



# Sedimentological characteristics of a late Miocene Contourite Channel System (The Rifian Corridor, Morocco)

W. de Weger



THE **DRIFTERS**  
RESEARCH GROUP  
BOTTOM CURRENTS & DEEP-WATER SEDIMENTATION

2021



# Sedimentological characteristics of a late Miocene Contourite Channel System

*Key areas: Morocco, Cyprus and South of Italy*

**Wouter de Weger**

Royal Holloway, University of London

This thesis is submitted to obtain the degree of Doctor of Philosophy (Geology) at the  
Royal Holloway University of London

May 2021

**Studentship with Contourite Project: JOINT INDUSTRY PROJECT – “Contourites”**

**REF. TOTAL: 4300003696 REF. BP: cw2153477**

VALUE OF THE AWARD:

Tuition fees: Equivalent to the value of the standard UK/EU student  
tuition fee for each academic year

Research grant: £117,000

DURATION OF THE AWARD: 3 years, full-time

Start Date: 19 October 2017

End Date: 18 October 2020

Extension end Date: 18 September 2021

## *Declaration of Authorship*

I, Wouter de Weger hereby declare that this thesis and the work presented herein is entirely my own. This thesis was completed whilst registered as a candidate at the Royal Holloway University of London, for the degree of Doctor of Philosophy (Geology). Where work has been completed in consultation or collaboration with other authors, this is clearly stated, and the relevant sources acknowledged.

Signed: *Wouter de Weger*

Date: *Friday the 14<sup>th</sup> of May 2021*

A handwritten signature in black ink, appearing to be 'Wouter de Weger', written in a cursive style.

## *Acknowledgements*

I would like to thank the following companies and people, without whom I would not have been able to do this PhD project, and without whom I could not have finalized this dissertation in its current form.

First and foremost, I would like to express my sincere gratitude to my supervisor Prof. Dr. Javier F. Hernández-Molina, who went to great lengths to set-up my research project, to set-up and manage “The Drifters Research Group” and its associated training sessions and, for his consistent support, trust, and guidance.

This project was funded by the Joint Industry Project supported by TOTAL, BP, ENI, ExxonMobil, Wintershall DEA, and TGS (formerly Spectrum), executed in the framework of “The Drifters Research Group”. Without their support this project would not have existed. Besides being grateful for offering me this opportunity, I would like to thank all company participants directly associated to this research project (in particular: Dr. F.H. Raison, Dr. E Stirling, Dr. G. Davoli, Dr. J.F. Fedele and M. Mohr) for their guidance, support, and for stimulating discussions on the topic.

I am furthermore very appreciative of the help and support given by the Office National des Hydrocarbures et the Mines (ONHYM), Morocco, to the General Director Madame A. Menkhadra, M. Nahim and Dr. A. Ait Salem. Not only did they provide me with data and required permissions to conduct fieldwork, two of its employees, Mr. M.A. Manar and Mr. Y. Astaty regularly joined me on field expeditions for which I’m grateful.

My gratitude is also expressed to Dr. D.G. Borisov, Prof. Dr. E.V. Ivanova and D.M. Korshunov from the Shirshov Institute of Oceanology, Russian Academy of Science and to E.I. Riazanova from Geoelement Ltd., Moscow, Russia, for their very pleasant collaboration in conducting a geochemical and mineralogical field study in Morocco.

I am furthermore very thankful to a great many colleagues and friends who contributed in many aspects of my PhD. First of all, many thanks to my co-supervisors, Prof. Dr. R. Flecker (Univ. of Bristol), Prof. W. Krijgsman (Utrecht Univ.) and advisor Dr. D. Chiarella (Royal Holloway Univ. of London). Thanks to my colleagues and friends from “The Drifters Research Group”, in particular: Sandra de Castro Santos, Adam Kirby, Oswaldo Mantilla, Lin Ng and Sara Rodriguez who significantly contributed to making this research project a very pleasant experience. Thanks to my co-authors, in particular those who have not yet been mentioned,



my friend Olmo Miguez-Salas (Univ. of Granada), Prof. Dr. F.J. Sierro (Univ. of Salamanca), Prof. Dr. F. Rodriguez Tovar, Prof. Dr. M. Bruno (Univ. of Cadiz) and G. Blackbourn (Blackbourn geoconsulting), for their scientific contributions and dedication to improve the manuscripts. Thanks to my friends in Morocco, Dr. Zakaria Yousfi and Abdel Mojid Kouissi who significantly supported me during my field campaigns, but also thanks to the many wonderful people I met in Morocco for making me feel welcome. Thanks to the many inspiring people I met, during conferences and training sessions, lecturers and professors at Utrecht University who paved my way through the sometimes erratic, but wonderful world of geosciences. Also, thanks to the Royal Holloway University of London, the Earth Sciences department (particularly Prof. Margaret Collinson, Dr. Amy Gough, Prof. Dr. Ian Watkinson and Kevin D'Souza), who supported, guided, supervised and accommodated me during this research project.

Finally, a great many thanks to my parents (John and Monique), Sisters (Mirte and Daphne), brother-in-law (Toine), nieces and nephew (Ilse, Hugo and Eva), my girlfriend Marjolein and our dog Nola, for shaping me the way I am and for always supporting me.

**Post vivia** – I would like to express my sincere gratitude to Prof. Heiko Hüneke (*External examiner, Univ. Greifswald, Germany*), Prof. emerit. D. Bosence (*Internal examiner, Royal Holloway Univ. of London*) and Prof. D. Waltham (*Independent chair, Royal Holloway Univ. of London*), for their roles in the examination committee and for making the viva such a pleasant experience.

## Autobiography

My name is Wouter de Weger, born on the 8th of August 1988 in 's-Hertogenbosch, the Netherlands. I grew up with an older sister (Mirte), a younger sister (Daphne), my mom (Monique), and my dad (John). During my childhood I dreamt of either becoming a veterinarian or a dentist, for which you need pre-university education. For this reason, I decided to advance my education for which I graduated in 2007. By this time, my wish to become a veterinarian had faded and I decided I wanted to become a dentist. Unfortunately, at the time, dentistry studies, due to a lack of positions, was based on a lottery that I did not make. An alternative was found in biomedical technology, I quickly realized however, that this was not for me, so I quit. During the remainder of the academic year, I worked a lot of construction, which happens to be one of my hobbies. The following academic year I retried the dentistry lottery without luck. In a study guide, borrowed from a friend, I stumbled upon Earth Sciences. As I have a great passion for the outdoors, which this study seemed to be able to facilitate, I started this study in September of 2008.



Although variably enthusiastic of studying, I quickly realized fieldwork was something I loved! As such, throughout my Bachelor I went on as many fieldtrips as possible, finishing with a bachelor thesis: “Transitional stratigraphy and palaeo-stratigraphy of a Barremian to Albian continental to marine depositional history”, based on a fieldtrip in the Galve- and Aliaga sub-basins in NE Spain. I received my bachelor’s degree on the 28th of February 2013. In September of 2013 I started my master’s degree in Earth Sciences in the Earth, Life and Climate (Integrated stratigraphy and sedimentary systems) programme with the addition of the M-profile, Geo-Resources. As it turned out, an excellent choice that led me to where I am writing this dissertation.

The Master’s degree comprised one academic year of taught classes, half a year of graduation by Research and half a year of Internship. The taught academic year was finalized with the MSc fieldtrip to Sorbas, Spain. It was during this fieldtrip where I met Walter Capella, a former PhD student at Utrecht University associated to the MEDGATE project, he was a field assistant during this trip. His research topic was to study the tectono-sedimentary evolution of the Rifian Corridor (Morocco) and the late Miocene isolation of the

Mediterranean. My research partner in Sorbas, Menno van Oorschot, and I were invited to join Walter on a fieldtrip to Morocco for our individual graduation Research, or MSc thesis.

The 12th of September 2014 we departed to Fes, Morocco, to find and investigate the sedimentary succession capturing the closure of the late Miocene Rifian Corridor. Six weeks, with only three days off, were spent in a country we grew to love. The resulting MSc thesis is titled: "Sequence stratigraphic analysis of the interaction between tectonically driven sedimentation and sediment transporting bottom currents in the foreland basin of the Rifian Corridor – Case study from the Gharb and Saiss basins, northern Morocco". This thesis, due to it describing sediment transporting bottom currents, caught the attention of Prof. Dr. F.J. Hernández-Molina, a contourite expert associated to the Royal Holloway University of London. He invited me to meet him in his office at RHUL in August of 2015, where he offered me the possibility to do a PhD in his upcoming consortium of "The Drifters" Research Group. This meeting was followed by a fieldtrip to Morocco, in search for Contourite outcrops in January of 2016. By this time, I already agreed to- and was very excited to do a PhD at the Royal Holloway University of London. In the meantime, I still had to do half a year of internship to obtain my MSc degree.

I ended up doing two internships that I really enjoyed and that enabled me to gain significant industry experience. The first being a 4-month internship at Panterra Geoconsulting where I did the core-description and analysed reservoir properties of both an Upper Carboniferous and a Lower Cretaceous core. The second, 6-month internship, was at TNO – Geological survey of the Netherlands, where I revised the paleomagnetic record of the Plio-Pleistocene fluvial deposits in the Lower Rhine Embayment. After the successful completion of these internships, I received my master's degree on the 31st of March 2016.

Since the offered PhD position was not yet finalized by this time, I took up the offer to work for the Geological Survey of the Netherlands on a project basis until the end of December 2017. Meanwhile, I was still awaiting confirmation about the PhD position and, by the time I almost gave up on the possibility as I was offered a job at an international engineering and consultancy firm, Javier (Prof. Dr. F.J. Hernández-Molina) contacted me that the contracts were finalized. I officially started my PhD on the 19th of October 2017.

# Contents

Declaration of Authorship .....	2
Acknowledgements.....	3
Autobiography.....	5
Abstract.....	13
<b>Lists of Figures, Tables and Abbreviations .....</b>	<b>14</b>
Tables and figures .....	15
Chapter II.....	15
Chapter II.....	16
Chapter IV .....	16
Chapter V .....	17
Chapter VI .....	20
Chapter VII .....	21
Chapter VIII .....	22
Abbreviations .....	24
<b>Chapter I .....</b>	<b>25</b>
1. Introduction .....	26
2. Aims and objectives.....	27
3. Outline.....	28
4. Scientific and Industrial significance.....	30
<b>Chapter II .....</b>	<b>32</b>
Part I.....	33
Study area and geology.....	33
1. Study location.....	34
1.1 Morocco .....	34
1.2 Study area .....	35
2. Geological Background of the western Mediterranean .....	36

2.1 Geology of the western Mediterranean.....	36
2.2 Rif-Betic Cordillera.....	36
2.3 Kinematics of the Betic-Rif orogenic system .....	40
3. Geology of the study area .....	42
4. Late Miocene Paleogeographic and Palaeoceanographic setting .....	45
4.1 Introduction .....	45
4.2 Evolution of the Late Miocene western Mediterranean seaways .....	46
4.3 The Strait of Gibraltar.....	51
4.4 Chronology of the Messinian Salinity Crisis.....	52
Part II.....	54
Deep-marine processes.....	54
5. Deep-marine sedimentary processes.....	55
5.1 Deep-water .....	55
5.2 Deep-water formation.....	57
5.3 Deep marine sedimentary processes .....	58
5.4 The deep-marine facies problem .....	71
REFERENCES.....	73
<b>Chapter III.....</b>	<b>85</b>
1. Introduction and approach .....	86
2. Literature studies .....	86
3. Fieldwork and analysis.....	87
4. Biostratigraphic dating and water-depth estimates.....	94
5. Petrography.....	95
6. Grain-size analysis .....	95
7. Geochemical and Magnetic susceptibility measurements .....	96
7.1 X-ray fluorescence.....	96
7.2 X-ray diffraction.....	97
7.3 Magnetic susceptibility.....	98



8. Identification of Ancient Contourites .....	98
9. Reproducibility, precedence and justification .....	100
10. Rationale .....	100
<b>Results .....</b>	<b>102</b>
Chapters IV – VII .....	102
<b>Chapter IV .....</b>	<b>103</b>
Late Miocene contourite channel system reveals intermittent overflow behavior ..	103
Abstract .....	104
Introduction .....	104
Regional setting.....	106
Sedimentary record.....	106
Decoding the paleo-MOW .....	109
Controls on overflow.....	111
Impact on thermohaline circulation.....	112
Acknowledgments.....	113
References cited.....	113
<b>Chapter V .....</b>	<b>116</b>
Contourite depositional system after the exit of a strait: case study from the late Miocene South Rifian Corridor, Morocco.....	116
Abstract.....	117
1. Introduction .....	118
2. Study area and geological setting.....	121
3. Palaeoceanographic setting .....	123
4. Methodology.....	124
5. Results .....	127
6. Depositional sub-environments .....	146
7. Discussion.....	150
8. Conclusions .....	159

acknowledgements .....	160
References .....	161
<b>Chapter VI .....</b>	<b>169</b>
Tide-dominated deltas responding to high-frequency sea-level changes, pre-Messinian Rifian Corridor, Morocco: DISCUSSION .....	169
Introduction .....	170
Spatiotemporal location of the outcrops .....	170
Shallow- vs Deep-water.....	172
Depositional setting: Sedimentological data and interpretation.....	174
Conclusion.....	175
References .....	175
<b>Chapter VII .....</b>	<b>177</b>
Abstract.....	178
1. Introduction .....	179
2. Study area and geological setting.....	181
3. Paleoceanographic setting .....	182
4. Methodology.....	184
5. Studied sections .....	185
6. Results.....	186
7. Discussion.....	209
8. Implications .....	217
9. Conclusions .....	218
10. Acknowledgements.....	219
References .....	220
<b>Chapter VIII.....</b>	<b>226</b>
General Discussion and Conclusions .....	226
(i) What are the main contributions of this research project? .....	227
(ii) How are contourite channel systems formed?.....	227

(iii) What are the main control factors of overflow induced contourite channel systems?	228
(iv) Which features make up a contourite system?	230
(v) What characterizes contourite channels and moats?	231
How can we improve on the terminology used for contourite depositional systems?	233
(vi) How are contourite channel systems sourced with sediment?	234
(vii) How do contourite channel systems interact with other deep-marine sedimentary processes?	237
(viii) Which sedimentary facies typify contourite channel fill sequences?	238
(ix) What are the identification criteria for sandy contourite channels?	239
(x) How is sediment distributed in contourite channels?	242
(xi) What factors control erosional and depositional features in contourite channel systems?	243
(xii) Are the studied outcrops, related to the paleo-MOW in a confined gateway, representative for sandy contourite systems on other continental margins?	243
(xiv) Why are there so few examples of contourite deposits in outcrop?	244
(xv) What are the implications of the new findings?	245
(xvi) What are the main limitations of this research project?	248
Conclusions	249
References	250
<b>Chapter IX</b>	<b>256</b>
Future Research	256
<b>Chapter X</b>	<b>258</b>
Co-Authored work	258
Co-Authored work	259
1.1 Publications	259
<b>Chapter XI</b>	<b>260</b>
Appendices – (Supplementary material)	260

Supplementary material Chapter VI.....	261
Supplementary material Chapter V.....	262
Supplementary material Chapter VI.....	265

## *Abstract*

Bottom currents are widely and increasingly more often recognized in deep-marine environments. However, the processes driving and controlling these bottom currents remain poorly understood. This partially results from their occurrence in near inaccessible deep-marine environments. Consequently, our knowledge of bottom currents significantly depends on studying their deposits.

Idealized facies of bottom current deposits (contourites) have been established for fine-grained contourite drifts in modern deep-marine sedimentary environments however, their sand-rich counter parts, related to stronger bottom-currents, have remained more elusive. Equivalent contourite facies in the ancient record have only been scarcely recognized, hindering the development of models that can be applied to industry geosciences and the reconstruction of past ocean circulation.

This Thesis presents a multidisciplinary field-focussed study on contourite deposits from the late Miocene Rifian Corridor in Morocco. A detailed geological analysis was carried out in the study area to characterise the paleogeographic setting and to analyse the potential of outcrops having a contouritic origin. Four sections were selected for detailed sedimentological analysis, including the characterisation of morphological, sedimentological, petrological, and ichnological elements. The results of these characterisations allowed us to reconstruct the newly identified contourite channel system associated to the late Miocene Mediterranean Outflow Water (paleo-MOW). Detailed facies analysis enables the characterisation of different contourite elements and the proposal of a novel contourite facies model.

The new findings of this research project furthermore include the characterisation of control factors on the behaviour of overflow, and thus the controls on bottom-current formation and their evolution. These control factors range from tectonically induced re-configuration of overflow controlling geological features, multi-scale orbitally controlled climate change and its effects on overflow behaviour as well as a strong modulation by tides. Unravelling these control factors from the sedimentary record, enabled the evaluation of the evolution of contourite depositional systems. This in-turn allows for the predictability of bottom-current induced sedimentary systems and strategies for both energy geosciences and hydrocarbon exploration.



# *Lists*

# Tables and figures

## Chapter II

### Part I

**Figure 2.1.** Location of Morocco, with in red, the study area. The Strait of Gibraltar (SoG) connects the Atlantic Ocean and the Mediterranean Sea. Modified from Google Earth.

**Figure 2.2.** Simplified geological map of southern Iberia and northern Morocco with the major tectonic domains and boundaries. (GB) Gharb Basin, (GuaB) Guadalquivir Basin, (GS) Gibraltar Strait, (HA) High Atlas, (M) Meseta, (MA) Middle Atlas, (Nf) Nekkror fault, (SB) Saïss Basin, (TASZ) Trans-Alboran Shear Zone. The red box indicates the location of the study area (from Gil de la Iglesia, 2015).

**Figure 2.3.** Structural map of southern Spain (S) and northern Morocco (M). Modified after Michard et al. 2002

**Figure 2.4.** Regional Geological map of the study area (modified after Saadi, et al., 1980). The grey-scale image represents a satellite image with a projection of the geological map. The location of the main sections are indicated by: A) Sidi Chahed, B) Kirmta, C) Fes-north, D) El Adergha and, E) Ain Kansera.

**Figure 2.5.** Composite stratigraphic- column of the Mesozoic and Tertiary rocks of the Saïss Basin. The sedimentary succession primarily studied falls within the Late Tortonian Blue Marls. Modified from Sani et al. (2007). (Note: not to scale)

**Figure 2.6.** Simplified paleogeographic maps of the Mediterranean area. (a) Schematic paleogeographic map of the Mediterranean area during Chattian. (b) Schematic paleogeographic map of the Mediterranean area during Burdigalian. (c) Schematic paleogeographic map of the Mediterranean area during Serravallian. (d) Schematic paleogeographic map of the Mediterranean area during Tortonian. Derived from Cornacchia, et al., 2018.

**Figure 2.7.** Tortonian reconstruction map of the western Mediterranean region.

**Figure 2.8.** Summary figure from Flecker et al. (2015) illustrating the main features of the Mediterranean's exchange history in the Late Miocene-Pliocene including lithology, Mediterranean salinity, a qualitative representation of gateway size and the probable drivers (tectonic, erosion, sea level) of changing dimensions, the Mediterranean's fresh water flux where E and P = evaporation and precipitation over the Mediterranean respectively and R is the river discharge into the Mediterranean Sea, and arrows representing one-way or two-way exchange between the Mediterranean and Atlantic.

### Part II

**Figure 2.9.** This figure shows the offshore zonation. Panel A shows the zonation of the Continental Shelf, down to water depths of 120 m. Panel B shows the zonation from the Continental Shelf (A) to Abyssal plains, down to water depths of over 6000 m. F. shore is short for foreshore. HCS stands for Hummocky cross-stratification. Figure modified after Wikipedia.

**Figure 2.10.** Schematic view of the ocean circulation (Kuhlbrodt et al., 2007). The red coloured bands show the main surficial currents. Deep-water formation, because of the increase in water density primarily related to cooling, is taking place at the yellow circles in the northern Atlantic (Labrador and Nordic Seas) and near Antarctica. This deep-water formation forces the current to sink and continue as the blue coloured bands, forming the main currents in deeper layers. In violet the Antarctic bottom water.

**Figure 2.11.** The range of processes contributing to fine-grained hemipelagic deposition in the deep-sea (after Stow, 1996)

**Figure 2.12.** Facies model for hemipelagites. This standardized model shows the cyclic variability between different input components. This state-of-the-art model is modified after Stow and Smillie, 2020.

**Figure 2.13.** Simplified models and facies models for rockfalls, slides, creep and slump deposits, debris flows and turbidity currents. The legend shows the dominant sedimentary composition based on grain-size; sand, mud/silt dominated and solid rock. Modified after Mulder, 2011; Lewis, 1971; Pickering, 1979; Reading, 1996; Stow et al., 1996; Bouma, 1962.

**Figure 2.14.** Facies model for fine-grained contourites. The contourite facies model on the left, modified after *Gonthier et al. (1984)*, shows the complete sequence of divisions C1-C5. The variations include typical partial sequences. *Copied from Stow and Smillie, 2020.*

**Figure 2.15.** Contourite Drift features modified after Rebesco et al., 2014 and references therein. Blue circles indicate the generalized core of the bottom current. Crosses within the blue circles indicate bottom currents away from the reader whilst black dots indicate a current flowing towards the reader.

## Chapter III

**Figure 3.1.** Satellite image of the study area (*derived from ZOOM Earth*). The study area is located in northern Morocco and comprises the cities (from west to east); Sidi Kacem, Meknes, Fes and Taza. The pin-marks indicate the location of prominent late Miocene outcrops. Numbers are associated to Table 1. The yellow pin-marks are indicative for newly discovered, likely late Miocene outcrops that have not been properly studied but have good potential for contourite studies. The red pin-marks are indicative for outcrops relevant for this study, but which were not considered vital for this research project. The green pin-marks indicate the location of the main outcrops used in this research project.

**Figure 3.2.** Overview of outcrops; (1) Bel Amri, (2) Msagra, (3) Haricha, (4) Madhouma, (5) Sidi Chahed, and (6) Kirmta. The numbers relate to both Figure 1 and Table 1. The panels on the left comprise satellite images (*derived from ZOOM Earth*), and the panels on the right represent pictures of the associated outcrop.

**Figure 3.3.** Overview of outcrops; (7) Lemda, (8) Moulay Yacoub, (9) Fes-north, (10) Sidi Harazem, (11) El Adergha, and (12) Ain Kansera. The numbers relate to both Figure 1 and Table 1. The panels on the left comprise satellite images (*derived from ZOOM Earth*), and the panels on the right represent pictures of the associated outcrop.

**Figure 3.4.** Workflow diagram for the identification of contourite potential of outcrops. This workflow or train-of-thought was used to determine the possible contourite origin of outcrops studied for this research project.

**Tabel 3.1.** Overview of visited outcrops. Numbers correspond to Figure 3.1. The table provides the location, general description, potential for contourite research, the data collected, publications on outcrops and the ages, depositional domains and remarks.

## Chapter IV

**Figure 4.1.** Paleogeographic reconstruction of the late Miocene western Mediterranean (*modified after Capella et al. 2017a*). Grey – subaqueous Prerif Ridges (PR). Red (lower) and orange (upper) arrows depict Mediterranean Outflow Water (MOW) branches. Globe shows MOW (orange) and main surficial (red) and deep-water circulation pattern (blue). Map data are ©2018 Google™ with topographic overlay from U.S. Geological Survey topographic maps (<http://earthpoint.us/TopoMap.aspx>).

**Figure 4.2.** Sedimentary log, panoramic pictures, and interpretations for the Sidi Chahed section (Morocco; 34.101566°N, 5.301466°W). Three sand units (from old to young; yellow, green, and red) represent channel-fill sequences. Rosette diagram shows paleocurrent directions. **(A)** Basal fill sequence of sandstone unit 1. **(B)** Typical stacking pattern of facies F4. **(C)** Two bedsets of facies F4 separated by F6. Beds below F6 show soft-sediment deformation, and overlying beds are erosive. Note near-perpendicular difference in paleocurrent directions. **(D)** Thin section with mixed compositional sand of facies F4, and transported, exsolved dolomite (Dol) rhomb.

**Figure 4.3.** Sedimentary log (see Fig. 2 for legend), panoramic pictures, and interpretations for the Kirmta section (Morocco; 34.170855°N, 5.239288°W). Rosette diagram shows paleocurrent directions. **(A-B)** Facies F3. **(C)** Sandstone unit 2 with tabular cross-stratified beds (F4). **(D-E)** Facies F6, with turbidite deposits below the uppermost sand unit.

**Figure 4.4.** Paleogeographic model of the late Miocene Rifian Corridor (Morocco) with lower (red) and upper (orange) branches of paleo-Mediterranean Outflow Water (MOW). Cross section A-A' shows intraslope subbasins that act as fairways in the frontal part of the imbricate wedge and are filled by three vertically stacked, color-labeled (1-3) sand units. Circles depict location of core for each paleo-MOW branch.

Supplementary material in appendix –

**Table S4.1.** Overview of recognized sedimentary facies and facies associations. The facies consist of F1) Blue marlstone, F2) Brownish sandy marlstone, F3) Planar bi-gradational sandstones, F4) Cross-stratified sandstone, F5) Trough-cross stratified sandstones, F6) Heterolithic convolute sandstones, F7) Normal graded compound sandstone beds and, F8) Monomictic conglomerates. Besides the facies, their general thickness, sedimentary structures, composition and interpretation are provided.

## Chapter V

**Figure 5.1. (A)** Satellite terrain image of the western-most Mediterranean region, southern Spain and north-west Africa. The globe on the right-hand corner shows the location of the study area and depicts the thermohaline circulation pattern (red – shallow and blue – deep), the orange arrow indicates the pathway of the MOW. In transparent blue a late Miocene palaeogeographic overlay of the Betic and Rifian corridors, NRC = North Rifian Corridor and SRC = South Rifian Corridor, after *de Weger et al. (2020)*. The location of the main geological features, such as the Gharb, Saiss and Taza-Guercif basins, the Prerifian Ridges and the Taza Strait are indicated. **(B)** Satellite image showing the location of the study areas. The abbreviations stand for the section names, FN = Fes-north and EA = El Adergha. **(C)** Late Miocene reconstruction through the SRC, cross-section A-A', of which the location is indicated in **(A)**. The SRC accommodated Atlantic-Mediterranean exchange of surficial Atlantic and Mediterranean Deep Water.

**Figure 5.2.** Regional geological map of the study area including the locations of the studied Upper Miocene outcrops; El Adergha (EA), Fes-north (FN) and Ain Kansera (EA) (*modified after Saadi et al., 1980*). Carb. Fact = carbonate factory, L = late, M = middle and E = early. Satellite images are derived from *GOOGLE Earth*.

**Figure 5.3.** Middle Miocene to late Pliocene lithostratigraphy of the Saiss Basin. The intercalated sandstone bodies in the late Tortonian to Messinian Blue Marl Formation belong to the sections studied herein.

**Figure 5.4.** Panoramic view of the El Adergha (A) and Fes-north (B) outcrops. These pictures highlight the general exposed geometries and the scale of the outcrops. Due to the location of the Fes-north section being far away from the nearest vantage point no better pictures are currently available.

**Figure 5.5.** Sedimentary logs for the Ain Kansera (*modified after Capella et al., 2017a*), Fes-north and El Adergha sections. Their location is provided in Fig. 2, and their relative distance, and distance to the Prerifian Ridges is indicated. Palaeocurrents are divided in two major components, along-slope Pc 1 (red) and down-slope Pc 2 (green). The main sedimentary features are indicated next to the log. HCS = hummocky cross-stratification, CS = cross-stratification, BG = bi-gradational and TD = turbidite (see text for interpretation).

**Figure 5.6.** Palaeogeographic reconstruction of the late Miocene South Rifian Corridor (7.51 to 7.25 Ma). The Prerifian Ridges (grey) might still have been submerged at this time. Red dots indicate sections studied herein. Yellow dots indicate sections previously studied, publications of these sections studied previously are denoted by superscript numbers (<sup>1</sup> Tulbure et al., 2017, <sup>2</sup> de Weger et al., 2020, <sup>3</sup> Capella et al., 2018). Green squares indicate the relative location of major cities in the area.

**Figure 5.7.** Sedimentary log for the El Adergha outcrop showing the facies, the facies associations, locations of the samples (Table S1) and the location of the pictures (see legend). **(A)** Main overview picture of the El Adergha section at an angle perpendicular to the outcrop. **(B)** Picture perpendicular to part of the outcrop showing facies, reference location of **(F)** and **(G)** and the location of sample EA4. **(C)** Eastward continuation of **(B)**. **(D)** Lowermost sandstone interval

consisting of facies F4 in sharp contact with facies F1. (E) Picture of turbidites stratigraphically located 100 m lower, embedded in the blue marls of facies F1.

(cont) Collage of examples of facies from the El Adergha outcrop. Picture letters correspond to those in (A) to (E). (F) Picture and line-drawing of the contact between facies F4 and F5 at 21 m in the log. Facies F4 is mottled, not easily captured by lines at this scale. (G) Picture and line-drawing of typical facies F5. The lowermost right corner is not well-exposed. (H) Top-view picture of bioclast (pecten) hash, imbrication bioclastic material not visible in picture. Note the 1 cm pecten shell in the middle top-view of the picture. (I) Bi-gradational stacking of facies F1-F2-F3-F2-F1. The F3 and F2 facies are intensely bioturbated leaving a mottled appearance. (J) Typical facies F4, consisting of laminated sandstone and mudstone and moderate bioturbation. (K) Turbidite deposits found roughly 100 m stratigraphically below the main studied interval, embedded in facies F1.

**Figure 5.8.** (A) Panoramic picture of the Fes-north outcrop with the panels indicating the locations of (B) to (E). (B) and (C) form a collage of the laterally (NW-SE) continuous section. Within these pictures the main facies distribution are indicated as well as locations for (F) to (K). (D) and (E) Line-drawings of (B) and (C) respectively. These line-drawings are made to emphasize bed-boundaries and internal structures. (D) Image clearly shows the tectonic tilt of the beds with respect to the near horizontal horizon. At the 5 m mark of the scale bar (4 m in the log) the mainly tabular beds with cross-stratification directed towards the left are overlain by S1 (slump 1) which is stratified mainly in the opposing direction. (E) This eastward lateral and upwards continuation of panel D (S1 for reference) shows that lateral facies changes are present. Furthermore, the termination of S1 against facies F6 (C) is visible. Within facies F6 SSD structures are visible. S2 overlies the more planar stratified facies F8 here.

(cont) Sedimentary log and picture collage of facies in the Fes-north outcrop. (F) Picture of facies F2 and F6, corresponding to 11 to 12 m in the log. Cross-stratification of facies F6 is directed towards the left (west). (G) Facies F8, alternating with facies F2. Facies F2 in this succession represents suspension fallout from a turbidity cloud. (H) Overview picture of the interval between 5.5 m and 8 m in the sedimentary log. The lower field of view shows facies F6 containing soft sediment deformation structures. This facies is overlain by facies F8. (I) Overview picture of the interval between 1 m and 5.5 m in the log. Here facies F3 and F6 are overlain by slump deposits of facies F9. (J) Picture showing both facies F3 and F7 and their stratigraphic relationship. On top of facies F7 a sharp basal contact with facies F6 is present. (K) Western-most expression of the exposed outcrop with stacked tabular beds of facies F6.

**Figure 5.9.** Overview of recognized ichnospecies: *Macaronichnus* (Mn), *Thalassinoides* (Th), *Planolites* (Pl), *Rosselia* (Rs), *Ophiomorpha* (Op) and undifferentiated (Undif.) traces. The addition of (l) stands for -like. Facies are indicated with the coloured and labelled circles. (A) to (F) are taken from the El Adergha sections and (G) to (J) from the Fes-north section.

**Figure 5.10.** Examples of cyclic thickening and thinning foreset intervals and cyclic alterations between angular and tangential toe-sets. These alternations are associated with cross-stratification and interpreted as the record of sandy bedforms migrating under unidirectional, tidal-modulated accelerating/decelerating currents. N = neap tide and S = spring tides.

**Figure 5.11.** Palaeogeographic reconstruction of the late Miocene Rifian corridors between 7.51 Ma and 7.25 Ma. The palaeo-MOW cascaded over the Taza Sill, through the Taza Strait into the South Rifian Corridor where it was forced against the northern margin by the Coriolis force. The Atlantic surficial water flowed through the South Rifian Corridor and Taza Strait into the Mediterranean. The studied sections, Fes-north (FN) and El Adergha (EA) were located closely to or within the contourite channel changing over time. The red arrow, indicating the core of the palaeo-MOW depicts the trajectory of highest current-velocities confined within the channel, whereas the palaeo-MOW water mass was less confined.

**Figure 5.12.** Sketch showing the relation between the facies (F1 to F9), facies associations and the different depositional and erosional elements from the proximal continental slope to the contourite drift. The facies associations are related to their dominant depositional process and associated current velocities. The panels in the bottom left corner show examples of observed facies stacking patterns. Soft sediment deformation structures (SSD) are regularly observed below facies F9.

**Figure 5.13.** (A) to (D) Influence of a tidal cycle on Atlantic Inflow Water (AIW) and Mediterranean Outflow Water (MOW) and the interface between the two. At high tide and low tide (A and C



respectively) the tidal current is zero and the MOW reaches its mean intensity. During the ebb phase (from high tide to low tide; **B**) the tidal current is directed towards the east and the MOW reaches its lowest velocity. Occasionally, the direction of the MOW can also be reversed. During the flood phase (from low tide to high tide; **D**) the tidal current is directed towards the west and the MOW reaches its highest velocity. **(E)** Summarizes the water mass characteristics during one tidal cycle. **(F)** Shows the long-term effect of a relative sea-level drop, by which the interface is located closer to the sill. The location of the interface to the sill affects the potential of Mediterranean Deep Water (MDW) to flow out of the Mediterranean.

**Figure 5.14.** The logs of the late Miocene Fes-north (Fn) and El Adergha (EA) sections show vertical sedimentary facies changes. The vertical stacking of facies has been correlated based on their depositional ages (7.51 to 7.25 Ma) as well as on facies which, based on the herein proposed facies model, can be correlated in an across contourite channel system profile. **(A)** Depicts the transition from blue marls to more sand-rich marls which might indicate the initiation of a palaeo-MOW (p-MOW) in the area. **(B)** Shows the clear transition from FA1 to facies related to bottom current processes. By this time, the palaeo-MOW became the dominant depositional process. **(C)** to **(E)** Depicts the subtle northward migration of the contourite depositional system (CDS) and a possible intensification of the palaeo-MOW. **(F)** and **(G)** Depicts a period with low-velocity bottom currents associated with a weak palaeo-MOW. During this period, gravitational deposits could be preserved, as they were not being significantly affected by bottom currents. **(H)** and **(I)** Depicts the southward migration of the CDS, where the channel (FA4) migrated of the drift (FA1).

**Table 5.1.** Sedimentary facies table (F1 to F9) showing the main sedimentological and ichnological characteristics and features of the studied deposits in the El Adergha (EA) and Fes-north (FN) outcrops.

**Table 5.2.** Sedimentary facies associations (FA) established for sedimentary deposits in the El Adergha (EA) and Fes-north (FN) outcrops.

Supplementary material in appendix –

**Table S5.1.** Modal analysis data based on 300-point counts in thin section. Proportions of solid rock components (i.e., all but porosity) are re-normalized to a total of 100%. Component abbreviations, from left to right: F = facies, Qm = monocrystalline quartz, Qp = polycrystalline quartz, Qt = quartz total, F = feldspar, Gg = green glauconite, Gb = brownish/yellowish glauconite, Gt = glauconite total, L = lithic fragments; c = carbonate, d = dolomite, cp = claystone pellets, ch = chert, fa = feldspar aggregates, qm = quartz-mica aggregates, Lt = lithic total, B = bioclastic; b = bivalves, f = foraminifera, e = echinoderm, ca = calcareous algae, u = undifferentiated, Bt = bioclast total, Cc = calcite cement, Fe = iron oxides/hydroxides, P% = porosity percentage, Gs = mean grain-size (ms = medium-grained sand, vfs = very-fine grained sand), S = sorting (m = medium, w = well, vw = very well).

**Figure S5.1.** Microphotographs for facies F4 and F5. Abbreviations: dp = detrital pellets, pf = planktonic foraminifera, bf = benthic foraminifera, dol = dolomite, gl = glauconite, ec = echinoderm fragments, hx = hexagonal quartz. **(A)** Microfacies of facies F4 with detrital pellets and planktonic foraminifera. **(B)** and **(C)** Microfacies of facies F5 with brownish gl, dp and exsolved dol **(B)** and ec fragments and bf **(C)**.

**Figure S5.2.** Microphotographs for facies F6 and F8. **(A)** Microfacies of F6 with ec spine and bf (see caption for Fig. S1 for abbreviations), the large crystal of calcite along the lower edge of the field-of-view contains silt-grade quartz grains and pods of argillaceous material. **(B)** to **(D)** Microfacies of F8 for El Adergha, rich in bc, pf and gl **(B)** and **(C)** and Fes-north, rich in pf, bc, gl and the occasional dol **(D)**. Minute dark specs are aggregates of iron oxides dissolved from the calcite cement.

## Chapter VI

**Figure 6.1** (herein). A) Regional geological map of the study area including the locations of the studied Upper Miocene outcrops; Ben Allou (BA) and El Adergha (EA), as well as the Pliocene Driouate (DR) outcrop. The South Rifian Corridor (SRC) was limited northwards by the Nappe and southwards by both the Moroccan Meseta in the southeast, and the Middle Atlas towards the south. The North Rifian Corridor (NRC) is located north of the Nappe. The square outlines the location of figure B. Carb. Factories is short for Carbonate factories, L = late, M = middle and E = early. (modified after *Saadi. et al., 1980*). B) Shows the geological map wrongly modified by Beelen et al. after *Chankeb, 2004*. Note that the Jurassic cover south of Fes and Meknes, or south of the Prerif Ridges is not present in the Saiss Basin but is related to the Middle Atlas.

**Figure 6.2** (herein). Temporal distribution of the studied outcrops used by Beelen et al. and based on other sources such as *Capella et al. (2017)*; *Chankeb (2004)*; *Saadi et al. (1980)* and *Taltasse (1953)*. BA = the Ben Allou outcrop and, EA = El Adergha.

Supplementary material in appendix –

**Fig. 1.** - Derived from Beelen et al., 2020 – Top: Paleogeographic reconstruction of the Rifian Corridors during the late Tortonian. Note that the Gibraltar Strait had not yet formed during this time (*Modified from Capella et al. 2017a*). White box in top right represents area of image shown below. White inset shows present day location of the study area. Bottom: Geological map showing all three outcrop locations visited in this study (Beelen et al., 2020): Ben Allou, El Adergha, Driouate, relative to the cities of Meknes and Fez. Geological map is modified from *Chenakeb (2004)*. All outcrop localities considered in this study are from upper Tortonian interval of the Saiss sub-basin in the Rif Foreland.

**Fig. 4.**- Derived from Beelen et al., 2020 – Three scale orders of cross strata in the calcarenites. A) The largest scale of 1-3-m-thick cross strata, showing both unidirectional and bidirectional cross-bedding and bounded by reactivation surfaces. B) The moderate scale has 20-100-cm-thick packages of mostly unidirectional cross-strata bounded by reactivation surfaces. C) The smallest cross-strata are less than 20 cm thick and show a dominance of bidirectional cross stratification and ripples, including some herringbone strata.

**Fig. 6.**- Derived from Beelen et al., 2020 – Images showing the details of subfacies 3b and 3c in the Ben Allou outcrop. A) Tabular sandstone beds bounded by mud drapes (subfacies 3c). B) 30-cm-thick intervals with bidirectional flaser bedding above a rippled surface (subfacies 3c). C) Prominent 5-cm-thick mud drape with mud crack (subfacies 3c). D) Rippled surface with *Rhizocorallium* (bottom left) (subfacies 3c). E) Large dewatering structure with red-colored hardgrounds at the base (subfacies 3b). F) Siderite-rich surface with pustular texture (possibly a fossil microbial mat, subfacies 3b). G) Bidirectional-current structure with dominant paleocurrent direction (blue) and subordinate paleocurrent direction (red) shown (subfacies 3b). H) Rhythmically bedded interval (subfacies 3b). I) Barnacle hash (subfacies 3b).

**Fig. 10.**- Derived from Beelen et al., 2020 – Images showing details of the Driouate outcrop. A) Pinkish, carbonaceous siltstones (facies 4) with roughly 30-cm-thick beds of micrite-rich caliche. These sediments are incised at the top by cross-stratified conglomerates (facies 5). B) Top of carbonaceous siltstones (facies 4) showing plant rootlets. C) Close-up view of cross-stratified conglomerates (facies 5) showing fining-upward beds and polymict clasts. D) Petrified tree trunk in cross-stratified conglomerates (facies 5). E) *Pylonichnus* trace fossils in facies 6. F) Layered, tuberous stromatolite in facies 6. G) Stromatolite with numerous insect-larva burrows in facies 6. H) Close-up of facies 6 showing bamboo or reed stalk imprint.

**Fig. 15.**- Derived from Beelen et al., 2020 – A) Exposure at Driouate. B) Interpretation: three complete cycles are identified, each having three facies. C) Possible interpretation of facies showing siltstones (facies 4) are linked to highstands while cross-stratified conglomerates (facies 5) are linked to lowstand and stromatolite bearing carbonate rocks (facies 6) are linked to transgression. Cycles are bounded at the bottom by erosional surfaces.

**Fig. 16.**- Derived from Beelen et al., 2020 – Tentative paleogeographic interpretation for the Saiss sub-basin area of the Southern Rifian Corridor. Top: five upper Tortonian outcrops and their paleocurrent directions as measured by *Capella et al. (2017a)*, suggesting a complex, likely rugose

southern coastline of the Rifian Corridor. Bottom: schematic paleogeographic interpretation for Ben Allou, El Adergha, and Driouate, showing Ben Allou situated at a bay.

**Table 2** of the supplementary material by Beelen et al. 2020 – Foraminiferal genera are roughly from shallow (left) to deeper (right), planktonic genera are in bold.

## Chapter VII

**Figure 7.1.** Paleogeographic reconstruction of the late Miocene Rifian Corridor, Morocco (modified after de Weger et al., 2020, 2021). The Betic and Rif, Middle Atlas, Prerif Ridges, and the Taza-Sill form the main geological features. The studied outcrops (Kirmta and Sidi Chahed) are related to different branches of the paleo-Mediterranean Outflow Water (MOW). The small globe depicts the location of the study area, the general ocean circulation pattern and in orange, the trajectory of the present-day MOW.

**Figure 7.2.** Satellite image of the study area near the city of Fes. The main sections described herein, **(A)** Sidi Chahed and **(B)** Kirmta are located north of the Prerif Ridges (PR). The locations of Fes-north **(C)**, El Adergha **(D)**, Ain Kansera **(E)** and, Sidi Harazem **(F)** sections, located south of the PR, are provided as a reference to previous work (see white box for references).

**Figure 7.3. (Above)** Overview figure of the Sidi Chahed outcrop **(A)** and associated sections **(B – E)**. The log on the left represents a generalized composite log through the three main 1<sup>st</sup> order sand units (SU), the black arrows indicate mean paleocurrent directions with respect to the north (up). **(A)** Panoramic picture of the outcrop. In yellow, green, and red respectively the paleochannels SU1, SU2 and SU3. The small grey circles depict the location of the sections **(B-I)** and the location of figure J.

>>> **(Right)** Sections **F – I** of the Sidi Chahed outcrop. **(J)** Drawing of the south western flank of the outcrops as indicated in **(A)**. This sketch shows the 1<sup>st</sup> order lower- (LBS) and upper-bounding surfaces (UBS) as well as the 2<sup>nd</sup> order bounding surfaces.

**Figure 7.4.** Overview figure of the Kirmta outcrop **(A)** and associated sections **(B – E)**. The log on the left represents a generalized log through the three 1<sup>st</sup> order sand units, the black arrows indicate the mean paleocurrent directions with respect to the north (up). **(A)** Panoramic picture of the outcrop photographed towards the north. In yellow, green, and red respectively the paleochannels SU1, SU2 and SU3. The small grey circles depict the location of the sections.

**Figure 7.5.** Outcrop pictures associated to the studied channelized features with facies labels. Pictures A, D, E, G, H and I are from the Sidi Chahed outcrop. Pictures B, C and F are from the Kirmta outcrop. The location of the pictures within the logs is provided in **Fig. 7.4** (orange circles). SSD = Soft Sediment Deformation. The people representative for scale are between 1.7 and 1.95 m.

**Figure 7.6.** Thin-section images of the three microfacies identified: **(A)** Microfacies I, **(B)** Microfacies II and, **(C)** Microfacies III. The pictures on the left-hand side are in plane polarized light whereas the pictures on the right hand side are in cross polarized light. The scale of the pictures is provided in the lower left corner. Abbreviations in the pictures stand for: gl – glauconite, br – bryozoan fragments, ec – echinoderm fragments, pf – planktonic foraminifers, bf – benthic foraminifers, dp – detrital pellets, commonly consisting of mud and, dol – dolomite.

**Figure 7.7.** The top panel is derived from de Weger et al. (2021) and shows the relation between facies F1-F9 defined therein. This facies model is used for comparison to the newly proposed facies model made herein (two bottom panels, one for the Sidi Chahed and one for the Kirmta outcrop at the bottom). This facies model shows the relation between facies and facies associations within the 1<sup>st</sup> order contourite channel, which transitions towards the drift (S/SW or left). The estimated current velocities for each depositional domain is included.

**Figure 7.8.** Simplified paleogeographic setting and terminology of the late Miocene, South Rifian Corridor contourite channel system.

**Figure 7.9.** Facies distribution within main sand-units (SU1-3) of the Sidi Chahed outcrop. **(A)** Panoramic picture with the main, concave-up sand units, indicated (from old to young), by the yellow (SU1), green (SU2) and red (SU3) lines. This color-scheme is also applied to the remaining figures. **(B)** Top-view of the outcrop with the black arrows indicating the main paleo-current direction and the dotted lines indicating the width of each sand unit. **(C)** Panoramic picture and

interpretation of part of Sand-Unit 1 as indicated in (A). (D) The southern flank of Sand-unit 1 and its interpretation. (E) The northern flank of Sand-Unit 1 and its interpretation.

**Figure 7.10.** Facies distribution within main sand-units (SU1-3) of the Kirmta outcrop. (A) Panoramic picture with the main, gently concave-up sand units, indicated (from old to young), by the yellow (SU1), green (SU2) and red (SU3). Facies in the east consist of laterally extensive F7.1 enclosed by facies association FA1. (B) Panoramic of the middle part of the outcrop with (C) the facies distribution interpretation below.

**Figure 7.11.** Multichannel (west-east oriented) seismic profile from the Gulf of Cadiz contourite depositional system showing the distribution of the erosive base of contourite channels developed coeval with regional discontinuities (from old to young;  $C_1 - C_9$ ). This profile is oriented in the direction of flow, roughly towards the North. Seismic line provided by REPSOL.

**Figure 7.12.** Sketch of the Sidi Chahed and Kirmta sections within the slope. This sketch furthermore depicts the 1<sup>st</sup> and 2<sup>nd</sup> order channels, their morphologies and their interrelationship.

**Figure 7.13.** Evolution of 2<sup>nd</sup> order channels and their related infill deposits. The secondary channels within the Sidi Chahed section (A and B) either prograde (A) or retrograde (B). The channel fill sequence in the Kirmta section is less complex due to weaker bottom currents and smaller bottom current velocity fluctuations.

**Figure 7.14.** Three-dimensional sandy contourite facies model showing the contourite channel and drift. Up current, or at the site of overflow, bottom current velocities are highest. Down-current bottom current velocities decrease. The bottom current core is the most energetic part within contourite systems, with decreasing current velocities away from the core. This model represents an idealized facies model where the facies distribution is a product of both sediment characteristics and current velocities.

**Table 7.1.** Sedimentary facies and facies associations table including the colour codes used throughout the chapter, sedimentary structures, thickness, grain-size, percentage of bioclastic component for the coarse grained sediments (Bc%, note: 0% bioclasts on the left side of the column, 100% bioclastic on the right side. Dotted line represents 50%), biogenic structures, estimated current velocities in cm/s ( $v \text{ cms}^{-1}$ ) and microfacies (MF).

**Table 7.2.** Modal analysis data based on 300-point modal analysis in thin section. Proportions of solid rock components (all but porosity) are renormalised to a total of 100%. Component abbreviations, from left to right: MF = micro facies, Qm = Monocrystalline Quartz, Qp = Polycrystalline Quartz, Qt = Quartz total, F = Feldspar, Gg = Green glauconite, Gb = Brownish/yellowish glauconite, Gt = Glauconite total, L = Lithic fragments; c = carbonate, d = dolomite, cp = claystone pellets, fa = feldspar aggregates, qm = quartz-mica aggregates, Lt = Lithic total, B = Bioclastic; b = bivalves, f = foraminifera, e = echinoderm, ca = calcareous algae, u = undifferentiated, Bt = Bioclast total, Cc = Calcite cement, Fe = Iron Oxides/Hydroxides, P% = porosity percentage, GS = Mean grain-size (ms = medium-grained sand, fs = fine grained sand), S = Sorting (w = well, vw = very well).

## Chapter VIII

**Figure 8.1.** Zonal section of the salinity (“density”) distribution along the axis of the Levantine intermediate current (*simplified after Wüst, 1961; Pinardi et al., 2019*). ENACW stands for Eastern North Atlantic Central Water. Note that this section is based on data from the winter season. The salinity distribution differs slightly during the summer season.

**Figure 8.2.** Schematic diagrams of the primary effects on overflow induced by tectonic activity and climate

**Figure 8.3.** Main characteristics of linear, large-scale contourite erosional features. The three main types are contourite moats, contourite channels and marginal valleys. Modified from *Hernández-Molina et al. (2008b)*.

**Figure 8.4.** Proposed terminology for contourite domains. USPB – Upper Stage Plane Bedforms, LSPB – Lower Stage Plane Bedforms, BCRS – Bottom Current Reworked Sands. Note that the pictured lateral variability of domains is not a requirement for contourite depositional systems. For drift types see Fig. 2.15.

**Figure 8.5.** The top panel is derived from *de Weger et al. (2021)* and shows the relation between facies F1-F9 defined therein. This facies model is used for comparison to the newly proposed facies model made herein (two bottom panels, one for the Sidi Chahed and one for the Kirmta outcrop at the bottom). This facies model shows the relation between facies and facies associations within the 1<sup>st</sup> order contourite channel, which transitions towards the drift (S/SW or left). The estimated current velocities for each depositional domain is included.

**Figure 8.6.** Evolution of contourite channels and the distribution of sediment with either reservoir (red) or seal (green) potential. A) The first stage of intra-slope sub-basin formation by the initiation and action of energetic bottom-currents. B) The across channel distribution of sediment with reservoir and seal potential. C) the final product of the natural evolution (up-slope migration) of the contourite channel and drift. A new phase of bottom-current activity is initiated by a newly generated bottom current > A.

## *Abbreviations*

ACC	Antarctic Circumpolar Current
AMOC	Atlantic Meridional Overturning Circulation
CDS	Contourite Depositional System
DSDP	Deep-Sea Drilling Programme
GB	Gharb Basin
GoCCS	Gulf of Cadiz Contourite System
GuaB	Gudalquivir Basin
HA	High Atlas
HCS	Hummocky Cross-Stratification
IODP	Integrated Ocean Drilling Programme
M	Moroccan Meseta
MA	Middle Atlas
MOW	Mediterranean Outflow/Overflow Water
MS	Magnetic Susceptibility
MSC	Mediterranean Salinity Crisis
MTD	Mass Transport Deposit
Nf	Nekkor fault
ODP	Ocean Drilling Project
<b>Paleo-MOW</b>	<b>Paleo (late Miocene) Mediterranean Outflow Water</b>
PCA	Principle Component Analysis
PLG	Primary Lower Gypsum
PR	Prerif Ridges
ROV	Remote Operated Vehicle
SB	Saiss Basin
SoG	Strait of Gibraltar
TAZS	Trans-Alboran Shear Zone
XRD	X-Ray Diffraction
XRF	X-Ray Fluorescence

# *Chapter I*

## **Introduction**

This chapter is divided in four sections, the first of which provides a brief introduction on the history of deep-sea-research and the current state of contourite research. It furthermore initiates on the problems that required the establishment of this research project. The second section elaborates on the aims and objectives that form the cornerstone of this project. The third section summarizes the outline of this thesis. The fourth section deals with the scientific and industrial significance of this research project.

# 1. Introduction

*“The World’s Ocean covers more than 70 percent of the planet’s surface, to date, we have explored approximately 5 percent”*

- NOAA, 2018 -

The origin of modern deep-sea exploration started in the year 1872, when the H.M.S. Challenger, commissioned by the Royal Society of London and the Royal Navy, set sail. During this expedition the general morphology of the ocean basins and the types of sediment they contained were established. The volume of *Murray & Renard (1891)* proceeding this voyage became the cornerstone of deep-sea sedimentology for a long time. Since then, oceanographers and geologists (among other disciplines) have made substantial progress in understanding the severely complex world’s oceans, a synthesis of which is nicely illustrated in the works of *Hernández-Molina et al. (2011)*.

The worldwide upsurge in research on deep-sea clastic deposits mainly coincided with the advent of the theory of turbidites, first recognized by *Kuenen & Migliorini (1950)*. During the 1960’s, the initial works of *Bouma (1962)*, the Bouma sequence, sparked the “turbidite revolution”. Despite the recognition of contourites in the 1960’s by *Heezen et al. (1966)*, turbidites evolved into an influential conceptual entity which overshadowed other deep-marine clastic depositional processes, as much so that decades later, *Shanmugam (2012)* dedicated a volume to provide the “much-needed” clarity by explaining the inherent problems with the prevailing practice of interpreting deep-water sands as “turbidites”. A second upsurge in research on deep-sea clastics coincided with the oil crisis in the 1970’s. This crisis stimulated deep-water oil and gas exploration which required a better understanding of deep-sea processes. This, in turn, sparked technological advances that enhanced the abilities for deep-sea research. With more widely available data on the deep-sea, the scientific community started to realize oceanographic processes have a substantial impact on climatic, sea-level and palaeoceanographic changes, which further stimulated deep-sea research. Examples of scientific programs that emerged from these realizations are the Deep Sea Driling Programme (DSDP), the Ocean Drilling Project (ODP) and the Integrated Ocean Drilling Programme (IODP). Associated to these developments, contourites started to gain more scientific attention and, particularly since the turn of the century, significant advances, and scientific contributions in contourite research were made. For comparison, the *google scholar* search engine records 2,610 results on “contourites” and 32,200 results



on “turbidites” by 2010. A decade later, 5,120 results are found on “contourites” and 68,300 results on “turbidites”.

Despite these advances, due to the near inaccessible environments of the deep-sea, most of the deep-marine realm and its associated processes are yet to be explored. Most of the works on contourites, as such, are based on 2D and 3D seismic profiles (*e.g. Faugeres et al. 1989; Paulat et al., 2019*) as they are relatively easy to acquire. Seismic studies however are generally of low-resolution and thus mainly focus on the large, fine-grained depositional features. Since less information is available from wells and cores, which also mainly focus on the fine-grained depositional features of contourites (*e.g. Gonthier et al., 1984; de Castro et al., 2020a, b; Hovikoski et al., 2020*), very little is known about the range of possible contourite facies, particularly for sandy contourites. This, in turn, hinders the recognition of contourite deposits in outcrop (*e.g. Huneke and Stow, 2008; Rebesco et al., 2014; Shanmugam, 2017*), even though outcrop studies regularly form the cornerstone of facies models, as was the case for “the Turbidite Revolution”.

## 2. Aims and objectives

By means of an extensive fieldwork-based study in northern Morocco where sandy contourite outcrops were previously recognized (*de Weger, 2016 (MSc thesis); Capella et al., 2017a*), I aimed to; i) get a better understanding of the regional context by which a solid background could be formed for the interpretation of observations, ii) get a better understanding of erosional and depositional processes within sandy contourite systems and, iii) to unravel which processes control the evolution of such a system. With these research aims I hoped to achieve a facies model for contourite channel systems, develop a better understanding of their evolution, establish their control factors and to identify recognition criteria for contourite deposits in the ancient record. Additionally, the findings should contribute to a better understanding of the implications of contourite channel systems for Energy Geosciences.

In order to achieve these aims our objective was to, i) obtain as much information on the region as possible, both in the form of existing literature but also to undertake several geological exploration trips in the area to get a broad consensus of the surrounding geology and to find new outcrops, ii) obtain a high-resolution record of large scale features such as

geometries, erosional bounding surfaces, general stacking patterns, and their dimensions, and, iii) to obtain a high resolution record of bed- to microfacies-scale erosional and depositional features and their lateral and vertical facies changes/evolution, especially within the contourite channels. Additional objectives were to acquire biostratigraphic, grain-size, geochemical, magnetic susceptibility and petrophysical data to complement our findings. Our objective for the final stages of this research project is to acquire a core of one of the sections to enable a continuous, very high-resolution record.

### 3. Outline

This thesis comprised nine chapters, three of which are preceding this paragraph.

#### *Preceding sections:*

- Section I is dedicated to acknowledging all companies, institutes and individuals who significantly contributed, in one way or another, to this thesis.
- Section II contains an autobiography in which I briefly describe the main events that led me to do this PhD.
- Section III contains lists of tables, figures, illustrations and appendices
- Section IV contains a list of abbreviations intended to make this thesis more accessible.

#### Introductory and background information

- Chapter I is divided in four sections, the first of which provides a brief introduction on the history of deep-sea-research and the current state of contourite research. It furthermore initiates on the problems that required the establishment of this research project. The second section elaborates on the aims and objectives that form the cornerstone of this project. The third section summarizes the outline of this thesis. The fourth section deals with the scientific and industrial significance of this research project.
- Chapter II is used to provide the reader with solid background information on the study location, geological background, paleogeographic and palaeoceanographic settings, and deep-sea sedimentary processes. This chapter comprises a literature study and results precede the findings of this research project.

- Chapter III outlines the methodologies used in this research project and presents the data acquired.

#### Results, interpretation, and discussion

- Chapters IV - VIII contain the results of this research project.
- Chapter IV consists of the first article that was published in GEOLOGY (2020), titled: “Late Miocene contourite channel reveals intermittent overflow behaviour”.
- Chapter V contains the second article published in SEDIMENTOLOGY (2021), titled: “Contourite depositional system after the exit of a strait: case study from the late Miocene Rifian Corridor, Morocco”.
- Chapter VI consists of a discussion article to a paper published by Beelen et al. (2020), titled: “Tide-dominated deltas responding to high-frequency sea-level changes, pre-Messinian Rifian Corridor, Morocco: DISCUSSION”.
- Chapter VII consists of the third full article that in its current state is ready to be submitted. This article is titled: “Sedimentary facies distribution within erosional and depositional contourite channels”.
- These chapters are followed by Chapter VIII which contains a synthesis of the results.
- Chapter IX is dedicated to the general discussion of the findings. In this chapter we discuss limitations, key findings, implications, and contributions.

#### Conclusions and recommendations

- Chapter X contains suggestions for future research. This chapter highlights proceedings based on new findings and areas of this research that need more elaborate research.
- Chapter XI contains the concluding remarks

#### Referencing and appendices

- Chapter XII is used to compile co-authored work, and the bibliography and references used throughout this thesis.
- Chapter XIII contains all appendices. These appendices include outsourced work, additional data, and partially finished work.

## 4. Scientific and Industrial significance

The results of this study are deemed highly relevant for and contribute to academia and industry.

Particularly in the early part of the 20<sup>th</sup> century several published articles and book chapters were dedicated to outline the palaeoceanographic and economic significance of contourite deposits. Examples of these works are; *“Economic and Palaeoceanographic Significance of Contourite Deposits”* edited by Viana and Rebesco (2007), *“Palaeoceanographic significance of contourite drifts”* by Knutz (2008), *“Identification of ancient contourites: problems and paeoceanographic significance”* by Huneke and Stow (2008), and *“Contourites: Physical oceanography, process sedimentology, and petroleum geology”* by Shanmugam (2017b).

Contourite deposits contain substantial information on ocean circulation and past climate change as the bottom currents that form these deposits are generated by a variety of oceanographic processes. These processes involve tidal forces, wind-driven transport, upwelling/downwelling and/or interhemispheric water-mass exchange (Knutz, 2008). Each of these processes are variable over different timescales and often relate to changes in global climate. These changes are likely captured as signatures in the contourite sedimentary record. Furthermore, particularly gateways that generate bottom currents, bring about changes in ocean circulation, affecting global climate. One of the best studied examples of a gateway that generates a contourite systems is the Strait of Gibraltar (SoG) and its associated Gulf of Cadiz Contourite Depositional System (GoCCDS). In the SoG, the generated present-day Mediterranean Outflow Water (MOW) is said to contribute to the Atlantic Meridional Overturning Circulation (AMOC) by as much as 15%, increasing the North Atlantic surface temperature by 1°C (Rogerson *et al.*, 2012). From this, it can also be inferred that changes in the MOW, captured in the geological record, contain significant information of global climate change. Despite a significant amount of data having been and being collected from the contourite system in the Gulf of Cadiz, it being situated far below sea-level, limits the acquired data to seismic reflection, bathymetric and core data (*e.g. Brackenridge, 2014*). Although much information can be obtained from this data, it is of relatively low resolution, except for the cores. Studies of *e.g. de Castro et al. (2020a, b)* however, mentioned that the sand-rich intervals in the acquired cores were not fully recovered due to them being unconsolidated. As such, the recovered data is incomplete for the entire range of contourite facies in the GoCCDS. Furthermore, small scale lateral facies variability cannot be deduced

from the datasets acquired. To overcome these limitations, I studied sandy contourite deposits from the late Miocene Rifian Corridor in Morocco. Our study enabled a very detailed description of 3-dimensional contourite features from which I was able to unravel a significant amount of information related to variability in the paleo-MOW and the effects on and produced by climate change. This study also allowed the description of contourite facies and the construction of facies models which enable the recognition of ancient sandy contourite deposits in outcrop.

The economic or industrial significance of contourites has increased considerably over the past decades with the advance of hydrocarbon exploration towards deeper waters and technological advances in deep-water observations, however, their economic potential are (in 2008) only in the primeval reconnaissance stages (*Viana, 2008*). Contourite deposits have seal (*e.g. Viana et al., 2007*), source (*e.g. Viana, 2008*), and reservoir potential (*e.g. Bulhoes et al., 2012; Mutti et al., 2014*) depending on the depositional characteristic of bottom currents. A contourite depositional system (CDS) is composed of a combination of depositional and erosional elements (*Hernández-Molina et al., 2008*). These elements are related to spatial and temporal changes in the bottom-current regime. The depositional elements, generally consisting of fine-grained sediment are related to slow convection and vertical settling under low-current velocities. These generally fine-grained deposits are often considered as potential seals (and source) in hydrocarbon exploration. The erosional elements, or sand-rich elements, of contourite depositional systems are more confined to the core of the bottom current, related to traction and saltation of sediment particles under higher current velocities. These coarser-grained deposits are generally considered as potential hydrocarbon reservoirs. The diversity in hydrodynamic behaviour within contourite depositional systems however creates a variety of facies within that system that have different petrophysical characteristics. To appraise potential hydrocarbon systems, a good understanding of the processes and products of contourite features is vital. Any advances, particular on contourite facies models, in contourite research is crucial for the predictability and economic viability of contourite deposits. In this thesis, by studying sandy contourites, we particularly contribute to the understanding of contourite deposits with reservoir potential.

# *Chapter II*

## **Background information**

This chapter is used to provide the reader with a solid background on the study location, its geological information, the paleogeographic and palaeoceanographic setting, and deep-sea sedimentary processes. This chapter furthermore comprises a literature study of results preceding the findings of this research project.

*Part I*

*Study area and geology*

# 1. Study location

This research project was initially supposed to be conducted on different outcrops with varying contourite elements in different countries. Since field examples of contourites are scarce and I did not have the opportunity yet to visit other outcrops (e.g. Angola and Colombia), this research project is restricted to northern Morocco (Fig. 2.1). Despite this limitation, due to the short duration of the project and the complexity of the outcrops in northern Morocco, sufficient data was acquired, and new outcrops were discovered for this study.

The following paragraphs summarize the regional and local geological framework of the Late Miocene Rifian Corridor. This regional geological framework is required to better understand the significance of the Rifian Corridor in accommodating Atlantic – Mediterranean water exchange whereas the regional geological framework is used to better understand the evolution of the Rifian Corridor itself.

## 1.1 Morocco

*- The following text is copied from Michard, et al. (2008) as it perfectly summarizes Morocco from a geological perspective -*

Morocco is one of the most fascinating lands in the world for studying geology. It is a friendly country, provided with a good network of roads. Most of Morocco being situated within the Mediterranean to Sub-Saharan climatic ones, with a mean annual precipitation ranging from 300 to 600 mm, it offers wide landscapes, with sub-surface rocks exposed in splendid outcrops. Last but not least, Morocco is located at a triple junction (Fig. 2.2) between a continent (Africa), an ocean (the Atlantic) and an active plate collision zone (the Alpine belt system). This results in a rugged topography with a wide range of outcropping terranes spanning from Archean to Cenozoic in age, as well as diverse tectonic systems from sedimentary basins to metamorphic fold belts. Minerals and fossils from Morocco are curated in museums the world over. Finally, it is worth emphasizing that the natural resources extracted from the Moroccan subsoil are important for the national economy (phosphate, Ag, Pb, Zn, barite, fluorspar, etc.). At the moment, there is also active offshore exploration for oil and gas.



## 1.2 Study area

The study area of this research project, located in northern Morocco, is roughly framed by the cities of Sidi Kacem (NW), Meknes (SW) and, Taza (E) (Figs. 2.1 and 2.2). The second largest city of Morocco, Fes, is found in the middle of the study area. This city formed the home base during several field campaigns.

The study area is in the triple-junction of three of the Major Geological domains of Morocco (Fig. 2.2), the Middle Atlas (MA) in the east, the Central Massive, or Meseta (M) in the west and the Rif towards the north. The main outcrops studied are related to late Miocene deposits in the Saiss-, Gharb- and wedge top Basins just north of Fes.

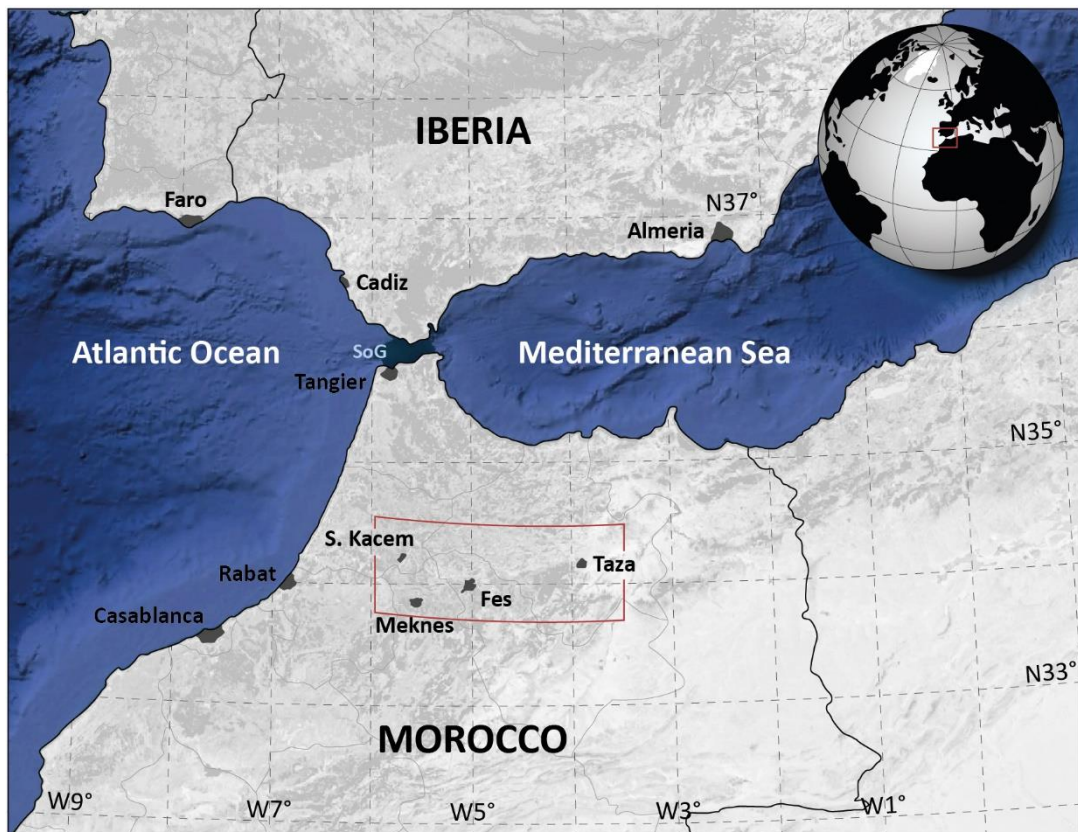


*Figure 2.1.* Location of Morocco, with in red, the study area. The Strait of Gibraltar (SoG) connects the Atlantic Ocean and the Mediterranean Sea. Modified from Google Earth.

## 2. Geological Background of the western Mediterranean

### 2.1 Geology of the western Mediterranean

The geological evolution of the western Mediterranean region exhibits a complex evolution of subduction initiation – “the initiation of western Mediterranean subduction varies from as old as ~120 Ma and ~80 Ma to as young as ~35 Ma (Hinsbergen et al., 2014)” - slab fragmentation and rollback, with an associated intense crustal deformation evolution within a context of slow Africa-Iberia and Africa-Europe convergence (e.g. Vissers and Meijer, 2012b). The western Mediterranean region is part of a convergent plate margin separating Africa and Europe and overlies a structurally complex mantle with remnants of subducted lithosphere (e.g. Spakman & Wortel, 2004; Bezada et al., 2013). This margin consists of marine basins which formed as back-arc basins since the Oligocene. Widespread extension associated with the formation of these basins led to considerable thinning of the continental crust (e.g., in the Alboran Sea) or the local initiation of sea floor spreading (e.g. in the southern Tyrrhenian and Provençal Basin) coeval with orogenesis in the adjacent mountain chains of the Rif-Betic cordillera (Rosenbaum et al. 2002).

### 2.2 Rif-Betic Cordillera

The arc shaped orogenic belt surrounding the Alboran Sea in the westernmost Mediterranean is formed by the Betic in southern Spain and the Rif in northern Morocco (Figs. 2.2 and 2.3). The Rif-Betic (fold-and thrust orogenic arc) forms the western most boundary of the larger-scale Alpine orogen that developed coeval to the opening of the western Mediterranean in the early Oligocene (e.g. Bidegaray-Batista & Arnedo, 2011). The Rif-Betic arc shows five major tectonic domains that together form the internal to external zones (Fig. 2.3).

The Internal Zone or the Alboran domain, comprises; (1) the Alboran back-arc basin and (2) the HP/LT metamorphic complexes which consists of allochthonous Paleozoic to Early Miocene rocks. These rocks were thrust on top of the External Zone during the Miocene (Crespo-Blanc & Campos, 2001). The External Zone consists of Mesozoic to Tertiary rocks

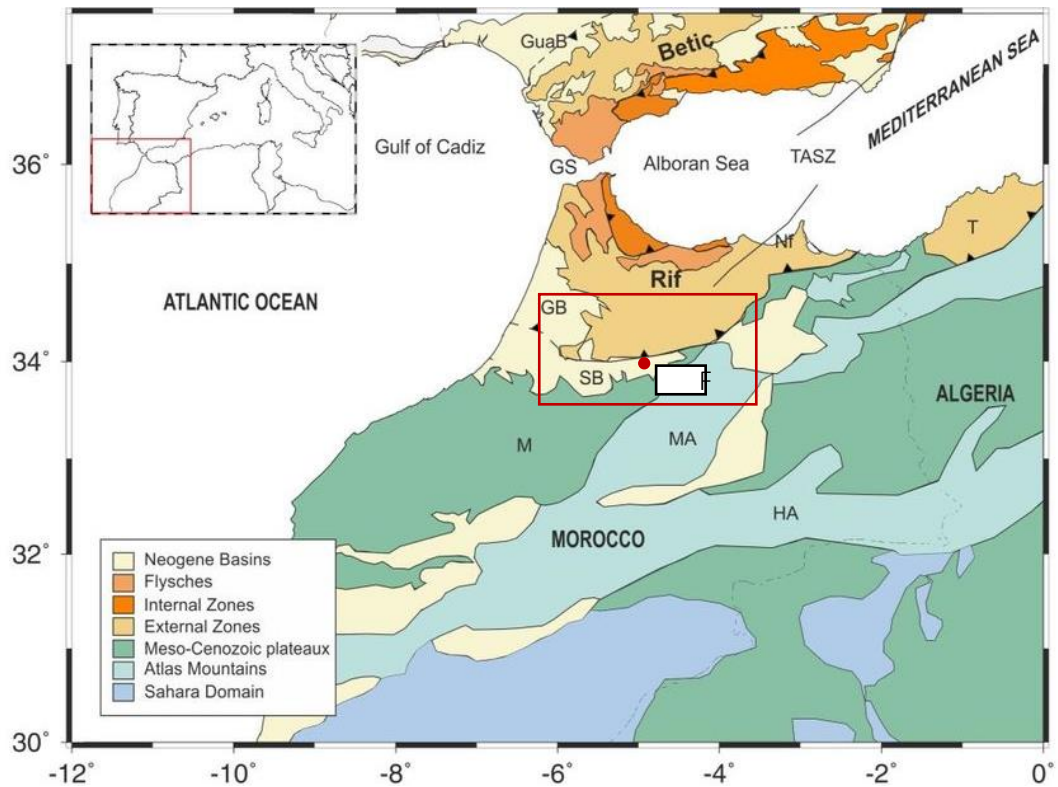


**Figure 2.2.** Simplified geological map of southern Iberia and northern Morocco with the major tectonic domains and boundaries. (GB) Gharb Basin, (GuaB) Guadalquivir Basin, (GS) Gibraltar Strait, (HA) High Atlas, (M) Meseta, (MA) Middle Atlas, (Nf) Nekor fault, (SB) Saiss Basin, (TASZ) Trans-Alboran Shear Zone. The red box indicates the location of the study area (from Gil de la Iglesia, 2015).

which represent the passive margin of Africa and Iberia deforming during Alpine orogeny. The external zone comprises deep marine clastic successions belonging to: (3) the Flysch units around the western side of the thrust belt, the (4) External Betics (separated in Pre- and Sub-Betic) and the External Rif, and (5) the Guadalquivir and Gharb foreland basins and their corresponding continuation into the Gulf of Cadiz (Martínez-García et al., 2011; Platt et al., 2003; Vergés & Fernández, 2012).

The earliest extension in the Rif-Betic zone was associated to rapid isothermal exhumation of high-pressure rocks in the Late Oligocene to Early Miocene (27 - 18 Ma) (Monie et al., 1994; Platt et al., 1998). Since the sea-floor of the Alboran Sea consists of rocks similar to those found in the Rif-Betic cordillera that are covered by Early Miocene syn-rift deposits and post-rift marine sediments, Rosenbaum et al. (2002) state that the region was subjected to widespread extension during the Middle Miocene which has led to the formation of this sea. Coeval with the extension of the Alboran Sea, thin-skinned thrusting and folding took place in the External Zones of the Rif-Betic cordillera (Platt & Vissers, 1989; Platzman et al., 2002; Crespo-Blanc & Campos, 2001) which was accompanied

by a considerable amount of block rotations around vertical axes causing clockwise rotation in the Rif and counterclockwise rotations in the Betic (*Allerton et al., 1993; Platzman et al., 2000; Lonergan & White, 1997*).

### *2.2.1 The Internal Zones*

The Internal Betics are formed by three main tectono-metamorphic complexes that are tectonically stacked, from bottom to top, the Nevado-Filabride, the Alpujarride and the Malaguide (Fig. 3). The contacts between different units within the Nevado-Filabride Complex are gently dipping ductile shear zones with westward sense of shear (*Martínez-Martínez et al., 2002*). The Alpujarride Complex, composed of Paleozoic to middle-upper Triassic rocks, shows severe differences in the metamorphic gradient across the contacts between units which crop out extensively in both the Betic-Rif fold belt and the Alboran basin. The Malaguide unit is made up of low-grade metamorphic Paleozoic basement and a Permo-Triassic sedimentary cover. This cover, in turn, is followed by a kilometer-thick discontinuous Jurassic to lower Miocene sedimentary succession with no signs of metamorphism (*Martín-Martín et al., 1997*). This unit was intruded by Oligocene and lower Miocene volcanism (*Turner et al., 1999*).

### *2.2.2 The External Zones*

The External Betics are mostly formed by the more proximal and shallower Prebetic and the deeper Subbetic domain. These domains were attained during the Jurassic opening of the Ligurian-Tethys corridor (*e.g., Gibbons & Moreno, 2002; Vera, 2004; Vilas et al., 2003*). The Prebetic domain was located along the south-eastern margin of the Iberian plate and underwent a second period of rifting during the Early Cretaceous. Rifting gave rise to SSE-dipping low-angle faults and the formation of half grabens (*Vilas et al., 2003*). The Subbetic domain was located further to the SSE above thinner crustal regions which comprised submarine Jurassic and Early Cretaceous volcanic and subvolcanic mafic rocks (*Vera et al., 1997*). Underneath the Jurassic rocks, upper Triassic evaporites constitute the present detachment level of the Rif-Betic fold-and-thrust system. The Late Cretaceous to Tertiary sedimentary successions displays the progressive evolution from passive to active margin at the onset of Africa convergence ~ 85 Ma (*Vera, 2000; van Hinsbergen et al., 2014*).

### 2.2.3 The Gibraltar Flysch units

The Gibraltar Flysch units are formed by siliciclastic rocks ranging from upper Jurassic to early-late Burdigalian age and are presently deformed as an accretionary prism, tectonically sandwiched above the External Subbetic fold-and-thrust system and below the high-pressure metamorphic rocks of the Internal Betics (*e.g., de Capoa et al., 2007; Luján et al., 2006; Bonardi et al., 2003; Crespo-Blanc and Campos, 2001*). The siliciclastic turbidites of the Flysch units (Mauretanian) were supplied by the stacked Internal Units of the Betic-Rif system since the earliest Miocene and up to the Late Burdigalian (*de Capoa et al., 2007*).

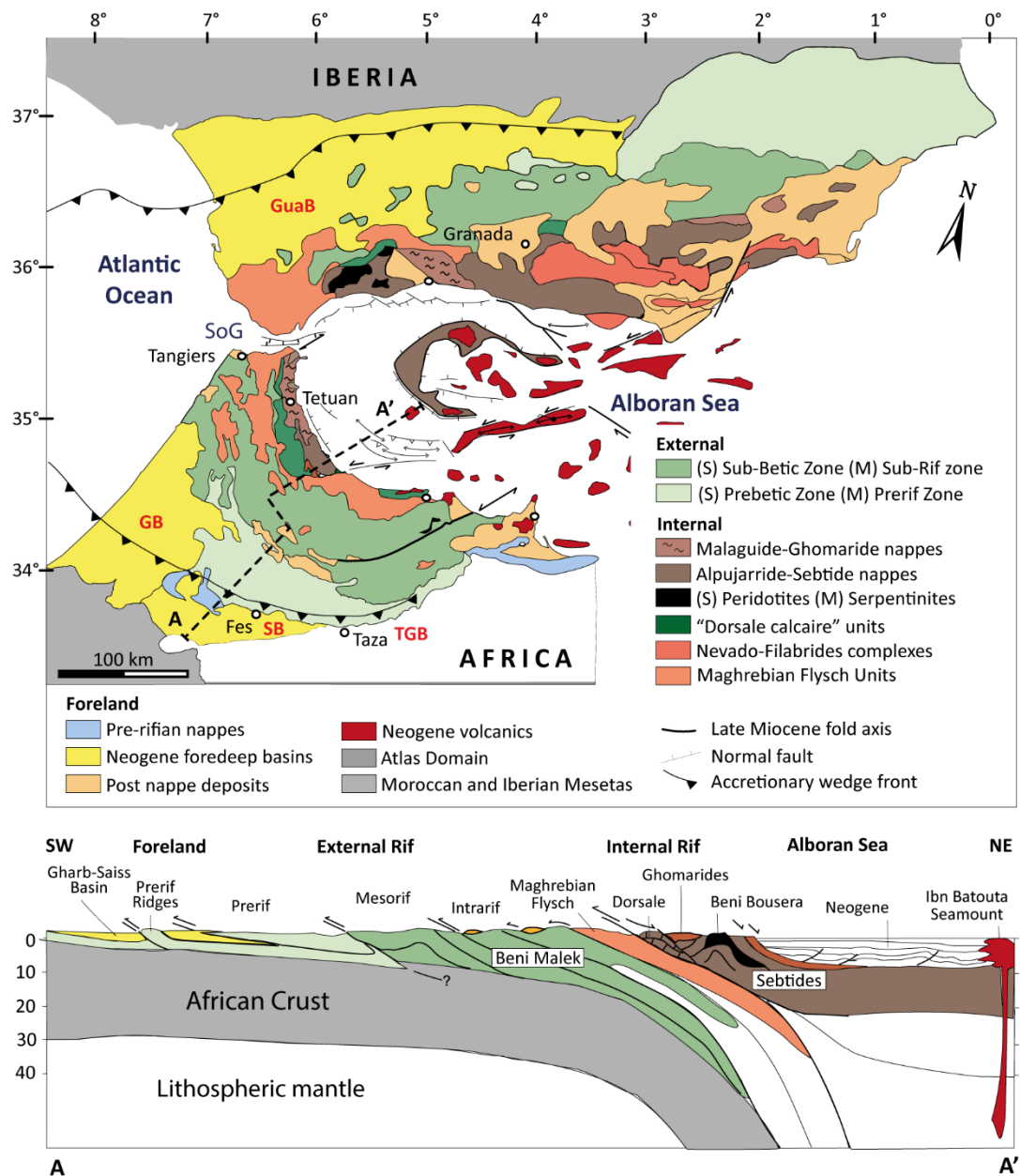


Figure 2.3. Structural map of southern Spain (S) and northern Morocco (M). Modified after Michard et al. 2002.

#### 2.2.4 The Gulf of Cadiz: Imbricate wedge

The Gulf of Cadiz Imbricate-, or Accretionary-Wedge, also known as the Allochthonous unit (*Medialdea et al., 2004*) or Olistostromes (*Maldonado et al., 1999*), is a thick, tongue-shaped tectonic unit that occupies a large area of the Atlantic, Moroccan and Iberia margins. This wedge, which is largely continuous with the external thrust belt, is defined as an active wedge above a narrow, east-dipping, subducting oceanic slab (*Gutscher et al., 2002*). The imbricate wedge was emplaced in the Tortonian (up till ~ 8 Ma) because of westward overthrusting by the Betic-Rif belt on the east Atlantic margins (*Medialdea et al., 2004*).

#### 2.2.5 The Alboran Basin

The Alboran basin is a back-arc basin occupying the inner side of the Betic-Rif system and formed mainly during the early Miocene (*e.g. Martínez-García et al., 2011*). The Western Alboran basin formed around 27-25 Ma and is floored by the Alpujarride metamorphic basement units that were affected by high grade metamorphic conditions before the late Oligocene to earliest Miocene (*Soto and Platt, 1999*). The eastern Alboran basin appears to be younger than the western Alboran basin, having formed at 12-10 Ma (*Booth-Rea et al., 2007*). The extensional evolution was accompanied by broad magmatism and several volcanic episodes (*Lustrino et al., 2011*). This extensional evolution was followed by compressional reorganization since the late Miocene to Holocene (*Chalouan et al., 1997*). The tectonic processes occurring in the basin during the Pliocene and Quaternary are, to a large degree, responsible for the present seafloor physiography of the basin (*Martínez-García et al., 2011*).

### 2.3 Kinematics of the Betic-Rif orogenic system

A cross-section through the central Rif (Fig. 2.3) by *Michard et al. (2002)* shows the structural relationships between different tectonic units with large but unconstrained thrust displacements. From the foreland to the hinterland, the Gharb basin is overthrust by the External Rif units; the Rides prerifaines, the Prerif and the Mesorif, which in turn are overthrust by the Intrarif units. These Internal Rif units consist, from top to bottom, by the less-metamorphic Ghomaride units (Malaguide in the Betics) and by the HP/LT metamorphic Sebtide units (Alpujarride in the Betics). The Sebtide units include the tectonic slivers of Beni Bousera periodites (Ronda peridotites in the Betics) which override all the previous Rif cover thrust sheets, each one corresponding to separated paleogeographic domains. A typical



foreland-ward propagation thrusting would imply a large-scale progressively younger age for the emplacement of the thrust sheets from the Internal Rif units to the External Rif units and its foreland.

The Internal Betics were thrust over the External Betics by early Oligocene times and thus right before the onset of the Alboran extension (*Martín-Algarra et al., 2000; Serra-Kiel et al., 1996*). The Fossilization of the Guadalquivir Allochthon during the latest Tortonian constrains the late major thrust displacement in the Guadalquivir foreland basin (*Verges & Fernandez, 2012*).

The shortening estimations for the External Betics vary from 64 to 85 km (*García-Hernández et al., 1980*), 100 km (*Banks & Warburton, 1991*) or  $96 \pm 67$  km once corrected for the true shortening direction along the Jaén cross-section proposed by *Platt et al. (2003)*. Thrusting and folding in the External Betics occurred along the main contractional detachment surface of the upper Triassic evaporitic level (Keuper). The Triassic evaporites were also reactivated into diapiric structures during the Tertiary (e.g. *Crespo-Blanc, 2007; Luján et al., 2003*). At the larger scale the upper Triassic evaporites represent the decoupling horizon separating the stratigraphy of the External and Internal units in both the Betic and the southern Rif segments, as already formulated by *Wildi (1983)* and more recently supported by *Chalouan et al. (2008)*.

### 3. Geology of the study area

The Geology of the study area (Figs. 2.4) comprises the Rides Prérifaines (*Daguin 1927*) or Prerifian Ridges (PR) of Morocco (**541 – 145 Ma**) which form the leading edge of the Rif chain. Works of (*Zizi 1996, 2002; Frizone de Lamotte et al. 2004*) show that a deep, flat structure of almost peneplained Palaeozoic substratum is positioned beneath a Triassic-Palaeocene succession (Fig. 2.5). In Early Mesozoic NE-SW-trending basins were formed by rifting, creating accommodation space for a Triassic syn-rift fluvial succession (continental Triassic redbeds), overlain by 500 - 1,000 m of anhydritic and halitic evaporites interbedded with basalts and dolomites of Triassic-Hettangian age (*Sani et. al., 2007*). Rifting continued during Pliensbachian to Bajocian resulting in the deposition of a shallow to deep marine syn-rift sequence. This rifting stage terminated in the Middle-Late Jurassic (*Sani et. al., 2007*).

The base of a thin middle to upper Cretaceous sequence (**100 - 56 Ma**), which is only exposed in the Dahar N'sour area, located approximately 18 km north to north-east of Meknes, (*Sani et al., 2007 and references therein*) is separated from Middle-Late Jurassic deposits by a significant hiatus (Fig. 2.5). *Faugeres, 1978* and *Zizi 1996* indicated that the Cretaceous and Paleocene sequence may represent a gulf (with limestones and marls), whilst other parts of the present Prerifian Ridges emerged (*Sani et al., 2007*).

Paleocene marls and marly limestones form the base of a thin unconformable sequence of Middle Miocene to Late Pliocene foredeep deposits (**56 – 5.33 Ma**). Wedged within this foredeep succession, which mainly consists of Beni Ammar White Marls ( $\pm 14 - 11$  Ma) that

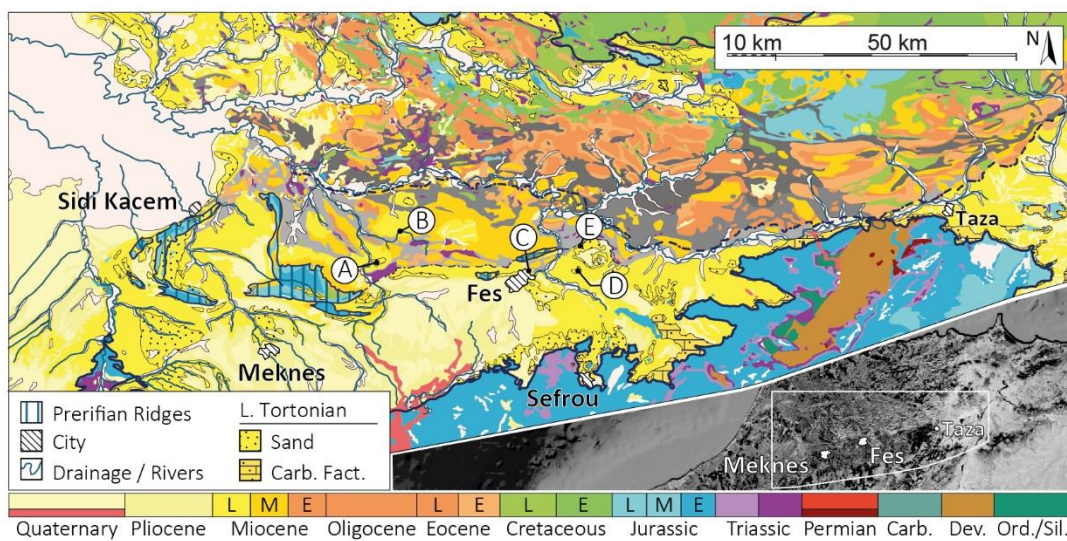


**Figure 2.4.** Regional Geological map of the study area (modified after *Saadi, et al., 1980*). The grey-scale image represents a satellite image with a projection of the geological map. The location of the main sections are indicated by: A) Sidi Chahed, B) Kirmta, C) Fes-north, D) El Adergha and, E) Ain Kansera.



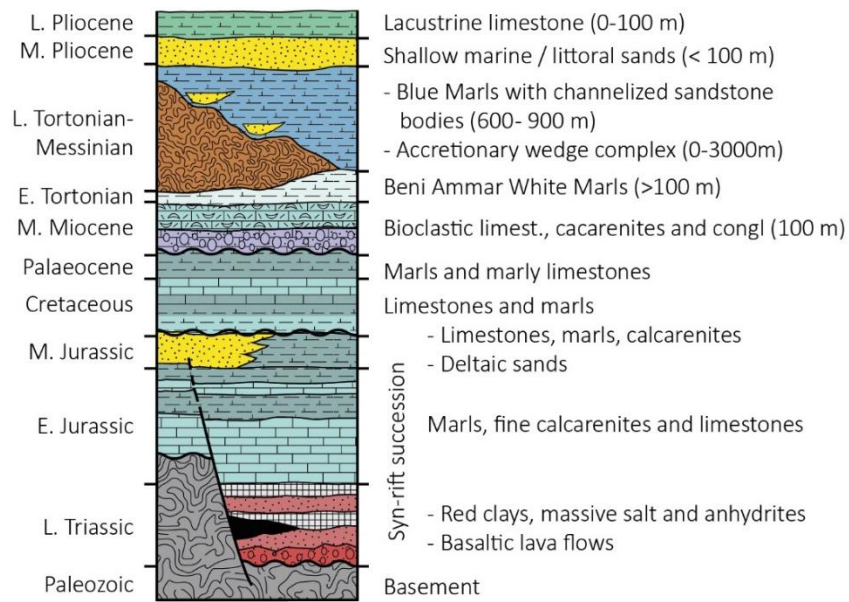


**Figure 2.5.** Composite stratigraphic- column of the Mesozoic and Tertiary rocks of the Saiss Basin. The sedimentary succession primarily studied falls within the Late Tortonian Blue Marls. Modified from Sani et al. (2007). (Note: not to scale)

were deposited when the Mediterranean area was still connected to the Indian Ocean in the west (Fig. 2.6), and the Blue Marl Formation ( $\pm 11 - 7$  Ma) (Sani et al., 2007), is the accretionary complex of the pre-Riffian nappe (thin-skinned deformation) (Figs. 2.4 and 2.5). The accretionary complex consists of a mélangé of different lithologies, mainly composed of limestones, sandstones and evaporates mixed with soft sediments, which are remnants of the foredeep succession. The thin-skinned emplacement of the Preriffian nappe allows for a division of pre-nappe foredeep succession (Beni Ammar White Marls) and a post-nappe foredeep succession (Blue Marl Formation). The blue marls consist of fine sediments with a majority of silt, containing some in-situ bivalves and echinoderms and show alternations of clay with a dominant very fine silt content to dominantly clay with medium-silt content. The Blue Marl Formation comprises sedimentological evidence of contourite processes and hence is the formation on which this thesis is primarily focussed. Above the blue marl member an approximately 100 m thick sand rich succession is deposited with locally unconformable deposits of littoral sands.

The pre-Riffian nappe emplacement within the foredeep is dated from the latest Tortonian-Messinian in the area of the Saiss basin to Pliocene in the Gharb basin (Sani et al., 2007). During Late Miocene, the Saiss basin acted as a subsiding marine basin whereas in Late Pliocene and Quaternary this basin consisted of a lacustrine environment (Taltasse, 1953; Feinberg, 1986). During the Pliocene, the Gharb Basin underwent rapid subsidence and was simultaneously exposed to thrusting by the Pre-Riffian thrust sheet (Feinberg, 1986;

*Flinch, 1994, Litto et al., 2001*). The northern edge of the Saïss Basin however, was subjected to significant compressive deformation and thrusting of the External Rif and Pre-Riffian ridges (*Bargach et al., 2004*).

During the Late Pliocene (**5.33 – 0 Ma**), the shallow marine and littoral sands that are exposed in the Dahar N'Sour area were overlain by lacustrine limestones in the Saïss Basin. *Taltasse (1953)* precisely evaluated the extension of this lacustrine environment, which is one of the most prominent features in the Saïss Basin and has a varying thickness from 10 up to 100 m. At the same time during Late Pliocene, a marine environment dominated to the west and north-west of the Gharb basin. The recent evolution of the area is exhibited by the Pliocene and Quaternary infill, affected by compressional and extensional deformation.

The current morphology of the Prerifian Ridges is the consequence of thick-skinned compressive tectonics with an anticlockwise rotation trend (*Sani et al., 2007*). The major Prerifian Ridges coincide with southwest verging thrust faults that are rooted in the basement, but also affect the Neogene foredeep sediments. Major faults strike NE-SW to N-S and mainly SW-SE to E-W (*Sani et al., 2007*). Frontal ramps of the Prerifian Ridges are roughly oriented WNW-ESE, whereas lateral ramps are oriented NE-SW, mainly parallel to the normal faults related to Mesozoic rifting. The Prerifian Ridges arcuate geometry in map view is strictly tied to the trends of the graben systems inherited since Late Triassic-Jurassic opening of the central Atlantic Ocean (*Faugeres 1978; Sani et. al., 2007*).

## 4. Late Miocene Paleogeographic and Palaeoceanographic setting

### 4.1 Introduction

The studied outcrops of the Late Miocene Rifian Corridor play an important role in the evolution of events that led up to the desiccation of the Mediterranean Sea in the Messinian, the Messinian Salinity Crisis (MSC). To better understand the role and the importance of this particular corridor, mainly its geological and hydrodynamic evolution, this paragraph summarizes the evolution of the Rifian Corridor within a regional geological context from the Jurassic inception of the Tethys Ocean to the MSC.

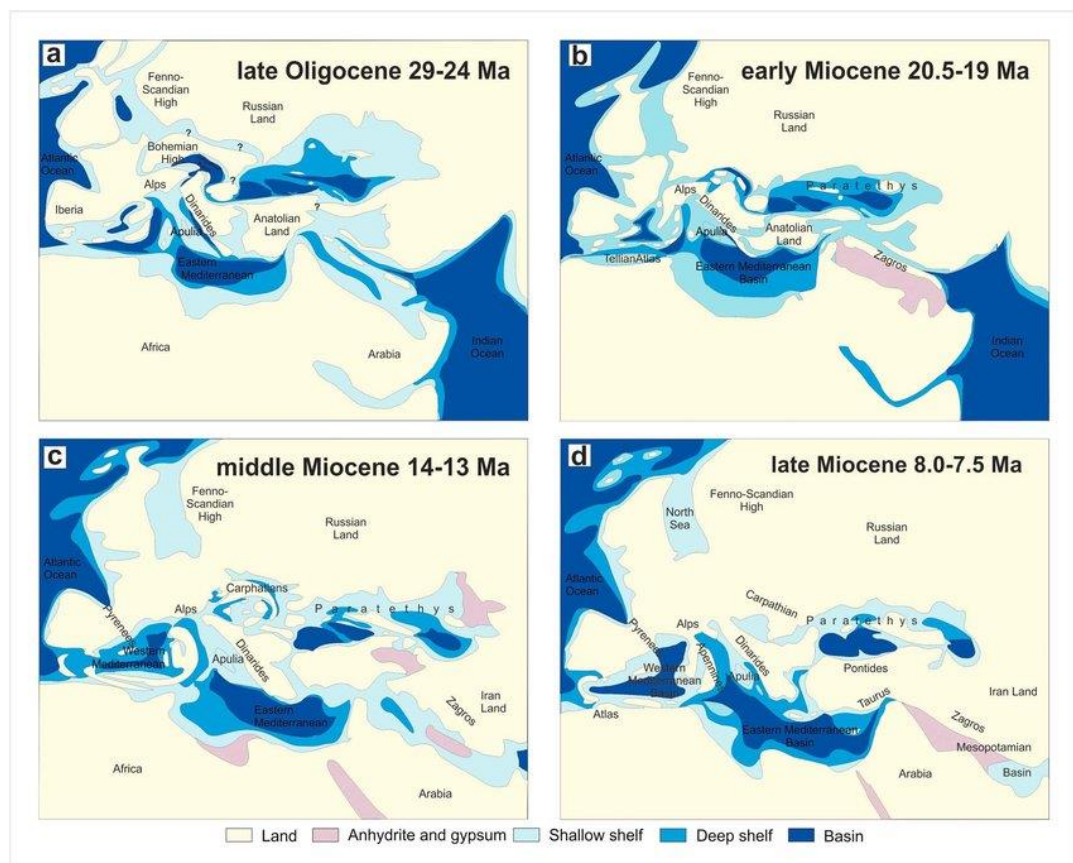


**Figure 2.6.** Simplified paleogeographic maps of the Mediterranean area. (a) Schematic paleogeographic map of the Mediterranean area during Chattian. (b) Schematic paleogeographic map of the Mediterranean area during Burdigalian. (c) Schematic paleogeographic map of the Mediterranean area during Serravallian. (d) Schematic paleogeographic map of the Mediterranean area during Tortonian. Derived from Cornacchia, et al., 2018.

Since the Jurassic inception of the Tethys Ocean, the western arm of the Atlantic-Tethys connection was located in the corridor region of Gibraltar between Morocco and Spain (Fig. 2.6; Flecker et al., 2015). From the Cretaceous to Middle Miocene, as part of the Ligurian-Maghrebian Ocean, an earlier and supposedly wider Mediterranean-Atlantic seaway existed (Do Couto et al., 2016; Jolivet et al., 2006). Its sedimentary remnants were incorporated in the Rif thrust-systems (Chalouan et al., 2008; Morley, 1988; Morley, 1992) during the orogenic phase that ceased in the late Tortonian creating the Betic-Rif arc (Crespo-Blanc et al., 2016; Do Couto et al., 2016; Jolivet et al., 2006; Hinsbergen et al., 2014; Verges and Fernandez, 2012). Up till the Middle-Late Miocene (14 - 11 Ma) the Mediterranean remained connected to the Indian Ocean (Hüsing et al., 2009). Closure of this eastern gateway fundamentally changed global ocean circulation by shutting off the circum-equatorial current (Bryden and Kinder, 1991; Reid, 1979) and drastically changed salinity and temperature in both the Mediterranean and the Para-Tethys (Karami et al., 2011). During the late Tortonian (~11.6 to 7.2 Ma), several gateways through southern Spain, northern Morocco and potentially Gibraltar connected the Mediterranean Sea with the Atlantic Ocean (Fig. 2.7, Capella et al., 2017a, 2018; Flecker et al., 2015). This complex network of gateway channels is obtained from the distribution of Late Miocene marine sediments that have been uplifted (~ 1 km) by compressional reorganization since the late Tortonian to Holocene. This compressional regime provided high enough uplift rates to close the Corridors (e.g. Chalouan et al., 1997; Capella et al., 2017). It however remains unclear how much of the bifurcating channel patterns reflects the primary configuration of the Late Miocene marine corridors and how much is a function of the preservation of the sediments after uplift and erosion (Flecker et al., 2015).

## 4.2 Evolution of the Late Miocene western Mediterranean seaways

As mentioned before, during the late Miocene, after closure of the Mediterranean connection of the Indian Ocean (14 - 11 Ma) (Hüsing et al., 2009), the Atlantic-Mediterranean connection comprised a complex network of gateway channels in the Gibraltar, southern Spain and northern Moroccan regions (Fig. 2.7). Gradual closure and/or partial restriction of these corridors marked the onset of the MSC. The Betic Corridor comprises the Guadalquivir Basin in southern Spain and its four main gateways connecting it to the Mediterranean Sea. The Spanish gateways (Betic Corridors) include; from east to west, 1) the North Betic Strait – including the Fortuna Basin, 2) the Guadix Basin, 3) the

Granada basin – including the Zagro Strait, and 4) the Guadalhorce Corridor. The Rifian Corridor, although still being discussed (see previous chapter, *e.g. Capella et al., 2018*), might have comprised two main corridors connecting the Mediterranean to the Gharb basin and eventually, the Atlantic Ocean. These corridors were the North-, and South- Rifian Corridor of which the latter is in the study area.

#### 4.2.1 Evolution of the Rifian Corridor

The pioneering paleogeographic reconstruction of Feinberg (*Feinberg, 1986*) and Wernli (*Wernli, 1988*) are still widely used today. These authors identified a post-orogenic marine sedimentary cover that unconformably overlies the Rif thrust systems (Miocene post-nappe). This marine cover therefore indicates a marine passage where water flowed over a submerged orogenic foreland. The Rifian Corridor (Fig. 2.7) evolved during the latest stage of collision of the Betic-Rif arc (*Sensu, Crampton and Allen, 1995; Sinclair, 1997; Mutti et al., 2003*) ending with the last pulse of Miocene nappe- or accretionary wedge stacking during the middle-late Tortonian, at around 8 Ma (*Do Couto et al., 2016; Hinsbergen et al., 2014*).

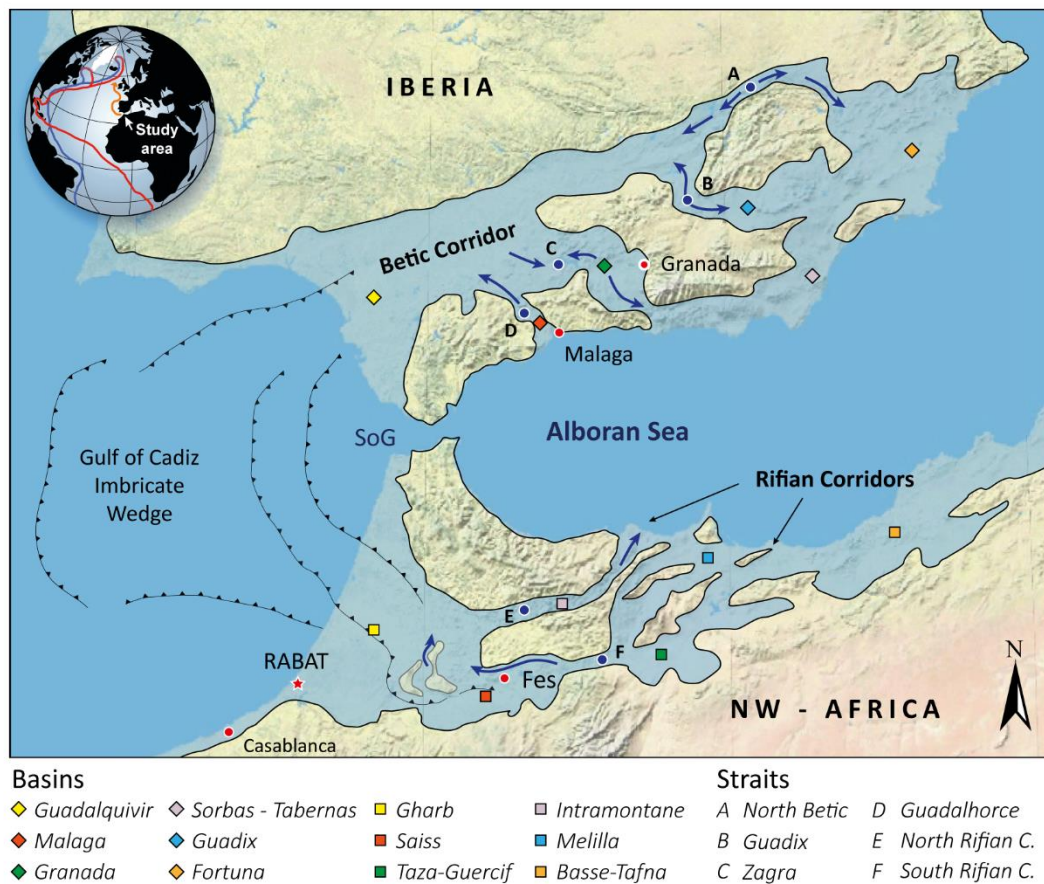


Figure 2.7. Tortonian reconstruction map of the western Mediterranean region.

This nappe-stacking took place in a submerged foreland which gradually shifted south to south-westward as a result of flexure caused by the Prerif Nappe emplacement, the frontal part of the orogenic wedge (*Capella et al., 2017b; Capella et al., 2018; Feinberg, 1986; Flinch, 1993; Gomez et al., 2000; Sani et al., 2007; Suter, 1980; Zouhri et al., 2002*).

The Rifian Corridor formed a gateway for Mediterranean-Atlantic water exchange. It was overlying the thrust-sheets composed of deep-marine sediments (Flysch and marls), at a time when they were already mostly emplaced (*Chalouan et al., 2008; Frizon de Lamotte, 1979; Feinberg, 1986; Wernli, 1988; Capella et al., 2017b*). The seaway was limited northwards by the earlier exhumed Rif orogenic wedge (*Iribarren et al., 2009*) and southwards by the Atlas Mountains (*Barbero et al., 2011*).

The main basins in which the Rifian Corridor, post 8 Ma sediments are preserved are the Saiss and Taza-Guercif basins to the south (Figs. 2.3 and 2.7), which were continuously connected forming the South Rifian Corridor (*Dayja et al., 2005; Krijgsman et al., 1999b*). Towards the north, the less connected Had Kourt, Taounate, Dhar Souk depocenters, which seem to connect to the Arbaa Taourit and Boudinar basins near the Mediterranean coast formed the northern strand of the Rifian corridor (*Achalhi et al., 2016; Tulbure et al., 2017*). The Gharb Basin was the western mouth of both strands of the Rifian Corridor and, following gateway closure, continued to record deposition as an Atlantic embayment (*e.g. Ivanovic et al., 2013; Wernli, 1988*).

The total thickness of post-orogenic cover reaches up to 2500 m, both in wedge-top and foredeep settings (*e.g., Flinch, 1994; Samara et al., 1997; Sani et al., 2007; Wernli, 1988*). This post-orogenic cover mostly consists of siliciclastic, marl-sandstone alternations called the “Blue Marls” or “Blue Marl Formation”. This clastic succession also includes, at limited locations, the products of carbonate factories. The location of these carbonate factories are the Gulf of Skoura, in the south-east part of the Saiss Basin, and the Melilla embayment, on the Mediterranean side of the corridor (*Saint-Martin and Cornee, 1996*). Between the Melilla embayment and the Taza-Guercif Basin, the products of coeval volcanic activity are mixed with the siliciclastic seaway deposits (*Wernli, 1988*).

Although the Rifian Corridor is commonly subdivided into a northern and a southern strand and two distinct Mediterranean-Atlantic connections are envisaged (*e.g., Achalhi et al., 2016; Flecker et al., 2015*), there are several patches of marine Blue Marl Formation that unconformably overlie the intervening accretionary wedge. These patches suggest a wider seaway that might have linked, at times, the southern and northern strands of the Rifian

Corridor (*Capella et al., 2017b*). Since the sedimentary thickness in the area of these patches is limited compared to for example the main depocenters, this might suggest the deposition on submarine highs or additional erosion due to subsequent uplift (*Capella et al., 2018*).

Based on the literature review paper by *Flecker et al. (2015)*, up till 2015, most recent work on the age refinement of the North Rifian corridor was carried out in the eighties by *Wernli (1988)*. *Wernli (1988)* found that all sediments were assigned to an undifferentiated Tortonian-Messinian marine zone that spans from 11.6 to 5.3 Ma. This, however, did not allow for more accurate age subdivisions. *Tulbure et al. (2017)* presented new calcareous plankton biostratigraphic data using an improved planktonic foraminiferal zone scheme that is based on an assemblage- (Developed by *Zachariasse, 1975* – elaborated by; *Langereis et al., 1984; Krijgsman et al., 1994, 1995, 1997, 1999b, 2002; and Hilgen et al. 1995*) rather than on a typology-based taxonomic concept (made and used by *Wernli, 1988*). Their results indicate an invariably late Tortonian age for the youngest open marine sediments throughout the basins that formed the northern strand of the Rifian Corridor (Fig. 2.7), and thus no marine sediments of Messinian age had been found. They furthermore state that high sediment rates have been observed shallowing in the top part of several North Rifian Corridor (NRC) succession that suggest that, although the marine connection through the NRC may have continued in the earliest Messinian, it was likely closed before  $\sim 7.1 - 6.9$  Ma [*Tulbure et al. 2017; Capella et al. 2017; Capella et al. 2018 (7.35 - 6.9 Ma)*], well before the onset of the Messinian Salinity Crisis. *Tulbure et al. (2017)* furthermore state that closure is likely related to a phase of enhanced and localised uplift in the Rif foreland.

*Krijgsman & Langereis (2000)* and *Krijgsman et al. (1999b)* dated a sedimentary continental to marine transition in the central southern Taza-Guercif Basin using astronomical tuning. Their results indicate closure of this part of the corridor to have occurred between 6.7 and 6.0 Ma. Their evidence however cannot preclude that there was a Mediterranean-Atlantic connection further north. *Ivanovich et al. (2013)* used Nd isotope data from the Taza-Guercif Basin which suggests that restriction took place towards the east, around 7.2 Ma. This restriction is said to have cut the connection to the Mediterranean whilst maintaining the connection between the Taza-Guercif Basin and the Atlantic.

*Capella et al. (2018, 2017)* obtained improved age-control derived from high-resolution biostratigraphy, paleoenvironmental indicators, sediment transport directions, and the analysis of published onshore subsurface (core and seismic datasets) and implied this to an integrated surface-subsurface paleogeographic reconstruction of the southern Rifian



Corridor. Their results indicate age constraints of 7.1 – 6.9 Ma for closure of the southern Rifian Corridor. They furthermore conclude that the Rifian Corridor was already closed in the early Messinian and hence did not contribute to the restriction events that resulted in the MSC.

Palaeomagnetic studies executed in the Taza-Guercif and Gharb basin by *Krijgsman and Garcés (2004)* demonstrated that no vertical axis rotations have occurred in these, and in the post-thrusting Melilla Basin since the Tortonian-Messinian. *Cifelli et al. (2008)* however, deduced anticlockwise rotations in upper Miocene thrust top sequences. Southward propagation of the thrust load appears to be a significant driver of closure of the Rifian corridors along with regional uplift attributed to slab dynamics (*Duggen et al., 2004*).

#### *4.2.2 Evolution of the Betic Corridors*

The most northerly corridor connecting the Guadalquivir Basin with the Mediterranean is the North Betic Strait (Fig. 2.7). This connection passes through the Fortuna and Lorca basins (Martin et al., 2009). Integrated stratigraphic studies by *Garces et al. (1998)* and *Krijgsman et al. (2000a, b)*, carried out in the Fortuna Basin at the eastern end of the North Betic Strait, indicate that sedimentation changed from marls to diatomites and evaporites during the Tortonian salinity crisis of the eastern Betics around 7.8 Ma (*Krijgsman et al., 2000a*). Deposition of continental deposits took place around 7.6 Ma suggesting that the North Betic Strait has not been the route that enabled Atlantic water to reach the Mediterranean during the MSC (*Krijgsman, 2000a*).

The relatively wide (12 – 15 km), open marine Guadix gateway (Fig. 2.7) might have permitted two-way flow in its early stages (*Flecker et al., 2015*). Upon becoming narrower, strong bottom currents flowed from the Mediterranean to the Atlantic, indicated by huge bioclastic sand and conglomerate dunes with internal cross-bedding (up to several meters) whereas Atlantic surface currents might have recharged the Mediterranean, flowing in the opposite direction (*Betzler et al., 2006*). Detailed timing of closure is still disputed. *Hüsing et al. (2010)* show that a major hiatus of at least 2 Myr exists between open marine sediments of ~7.85 Ma and continental deposits dated at 5.5 Ma. The presence of this unconformity means that the Guadix Basin corridor does not record the closure of the corridor, and hence might have accommodated water exchange during MSC Stages 1 and 2 (*Flecker et al. 2015*).

The Granada basin (Fig. 2.7) was connected to the Guadalquivir Basin and the Mediterranean via the Zagra strait (*Martin et al., 2014*). The restriction of the Granada Basin



has been dated by *Corbi et al. (2012)* who indicate a short phase of evaporite precipitation between 7.37 to 7.24 Ma. This phase is followed by poorly constrained continental sedimentation. This confirms the conclusions of *Dabrio et al. (1978)*, *Martin et al. (1984)* and *Braga et al. (1990)* that the Granada Basin cannot have been the route by which the Mediterranean received Atlantic water during any part of the Messinian.

Compared to the other Betic basins, the history of the Guadalhoce corridor (Fig. 2.7) is less well understood. The sedimentary record of the Guadalhoce corridor consists predominantly of siliciclastic, unidirectional crossbedded sets over 100 m in length and thicknesses ranging from 10 to 20 m (*Martin et al., 2001*). From these structures the depth is deducted to have been at least 60 – 120 m and subject to extremely fast flowing (1.0 – 1.5 ms<sup>-1</sup>) unidirectional bottom currents directed towards the northwest (*Martin et al., 2001*). Foraminifera assemblages of the bottom of a carbonate unit have obtained an early Messinian age (7.2 – 6.3 Ma; *Martin et al., 2001*). *Perez-Asensio et al. (2012)* interpreted a change in benthic  $\delta^{18}\text{O}$  in the Guadalquivir basin at 6.18 Ma as indicating closure of the Guadalhoce corridor. Since, however, no Messinian aged sediment is preserved or is yet to be found in the Guadalhoce corridor, this corridor might or might not have acted as a gateway throughout the MSC.

### 4.3 The Strait of Gibraltar

Although several authors previously described a possible gateway through the Strait of Gibraltar (Fig. 2.7) during the Mediterranean Salinity Crisis (MSC) (*e.g. Capella et al., 2017; Flecker et al., 2015; etc.*), *Krijgsman et al. (2018)* recently published a paper stating that the Gibraltar Corridor was the only remaining open seaway connecting the Atlantic and the Mediterranean during the MSC (Figs. 2.1 and 2.7). *Hsü et al. (1973a, b)* already realized that intermittent input of Atlantic water to the Mediterranean was necessary to explain the huge amount of halite in the deep basins of the Mediterranean. Until recently, since the Betic and Rifian Corridors appear to have been closed prior to the onset of the MSC, the exact location of the marine Messinian passageway remained elusive.

Although the main focus has been evolving around finding evidence for open gateway connections prior and during the MSC, there is also evidence for a distinct period at which Morocco and Spain were connected. This evidence is derived from the ability of mammal migration between Morocco and Spain, before 6.1 Ma (*Agustí et al., 2006; Benammi et al., 1996; Gilbert et al., 2013*).

## 4.4 Chronology of the Messinian Salinity Crisis

The oldest concepts of a “Messinian Salinity Crisis” date back to the works of *Selli* in the fifties (*Selli, 1954, 1960*). The Deep-Sea Drilling Project (DSDP) Leg 13 in the Mediterranean basins recovered km-thick evaporites that led to the initial picture of a deep-desiccated Mediterranean during the Messinian (*Hsü et al., 1973a, b*). *Krijgsman et al. (1999a)* defined the MSC as the interval of evaporite deposition and Lago Mare sedimentation in the Mediterranean before the Pliocene flooding 5.33 Ma (*Lourens et al. 1996*). The Mediterranean-wide extent of the Messinian evaporites was further established from seismic profiles, deep-sea cores and land-based sections (for a review, see *Roveri et al., 2014a*). The MSC is widely considered as one of the most dramatic events in oceanic change of the past 20 million years (e.g. *Hsü et al., 1973; Ryan et al., 1973; Hilgen et al., 1995*).

The pre-evaporitic phase of the MSC was characterized by marked palaeoceanographic changes culminating in the deposition of huge volumes of evaporites in shallow and deep/intermediate settings of the Mediterranean (*Gennari et al., 2018*). The most pronounced steps of this palaeoceanographic evolution (Fig. 2.8) occurred at 7.15, 6.7, 6.4 - 6.29 and 6.1 - 6.0 Ma (see *Kouwenhoven et al. 2006*, and references therein). According to *Krijgsman et al. (1999a, b)*, *Krijgsman & Langereis (2000)* and *Kouwenhoven et al. (2003, 2006)*, the first two steps (7.15 and 6.7 Ma) were related to the tectonic narrowing and/or closure of the Atlantic connections in the Rifian corridors that might have completely shut down the Mediterranean deep circulation. There, however, also seems to be a relation with the eccentricity cycles since the palaeoceanographic steps roughly follow 400 kyr cycles (*Blanc-Valleron et al., 2002; Kouwenhoven et al., 2006*). Moreover, *Krijgsman et al. (1999)* state that the sedimentary cycles of the pre-evaporites are dominantly controlled by precession-induced changes in circum-Mediterranean climate.

The palaeoceanographic step from 6.4 Ma shows abrupt fluctuation of the Plankton/Benthos ratios representing anoxic conditions during insolation maxima and strongly reduced planktonic layers during insolation minima (*Sierro et al., 2003*). The last step before the onset of the MSC at 5.971 Ma occurred between 6.1 and 6.0 Ma and certifies the final decrease of calcareous microfossils (*Manzi et al., 2007; Lozar et al., 2010; Manzi et al., 2013*) indicating intolerable living conditions.

*Krijgsman et al. (2018)* indicate that evidence has been accumulating over the last decades, proof that the Messinian sequences in the Mediterranean required regular sea-

level and at least one continuously open Atlantic connection to provide enough salts for repeated events of gypsum and halite deposition (*Krijgsman and Meijer, 2008; Stefano et al., 2010; Simon and Meijer, 2017*).

The onset of the first MSC Stage, Stage 1 (Fig. 2.8), resulted in the deposition of the Primary Lower Gypsum (PLG) between 5.97 and 5.6 Ma (*Roveri et al., 2014a*). During this stage the Mediterranean salinity was potentially above 130 gkg<sup>-1</sup> or roughly 130 ppt (*Krijgsman et al., 2018*), for comparison, the current Mediterranean has a very high salinity of 38 ppt. *Stefano et al. (2010)* and *Simon et al. (2017)* proved, by means of numerical modelling, that at least one gateway must have persisted for the Mediterranean-wide evolution of the PLG. Their findings are supported by *Topper et al. (2011)* who state that the chemical (strontium) composition can only be explained by an open connection.

The most extreme stage during the MSC is the 2<sup>nd</sup> stage (Fig. 2.8), during this stage, up to 6% of the global ocean salt was stored in the Mediterranean basin (*Ryan, 2009*). This up to 3 km thick deposit has been deposited in less than 50 – 60 kyr between 5.6 and 5.55 Ma.

The 3<sup>rd</sup> stage of the MSC (Fig. 2.8) contains the Upper Gypsum or Lago-mare stage, deposited between 5.55 and 5.33 Ma (*Roveri et al., 2014a*). An open Atlantic corridor has also been proved to have existed during this stage (*Stefano et al., 2010; Simon et al., 2017*).

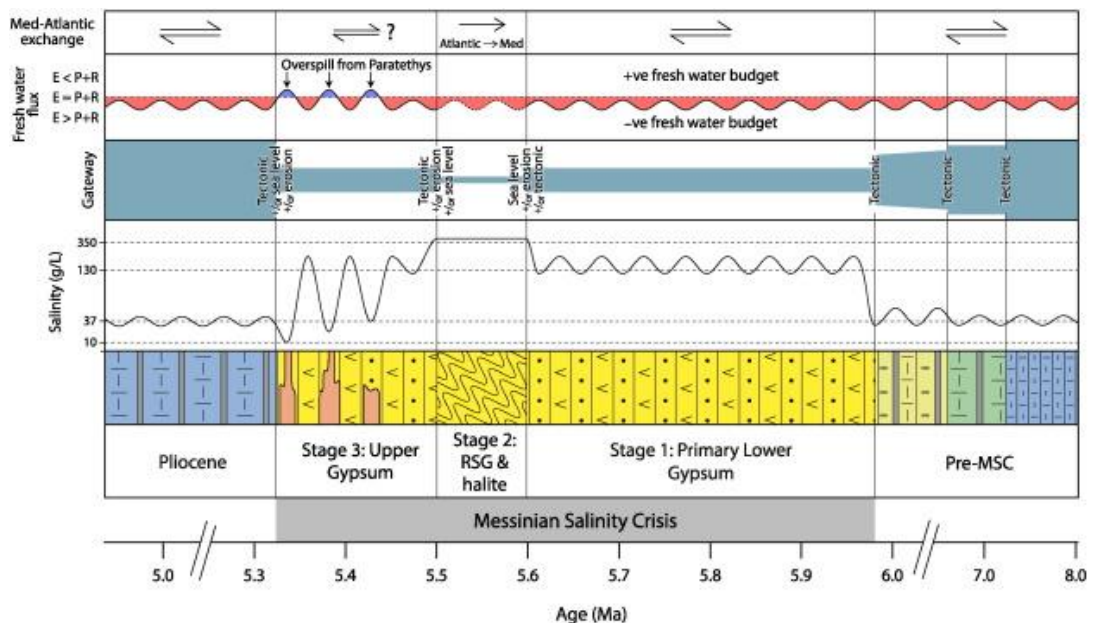


**Figure 2.8.** Summary figure from *Flecker et al. (2015)* illustrating the main features of the Mediterranean's exchange history in the Late Miocene-Pliocene including lithology, Mediterranean salinity, a qualitative representation of gateway size and the probable drivers (tectonic, erosion, sea level) of changing dimensions, the Mediterranean's fresh water flux where *E* and *P* = evaporation and precipitation over the Mediterranean respectively and *R* is the river discharge into the Mediterranean Sea, and arrows representing one-way or two-way exchange between the Mediterranean and Atlantic.

## *Part II*

### *Deep-marine processes*

## 5. Deep-marine sedimentary processes

### 5.1 Deep-water

As we aim to better understand deep-marine modern and ancient sedimentary processes, it is important to define the deep marine realm.

The term “deep” is defined by the *Cambridge Dictionary* as: “going or being a long way down from the top or surface or being of a particular distance from the top to the bottom”. Since the definition of “deep” is relative, the term “deep-water” bears different meanings depending on its use. For example, Geologists use the term to denote the deep-water depositional origin of the subsurface, whereas drilling engineers use the term to denote the present-day drilling depths for the target reservoir, irrespective of its depositional origin (*Shanmugam, 2012*).

“Since this thesis has a geological background, I aim to define the term deep-water from a geological perspective”

The influential works of *Pickering et al. (1989)* uses the term “deep-water” to describe environments that occur exclusively below storm wave base (Fig. 2.9A). *Shanmugam (2012)* however, argues that the depth of the “storm wave base” is not a constant value and varies, for example, with the wide range of wind velocities created by tropical cyclones.

Within the scope of this thesis, the term “deep-water” is used to refer to bathyal water-depth environments. The continental slope and thus the start of deep-water, approximately corresponds to this bathyal zone (Fig. 2.9B, 120 – 3500 m). The bathyal zone starts downward from the shelf break (or shelf edge), which is defined by a change in slope gradient from  $< 1^\circ$  (continental shelf), to roughly  $3 - 5^\circ$  (along the continental slope). Occasionally this gradient can exceed  $20^\circ$  in areas where canyons are incising the slope and shelf. Distally of the continental slope, on the rise, the slope gradient decreases to  $1 - 2^\circ$  and the relief becomes smoother. Because of this decrease in gradient, the continental rise is the preferred area for final deposition of terrigenous sediment that bypassed the shelf and slope areas. Together, the continental shelf, slope and rise form the continental margin. The margin can be passive and tectonically quiescent (North Atlantic margin) or active and tectonically dynamic (circum-Pacific margins) where instead of a continental rise a trench characterises the margins.

The continental rise passes into the abyssal plain, which represents the largest oceanic domain, from about 3500 m water depth. The mean water depth of this, at a large scale, “flat” marine realms is ~ 3800 m. Often its “flatness” is heavily disrupted by tectonic and volcanic features, accumulations of sediments forming drifts and levees, diapirs and dissolution structures. In subduction areas, the presence of a subduction trench generates the deepest oceanic environments, down to 11,020 m (Mariana Trench).

Mosher *et al.* (2017) recently published a paper on the influence of deep-water sedimentary processes in shaping the continental margins (*e.g.* Heezen *et al.*, 1966; Embly & Langseth, 1977; Wynn *et al.*, 2000). They indicate the importance of the interaction between the Bathyal zone and the sedimentary processes in shaping the continental margin and thus affecting the depth of deep water.

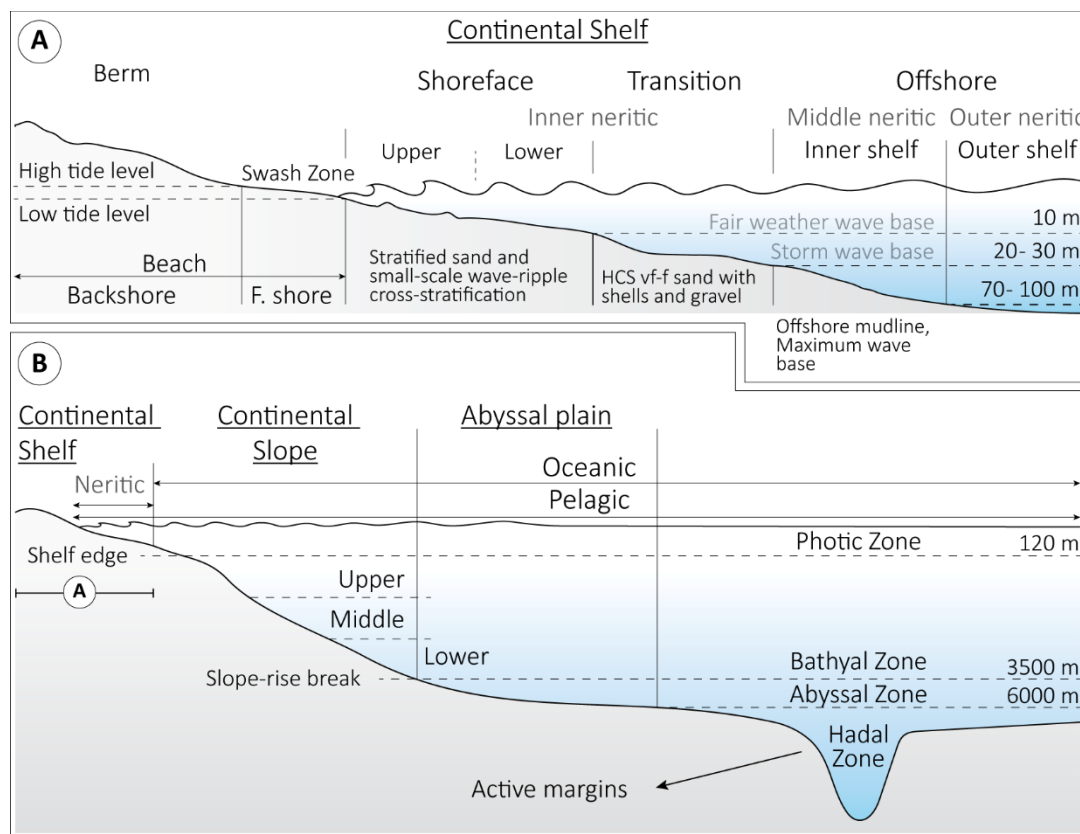
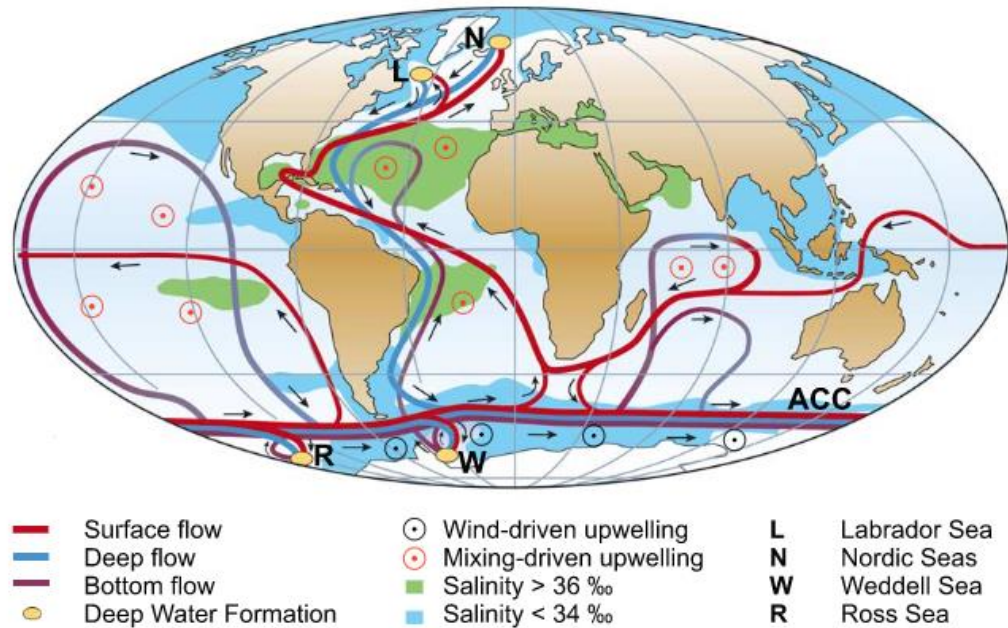


Figure 2.9. This figure shows the offshore zonation. Panel A shows the zonation of the Continental Shelf, down to water depths of 120 m. Panel B shows the zonation from the Continental Shelf (A) to Abyssal plains, down to water depths of over 6000 m. F. shore is short for foreshore. HCS stands for Hummocky cross-stratification. Figure modified after Wikipedia.



**Figure 2.10.** Schematic view of the ocean circulation (Kuhlbrodt et al., 2007). The red coloured bands show the main surficial currents. Deep-water formation, because of the increase in water density primarily related to cooling, is taking place at the yellow circles in the northern Atlantic (Labrador and Nordic Seas) and near Antarctica. This deep-water formation forces the current to sink and continue as the blue coloured bands, forming the main currents in deeper layers. In violet the Antarctic bottom water.

## 5.2 Deep-water formation

The Oceans are stratified into distinct layers. This stratification results from different physical and chemical properties of water masses. Deep waters of the ocean are primarily formed in marginal seas or shallow shelf regions where the water properties are increased in density. These density increases result from cooling, cold water is denser than warm water, and/or due to ice formation or strong evaporation which enhances density by increased salinity (Rebesco et al. 2014, and references therein). The division between an upper warm-, and a deep cold-water mass, is the so called “thermocline”.

The principle deep-marine bottom water is formed by the cooling and sinking of surface water at high latitudes. This dense water formation powers the thermohaline circulation throughout the world’s oceans (Fig. 2.10). Bottom waters of the thermohaline circulation generally move very slowly through ocean basins, at velocities no greater than 1-2 cm s<sup>-1</sup> but under specific circumstances they can reach velocities in the order of ms<sup>-1</sup> (Stow et al., 2009).

### 5.3 Deep marine sedimentary processes

The noun *sediment* comes from the Latin word *sedimentum*, which means settling or sinking down, a form of the verb “*sedere*”, to sit or settle. In Earth and environmental sciences, sediment has a wide context that includes many forms of organic and mineral matter (Leeder, 2009). The term “sedimentation” describes the process of accumulating sediments in the form of layers or beds and includes all events that take place during particle formation, through transport to final deposition of the sedimentary particles. It also includes all the consolidation processes, as well as the associated biochemical and chemical changes and biological processes during and after deposition.

Sediment in the deep-sea, or deep water sediment, consists of either, (1) clastic particles derived from eroded rocks and sediment outcropping either on the emerged continents of previously deposited sediment in marine environments, (2) particles generated by volcanic eruptions, (3) particles formed by living organisms, including organic matter, skeletal hard parts of calcareous, opaline or phosphatic composition, and faecal particles, and (4) particles formed by chemical precipitation of the elements contained in the salty sea water. Most of the chemical processes include micro-biotic reactions and are thus grouped under the term “biochemical processes” (e.g. Hüneke & Mulder, 2011).

Herein I will mainly focus on the sedimentary processes responsible for the deposition of deep-water sandstones.

Stow *et al.* (1996) indicated that the main control on the style of deep-water sedimentation is sediment supply, followed by the control of plate tectonic configurations, climate and sea level. The controls of sediment supply include grain size, composition, volume, and the rate and frequency at which sediment is made available for deposition. The depositional style is governed by tectonic activity and resulting morphology of both the distant and immediate source areas, by climate, in particular its influence on the supply of sediment to the shelf and shoreline, and by the regularity, magnitude and frequency of flows from the source region.

The three main groups of processes that are capable of eroding, transporting and depositing clastic material within the deep sea are: i) pelagic and hemipelagic settling, ii) episodic re-suspension or gravitational processes and iii) semi-permanent bottom current processes (Figs. 2.11). Each of these processes will be described below. In addition to these processes, some deep-sea deposits are formed by in-situ authigenic processes. These



processes are not treated herein as they mainly comprise geochemical alternations of previously deposited sediment.

### 5.3.1 Pelagic and hemipelagic sedimentation

The term “pelagic” is defined as “relating to the open ocean” by the Oxford dictionary, whereas “hemi-“ the prefix of hemipelagic, is defined as “half”. In geology, pelagic is referred to as sediment which is generated in the open sea (Fig. 2.11). Pelagic sediment is mainly composed of biogenic material diluted by a proportion (<10%) of non-biogenic, terrestrial components (Stow and Tabrez, 1998). More proximally, close to the continental margins and in enclosed basins, clastic supply is more abundant and further dilutes (hemipelagic) the rain of biogenic debris by an increased supply of terrigenous silt- and clay-sized sediment. The process of sedimentation is controlled by the slow and relatively steady fallout of biogenic debris generated largely in the upper part of the water column and terrigenous fine-grained particles (Fig. 2.11, Stow, 1985).

More specifically, hemipelagites are fine-grained sediments that typically form in the marginal outer shelf and slope. They form the principal marine sediment types, also known as ‘background,’ facies of many deep-water successions (Stow, 1985; Stow et al., 1996; Pickering and Hiscott, 2016). The principal facies model for hemipelagites along with variances in composition resulting from sediment source is shown in Figure 2.12.

Hemipelagites have close similarities with other deep-water facies as sedimentary processes are commonly associated, including i) pelagites, both biogenic oozes and abyssal red clays; ii) muddy contourites; iii) fine-grained turbidites; and iv) hemiturbidites. A

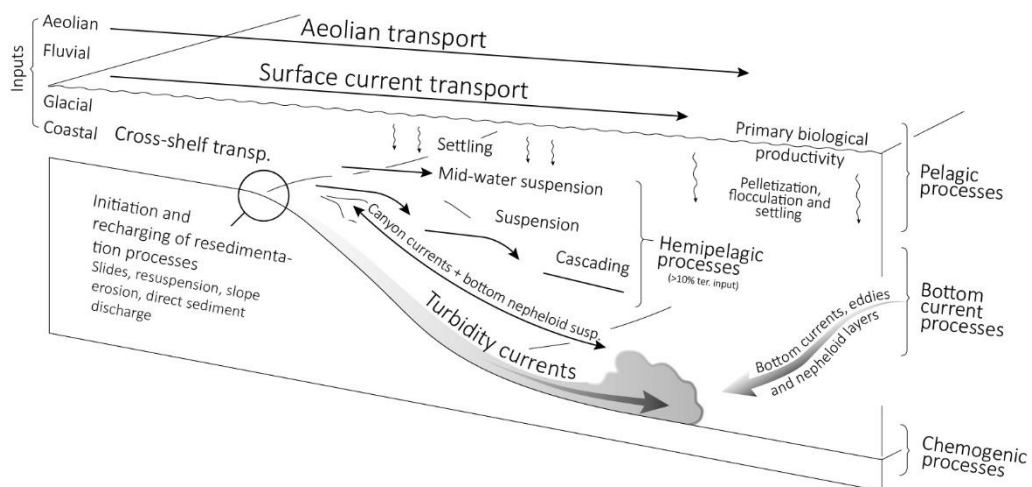
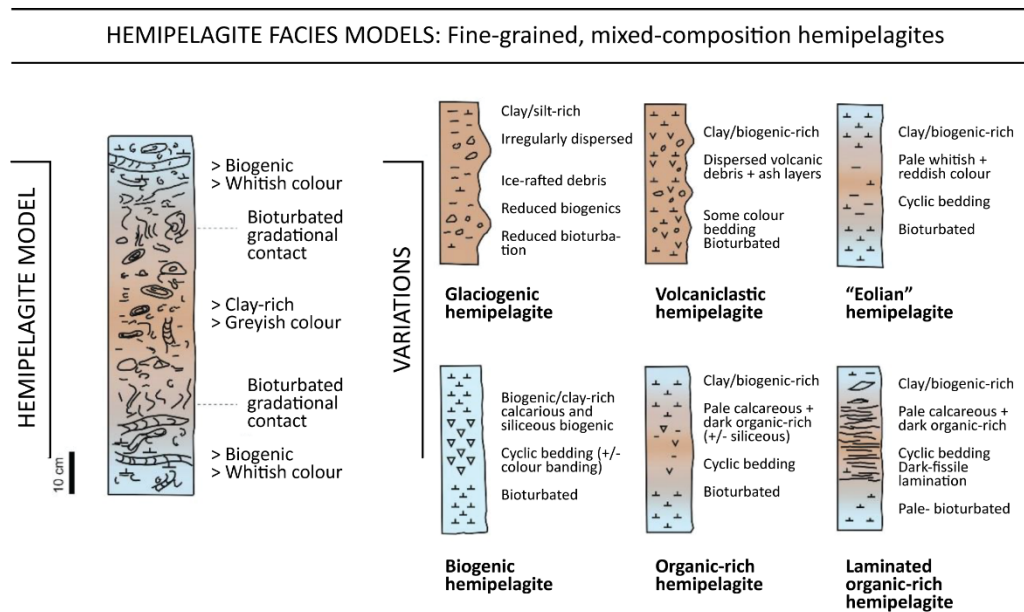


Figure 2.11. The range of processes contributing to fine-grained hemipelagic deposition in the deep-sea (after Stow, 1996)

complete gradation between hemipelagites and muddy contourites as bottom current velocities increase. The complete gradation between hemipelagites and open ocean pelagites is associated to increasing distances from land and diminishing terrestrial input. Hemiturbidites are sediments with partly muddy turbidite and partly hemipelagite characteristics (Stow and Wetzel, 1990).



**Figure 2.12.** Facies model for hemipelagites. This standardized model shows the cyclic variability between different input components. This state-of-the-art model is modified after Stow and Smillie, 2020.

### 5.3.2 Episodic re-suspension processes

Einsele (1991) stated that re-sedimentation processes are the main processes whereby large volumes of sediment are transported into deep water from an original shallow-water setting. These processes all depend upon the down-slope component of gravity acting upon material stored on or moving down a slope Nardin et al. (1979). Re-sedimentation or gravity driven processes include rock falls, slides and slumps, debris flows, liquified and fluidized flows & turbidity currents (Fig. 2.13). Stow et al. (1996) indicated that all these processes may be classified as subaqueous mass movement and most of them as sediment gravity flows. The only process that falls outside such a classification are rock falls and slides.

Submarine gravity processes are classified according to the mechanical behaviour of the process, the particle-support mechanism, the concentration, or the longitudinal change in their deposits. Sediment gravity flows are all mixtures, in varying proportions, of water and sediment particles. For these mixtures to move and deform internally, particles must be

dilated allowing them to move relative to one another. The various clast-support mechanisms provide a further basis for subdivision.

The most used classification in literature for the present-day deep-water environment uses this particle support mechanism to classify gravity processes (*e.g. Stow et al., 1996; Lowe, 1979, 1982; Nardin et al., 1979; Middleton and Hampton, 1973*). The classification based on deposits (*e.g. Mutti and Ricci Lucchi, 1975; Pickering et al., 1989*) is extensively used in research on ancient environments and in the oil industry. It is based on the sedimentary facies and their evolution along the pathway of the flow.

The main types of flow processes (Fig. 2.13) are rock (rock falls) or consolidated material avalanching, creeping and failures, slides and slumps, flows (cohesive and non-cohesive), water-dominated flow and turbulent flow (*e.g. Mulder, 2011*).

#### *5.3.2.1 Consolidated gravitational processes*

##### *Rock falls*

Rock falls (Fig. 5) are short-lived events in which blocks of lithified material fall down a steep subaqueous slope with minimal interference between falling clasts. Subaqueous slopes steep enough to accommodate this type of movement are confined to active fault scarps, the margins of carbonate platforms and the heads of some steeply incised canyons. Rock falls might be triggered by external events such as earthquakes or major storms. Rock fall related deposits consist of wedges of chaotic breccia (talus apron). These breccias commonly have very high initial porosities which tend to be filled by pelagic and hemipelagic sediment. Large single clasts may fall into finer-grained sediment at the foot of the slope as olistoliths (chaotic mass of heterogeneous consolidated material >10 m) and disturb the original structure and fabric of that material.

The avalanching of discrete blocks (m to 100's of metres) occurs only in places where consolidated sediment or rock crops out from steep subaqueous slopes or cliffs. Rock avalanching is most frequently occurrent in volcanoclastic environments (*Carey and Schneider, 2011*).

##### *Rock slides*

Rock slides involve large blocks that move in isolation or as clusters in continuous contact with underlying sediments (Fig. 5). The blocks move without internal deformation as all the shear is concentrated on basal slip surfaces. Slide deposits might make major contributions

to the deposits of continental slopes and rises and are characterized by large, often isolated blocks of material, predominantly limestones, in otherwise fine-grained background sediment.

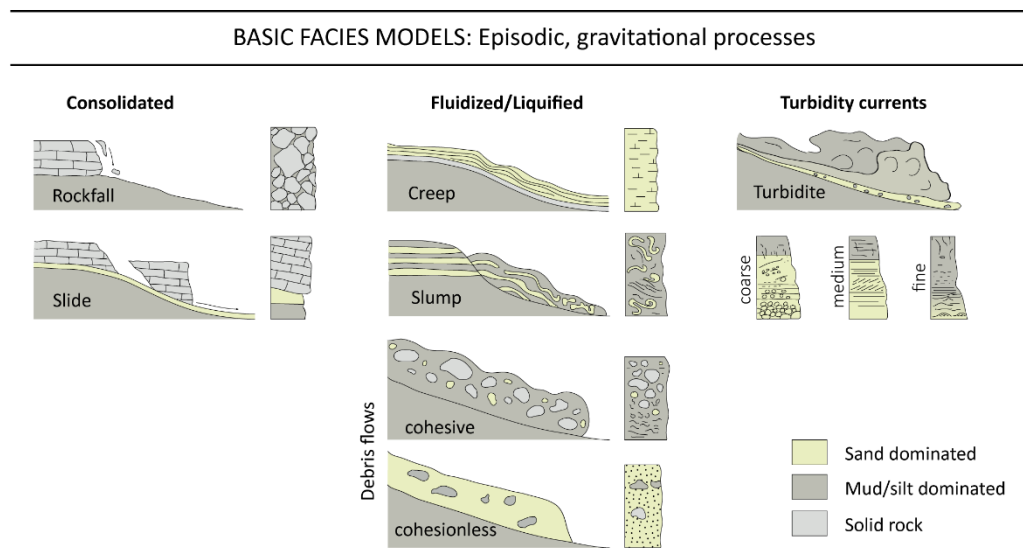


**Figure 2.13.** Simplified models and facies models for rockfalls, slides, creep and slump deposits, debris flows and turbidity currents. The legend shows the dominant sedimentary composition based on grain-size; sand, mud/silt dominated and solid rock. Modified after Mulder, 2011; Lewis, 1971; Pickering, 1979; Reading, 1996; Stow et al., 1996; Bouma, 1962.

### 5.3.2.2 Concept of Mass Transport Deposits (MTDs)

Mass-transport deposits are sedimentary, stratigraphic successions that were remobilized after initial deposition but prior to substantial lithification and transported downslope by gravitational processes as non-Newtonian rheological units (Bingham plastics or dilatant fluids) (Meckel, 2010).

#### Slumps

*Slumps share many features of slides.* They may occur over a wide range of scales with the largest slump layers covering many hundreds of square kilometres. They may occur on very low-gradient slopes, especially where sedimentation rates of fine-grained sediments are high. For slumps, the bulk of displacement is concentrated on a basal slip surface, however, the mass of moving material is commonly unconsolidated and undergoes complex internal deformation as it moves downslope (Fig. 2.13).

The two-dimensional model of Lewis (1971) shows that the head areas of slumps are dominated by extensional structures in the form of normal, commonly listric faults, while the downslope part of the slump, where movement ceases, tends to be dominated by

compressional structures such as folds and thrusts which ramp up from the basal complex as a result of internal components moving relative to each other. Since slumping involves plastic deformation, a slump will freeze once applied shear falls below some critical value. This freezing may not occur at the same time throughout a slumping sheet and certain parts will move after other parts have stopped, adding to the complexity of internal deformation. Within slump sheets, therefore, it is common to find a very wide variety of styles of deformation ranging from brittle to highly ductile, sometimes occurring in proximity (e.g. *Martinsen & Bakken, 1990*). *Pickering (1979)* indicates that, following initial slump movement, retrogressive failures in the head area may lead to a succession of smaller, later flows. Furthermore, the area from which the largest slumps are removed may become sites for the development of slope channels and conduits for the transfer of later sediments to deep water.

Slump deposits vary in thickness from a few cm to over 100 m's and are recognized by the presence of pervasive deformation structures within which it often is still possible to recognize remnants of original bedding and lamination. The distinction between slump folded units and the products of tectonic deformation can be based on: (1) the presence of undeformed beds above and below, (2) the erosional truncation of folds on the top surface, and (3) immediately overlying beds which rapidly eliminate any relief on the top surface of the slump and restore a horizontal surface. Sediment slides and slumps caused by slope failure can transform and disaggregate by liquefaction, fluidization and downslope surface shear into debris flows (*Leeder, 2011*).

### *Sediment creep*

Sediment creep (Fig. 2.13) is a long-term process of slow strain (*Mulder and Cochonat, 1996*). This strain is the result of sediment loading on an inclined slope. Continuous or theological creep results from the breaking and re-establishment of electro-chemical bonds between particles. Intermittent creep results from physical or biological displacement normal to the slope with downslope readjustment. Freeze-thaw is a major mechanism in subaerial settings, burrowing organisms may provide the main agent for destabilizing (thawing) the sediment (*Reading, 1996*).

Creep deposits are poorly documented but might be inferred from subtle surface morphology on modern slopes (*Stow et al., 1996*). When shear stress is high, creep may be a precursor to creep rupture and the initiation of a slump or slide (*Nardin et al., 1979*).

### Debris flows

Debris flows are plastic flows in which sediment and water are fully mixed and original bedding and lamination is thus largely destroyed. Stow et al. (1996) subdivided these debris flows into cohesive and non-cohesive types based on the clast-support mechanism (Fig. 2.13).

Johnson (1970) and Nemeč & Steel (1984) for example, indicate that cohesive debris flows (mudflows) occur where the cohesive strength of the matrix is the dominant clast-support mechanism and is considerably supplemented by buoyancy. Since these cohesive flows are not responsible for depositing sands in deep waters, they will not be further discussed.

Non-cohesive debris flow, or grain flows, derive their mobility from intergranular collisions which creates dispersive pressure from grain-to-grain interactions (e.g. Bagnold, 1954; Middleton and Hampton, 1973). Stow et al. (1996) state that grain flows are best developed in well-sorted sand and gravel and only occur in a pure form on steep slopes, typically as a grain avalanching when the angle of rest is exceeded. Mulder (2011) however, states that this process occurs uniquely in sand or coarse silts and necessitates steep slopes ( $> 18^\circ$ ) to be maintained. The relevance of such processes to major re-sedimentation is minimal though grain flows of sand occur in the steep heads of submarine canyons (Stow et al., 1996).

The velocity of non-cohesive (granular) flows decreases primarily due to a decrease in slope. Erosion features are frequent at the base of these flows. Stow et al. (1996) wrote that intergranular collision is important in layers of well-sorted sediment subjected to powerful shearing on a bed by an overriding current. Grain flow-like processes may then operate in conjunction with powerful turbidity currents flowing on low gradient slopes where the current sustains a traction carpet of colliding grains close to the bed. One property of grain flows is that, through the operation of dispersive pressure and so-called "kinetic sieving", larger particles work their way into higher parts of the shearing layer. As grain flows have the rheological properties of a plastic, the distribution of clast sizes is commonly preserved as inverse grading. This inverse grading is a common feature of the lower parts of conglomeratic turbidite beds. Grain flows therefore are of little significance on their own and equivalent processes may occur in association with other types of current.

Shanmugam (2006) summarizes his chapter on debris flows by stating that sandy debris flows have developed a variety of sedimentological features of which some may have been

misinterpreted as deposits of turbidity currents (e.g. normal grading), or even as tectonic features (e.g., duplex structures). Because of the complexity of the features in sandy debris flow there are no simple vertical facies models. For the same reason, interpretation of sandy debris flows in the rock record would require excruciatingly detailed observations of intricate sedimentary features.

### *Liquified and fluidized flows*

Liquefied and fluidized flows both depend upon the behaviour of pore fluid in granular systems. Though neither is important in sustaining long-distance sediment transport, both may be active during initiation of movement and during deposition from decelerating turbidity currents.

Sediment liquefaction occurs when a metastable grain packing texture is suddenly disturbed, commonly from shock due to e.g. surge, storm waves or earthquakes. The sudden shift towards a closer grain packing creates excess pore fluid and, until the fluid escapes, intergranular friction is broken down as a result of the excess fluid- or interstitial-pressure (*Middleton & Hampton, 1973*). Liquified flows are defined by *Nardin et al. (1979)* as cohesionless flows supported by the upward displacement of fluid in a loosely packed structure. Fluidization is often closely associated with liquefaction in that the resulting upward movement of fluid then supports the grains. It is thus a process that might occur during dewatering of a liquefied layer. Fluidization only lasts as long as pore fluid is available. Fluidization in deep-sea sands acts therefore as an adjunct to liquefaction and evidence for it lies in the same range of structures that liquefaction produces (*e.g. Lowe & LoPiccolo, 1974; lowe, 1975*).

Depending on the slope gradient, the thickness of the liquefied layer and the rate of fluid loss, the moving layer will either refreeze or it will accelerate and transform into a more dilute flow such as a turbidity current. Very short-lived liquefaction will lead to deformation of any original lamination while more sustained loss of strength may lead to total homogenization.

### *5.3.3 Turbidity currents*

The Cambridge dictionary defines the noun “turbulence” (currents) as a strong, uneven current in air or water. A turbidity current defined herein is a sediment flow with Newtonian rheology and turbulent state in which sediment is supported by turbulence and from which deposition occurs through suspension settling. Turbidity currents are the *most important*

transporters of coarse-grained sediment into deep water and, while they have sparsely been observed directly in deep-marine settings, they have been inferred through observations of sequential breaks in submarine telegraph cables (*Heezen & Hollister, 1971*). Turbidity currents are known directly from lakes, laboratory experiments and they have a well-founded theoretical basis, much of our knowledge of turbidity current deposition is inferred from extensive studies of their deposits, turbidites (*Stow et al., 1996*).

*Bagnold (1962)* and *Southard & Mackintosh (1981)* indicate that within an active turbidity current, the upwards components of turbulent fluid motion provides the main grain support mechanism and this behaviour can be sustained over long distances through a feedback loop known as auto suspension. In this dynamic equilibrium: (1) turbulence is generated by the flow, (2) flow results from the excess density of the suspension, (3) excess density results from the suspended load, and (4) the suspended load is maintained by turbulence.

The deposits formed by turbidity currents are known as turbidites (Fig. 2.13). These highly diverse deposits are found in many deep-water settings, forming successions up to kilometres in thickness. Turbidite beds range in thickness from a few millimetres to several meters, being composed of grain sizes ranging from mud to gravel (*Reading, 1996*). The widely accepted facies model for medium-grained sand-mud turbidites was presented by *Bouma in 1962*. This model includes a range of erosional, sharp-based beds (sole marks, tool marks, flute marks and load casts) with an ordered, stacked, sequence of five internal lamination styles. This ordered style of deposition is derived from the gradual transition in flow characteristics during the life-span of a turbidity current; (massive or graded) from upper flow regime flows or high sedimentation rates that don't allow the formation of bedforms or lamination (*Walton, 1967*), (parallel lamination) plane bed transport in the upper flow regime, followed by flow deceleration, (ripple cross-lamination) reflecting the fallout of sand or silt while lower flow regime current ripples were moving on the bed, (normal graded) suspension settling resulting in delicate grain sorting.

#### *5.3.4 Bottom current sedimentation*

Contourites are the sedimentary products of bottom currents. The term was originally used specifically to describe sediments in the deep sea affected by contour parallel (along slope) thermohaline driven bottom currents (*Heezen et al., 1966*). Currently, the term contourite is used to define all those sediments deposited or substantially reworked by the persistent action of bottom currents independent of their driving force (*Rebesco and Camerlenghi, 2008*). The depositional depth of contourites has since been widened as well,



ranging from shallower water, upper slope, and outer shelf depths, as well as in large lakes and inland seas to the deep see (Stow and Smillie, 2020).

The main difference between bottom currents and other deep marine sedimentary systems is the duration in which they can affect the pattern of sedimentation. Whereas gravitational processes are periodic short-lived events, bottom currents can be semi-continuous for extended periods. These bottom currents are however affected by short- and longer scale phenomenon's that might affect their hydrodynamic properties intermittently (e.g. de Weger et al. 2020).

At least three different processes generate bottom currents in deep-water settings; i) wind, ii) thermohaline differences and iii) deep-water tides (e.g. Rebesco et al., 2014). Each of these processes can be affected by other short-lived marine processes such as; eddies, benthic storms, tsunamis, tectonic events, orbitally controlled climate change etc.

Bottom currents can erode, transport, deposit and rework sediments. Sediment particles can be transported by the bottom currents via traction, saltation or suspension. The effect of bottom currents on sedimentation depends on the type of sediment affected by the current, the density of the water mass and the velocity of the current.

The Coriolis Force is considered the dominant force in steering water masses. *Gustave-Gaspard Coriolis*, who first described this force in 1836, showed that in a rotating frame of reference the inertial force acts to the right of the direction of body motion for counterclockwise rotation of the reference frame or to the left of clockwise rotation. E.g. if a water mass moves away from the equator towards the north, this water mass will be deflected towards the right (east). If a water mass moves away from the equator towards the south, this water mass will be deflected towards the left (east). This forcing implies that bottom currents not necessarily follow the path of least resistance but can be forced through narrow passages (with a resulting increase in flow-velocity), over topography and against continental margins with resulting changes in flow velocity. In this respect, many bottom currents are a semi-permanent part of the thermohaline circulation pattern, and sufficiently competent in parts to erode, transport and deposit sediments (Stow et al., 2002).

*The principal characteristics of bottom currents summarized based on Stow et al. (2008) is as follows:*

1. *The net flow of bottom currents is along slope as a result of the thermohaline circulation (Heezen et al., 1966). Bottom-currents can however also flow up-, down-slope, around*

and over topographic obstacles or irregularities (Stow et al., 2002a; Rebesco and Camerlenghi, 2008; Hernández-Molina et al., 2008). This deviation from along-slope movement is generally the result of deep-water formation and the steering/forcing by the Coriolis force respectively (e.g. Ambar and Howe, 1979; Dickson and Brown, 1994; Price and Barringer, 1994; Girton and Sanford, 2003; Rahmstorf, 2006; Kuhlbrodt et al., 2007). The level within the water column at which maximum flow occurs is dependent on the density of the water mass involved (Munk and Wunsch, 1998; Wells and Wettlaufer, 2005; Wahlin and Cenedes, 2006; Legg et al., 2009; Akimova et al., 2011). Major effects on sedimentation occur where the flow impinges on the sea floor.

2. Bottom currents typically act as broad sluggish movement of specific water masses with mean flow velocities below  $10 \text{ cm s}^{-1}$  over low gradient slopes and in ocean basins. More restricted or confined intermediate flow velocities are in the range of  $10\text{-}30 \text{ cm s}^{-1}$ . Over steeper slopes and around topographic obstacles, highly restricted high velocity flows reach speeds over  $30 \text{ cm s}^{-1}$  through narrow gateways, passages and over shallow sills (Stow et al., 1996b). The sediment type affected by the bottom current depends mainly on the velocity of the bottom current. A diagram depicting sediment type and bedforms in relation to current velocity, the bedform velocity matrix after Stow et al. (2009), gives a good representation of this relation.
3. Bottom currents are highly variable in location, direction and velocity over relatively short timescales (from hours to months). Deep tidal effects cause velocity increase decrease and flow reversals (e.g. Shanmugam, 2008). Seasonal changes in flow velocity can result from variations in water mass properties generated in the source regions. Large eddies can significantly affect bottom currents depending on their relative movement (e.g. Serra et al., 2010). Flow velocities are directly affected by changes in slope gradient and topographic irregularities along its course (e.g. Hernández-Molina et al., 2008). This kind of variability leads to many cycles of deposition, non-deposition and erosion during contourite accumulation and generates significant hydrodynamic difference, affecting the style of sedimentation within short distances.
4. Eddy kinetic energy, sea-surface topographic variations and surface current instabilities can all be transmitted through the water column and so result in marked variations in kinetic energy at the sea floor (e.g. Stow et al., 2002a; Rebesco, 2005; He et al., 2008). In places, this leads to an alternation of short (days to weeks) episodes of higher velocity

*benthic storms (Hollister et al., 1974; Hollister and McCave, 1984), and longer periods (weeks to months) of lower velocity.*

5. *Bottom currents also show longer period variability or intermittency (from decadal to millennial). Some of this intermittency is directly related to climate and sea-level change, for example at the scale of Milankovitch cyclicity, which in turn influences the density properties of the deep-water masses generated in the source area as well as the volume of deep-water generated and, in some cases, the amount of water that escapes through oceanic gateways to feed thermohaline circulation (e.g. de Weger et al., 2020). Furthermore, tectonic events can significantly control and or affect bottom currents by reconfiguration of gateways and sills, affecting the deep-water formation and water mass characteristics.*

### Contourites

Contourites are the sediments deposited or significantly affected by the action of bottom currents (Stow et al., 2002; Stow and Faugeres, 2008). As previously described, semi-permanent deep marine bottom currents interact and are affected by other deep-water processes. Bottom currents, although capable of eroding and transporting sediment, largely depend on sediment sourcing from pelagic, hemi-pelagic and gravitational processes. Contourites generally incorporate fine-grained material from these processes, which may be transported over long distances before their ultimate deposition (Stow and Faugeres, 2008). Bottom currents are also capable of eroding and winnowing the sea floor and to prevent deposition, causing hiatuses and/or hardgrounds in the sedimentary record.

Due to their wide range of hydrodynamic conditions and their dependence on sediment supply, contourites deposit a wide range of facies. The contourite facies, as described in Stow and Faugeres (2008), consist of; i) Siliciclastic, ranging from muddy to gravel grades, ii) shale, iii) volcanoclastic, iv) Calcareous bioclastic, ranging from calcilutites to calcirudite grade, v) Siliceous bioclastic, vi) chemogenic and other contourite-related facies. However, these contourite facies divisions do not even include mixed depositional features such as turbidites affected by bottom currents.

Despite the wide range of recognized contourite facies there is only one generally accepted contourite facies model, the bi-gradational sequence (Fig. 2.14). This model, originally from Gonthier et al. (1984) and Faugeres et al. (1984) and later revised by Stow and Faugeres (2008) is based on gradual changes in flow velocity of the bottom current. This

gradual change is related to an increase (reversed grading – facies C1, C2 and C3) and a subsequent decrease (normal grading – facies C3, C4 and C5) of the bottom current velocity and thus its gradually changing ability to transport, erode and deposit sediment of different grades. This model is applied to all contourite facies, suggesting that the process is the same for all facies and that only the source of the sediment is responsible for the large variety of contourite facies.

Variations to the standard bi-gradational sequence have been proposed (*Stow and Faugeres, 2008*), however they differentiate between fine- and sand-grade lithofacies within the same bi-gradational model without distinct recognition criteria other than a bi-gradational co-occurrence. Also, the possible presence of partial, or composite sequences further hampers the differentiation with other deep marine facies.

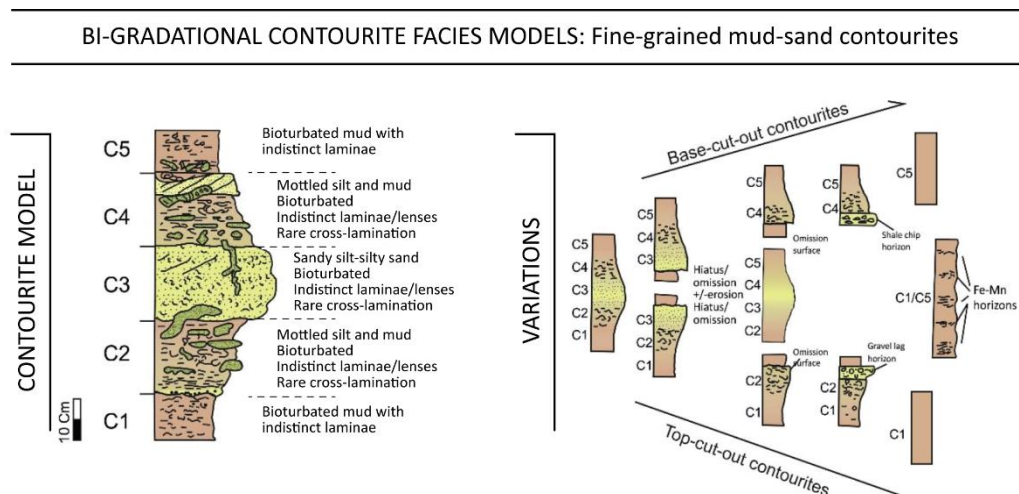


**Figure 2.14.** Facies model for fine-grained contourites. The contourite facies model on the left, modified after Gonthier et al. (1984), shows the complete sequence of divisions C1-C5. The variations include typical partial sequences. Copied from Stow and Smillie, 2020.

### 5.3.5 Mixed systems

Ocean basins are regularly affected by an interplay of hydrodynamic and sedimentary processes. The sedimentary processes as described above range from short lived, periodic events (gravitational processes) to semi-continuous long-lived events (contourites). Where multiple sedimentary processes occur simultaneously, they affect one-another, forming mixed systems. The sedimentary record of these mixed systems might deviate from those affected by a singular process. *Mulder et al. (2008)* synthesised the mixed occurrence of turbidite-contourite systems and several publications were dedicated to this topic during

recent years (e.g. Gong et al., 2016; Sansom, 2018; Fonnesu et al., 2020; Fuhrmann et al., 2020; Rodrigues et al., 2021).

## 5.4 The deep-marine facies problem

Over the years, several attempts have been made to classify deep-marine processes based on the mechanical behavior of flow, the transport mechanisms and, the clast-support systems, so that a plethora of terminology and confusing (partial) synonyms exists. This resulted from the aim to oversimplify the true complexity of processes, from initiation to deposition, and their relationship to depositional products (Stow et al., 1996).

A worldwide upsurge in research on deep-sea clastic deposits coincided with the advent of the theory of turbidity currents in the early part of the 1950's. During the past six decades, the initial works of Bouma (1962), the Bouma-sequence, which describes the depositional sequence of turbidites, evolved into an influential conceptual entity that was easily applied and understood. As research on turbidites evolved quickly and was widely applicable to deep-marine facies in outcrops, other deep-marine processes were easily overlooked, as much so that Shanmugam (2012) dedicated a volume to provide the "much-needed" clarity by explaining the inherent problems with prevailing practice of interpreting deep-water sands as "turbidites".

The continuous advances in ocean research have increasingly shown the severe complexity of ocean dynamics and its effects on sedimentation but also climate. Particularly with respect to advances in hydrocarbon exploration towards deeper waters and to lesser-understood plays, a need to better determine the origin of reservoir deposits that lacked the, what is commonly referred to as "typical" turbidite signature, was recognized (Viana, 2008).

Unlike turbidites and other gravity-flow-derived deposits, research on contourites has not made significant advances since its first description in 1964 by Heezen and Hollister (1964). The advances that have been made have mainly been confined to a much more academic rather than an economically valuable approach and has thus been limited to conventional shallow penetration, high-resolution 2-D seismic data and shallow piston coring (Viana, 2008) restricting the ability to study contourites in detail. An example of the limited interest from the scientific community has been quoted very strikingly by Eggenhuisen (pers. comm, 2019) after a multidisciplinary team of which he was part, ran its first experiments on the

interaction between turbidity- and bottom-currents in the EUROTANK in Utrecht, the Netherlands:

*“We are able to model and predict turbidity currents and their deposits in controlled flume experiments. These experiments thus far lacked the inclusion of other deep-water processes as we (the turbidite research focused community) expected their velocity and impact to be of such magnitude that they would overprint secondary processes. For this reason, we were amazed to see that these relatively low-velocity bottom currents, directed perpendicular to the turbidity current, have such a strong effect on the style of deposition.”*

- The first results of these experiments are published in *Miramontes et al. 2020* –

This quote shows that, the much-needed simplification, should not refrain us from looking at the bigger and very complex picture as the smallest of processes might have a significant impact on dominant processes.

This brings us to the second deep-water facies problem. This problem relates to the research developments that have been made since the discovery of contourite facies, the contourite facies model (*Gonthier et al., 1984*). As mentioned earlier, this model is based on the gradual changes in semi-permanent bottom current velocities and its effects on sedimentation. Despite the subdivisions made, the model suggests that the process behind contourite sedimentation is solely based on these gradual changes in flow velocity and that the source of the sediment is the dominant factor for the resulting contourite facies. As the sourced sediment is highly variable in composition, this makes sense. However, the model does not consider the full extent of the depositional environment and the broad range of morphological features in contourite systems (Fig. 2.15), meaning that the contourite facies model is not applicable to the wide spectrum of the different contourite depositional elements existing in a contourite system. So although a widely applicable model is present, it doesn't cover the full spectrum of contourite facies, nor in many cases, does it provide sufficient recognition criteria to distinguish contourites from other deep-marine deposits.

---

## EXAMPLES OF CONTOURITE DRIFT FEATURES

---

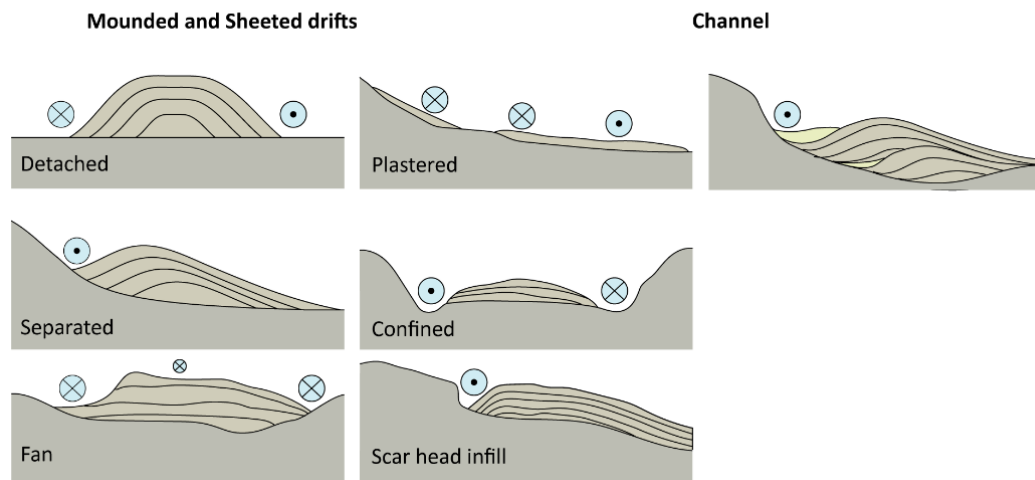


**Figure 2.15.** Contourite Drift features modified after Rebesco et al., 2014 and references therein. Blue circles indicate the generalized core of the bottom current. Crosses within the blue circles indicate bottom currents away from the reader whilst black dots indicate a current flowing towards the reader.

## REFERENCES

- Achalhi, M., Münch, P., Cornée, J. J., Azdimousa, A., Melinte-Dobrinescu, M., Quillévéré, F., ... & Moussa, A. B. (2016). The late Miocene Mediterranean-Atlantic connections through the North Rifian Corridor: New insights from the Boudinar and Arbaa Taourirt basins (northeastern Rif, Morocco). *Palaeogeography, Palaeoclimatology, Palaeoecology*, 459, 131-152.
- Agustí, J., Garcés, M., & Krijgsman, W. (2006). Evidence for African-Iberian exchanges during the Messinian in the Spanish mammalian record. *Palaeogeography, Palaeoclimatology, Palaeoecology*, 238(1-4), 5-14.
- Akimova, A., Schauer, U., Danilov, S., & Núñez-Riboni, I. (2011). The role of the deep mixing in the Storfjorden shelf water plume. *Deep Sea Research Part I: Oceanographic Research Papers*, 58(4), 403-414.
- Allerton, S., Lonergan, L., Platt, J. P., Platzman, E. S., & McClelland, E. (1993). Palaeomagnetic rotations in the eastern Betic Cordillera, southern Spain. *Earth and Planetary Science Letters*, 119(3), 225-241.
- Ambar, I., & Howe, M. R. (1979). Observations of the Mediterranean outflow—I mixing in the Mediterranean outflow. *Deep Sea Research Part A. Oceanographic Research Papers*, 26(5), 535-554.
- Bagnold, R. A. (1954). Experiments on a gravity-free dispersion of large solid spheres in a Newtonian fluid under shear. *Proc. R. Soc. Lond. A*, 225(1160), 49-63.
- Bagnold, R. A. (1962). Auto-suspension of transported sediment; turbidity currents. *Proc. R. Soc. Lond. A*, 265(1322), 315-319.
- Banks, C. J., & Warburton, J. (1991). Mid-crustal detachment in the Betic system of southeast Spain. *Tectonophysics*, 191(3-4), 275-289.
- Barbero, L., Jabaloy, A., Gómez-Ortiz, D., Pérez-Peña, J. V., Rodríguez-Peces, M. J., Tejero, R., ... & Asebriy, L. (2011). Evidence for surface uplift of the Atlas Mountains and the surrounding peripheral plateaux:

- Combining apatite fission-track results and geomorphic indicators in the Western Moroccan Meseta (coastal Variscan Paleozoic basement). *Tectonophysics*, 502(1-2), 90-104.
- Bargach, K., Ruano, P., Chabli, A., Galindo-Zaldívar, J., Chalouan, A., Jabaloy, A., & Akil, M. (2004). Ahmamou M Sanz De Galdeano C. Benmakhlof M, 521-540.
- Benammi, M., Calvo, M., Prévot, M., & Jaeger, J.J. (1996). Magnetostratigraphy and paleontology of Ait Kandoula basin (High Atlas, Morocco) and the African-European late Miocene terrestrial fauna exchanges. *Earth and Planetary Science Letters*, 145(1), 15-29.
- Betzler, C., Braga, J. C., Martín, J. M., Sanchez-Almazo, I. M., & Lindhorst, S. (2006). Closure of a seaway: stratigraphic record and facies (Guadix basin, Southern Spain). *International Journal of Earth Sciences*, 95(5), 903-910.
- Bezada, M. J., Humphreys, E. D., Toomey, D. R., Harnafi, M., Dávila, J. M., & Gallart, J. (2013). Evidence for slab rollback in westernmost Mediterranean from improved upper mantle imaging. *Earth Planet. Sci. Lett*, 368, 51-60.
- Bidegaray-Batista, L., & Arnedo, M. A. (2011). Gone with the plate: the opening of the Western Mediterranean basin drove the diversification of ground-dweller spiders. *BMC evolutionary biology*, 11(1), 317.
- Bjørlykke, K., & Jahren, J. (2010). Sandstones and sandstone reservoirs. In *Petroleum Geoscience* (pp. 113-140). Springer, Berlin, Heidelberg.
- Blanc-Valleron, M. M., Pierre, C., Caulet, J. P., Caruso, A., Rouchy, J. M., Cespuglio, G., ... & Di Stefano, E. (2002). Sedimentary, stable isotope and micropaleontological records of paleoceanographic change in the Messinian Tripoli Formation (Sicily, Italy). *Palaeogeography, Palaeoclimatology, Palaeoecology*, 185(3-4), 255-286.
- Bonardi, G., de Capoa, P., Di Staso, A., Estévez, A., Martín-Martín, M., Martín-Rojas, I., ... & Tent-Manclús, J. E. (2003). Oligocene-to-Early Miocene depositional and structural evolution of the Calabria–Peloritani Arc southern terrane (Italy) and geodynamic correlations with the Spain Betics and Morocco Rif. *Geodinamica Acta*, 16(2-6), 149-169.
- Booth-Rea, G., Ranero, C. R., Martínez-Martínez, J. M., & Grevemeyer, I. (2007). Crustal types and Tertiary tectonic evolution of the Alborán sea, western Mediterranean. *Geochemistry, Geophysics, Geosystems*, 8(10).
- Bouma, A. H. 1962. *Sedimentology of some flysch deposits*. Elsevier, Amsterdam. 168 pp. x975. Sedimentary structure of Philippine Sea and Sea of Japan sediments, DSDP, Leg, 3, 489-97.
- Brackenridge, R. E. (2014). *Contourite sands in the Gulf of Cadiz: characterisation, controls and wider implications for hydrocarbon exploration* (Doctoral dissertation, Heriot-Watt University).
- Braga, J. C., Martín, J. M., & Alcalá, B. (1990). Coral reefs in coarse-terrigenous sedimentary environments (Upper Tortonian, Granada Basin, southern Spain). *Sedimentary Geology*, 66(1-2), 135-150.
- Bryden, H. L., & Kinder, T. H. (1991). Steady two-layer exchange through the Strait of Gibraltar. *Deep Sea Research Part A. Oceanographic Research Papers*, 38, S445-S463.
- Capella, W., Hernández-Molina, F. J., Flecker, R., Hilgen, F. J., Hssain, M., Kouwenhoven, T. J., van Oorschot, M., Sierro, F. J., Stow, D. A. V., Trabuco-Alexandre, J., Tulbure, M. A., de Weger, W., Yousfi, M.Z., Krijgsman, W. (2017a). Sandy contourite drift in the late Miocene Rifian Corridor (Morocco): Reconstruction of depositional environments in a foreland-basin seaway. *Sed. Geol.*, 355, 31-57.
- Capella, W., Matenco, L., Dmitrieva, E., Roest, W. M., Hessels, S., Hssain, M., ... & Krijgsman, W. (2017b). Thick-skinned tectonics closing the Rifian Corridor. *Tectonophysics*, 710, 249-265.
- Capella, W., Barhoun, N., Flecker, R., Hilgen, F. J., Kouwenhoven, T., Matenco, L. C., ... & Krijgsman, W. (2018). Palaeogeographic evolution of the late Miocene Rifian Corridor (Morocco): Reconstructions from surface and subsurface data. *Earth-Science Reviews*.
- Carey, S. N., & Schneider, J. L. (2011). Volcaniclastic processes and deposits in the deep-sea. In *Developments in sedimentology* (Vol. 63, pp. 457-515). Elsevier.
- Chalouan, A., Saji, R., Michard, A., & Bally, A. W. (1997). Neogene tectonic evolution of the southwestern Alboran Basin as inferred from seismic data off Morocco. *AAPG bulletin*, 81(7), 1161-1184.



- Chalouan, A., Michard, A., El Kadiri, K., Negro, F., de Lamotte, D. F., Soto, J. I., & Saddiqi, O. (2008). The Rif Belt. In *Continental evolution: the geology of Morocco* (pp. 203-302). Springer Berlin Heidelberg.
- Cifelli, F., Mattei, M., & Porreca, M. (2008). New paleomagnetic data from Oligocene–upper Miocene sediments in the Rif chain (northern Morocco): insights on the Neogene tectonic evolution of the Gibraltar arc. *Journal of Geophysical Research: Solid Earth*, 113(B2).
- Corbí, H., Lancis, C., García-García, F., Pina, J. A., Soria, J. M., Tent-Manclús, J. E., & Viseras, C. (2012). Updating the marine biostratigraphy of the Granada Basin (central Betic Cordillera). Insight for the Late Miocene palaeogeographic evolution of the Atlantic–Mediterranean seaway. *Geobios*, 45(3), 249-263.
- Cornacchia, I., Agostini, S., & Brandano, M. (2018). Miocene oceanographic evolution based on the Sr and Nd isotope record of the Central Mediterranean. *Paleoceanography and Paleoclimatology*, 33(1), 31-47.
- Crampton, S. L., & Allen, P. A. (1995). Recognition of forebulge unconformities associated with early-stage foreland basin development: example from the North Alpine Foreland Basin. *AAPG bulletin*, 79(10), 1495-1514.
- Crespo-Blanc, A., & Campos, J. (2001). Structure and kinematics of the South Iberian paleomargin and its relationship with the Flysch Trough units: extensional tectonics within the Gibraltar Arc fold-and-thrust belt (western Betics). *Journal of Structural Geology*, 23(10), 1615-1630.
- Crespo-Blanc, A. (2007). Superimposed folding and oblique structures in the palaeomargin-derived units of the Central Betics (SW Spain). *Journal of the Geological Society*, 164(3), 621-636.
- Crespo-Blanc, A., Comas, M., & Balanyá, J. C. (2016). Clues for a Tortonian reconstruction of the Gibraltar Arc: structural pattern, deformation diachronism and block rotations. *Tectonophysics*, 683, 308-324.
- Dabrio, C. J., Fernández, J., Peña, J. A., Ruiz Bustos, A., & Sanz de Galdeano, C. M. (1978). Rasgos sedimentarios de los conglomerados miocénicos del borde noreste de la Depresión de Granada. *Estudios Geológicos*, 34, 89-97.
- Daguin, F., (1927). Contribution á l'étude géologique de la région Pré-rifaine (Maroc septentrional). *Notes Mém. Serv. Géol. Maroc* 1:1–413.
- Dayja, D., Janin, M. C., & Boutakiout, M. (2005). Biochronologie et corrélation des bassins néogènes du Couloir sud-rifain (Maroc) fondées sur les événements de foraminifères planctoniques et de nannofossiles calcaires. *Revue de micropaléontologie*, 48(3), 141-157.
- de Capoa, P., Di Staso, A., Perrone, V., & Zaghoul, M. N. (2007). The age of the foredeep sedimentation in the Betic–Rifian Mauretanian units: a major constraint for the reconstruction of the tectonic evolution of the Gibraltar Arc. *Comptes Rendus Geoscience*, 339(2), 161-170.
- de Castro, S., Hernández-Molina, F. J., Rodríguez-Tovar, F. J., Llave, E., Ng, Z. L., Nishida, N., & Mena, A. (2020a). Contourites and bottom current reworked sands: Bed facies model and implications. *Marine Geology*, 428, 106267.
- de Castro, S., Hernández-Molina, F. J., de Weger, W., Jiménez-Espejo, F. J., Rodríguez-Tovar, F. J., Mena, A., ... & Sierro, F. J. (2020b). Contourite characterization and its discrimination from other deep-water deposits in the Gulf of Cadiz contourite depositional system. *Sedimentology*.
- de Weger, W. (2016). Sequence stratigraphic analyses of the interaction between tectonically driven sedimentation and sediment transporting bottom currents in the foreland basin of the Rifian Corridor-Case study from the Gharb and Saïss basins, northern Morocco (Master's thesis).
- de Weger, W., Hernández-Molina, F. J., Flecker, R., Sierro, F. J., Chiarella, D., Krijgsman, W., & Manar, M. A. (2020). Late Miocene contourite channel system reveals intermittent overflow behavior. *Geology*, 48(12), 1194-1199.
- Dickson, R. R., & Brown, J. (1994). The production of North Atlantic Deep Water: sources, rates, and pathways. *Journal of Geophysical Research: Oceans*, 99(C6), 12319-12341.
- Do Couto, D., Gorini, C., Jolivet, L., Le Bret, N., Augier, R., Gumiaux, C., ... & Auxietre, J. L. (2016). Tectonic and stratigraphic evolution of the Western Alboran Sea

- Basin in the last 25 Myrs. *Tectonophysics*, 677, 280-311.
- Duggen, S., Hoernle, K., van den Bogaard, P., & Harris, C. (2004). Magmatic evolution of the Alboran region: the role of subduction in forming the western Mediterranean and causing the Messinian Salinity Crisis. *Earth and Planetary Science Letters*, 218(1), 91-108.
- Einsele, G. (1991). Submarine mass flow deposits and turbidites. *Cycles and events in stratigraphy*, 313-339.
- Embley, R. W., & Langseth, M. G. (1977). Sedimentation processes on the continental rise of northeastern South America. *Marine Geology*, 25(4), 279-297.
- Faugères, J. C. (1978). Les Rides sud-rifaines: Evolution sédimentaire et structurale d'un bassin atlantico-mesogéen de la marge africaine.
- Faugères, J. C., Gonthier, E., & Stow, D. A. (1984). Contourite drift molded by deep Mediterranean outflow. *Geology*, 12(5), 296-300.
- Faugeres, J. C., Legigan, P., Maillet, N., & Latouche, C. (1989). 18. Pelagic, turbiditic, and contouritic sequential deposits on the Cape Verde Plateau (Leg 108, Site 659, Northwest Africa): Sediment record during Neogene time. In *Proc. Ocean Drill. Program Sci. Results* (Vol. 108, pp. 311-327).
- Feinberg, H. (1986). Les séries tertiaires des zones externes du Rif (Maroc): biostratigraphie, paléogéographie et aperçu tectonique (No. 315). Éditions du Service géologique du Maroc.
- Flecker, R., Krijgsman, W., Capella, W., de Castro Martins, C., Dmitrieva, E., Mayser, J. P., ... & Tulbure, M. (2015). Evolution of the Late Miocene Mediterranean–Atlantic gateways and their impact on regional and global environmental change.
- Flinch, J. F. (1994). Tectonic evolution of the Gibraltar Arc (Doctoral dissertation, Rice University).
- Fonnesu, M., Palermo, D., Galbiati, M., Marchesini, M., Bonamini, E., & Bendias, D. (2020). A new world-class deep-water play-type, deposited by the syndepositional interaction of turbidity flows and bottom currents: The giant Eocene Coral Field in northern Mozambique. *Marine and Petroleum Geology*, 111, 179-201.
- Frizon de Lamotte, D. (1979). Contribution à l'étude de l'évolution structural du Rif oriental (Maroc) (Doctoral dissertation, PhD thesis). Université Paris 6, France).
- Frizon de Lamotte, D., Crespo-Blanc, A., Saint-Bézar, B., Comas, M., Fernández, M., Zeyen, H., Ayarza, P., Robert-Charrue, C., Chalouan, A., Zizi, M., Teixell, A., Arboleya, M. L., Alvarez-Lobato, F., Julivert, M., Michard, A. (2004). TRANSMED Transect I. In: Cavza, W., Roure, F., Spakman, W., Stampfli, G. M., Ziegler, P. A. (eds) *The TRANSMED Atlas—the Mediterranean Region from crust to mantle*. Springer, Berlin Heidelberg New York.
- Fuhrmann, A., Kane, I. A., Clare, M. A., Ferguson, R. A., Schomacker, E., Bonamini, E., & Contreras, F. A. (2020). Hybrid turbidite-drift channel complexes: An integrated multiscale model. *Geology*, 48(6), 562-568.
- Garcés, M., Krijgsman, W., & Agustí, J. (1998). Chronology of the late Turolian deposits of the Fortuna basin (SE Spain): implications for the Messinian evolution of the eastern Betics. *Earth and planetary science Letters*, 163(1-4), 69-81.
- García-Hernández, M., López-Garrido, A. C., Rivas, P., Sanz de Galdeano, C., & Vera, J. A. (1980). Mesozoic palaeogeographic evolution of the external zones of the Betic Cordillera. *Geologie en Mijnbouw*, 59(2), 155-168.
- Gennari, R., Lozar, F., Turco, E., Dela Pierre, F., Lugli, S., Manzi, V., ... & Taviani, M. (2018). Integrated stratigraphy and paleoceanographic evolution of the pre-evaporitic phase of the Messinian salinity crisis in the Tokhni section (Cyprus island). *Newsletters on Stratigraphy*, 51(1), 33-55.
- Gibbons, W., & Moreno, T. (Eds.). (2002). *The geology of Spain*. Geological Society of London.
- Gil de la Iglesia, A. (2015). Seismic structure of the crust beneath the Rif Cordillera (Doctoral dissertation, Universitat de Barcelona).
- Gibert, L., Scott, G. R., Montoya, P., Ruiz-Sánchez, F. J., Morales, J., Luque, L., ... & Lería, M. (2013). Evidence for an African-Iberian mammal dispersal during the pre-evaporitic Messinian. *Geology*, 41(6), 691-694.
- Girton, J. B., & Sanford, T. B. (2003). Descent and modification of the overflow plume in the Denmark Strait. *Journal of Physical Oceanography*, 33(7), 1351-1364.

- Gomez, F., Barazangi, M., & Demnati, A. (2000). Structure and evolution of the Neogene Guercif Basin at the junction of the Middle Atlas Mountains and the Rif thrust belt, Morocco. *AAPG bulletin*, 84(9), 1340-1364.
- Gong, C., Wang, Y., Zheng, R., Hernández-Molina, F. J., Li, Y., Stow, D., ... & Brackenridge, R. E. (2016). Middle Miocene reworked turbidites in the Baiyun Sag of the Pearl River Mouth Basin, northern South China Sea margin: processes, genesis, and implications. *Journal of Asian Earth Sciences*, 128, 116-129.
- Gonthier, E. G., Faugères, J. C., Stow, D. A. V. (1984). Contourite facies of the Faro drift, Gulf of Cadiz. *J. Geol. Soc. London, Special Publications*, 15(1), 275-292.
- Coriolis, G. G. (1836). Sur un moyen de tracer des courbes données par des équations différentielles. *Journal de Mathématiques Pures et Appliquées*, 1, 5-9.
- Gutscher, M. A., Malod, J., Rehault, J. P., Contrucci, I., Klingelhoefer, F., Mendes-Victor, L., & Spakman, W. (2002). Evidence for active subduction beneath Gibraltar. *Geology*, 30(12), 1071-1074.
- He, Y., Duan, T., Gao, Z., 2008. Sediment entrainment, in: Rebesco, M., Camerlenghi, A. (Eds.), *Contourites. Developments in Sedimentology*, 60 (this volume) pp. 99–120.
- Heezen, B. C., Hollister, C. D., & Ruddiman, W. F. (1966). Shaping of the continental rise by deep geostrophic contour currents. *Science*, 152(3721), 502-508.
- Heezen, B. C., & Hollister, C. D. (1971). *Face of the deep*, 659 pp. Oxford University Press, New York. 10.2.3, 10.3.7
- Hernández-Molina, F. J., Llave, E., Stow, D. A. V. (2008). Continental slope contourites. *Dev. Sedimentol.*, 60, 379-408.
- Hernández-Molina, F. J., Stow, D. A., Llave, E., Rebesco, M., Ercilla, G., Van Rooij, D., ... & Voelker, A. H. (2011). Deep-water circulation: processes & products (16–18 June 2010, Baiona): introduction and future challenges.
- Hilgen, F. J., Krijgsman, W., Langereis, C. G., Lourens, L. J., Santarelli, A., & Zachariasse, W. J. (1995). Extending the astronomical (polarity) time scale into the Miocene. *Earth and Planetary Science Letters*, 136(3-4), 495-510.
- Hinsbergen, D. J., Vissers, R. L., & Spakman, W. (2014). Origin and consequences of western Mediterranean subduction, rollback, and slab segmentation. *Tectonics*, 33(4), 393-419.
- Hollister, C.D., McCave, I.N., 1984. Sedimentation under deep-sea storms. *Nature* 309, 220–225.
- Hollister, C.D., 1993. The concept of deep-sea contourites. *Sediment. Geol.* 82, 5–11.
- Hovikoski, J., Uchman, A., Weibel, R., Nøhr-Hansen, H., Sheldon, E., Ineson, J., Bjerager, M., Therkelsen, J., Olivarius, M., Larsen, M., Alsen, P., Bojesen-Koefoed, J. (2020). Upper Cretaceous bottom current deposits, north-east Greenland. *Sedimentology*. <https://doi.org/10.1111/sed.12764>
- Hsü, K. J., Ryan, W. B. F., & Cita, M. B. (1973a). Late Miocene desiccation of the Mediterranean. *Nature*, 242(5395), 240-244.
- Hsü, K. J. (1973b). The origin of the Mediterranean evaporites. Initial reports of the deep sea drilling project, 13, 1203-1231.
- Hüneke, H., and Stow, D. A. V. (2008). Identification of ancient contourites: problems and palaeoceanographic significance. *Dev. Sedimentol.*, 60, 323-344.
- Hüneke, H., & Mulder, T. (2011). *Deep-Sea Sediments (Developments in Sedimentology)*.
- Hüsing, S. K., Zachariasse, W. J., Van Hinsbergen, D. J., Krijgsman, W., Inceöz, M., Harzhauser, M., ... & Kroh, A. (2009). Oligocene–Miocene basin evolution in SE Anatolia, Turkey: constraints on the closure of the eastern Tethys gateway. *Geological Society, London, Special Publications*, 311(1), 107-132.
- Hüsing, S. K., Oms, O., Agustí, J., Garcés, M., Kouwenhoven, T. J., Krijgsman, W., & Zachariasse, W. J. (2010). On the late Miocene closure of the Mediterranean–Atlantic gateway through the Guadix basin (southern Spain). *Palaeogeography, Palaeoclimatology, Palaeoecology*, 291(3-4), 167-179.
- Iribarren, L., Vergés, J., & Fernández, M. (2009). Sediment supply from the Betic–Rif orogen to basins through Neogene. *Tectonophysics*, 475(1), 68-84.
- Ivanovic, R. F., Flecker, R., Gutjahr, M., & Valdes, P. J. (2013). First Nd isotope record of Mediterranean–Atlantic water exchange through the Moroccan Rifian Corridor during the Messinian salinity

- crisis. *Earth and Planetary Science Letters*, 368, 163-174.
- Johnson, A. M. (1970). Physical processes in geology: A method for interpretation of natural phenomena; intrusions in igneous rocks, fractures, and folds, flow of debris and ice. Freeman, Cooper.
- Jolivet, L., Augier, R., Robin, C., Suc, J. P., & Rouchy, J. M. (2006). Lithospheric-scale geodynamic context of the Messinian salinity crisis. *Sedimentary geology*, 188, 9-33.
- Karami, M. P., De Leeuw, A., Krijgsman, W., Meijer, P. T., & Wortel, M. J. R. (2011). The role of gateways in the evolution of temperature and salinity of semi-enclosed basins: An oceanic box model for the Miocene Mediterranean Sea and Paratethys. *Global and Planetary Change*, 79(1-2), 73-88.
- Knutz, P. C. (2008). Palaeoceanographic significance of contourite drifts. *Developments in Sedimentology*, 60, 511-535.
- Kouwenhoven, T. J., Hilgen, F. J., & Van der Zwaan, G. J. (2003). Late Tortonian–early Messinian stepwise disruption of the Mediterranean–Atlantic connections: constraints from benthic foraminiferal and geochemical data. *Palaeogeography, Palaeoclimatology, Palaeoecology*, 198(3-4), 303-319.
- Kouwenhoven, T. J., Morigi, C., Negri, A., Giunta, S., Krijgsman, W., & Rouchy, J. M. (2006). Paleoenvironmental evolution of the eastern Mediterranean during the Messinian: Constraints from integrated microfossil data of the Pissouri Basin (Cyprus). *Marine Micropaleontology*, 60(1), 17-44.
- Krijgsman, W., Hilgen, F. J., Langereis, C. G., & Zachariasse, W. J. (1994). The age of the Tortonian/Messinian boundary. *Earth and Planetary Science Letters*, 121(3-4), 533-547.
- Krijgsman, W., Hilgen, F. J., Langereis, C. G., Santarelli, A., & Zachariasse, W. J. (1995). Late Miocene magnetostratigraphy, biostratigraphy and cyclostratigraphy in the Mediterranean. *Earth and Planetary Science Letters*, 136(3-4), 475-494.
- Krijgsman, W., Hilgen, F. J., Negri, A., Wijbrans, J. R., & Zachariasse, W. J. (1997). The Monte del Casino section (northern Apennines, Italy): a potential Tortonian/Messinian boundary stratotype?. *Palaeogeography, Palaeoclimatology, Palaeoecology*, 133(1-2), 27-47.
- Krijgsman, W., Hilgen, F. J., Raffi, I., Sierro, F. J., & Wilson, D. S. (1999a). Chronology, causes and progression of the Messinian salinity crisis. *Nature*, 400(6745), 652.
- Krijgsman, W., Langereis, C. G., Zachariasse, W. J., Boccaletti, M., Moratti, G., Gelati, R., ... & Villa, G. (1999b). Late Neogene evolution of the Taza–Guercif Basin (Rifian Corridor, Morocco) and implications for the Messinian salinity crisis. *Marine Geology*, 153(1-4), 147-160.
- Krijgsman, W., Garcés, M., Agustí, J., Raffi, I., Taberner, C., & Zachariasse, W. J. (2000a). The ‘Tortonian salinity crisis’ of the eastern Betics (Spain). *Earth and Planetary Science Letters*, 181(4), 497-511.
- Krijgsman, W., & Langereis, C. G. (2000b). Magnetostratigraphy of the Zobzit and Koudiat Zarga sections (Taza-Guercif basin, Morocco): implications for the evolution of the Rifian Corridor. *Marine and Petroleum Geology*, 17(3), 359-371.
- Krijgsman, W., Blanc-Valleron, M. M., Flecker, R., Hilgen, F. J., Kouwenhoven, T. J., Merle, D., ... & Rouchy, J. M. (2002). The onset of the Messinian salinity crisis in the Eastern Mediterranean (Pissouri Basin, Cyprus). *Earth and Planetary Science Letters*, 194(3-4), 299-310.
- Krijgsman, W., & Garces, M. (2004). Palaeomagnetic constraints on the geodynamic evolution of the Gibraltar Arc. *Terra Nova*, 16(5), 281-287.
- Krijgsman, W., & Meijer, P. T. (2008). Depositional environments of the Mediterranean “Lower Evaporites” of the Messinian salinity crisis: constraints from quantitative analyses. *Marine Geology*, 253(3-4), 73-81.
- Krijgsman, W., Capella, W., Simon, D., Hilgen, F. J., Kouwenhoven, T. J., Meijer, P. T., ... & Flecker, R. (2018). The Gibraltar Corridor: Watergate of the Messinian Salinity Crisis. *Marine Geology*.
- Kuenen, P. H., & Migliorini, C. I. (1950). Turbidity currents as a cause of graded bedding. *The Journal of Geology*, 58(2), 91-127.
- Kuhlbrodt, T., Griesel, A., Montoya, M., Levermann, A., Hofmann, M., & Rahmstorf, S. (2007). On the driving processes of the Atlantic meridional overturning circulation. *Reviews of Geophysics*, 45(2).

- Langereis, C. G., Zachariasse, W. J., & Zijderveld, J. D. A. (1984). Late Miocene magnetobiostratigraphy of Crete. *Marine micropaleontology*, 8(4), 261-281.
- Leeder, M. R. (2009). *Sedimentology and sedimentary basins: from turbulence to tectonics*. John Wiley & Sons.
- Leeder, M. R. (2011). Tectonic sedimentology: sediment systems deciphering global to local tectonics. *Sedimentology*, 58(1), 2-56.
- Legg, S., Briegleb, B., Chang, Y., Chassignet, E. P., Danabasoglu, G., Ezer, T., ... & Yang, J. (2009). Improving oceanic overflow representation in climate models: the gravity current entrainment climate process team. *Bulletin of the American Meteorological Society*, 90(5), 657-670.
- Lewis, K. B. (1971). Slumping on a continental slope inclined at 1–4. *Sedimentology*, 16(1-2), 97-110.
- Litto, W., Jaaïdi, E., Medina, F., & Dakki, M. (2001). Seismic study of the structure of the northern margin of the Gharb Basin (Morocco): Evidence for a late Miocene distension. *Eclogae Geologicae Helveticae*, 94(1), 63-74.
- Lonergan, L., & White, N. (1997). Origin of the Betic-Rif mountain belt. *Tectonics*, 16(3), 504-522.
- Lourens, L. J., Antonarakou, A., Hilgen, F. J., Van Hoof, A. A. M., Vergnaud-Grazzini, C., & Zachariasse, W. J. (1996). Evaluation of the Plio-Pleistocene astronomical timescale. *Paleoceanography*, 11(4), 391-413.
- Lowe, D. R., & LoPiccolo, R. D. (1974). The characteristics and origins of dish and pillar structures. *Journal of Sedimentary Research*, 44(2).
- Lowe, D. R. (1975). Water escape structures in coarse-grained sediments. *Sedimentology*, 22(2), 157-204.
- Lowe, D. R. (1979). Sediment gravity flows: their classification and some problems of application to natural flows and deposits.
- Lowe, D. R. (1982). Sediment gravity flows; II, Depositional models with special reference to the deposits of high-density turbidity currents. *Journal of Sedimentary Research*, 52(1), 279-297.
- Lozar, F., Violanti, D., Pierre, F. D., Bernardi, E., Cavagna, S., Clari, P., ... & Trenkwalder, S. (2010). Calcareous nannofossils and foraminifers herald the Messinian salinity crisis: the Pollenzo section (Alba, Cuneo; NW Italy). *Geobios*, 43(1), 21-32.
- Luján, M., Storti, F., Balanyá, J. C., Crespo-Blanc, A., & Rossetti, F. (2003). Role of décollement material with different rheological properties in the structure of the Aljibe thrust imbricate (Flysch Trough, Gibraltar Arc): an analogue modelling approach. *Journal of Structural Geology*, 25(6), 867-881.
- Luján, M., Crespo-Blanc, A., & Balanyá, J. C. (2006). The Flysch Trough thrust imbricate (Betic Cordillera): A key element of the Gibraltar Arc orogenic wedge. *Tectonics*, 25(6).
- Lustrino, M., Duggen, S., & Rosenberg, C. L. (2011). The Central-Western Mediterranean: anomalous igneous activity in an anomalous collisional tectonic setting. *Earth-Science Reviews*, 104(1-3), 1-40.
- Maldonado, A., Somoza, L., & Pallarés, L. (1999). The Betic orogen and the Iberian–African boundary in the Gulf of Cadiz: geological evolution (central North Atlantic). *Marine Geology*, 155(1-2), 9-43.
- Manzi, V., Roveri, M., Gennari, R., Bertini, A., Biffi, U., Giunta, S., ... & Riva, A. (2007). The deep-water counterpart of the Messinian Lower Evaporites in the Apennine foredeep: the Fananello section (Northern Apennines, Italy). *Palaeogeography, Palaeoclimatology, Palaeoecology*, 251(3-4), 470-499.
- Manzi, V., Gennari, R., Hilgen, F., Krijgsman, W., Lugli, S., Roveri, M., & Sierro, F. J. (2013). Age refinement of the Messinian salinity crisis onset in the Mediterranean. *Terra Nova*, 25(4), 315-322.
- Martin, J., Ortega-Huertas, M., & Torres-Ruiz, J. (1984). Genesis and evolution of strontium deposits of the Granada Basin (southeastern Spain): evidence of diagenetic replacement of a stromatolite belt. *Sedimentary geology*, 39(3-4), 281-298.
- Martín, J. M., Braga, J. C., & Betzler, C. (2001). The Messinian Guadalhorca corridor: the last northern, Atlantic–Mediterranean gateway. *Terra Nova*, 13(6), 418-424.
- Martín, J. M., Braga, J. C., Aguirre, J., & Puga-Bernabéu, Á. (2009). History and evolution of the North-Betic Strait (Prebetic Zone, Betic Cordillera): a narrow, early Tortonian, tidal-dominated, Atlantic–Mediterranean marine passage. *Sedimentary Geology*, 216(3-4), 80-90.
- Martín, J. M., Puga-Bernabéu, Á., Aguirre, J., & Braga, J. C. (2014). Miocene Atlantic-

- Mediterranean seaways in the Betic Cordillera (Southern Spain).
- Martin-Algarra, A. (1987). Evolucion geologica alpina del contacto entre las Zonas Internas y las Zonas Externas de la Cordillera Betica [Ph. D. thesis]: Granada. Spain, University of Granada.
- Martínez-García, P., Soto, J. I., & Comas, M. (2011). Recent structures in the Alboran Ridge and Yusuf fault zones based on swath bathymetry and sub-bottom profiling: evidence of active tectonics. *Geo-Marine Letters*, 31(1), 19-36.
- Martínez-Martínez, J. M., Soto, J. I., & Balanyá, J. C. (2002). Orthogonal folding of extensional detachments: structure and origin of the Sierra Nevada elongated dome (Betics, SE Spain). *Tectonics*, 21(3).
- Martinsen, O. J., & Bakken, B. (1990). Extensional and compressional zones in slumps and slides in the Namurian of County Clare, Ireland. *Journal of the Geological Society*, 147(1), 153-164.
- Meckel III, L. D. (2010). Sand-Prone Submarine Mass-Transport Deposits: Reservoir Characteristics and Classification of an Underappreciated Deepwater Facies.
- Medialdea, T., Vegas, R., Somoza, L., Vázquez, J. T., Maldonado, A., Diaz-del-Rio, V., ... & Fernández-Puga, M. C. (2004). Structure and evolution of the "Olistostrome" complex of the Gibraltar Arc in the Gulf of Cádiz (eastern Central Atlantic): evidence from two long seismic cross-sections. *Marine Geology*, 209(1-4), 173-198.
- Michard, A., Chalouan, A., Feinberg, H., Goffé, B., & Montigny, R. (2002). How does the Alpine belt end between Spain and Morocco?. *Bulletin de la Société géologique de France*, 173(1), 3-15.
- Michard, A., Saddiqi, O., Chalouan, A., & de Lamotte, D. F. (Eds.). (2008). Continental evolution: The geology of Morocco: Structure, stratigraphy, and tectonics of the Africa-Atlantic-Mediterranean triple junction (Vol. 116). Springer.
- Middleton, G. V., & Hampton, M. A. (1973). Part I. Sediment gravity flows: mechanics of flow and deposition.
- Miramontes, E., Eggenhuisen, J. T., Jacinto, R. S., Poneti, G., Pohl, F., Normandeau, A., ... & Hernández-Molina, F. J. (2020). Channel-levee evolution in combined contour current-turbidity current flows from flume-tank experiments. *Geology*, 48(4), 353-357.
- Monié, P., Torres-Roldán, R. L., & García-Casco, A. (1994). Cooling and exhumation of the western Betic Cordilleras,  $^{40}\text{Ar}/^{39}\text{Ar}$  thermochronological constraints on a collapsed terrane. *Tectonophysics*, 238(1-4), 353-379.
- Morley, C. K. (1988). The tectonic evolution of the Zoumi Sandstone, western Moroccan Rif. *Journal of the Geological Society*, 145(1), 55-63.
- Morley, C. K. (1992). Tectonic and sedimentary evidence for synchronous and out-of-sequence thrusting, Larache-Acilah area, Western Moroccan Rif. *Journal of the Geological Society*, 149(1), 39-49.
- Mosher, D. C., Campbell, D. C., Gardner, J. V., Piper, D. J. W., Chaytor, J. D., & Rebesco, M. (2017). The role of deep-water sedimentary processes in shaping a continental margin: The Northwest Atlantic. *Marine Geology*, 393, 245-259.
- Mulder, T., & Cochonat, P. (1996). Classification of offshore mass movements. *Journal of Sedimentary research*, 66(1), 43-57.
- Mulder, T., Faugères, J. C., & Gonthier, E. (2008). Mixed turbidite-contourite systems. *Developments in Sedimentology*, 60, 435-456.
- Mulder, T. (2011). Gravity processes and deposits on continental slope, rise and abyssal plains. In *Developments in Sedimentology* (Vol. 63, pp. 25-148). Elsevier.
- Munk, W., & Wunsch, C. (1998). Abyssal recipes II: Energetics of tidal and wind mixing. *Deep Sea Research Part I: Oceanographic Research Papers*, 45(12), 1977-2010.
- Murray, J., & Renard, A. F. (1891). Report on deep-sea deposits based on the specimens collected during the voyage of HMS Challenger in the years 1872 to 1876. HM Stationery Office.
- Mutti, E., & Ricci Lucchi, F. (1975). Turbidite Facies and Facies Associations. In *Examples of Turbidite Facies and Facies Associations from Selected Formations of the Northern Apennines*. *Sedimentology*, Nice France, field trip guidebook All, 21-36.
- Mutti, E., Tinterri, R., Benevelli, G., di Biase, D., & Cavanna, G. (2003). Deltaic, mixed and turbidite sedimentation of ancient foreland basins. *Marine and Petroleum Geology*, 20(6-8), 733-755.

- Nardin, T. R., Hein, F. J., Gorsline, D. S., & Edwards, B. D. (1979). A review of mass movement processes sediment and acoustic characteristics, and contrasts in slope and base-of-slope systems versus canyon-fan-basin floor systems.
- Nemec, W., & Steel, R. (1984). Alluvial and coastal conglomerates: their significant features and some comments on gravelly mass-flow deposits.
- Nichols, G. (2009). *Sedimentology and stratigraphy*. John Wiley & Sons.
- NOAA, National Ocean Services, U.S. Department of Commerce (2018), How much of the ocean have we explored? <https://oceanservice.noaa.gov/facts/exploration.html>
- Paulat, M., Lüdmann, T., Betzler, C., Eberli, G. P. (2019). Neogene palaeoceanographic changes recorded in a carbonate contourite drift (Santaren Channel, Bahamas). *Sedimentology*, 66(4), 1361-1385.
- Pérez-Asensio, J. N., Aguirre, J., Schmiedl, G., & Civis, J. (2012). Impact of restriction of the Atlantic-Mediterranean gateway on the Mediterranean Outflow Water and eastern Atlantic circulation during the Messinian. *Paleoceanography*, 27(3).
- Pickering, K. T. (1979). Possible retrogressive flow slide deposits from the Kongsfjord Formation: a Precambrian submarine fan, Finnmark, N. Norway. *Sedimentology*, 26(2), 295-306.
- Pickering, K. T., Hiscott, R. N., & Hein, F. J. (1989). *Deep-marine environments: clastic sedimentation and tectonics*. Allen & Unwin Australia.
- Pickering, K. T., & Hiscott, R. N. (2016). *Deep Marine Systems. Processes, Deposits, Environments, Tectonics and Sedimentation*, 657 pp., AGU and Wiley.
- Platt, J. P., & Vissers, R. L. M. (1989). Extensional collapse of thickened continental lithosphere: A working hypothesis for the Alboran Sea and Gibraltar arc. *Geology*, 17(6), 540-543.
- Platt, J. P., Soto, J. I., Whitehouse, M. J., Hurford, A. J., & Kelley, S. P. (1998). Thermal evolution, rate of exhumation, and tectonic significance of metamorphic rocks from the floor of the Alboran extensional basin, western Mediterranean. *Tectonics*, 17(5), 671-689.
- Platt, J. P., Allerton, S., Kirker, A., Mandeville, C., Mayfield, A., Platzman, E. S., & Rimi, A. (2003). The ultimate arc: Differential displacement, oroclinal bending, and vertical axis rotation in the External Betic-Rif arc. *Tectonics*, 22(3).
- Platzman, E., Platt, J. P., Kelley, S. P., & Allerton, S. (2000). Large clockwise rotations in an extensional allochthon, Alboran Domain (southern Spain). *Journal of the Geological Society*, 157(6), 1187-1197.
- Price, J. F., & Baringer, M. O. N. (1994). Outflows and deep water production by marginal seas. *Progress in Oceanography*, 33(3), 161-200.
- Rahmstorf, S. (2006). Thermohaline ocean circulation. *Encyclopedia of quaternary sciences*, 5.
- Reading, H. G. (1996). *Sedimentary Environments: Processes, Facies and Stratigraphy*. 3rd. Edition. Blackwell Science. Oxford.
- Rebesco, M. (2005). *Contourites*//Encyclopedia of Geology/Selley, RC, Cocks, LRM, Plimer, IR.
- Rebesco, M., & Camerlenghi, A. (Eds.). (2008). *Contourites*. Elsevier.
- Rebesco, M., Hernández-Molina, F. J., Van Rooij, D., Wåhlin, A. (2014). Contourites and associated sediments controlled by deep-water circulation processes: state-of-the-art and future considerations. *Mar. Geol.*, 352, 111-154.
- Reid, J. L. (1979). On the contribution of the Mediterranean Sea outflow to the Norwegian-Greenland Sea. *Deep Sea Research Part A. Oceanographic Research Papers*, 26(11), 1199-1223.
- Rodrigues, S., Hernández-Molina, F. J., & Kirby, A. (2021). A late Cretaceous mixed (turbidite-contourite) system along the Argentine margin: paleoceanographic and conceptual implications. *Marine and Petroleum Geology*, 123, 104768.
- Rogerson, M., Rohling, E. J., Bigg, G. R., Ramirez, J. (2012). Paleoceanography of the Atlantic-Mediterranean exchange: Overview and first quantitative assessment of climatic forcing. *Rev. Geophys.*, 50(2), RG2003.
- Rosenbaum, G., Lister, G. S., & Duboz, C. (2002). Reconstruction of the tectonic evolution of the western Mediterranean since the Oligocene. *Journal of the Virtual Explorer*, 8, 107-130.
- Roveri, M., Flecker, R., Krijgsman, W., Lofi, J., Lugli, S., Manzi, V., ... & Govers, R. (2014a). The Messinian Salinity Crisis: past and

- future of a great challenge for marine sciences. *Marine Geology*, 352, 25-58.
- Ryan, W.B.F. et al. Initial reports of the Deep-Sea Drilling Project Vol. 13 (US Govt Printing Office, Washington, 1973).
- Ryan, W. B. (2009). Decoding the Mediterranean salinity crisis. *Sedimentology*, 56(1), 95-136.
- Saadi, S. E. M., Hiladi, E.A., and Boudda, A. (1980). Editions du Service Géologique du Maroc. Notes et Memoires N°. Maquette achevée en 1975).
- Saint Martin, J. P., & Cornee, J. J. (1996). The Messinian reef complex of Melilla, northeastern Rif, Morocco.
- Samara, F., Benyaich, A., Dakki, M., Hcaine, M., & Bally, A. W. (1997). Origine et inversion des bassins miocènes supra-nappes du Rif Central (Maroc) Étude de surface et de subsurface: Exemple des Bassins de Taouinate et de Tafrannt. *Geodinamica Acta*, 10(1), 30-40.
- Sani, F., Zizi, M., & Bally, A. W. (2000). The Neogene–Quaternary evolution of the Guercif Basin (Morocco) reconstructed from seismic line interpretation. *Marine and Petroleum Geology*, 17(3), 343-357.
- Sansom, P. (2018). Hybrid turbidite–contourite systems of the Tanzanian margin. *Petroleum Geoscience*, 24(3), 258-276.
- Selli, R. (1954). Il bacino del Metauro: Giorn. Geol., set, 2, 1-268.
- Selli, R. (1960). Il Messiniano Mayer-Eymar 1867. Proposta di un neostratotipo. *Giornale di Geologia*, 28(2), 1-33.
- Serra-Kiel, J., Martín-Martín, M., El Mamoune, B., Martín-Algarra, A., JA, M. P., Tosquella i Angrill, J., ... & Serrano, F. (1998). Bioestratigrafía y litoestratigrafía del Paleógeno del área de Sierra Espuña (Cordillera Bética oriental, SE de España). *Acta Geologica Hispanica*, 1998, vol. 31, num. 1-3, p. 161-182.
- Serra, N., Ambar, I., & Boutov, D. (2010). Surface expression of Mediterranean Water dipoles and their contribution to the shelf/slope–open ocean exchange. *Ocean Science*, 6(1), 191-209.
- Shanmugam, G. (2006). Deep-water processes and facies models: Implications for sandstone petroleum reservoirs (Vol. 5). Elsevier.
- Shanmugam, G. (2008). Deep-water bottom currents and their deposits. *Developments in sedimentology*, 60, 59-81.
- Shanmugam, G. (2012). New perspectives on deep-water sandstones: Origin, recognition, initiation, and reservoir quality (Vol. 9). Elsevier.
- Shanmugam, G. (2017). The contourite problem. In *Sediment provenance*, 183-254. Elsevier.
- Shanmugam, G. (2017b). Contourites: Physical oceanography, process sedimentology, and petroleum geology. *Petroleum exploration and development*, 44(2), 183-216.
- Sierro, F. J., Flores, J. A., Francés, G., Vazquez, A., Utrilla, R., Zamarréño, I., ... & Barcena, M. A. (2003). Orbitally-controlled oscillations in planktic communities and cyclic changes in western Mediterranean hydrography during the Messinian. *Palaeogeography, Palaeoclimatology, Palaeoecology*, 190, 289-316.
- Simon, D., & Meijer, P. T. (2017). Salinity stratification of the Mediterranean Sea during the Messinian crisis: A first model analysis. *Earth and Planetary Science Letters*, 479, 366-376.
- Simon, D., Marzocchi, A., Flecker, R., Lunt, D. J., Hilgen, F. J., & Meijer, P. T. (2017). Quantifying the Mediterranean freshwater budget throughout the late Miocene: New implications for sapropel formation and the Messinian Salinity Crisis. *Earth and Planetary Science Letters*, 472, 25-37.
- Sinclair, H. D. (1997). Tectonostratigraphic model for underfilled peripheral foreland basins: An Alpine perspective. *Geological Society of America Bulletin*, 109(3), 324-346.
- Soto, J. I., & Platt, J. P. (1999). Petrological and structural evolution of high-grade metamorphic rocks from the floor of the Alboran Sea basin, western Mediterranean. *Journal of Petrology*, 40(1), 21-60.
- Southard, J. B., & Mackintosh, M. E. (1981). Experimental test of autosuspension. *Earth Surface Processes and Landforms*, 6(2), 103-111.
- Spakman, W., & Wortel, R. (2004). A tomographic view on western Mediterranean geodynamics. In *The TRANSMED atlas. The Mediterranean region from crust to mantle* (pp. 31-52). Springer, Berlin, Heidelberg.
- Stefano, L., Vinicio, M., Marco, R., & Charlotte, S. B. (2010). The Primary Lower Gypsum in the Mediterranean: a new facies interpretation for the first stage of the



- Messinian salinity crisis. *Palaeogeography, Palaeoclimatology, Palaeoecology*, 297(1), 83-99.
- Stow, D. A. V. (1985). Deep-sea clastics: where are we and where are we going?. Geological Society, London, Special Publications, 18(1), 67-93.
- Stow, D. A., & Wetzel, A. (1990). Hemiturbidite: a new type of deep-water sediment. In *Proceedings of the ocean drilling program, scientific results (Vol. 116, pp. 25-34)*. College Station, TX: Ocean Drilling Program.
- Stow, D.A.V., Reading, H.G. & Collinson, J.D. (1996). *Deep seas, Sedimentary Environments: Processes, Facies and Stratigraphy*. 3rd Edition - (Reading, H.G., 1996). Blackwell Science. Oxford
- Stow, D. A., & Tabrez, A. R. (1998). Hemipelagites: processes, facies and model. *Geological Society, London, Special Publications*, 129(1), 317-337.
- Stow, D. A.V., Faugères, J. C., Howe, J. A., Pudsey, C. J., & Viana, A. R. (2002a). Bottom currents, contourites and deep-sea sediment drifts: current state-of-the-art. *Geological Society, London, Memoirs*, 22(1), 7-20.
- Stow, D. A. V., Hunter, S., Wilkinson, D., & Hernández-Molina, F. J. (2008). The nature of contourite deposition. *Developments in sedimentology*, 60, 143-156.
- Stow, D. A. V., & Faugères, J. C. (2008). Contourite facies and the facies model. *Developments in Sedimentology*, 60, 223-256.
- Stow, D. A., Hernández-Molina, F. J., Llave, E., Sayago-Gil, M., Díaz del Río, V., & Branson, A. (2009). Bedform-velocity matrix: the estimation of bottom current velocity from bedform observations. *Geology*, 37(4), 327-330.
- Stow, D., & Smillie, Z. (2020). Distinguishing between Deep-Water Sediment Facies: Turbidites, Contourites and Hemipelagites. *Geosciences*, 10(2), 68.
- Suter, G. (1980). Carte géologique de la Chaîne Rifaine, échelle 1: 500.000. Ministère de l'Énergie et des Mines du Maroc, Direction de la Géologie, Rabat. Notes Mem Serv Geol Maroc 245a.
- Taltasse, P. (1953). Recherches géologiques et hydrogéologiques dans le Bassin lacustre de Fès-Meknè s. Notes Mem Serv. Géol Maroc 115:1-300
- Turner, S. P., Platt, J. P., George, R. M. M., Kelley, S. P., Pearson, D. G., & Nowell, G. M. (1999). Magmatism associated with orogenic collapse of the Betic-Alboran domain, SE Spain. *Journal of Petrology*, 40(6), 1011-1036.
- Topper, R. P. M., Flecker, R., Meijer, P. T., & Wortel, M. J. R. (2011). A box model of the Late Miocene Mediterranean Sea: Implications from combined 87Sr/86Sr and salinity data. *Paleoceanography*, 26(3).
- Tucker, M. E. (1996). *The Field Description of Sedimentary Rocks*. Open University Press.
- Tulbure, M. A., Capella, W., Barhoun, N., Flores, J. A., Hilgen, F. J., Krijgsman, W., ... & Yousfi, M. Z. (2017). Age refinement and basin evolution of the North Rifian Corridor (Morocco): No evidence for a marine connection during the Messinian Salinity Crisis. *Palaeogeography, Palaeoclimatology, Palaeoecology*, 485, 416-432.
- Vera, J. A., Molina, J. M., Montero, P., & Bea, F. (1997). Jurassic guyots on the Southern Iberian Continental Margin: a model of isolated carbonate platforms on volcanic submarine edifices. *Terra Nova*, 9(4), 163-166.
- Vera, J. A. (2000). El Terciario de la Cordillera Bética: estado actual de conocimientos. *Rev. Soc. Geol. España*, 13(2), 345-373.
- Vera, J. A. (Ed.). (2004). *Geología de España*. IGME.
- Vergés, J., & Fernández, M. (2012). Tethys–Atlantic interaction along the Iberia–Africa plate boundary: The Betic–Rif orogenic system. *Tectonophysics*, 579, 144-172.
- Viana, A. R., & Rebesco, M. (Eds.). (2007). *Economic and palaeoceanographic significance of contourite deposits*. Geological Society of London.
- Viana, A. R. (2008). Economic relevance of contourites. *Dev. Sedimentol.*, 60, 491-510.
- Vilas, L., Martín-Chivelet, J., & Arias, C. (2003). Integration of subsidence and sequence stratigraphic analyses in the Cretaceous carbonate platforms of the Prebetic (Jumilla–Yecla Region), Spain. *Palaeogeography, Palaeoclimatology, Palaeoecology*, 200(1-4), 107-129.
- Vissers, R. L. M., & Meijer, P. T. (2012). Iberian plate kinematics and Alpine collision in the Pyrenees. *Earth-Science Reviews*, 114(1-2), 61-83.
- Wählin, A. K., & Cenedese, C. (2006). How entraining density currents influence the stratification in a one-dimensional ocean basin. *Deep Sea Research Part II: Topical*

- Studies in Oceanography, 53(1-2), 172-193.
- Walton, E. K. (1967). The sequence of internal structures in turbidites. *Scottish Journal of Geology*, 3(2), 306-317.
- Wells, M. G., & Wettlaufer, J. S. (2005). Two-dimensional density currents in a confined basin. *Geophysical & Astrophysical Fluid Dynamics*, 99(3), 199-218.
- Wernli, R. (1988). *Micropaléontologie du Néogène post-nappes du Maroc septentrional et description systématique des foraminifères planctoniques*. Editions du Service géologique du Maroc.
- Wildi, W. (1983). La chaîne tello-rifaine (Algérie, Maroc, Tunisie): structure, stratigraphie et évolution du Trias au Miocène. *Revue de géographie physique et de géologie dynamique*, 24(3), 201-297.
- Wynn, R. B., Masson, D. G., Stow, D. A., & Weaver, P. P. (2000). The Northwest African slope apron: a modern analogue for deep-water systems with complex seafloor topography. *Marine and Petroleum Geology*, 17(2), 253-265.
- Zachariasse, W. J. (1975). *Planktonic foraminiferal biostratigraphy of the Late Neogene of Crete (Greece)* (Doctoral dissertation, Utrecht University).
- Zizi, M. (1996). *Triassic-Jurassic extensional systems and their Neogene reactivation in northern Morocco (the Rides pré-rifaines and Guercif basin)* (Doctoral dissertation).
- Zouhri, L., Lamouroux, C., Vachard, D., & Pique, A. (2002). Evidence of flexural extension of the Rif foreland: The Rharb-Mamora basin (northern Morocco). *Bulletin de la Société Géologique de France*, 173(6), 509-514.

# *Chapter III*

## **Methodology and Data**

This chapter outlines the methodologies used in this research project and presents the data acquired.

## 1. Introduction and approach

The Gulf of Cadiz is the best studied and most well-known contourite depositional system to date. The problem however with studying active deep-water settings is that they are relatively inaccessible. As a result, sedimentary data acquired is limited to, in the best case; cores, reflection seismic data and ROV footage (*e.g. Fauget et al., 1999; Llave et al., 2001; Rebesco et al., 2001; Stow et al., 2009, 2013; Roque et al., 2012; Hernández-Molina et al., 2014a*). Although a significant amount of information is obtained from such studies and their acquired data sets, detailed sedimentary information regarding bedform morphologies, bedforms, sedimentary stacking patterns and lateral facies changes are not properly recognized. Furthermore, modern systems mostly comprise unconsolidated sediment. These unconsolidated sediments, particularly for sandy deposits, are often not recovered by cores, further hampering their understanding (*Expedition 339 scientists, 2012; Brackenridge et al., 2018; de Castro et al., 2021*).

The Gulf of Cadiz contourite depositional system is mainly formed by the outflow of Mediterranean overflow water into the Atlantic (*Llave et al., 2007*). A similar system and thus a similar depositional setting occurred during the Late Miocene, not in the Gibraltar Strait but in the Rifian Corridor. Remnants of this bottom current controlled corridor are exposed in outcrops in the Fes-Mekness region (*e.g. De Weger, 2015; Capella et al., 2017a*).

By conducting a field-based study in the Late Miocene record of the Rifian Corridor, which thus forms a good analogue for the Gulf of Cadiz CDS and vice versa, a broader dataset is acquired which enables answering questions left by the limitations of only studying modern systems. Furthermore, the research conducted allows the construction of facies models related to different aspects of contourite depositional systems and the changes between them.

## 2. Literature studies

Previously numerous, geology related studies have been carried out in the study area and the region surrounding it. These studies covered many aspects of Earth sciences that lead to a better understanding of the Late Miocene geological and hydrological framework relevant for this study. The main studies are related to, dating of the rock record, structural geology, sedimentology but also oceanography and physical modelling.

The published work of these studies was used to form a geological and hydrological framework by means of a literature study. The newly acquired data was analyzed in respect to- and applied to this framework. Newly obtained results that deviated from previous interpretations or that were not in line with previous interpretations were detailly revised and discussed but observations herein are regarded decisive as they are based on new observations.

Besides literature studies linking directly to the study area, numerous other topics and areas have been investigated to provide the needed background knowledge and comparison to the objective of this study. Topics that were widely studied mainly related to: contourites, gateways, deep-water sedimentation and processes, oceanography, hydrodynamic behavior of water-masses and tides, tectonic evolution of foreland basins and, on a smaller scale, sediment composition and provenance.

### ***3. Fieldwork and analysis***

*- The Methodology of analyzing sedimentary rocks, recording data an interpreting them in terms of processes and environments. The value of the interpretations that comes from the results is determined by the quality of the data collected -*

*Gary Nichols, 2009*

Sedimentology is the interpretation of sediments and sedimentary rocks in terms of processes of transport and deposition and how they are distributed in space and time in sedimentary environments. This sort of sedimentological analysis requires data which in this case is collected from exposures of rocks. A satisfactory analysis of sedimentary environments and their stratigraphic context requires a sound basis of field data that is predominantly acquired by sedimentological fieldwork (*Nichols, 2009*). Sedimentological fieldwork forms the cornerstone of this thesis.

Prior to detailed data collection a regional reconnaissance mission was carried out in, and covering most of, the study area (Figs. 3.1, 3.2 and 3.3). During this reconnaissance several previously documented outcrops, *Haricha, Madhouma, Sidi Chahed, Lemda, Moulay Yacoub, Sidi Harazem, El Adergha, Ain Kansera, Bir Tam Tam and Taza (Taza-Guercif Basin)* were visited and several new outcrops were discovered; *Bel Amri, Msagra, Kirmta and Fes-north* (Table 3.1 – Figs 3.1, 3.2 and 3.3). Based on the location, accessibility, exposure and sedimentary facies, the *Sidi Chahed, Kirmta, Fes-north* and *El Adergha* outcrops were

deemed most scientifically valuable for this research project, considering the limited duration of the project.

Data collection of the four selected outcrops started with the construction of graphic sedimentary logs. These logs are a graphical method to represent the hierarchical series of beds of sediment and sedimentary rocks. Although many different schemes are used to construct these logs, the format used herein closely resembles that of *Tucker (1996)*, where the focus lied on; relief, grain-size, internal bedding structure, sedimentary structures, composition, and additional descriptions. Furthermore, data acquired such as samples, photographs, transport direction and fossil content were carefully noted.

The logs were constructed on a variety of different scales. The scales depended both on the size of the sedimentary beds and structures as well as on the amount of detailed required. As this study aims to identify contourite recognition criteria, in general the scale required cm-scale observations and thus the scale of the log needed to be as such that these observations could be incorporated.

Additional to sedimentary logging field sketches were made to outline the larger morphological features. Within these drawings the location from where the sedimentary log was obtained was presented. These sketches are important to pinpoint the sedimentary succession of the log within these morphological features. In this way, facies and facies stacking patterns could be associated to larger scale features.



**Figure 3.1.** Satellite image of the study area (derived from ZOOM Earth). The study area is located in northern Morocco and comprises the cities (from west to east); Sidi Kacem, Meknes, Fes and Taza. The pin-marks indicate the location of prominent late Miocene outcrops. Numbers are associated to Table 1. The yellow pin-marks are indicative for newly discovered, likely late Miocene outcrops that have not been properly studied but have good potential for contourite studies. The red pin-marks are indicative for outcrops relevant for this study, but which were not considered vital for this research project. The green pin-marks indicate the location of the main outcrops used in this research project.





*Figure 3.2. Overview of outcrops; (1) Bel Amri, (2) Msagra, (3) Haricha, (4) Madhouma, (5) Sidi Chahed, and (6) Kirmia. The numbers relate to both Figure 1 and Table 1. The panels on the left comprise satellite images (derived from ZOOM Earth), and the panels on the right represent pictures of the associated outcrop.*





**Figure 3.3.** Overview of outcrops; (7) Lemda, (8) Moulay Yacoub, (9) Fes-north, (10) Sidi Harazem, (11) El Adergha, and (12) Ain Kansera. The numbers relate to both Figure 1 and Table 1. The panels on the left comprise satellite images (derived from ZOOM Earth), and the panels on the right represent pictures of the associated outcrop.



Table 3.1. Overview of visited outcrops. Numbers correspond to Figure 3.1. The table provides the location, general description, potential for contourite research, the data collected, publications on outcrops and the ages, depositional domains and remarks.

Nr	Name and location	General description	Potential for contourite research				Data collected	Publications	Age, depositional domain, and remarks
			New	Low	Mod	High			
1	<b>Bel Amri</b> 34.088070 5.948792	The outcrop measures roughly 1 km in width and its well exposed western, N-S striking flank is 70 m high. The lithology consists of blue marls followed by a semi gradational transition to massive and likely cross-stratified sandstone					General observations	Based on the Geological map by <i>Saadi et al. (1980)</i> this outcrop is aged between the Tortonian to Pliocene. Its location on the western foot of the Prerif Ridges in the Gharb basin, along with its sedimentary facies indicate a possible contouritic origin.	
2	<b>Msagra</b> 34.067767 5.878186	This outcrop has a Badlands appearance consisting of blue marls with sandstone intercalations. The sandstones might represent turbidite and/or sandy contourite deposits belonging to channel-drift transitional and drift elements.					General observations	Based on the Geological map by <i>Saadi et al. (1980)</i> this outcrop is Tortonian to Messinian in age. Its location on the western foot of the Prerif Ridges in the Gharb basin, along with its sedimentary facies indicate a possible contouritic origin.	
3	<b>Haricha</b> 34.286064 5.644314	Located on top of the accretionary wedge and consists of, from bottom to top, a turbidite dominated succession, blue marls, an in abundance upwards increasing turbidite succession followed by apparent massive, well sorted sandstones that, upon closer examination show cross-stratification and has a possible contouritic origin.					General observations and lacquer-peels	<i>SCP/ERICO report, 1991</i> <i>De Weger, 2015 (MSc)</i> <i>Capella et al., 2017a</i> <i>Capella, 2017 (Thesis)</i> <i>Capella et al., 2018</i>	Dated between 7.25 and 6.45 Ma deposited in a shelf-slope transitional domain (150 – 300 m water depth).
4	<b>Madhouma</b> 33.915372 5.315206	Basal massive, very clayey blue marlstones which grade upwards to sandy marlstones. In the western flank these marlstones are truncated by conglomeratic, lacustrine limestones whereas in the eastern flank the marlstones are truncated by up to 30 m thick sandstones deposited in shallow marine to surficial environments.					General observations	<i>Wernli, 1988</i> <i>Barbieri and Ori, 2000</i> <i>De Weger, 2015 (MSc)</i> <i>Capella, 2017 (Thesis)</i> <i>Capella et al., 2018</i>	Dated between 7.25 and 6.35 Ma deposited in a shallowing upward sequence from middle shelf to continental domains (150 – 0 m water depth).
5	<b>Sidi Chahed</b> 34.102576 5.300959	Formerly referred to as the Ben Allou outcrop in the works of <i>Capella</i> . This outcrop consists of blue marls, sandy marlstones and three sandstone units. The deposits are interpreted as remnants of a contourite channel system.					Logs - > 370 m Thin sections - 62 Biostrat. samples - 5 Petrophys. samples - 1 XRF measurements - 380 XRD measurements - 44 MS measurements - 511	<i>Capella et al., 2017a</i> <i>Capella, 2017 (Thesis)</i> <i>Capella et al., 2018</i> <i>De Weger et al., 2019</i> <i>Miguez-Salas and Rodriguez-Tovar, 2020</i> <i>De Weger et al., 2020</i> <i>Miguez-Salas et al., 2020, 2021</i> <i>De Weger et al., 2021b</i>	Dated between 7.80 and 7.51 Ma deposited in an outer shelf to upper bathyal domain (150 – 400 m water depth).

6	<b>Kirmia (Kirmta)</b> 34.170706 5.238689	This outcrop was discovered in 2017 and, similarly as the Sidi Chahed outcrop consists of blue marls, sandy marlstones and three sandstone units. The deposits are interpreted as remnants of a contourite channel system					Logs - > 200 m Thin sections - 7 Biostrat. samples - 12 XRF measurements - 105 XRD measurements - 39 MS measurements - 531	<i>De Weger et al., 2019</i> <i>De Weger et al., 2020</i> <i>De Weger et al., 2021b</i> <i>Miguez-Salas et al., 2021</i>	Dated between 7.80 and 7.51 Ma in an outer shelf to upper slope depositional domain (150 – 300 m water depth).
7	<b>Lemda</b> 34.238377 5.221680	Located on top of the accretionary wedge, dominated by the presence of blue marlstones, with an upward increasing sand content and sandstone intercalations. <i>Capella (2017)</i> and <i>Capella et al. (2018)</i> indicated that the high percentages of excellently preserved planktonic foraminifera are typical of environments swept by permanent bottom currents.					General observations	<i>Capella, 2017 (Thesis)</i> <i>Capella et al., 2018</i>	Dated between 7.80 and 7.51 Ma deposited in shallowing upward upper bathyal to shelf domains (500 – 150 m water depth). This outcrop has poor surficial exposure, but the presence of cross-stratification and possible bi-gradational sequences make them suitable for contourite research.
8	<b>Moulay Yacoub</b> 34.112359 5.169416	The composite Moulay Yacoub section is roughly 800 m thick consisting of mud-dominated deposits with irregular intercalations of sandstones with a turbiditic origin.					General observations	<i>Wernli, 1988</i> <i>SCP/ERICO report, 1991</i> <i>Capella, 2017 (Thesis)</i> <i>Capella et al., 2018</i>	Dated between 7.92 and 6.35 Ma deposited in upper bathyal, shallowing upwards to middle shelf domains.
9	<b>Fes-north</b> 34.076207 4.964352	This outcrop was discovered in 2017 and consists of a 12 m thick sandstone dominated succession truncating blue marls. The sandstones have been deposited gravitational processes and contour currents.					Logs - > 20 m Thin sections - 2 Biostrat. samples - 5	<i>De Weger et al., 2021a</i>	Dated between 7.51 and 7.28 Ma deposited in the upper slope. This outcrop is relatively small and is recommended to be investigated further.
10	<b>Sidi Harazem</b> 34.045989 4.853723	The Sidi Harazem outcrop mainly consists of marlstones and sandstones of which the latter are interpreted as turbidites.					General observations	<i>Capella et al., 2017a</i> <i>Capella, 2017 (Thesis)</i> <i>Miguez-Salas et al., 2021</i>	Dated between 7.80 and 7.51 Ma deposited in the upper slope (250 – 400 m water depth).
11	<b>El Adergha</b> 34.076427 4.861719	The El Adergha outcrop consists of a lower, bleu marlstone sequence, and an upper, sandstone dominated succession with a thickness of roughly 30 meters. This section is interpreted as a relic of a contourite channel system.					Logs - > 60 m Thin sections - 6 Biostrat. samples - 3 XRF measurements - 104 XRD measurements - 39 MS measurements - 102	<i>Capella et al., 2017a</i> <i>Capella, 2017 (Thesis)</i> <i>Capella et al., 2018</i> <i>De Weger et al., 2019</i> <i>De Weger et al., 2021</i> <i>Miguez-Salas and Rodriguez-Tovar, 2020</i> <i>Miguez-Salas et al., 2020</i>	Dated between 7.35 and 7.25 Ma deposited in an upper-slope to outer shelf domain (300 – 150 m water depth).

12	<b>Ain Kansera</b> 34.126666 4.856640	Resting unconformably on the accretionary wedge is this 60-meter-thick outcrop. Bleu marlstones are present at the base, grading upwards to coarse grained, sandstone. The sandstones are interpreted to have formed in infralittoral environments.				General observations	<i>Capella et al., 2017a</i> <i>Capella, 2017 (Thesis)</i> <i>Capella et al., 2018</i> <i>Miguez-Salas et al., 2021</i>	Dated between 7.51 and 7.35 Ma deposited in inner shelf environments (100 – 15 m water depth).
13	<b>Bir Tam Tam</b> 34.032835 4.677842	This section consists of several, laterally and vertically limited sandstone outcrops (composite roughly 20 m) wedged within a silty marlstone successions. The heterolithic facies recognized are very similar to those of channel-drift transitional contourite elements as described herein.				General observations	<i>Capella, 2017 (Thesis)</i> <i>Capella et al., 2018</i>	Dated between 7.58 and 7.35 Ma deposited in outer shelf to upper bathyal environments. Despite the outcrops being of limited lateral and vertical exposure, due to the scientific advances made herein I recommend studying these outcrops in more detail.
14	<b>Taza</b> 34.285895 3.954915	The Taza outcrop, herein referred to as a representative for the Taza-Guercif basin, predominantly consists of marlstones with sandstone intercalations of turbiditic origin.				General observations	e.g. <i>Krijgsman et al., 1999 Krijgsman et al., 2000</i> <i>Gelati et al., 2000</i> <i>Pratt et al., 2016</i>	The Miocene Taza-Guercif basin fill succession predominantly consists of marlstones with turbiditic sandstone intercalations. Despite this basin being located eastward of the westward overflow at the Taza-Sill, this area might, although less likely, host evidence of contourite deposits

## 4. Biostratigraphic dating and water-depth estimates

The age of the rock formation studied, the Blue Marl Formation, has previously been relatively well constrained from the Middle- to Late Miocene. Furthermore, some of the sites studied have previously undergone biostratigraphic examination.

To complement the biostratigraphic dating and to date new sections, 28 additional samples were collected from blue marls surrounding the dominantly sandy, indurated sections. Utmost care had been taken to sample fresh, un-weathered material. This meant that exposed material needed to be excavated to uncover sediment not affected by the elements. Usually this led to removal of at least 50 cm of exposed marls.

The rock samples were sent to the University of Salamanca, Spain, where they were prepared and analysed by Prof. Dr. F.J. Sierro.

The biostratigraphic framework for these Late Miocene samples is mainly based on the quantitative changes of the planktic foraminifer assemblage and changes in the proportion of the species. The samples have been compared to the works of *Capella et al. (2017a)* to have a continuous stratigraphic succession. The biostratigraphic framework published in *Capella et al. (2017a)* and *Talbure et al. (2017)* has been used to date these samples based on quantitative changes in abundance of keeled and unkeeled *Globorotalids*, mainly *G. menardii* 4, abundant until 7.51 Ma, the interval between 7.51 and 7.35 Ma with very rare *G. menardii* 4 and 5, and *G. menardii* 5 which was abundant since 7.35 Ma.

The water-depth during deposition has been inferred based on the benthic foraminifera assemblages of the biostratigraphic samples, similarly as in the works of *Capella et al. (2017a)*. The specific assemblages and relative abundance of benthic-species were associated to depth ranges from literature (e.g. *Perez-Asensio et al., 2012; Capella et al., 2017a*). The mixed shallow- (e.g. *Lobatula, Elphidium, Ammonia, Discorbis, Nonion* and *Buoeanum*) and deep-water species (e.g. *Fombotia, Melonis, Gyroidina, Bulimina, Syphonina, Lagena, Globobulima Cibicidoides, Planulina, Uvigerina, Bolivina, Cibicidoides, Bolvina alata, Syphonina, Sphaeroidina, Lenticulina, Pullenia, Lagena, Dentalina, Cassidulina*) is considered to be the result of downslope transport. Due to downslope transport, the deeper-water species are most reliable in depositional depth estimates.

## *5. Petrography*

In total 20 hand-sized rock specimens were collected from sedimentary intervals where they were expected to contribute most to understanding the depositional history. The rock-specimen were carefully recovered from the sedimentary record, considering that they were not severely affected by the elements. The new samples collected are complementary to 59 samples collected during a reconnaissance mission in 2016. The additional samples were selected to cover the full variety of indurated rock compositions present in the sections. Fine-grained sediment or unconsolidated sediment was not collected for thin-section analysis as they would not survive transport. Samples collected for biostratigraphy were also analyzed for sedimentary composition, albeit less detailly.

Seventy-nine (x2) thin sections, 2 thin sections per sample, were realized by the geology technician at Royal Holloway University of London. One of each sample set was impregnated with dyed resin to highlight original porosity. All thin-sections were provided with glass coverslips and were examined under a Nikon Optiphot-pol petrographic microscope with integral Canon EOS-50D camera system. Modal analysis was carried out on eight of the samples by determining the composition at 300 points using a stepping stage and associated PETROG software. Grain-size analysis was conducted on the sand-grain (quartz and feldspar, not bioclasts and glauconite pellets etc.) population of one of the samples. One hundred grains were selected at random within the thin-section, and the longest axis of each was measured on the microscope graticule.

## *6. Grain-size analysis*

Grain-size analysis was conducted on a particular cored interval covering the bi-gradational interval in the El Adergha section. This interval was cored in an unconventional way. First the surface was cleaned to remove weathered material and to obtain a strait vertical surface. Grooves were created with chisels and hammers 10 cm apart and roughly 5-7 cm deep. These grooves accommodated a 1-m plastic cable tray. Once the tray was in position the rock surrounding the tray was carefully removed to reveal a continuous, 1m long, 9 cm wide and 5 cm thick core. In total 4 of these 1m cores were recovered, 2 times the bi-gradational interval. These cores was capped with the cable tray lid, wrapped in foil, and shipped to the Royal Holloway University of London. One of these 2-meter cored intervals was sampled for grain-size analysis. Nineteen samples measuring roughly 1 cm<sup>3</sup>

were shipped to the University of Bordeaux, EPOC laboratory (France), where grain-size measurements were conducted both on the bulk and a de-carbonated sample, using a Malvern Mastersizer S laser micro-granulometer. This device measured a grain-size range of 0.02 to 2000  $\mu\text{m}$  (clay to sand). A value of 1.33 was adopted as the particle refractive index.

## ***7. Geochemical and Magnetic susceptibility measurements***

*- The composition and physical properties of sedimentary rocks are to a large extent controlled by chemical processes during weathering, transport and during burial. We can not avoid studying chemical processes if we want to understand the physical properties of sedimentary rocks. Sediment transport and distribution of sedimentary facies is strongly influenced by the sediment composition such as the content of sand/clay ratio and the clay mineralogy. The primary composition is the starting point for the diagenetic processes during burial –*

*Knut Bjørlykke, 2010*

### **7.1 X-ray fluorescence**

The chemical composition of the rock was analyzed using the Olympus Vanta C hand-held XRF analyzer. These measurements, done directly on the rock surface, required fresh exposure of the rock. Fresh exposure was achieved by chiseling or grinding (portable grinder) away the surface layer of the rock record that was exposed to the elements. Generally, this meant that 2 – 5 cm of this surface was removed. Care was taken that the material sampled was not contaminated by the tools used. This was achieved by only measuring surfaces cleared by chips of the rock. The measurement time, or Geochem mode, was set to 2 minutes for each sample.

Correlation matrices were constructed to show the statistical relationship between individual normalized elements. Normalization was achieved by dividing the individual element counts by the total counts for each measurement.

The data was further subjected to standardization. As a result of standardization, a distribution of each variable is characterized by mean value = 0 and standard deviation = 1.

In order to visualize the data, the number of dimensions of the data set was decreased down to 3 using the principal component approach<sup>1</sup>. Different approaches were used for clustering to get the best result (for 2 and 3 clusters). The used algorithm of clustering is called Agglomerative clustering<sup>2</sup>.

The best results were achieved during the clustering of the data which dispersion was increased using the Principal Component Analysis (PCA). In this case the number of dimensions of the parameter space is equal to 5. The visualization of the results in 3D plot in this case is a projection of 5D parameter space on the 3D parameter space (see fig. in attachment).

<sup>1</sup><https://scikit-learn.org/stable/modules/decomposition.html#pca>

<sup>2</sup>[https://scikit-learn.org/stable/auto\\_examples/cluster/plot\\_agglomerative\\_clustering.html#sphx-glr-auto-examples-cluster-plot-agglomerative-clustering-py](https://scikit-learn.org/stable/auto_examples/cluster/plot_agglomerative_clustering.html#sphx-glr-auto-examples-cluster-plot-agglomerative-clustering-py)

## 7.2 X-ray diffraction

X-ray diffraction (XRD) patterns were collected for mineral identification and quantification. The mineral composition of samples has been measured using the TERRA Mobile XRD System, provided by the LLC “Olympus Moscow”. The surface (~ 5 – 10 cm) of the rock to be sampled was carefully removed using a chisel and a grinder to diminish the effect of surface weathering. Care was taken that the material sampled was not contaminated by the tools used. This was achieved by only measuring surfaces cleared by chips of the rock.

Sampling took place with a resolution of 50 cm. The samples were grinded using a purpose build portable grinding machine that was carefully cleaned between samples. After grinding, the samples were sieved through a 100-micron mesh. A portion of the resulting powder (15g per sample) was placed in a cuvette (sample holder) and subjected to the XRD analysis with the following parameters: step = 0.09, expositions = 50 and an analysis time of 15 minutes. The resulting raw data was processed using the Profex 3.1.3 software using a standard mineralogical database. Muscovite, illite and smectite were considered together as hydromicas.

### 7.3 Magnetic susceptibility

Magnetic Susceptibility measurements (MS) were performed using the Bartington MS3 system and the Bartington MS2E point surface sensor. Measurements were performed on the rock surface previously cleared for XRF sampling. The vertical sample resolution was either 5 or 20 cm. To avoid damaging the MS equipment, measurements were only made in relatively easily accessible parts of the outcrop.

## 8. *Identification of Ancient Contourites*

Since the identification of ancient contourite outcrops has proven problematic in the past (for references see Chapter II, Paragraph 5.4), one of the goals of this research project was to establish a work-flow which should benefit the recognition of contourites or bottom-current reworked deposits in outcrop. However, a workflow was already required to establish the contourite potential of the outcrops considered in this thesis. The workflow, or train of thought used in determining a possible contouritic origin of the outcrop deposits in northern Morocco is provided in figure 3.4.

The determination of contourite potential in outcrop heavily leans on the geological framework as recognition criteria (besides the bi-gradational model for fine grained contourites) are lacking. As such, first the depositional water depth has to be established to determine the possibility of water-stratification. Furthermore, the geological framework, might provide a setting in which bottom currents are likely, as was the case for the Rifian Corridor and the water exchange between the Atlantic and the Mediterranean. The second step requires knowledge of the processes that generate bottom currents; density driven currents, wind-driven currents, deep-water tidal currents and internal waves. Knowledge of these processes enables the establishment of what type of deposits and sedimentary structures that could have been formed. If the geological framework is such that bottom currents might have played a role in sedimentation, the deposits found need to be compared to well established facies for deep water deposits. If significant deviations from well established deep water facies models occur, a bottom current needs to be considered, taking in mind the dynamics of this current and its effect on the deposits studied. Newly established recognition criteria based on the findings of this study can be found in Chapters IV – XIII.



## GEOLOGICAL FRAMEWORK

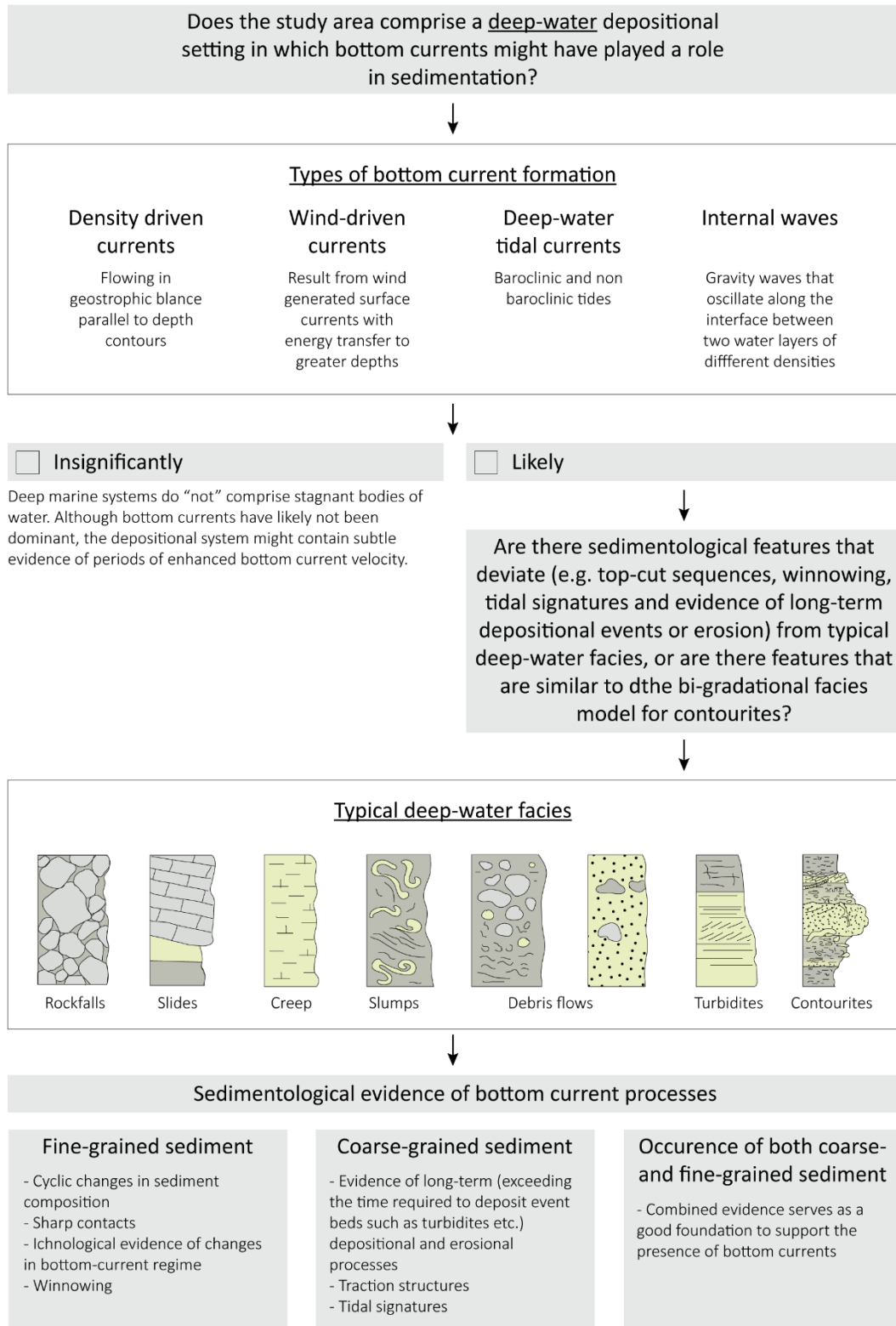


*Figure 3.4. Workflow diagram for the identification of contourite potential of outcrops. This workflow or train-of-thought was used to determine the possible contourite origin of outcrops studied for this research project.*

## *9. Reproducibility, precedence and justification*

The reproducibility of the sedimentary logs is dependent on the location of its construction. Significant lateral facies changes occur over short distances affecting the sedimentary stacking pattern to be observed in vertical succession. These lateral facies changes, however significant, should not result in drastically diverging sedimentary stacking patterns and their interpretation. Logging trajectories had been carefully chosen to accommodate a relatively easily accessible and vertically continuous sedimentary succession that can be back tracked. The starting point GPS-coordinates of each all logs can be provided upon request.

Samples and their location are provided in the sedimentary log, and as the sedimentary log is reproducible, samples can be obtained from the same interval. Care however has to be taken in obtaining material that is not affected by weathering.

Sample analysis was conducted as described in paragraph 3 (Fieldwork and analysis). If care is taken to reproduce analytical techniques and settings, the outcome of the analysis should be similar if not the same.

As the techniques described in paragraph 3 (Fieldwork and analysis) are considered standard techniques. Similar, if not the same techniques have been used for comparable research projects. Comparable endeavors in the study area also used the same techniques, acquiring similar data. Data interpretation however depends on the background knowledge, comparison to similar datasets and their previous interpretation, and general models created for those datasets. Although interpretation should follow grounded reasoning, a given dataset can result in deviating interpretations that usually evolve over time as the dataset and understanding of the data improves. As such, it is strongly believed that the work herein forms the most-up to date interpretation of the study area, based on a solid foundation with the addition of newly formed ideas and interpretations based on grounded reasoning.

## *10. Rationale*

No matter the type of research, alternative approaches are possible. These alternative approaches, in this case, however, mainly constitute the specialization of a certain research direction. As, herein, the main focus was to find, study, interpret, and generalize sedimentary

facies in the form of a facies model, the basic field techniques and samples used and described herein (sedimentary description of the rock record, thin-section analysis and dating of the rock record by means of biostratigraphy) form the most solid foundation to establish the goals initially set-out, taking into account the limited time of the research project.

Data that was additionally acquired; grain-size analysis, geochemical data and magnetic susceptibility data are considered supplementary. This supplementary data however significantly helps the interpretation of the studied rock record and forms a first step in more detailly determining contourite processes and facies, establishing a foundation for future studies.

The current dataset could be elaborated with a higher quantity of samples, additional samples for other analytical techniques and the data already acquired could be subjected to different analysis. However, in the scope of this research project, sufficient, trustworthy data was acquired to answer the research questions and to establish a framework for future studies. If in the future, a higher resolution dataset is required, this current dataset forms the cornerstone to determine the samples needed for these studies.

# *Results*

## *Chapters IV – VII*

### **Results**

These chapters contain the results of this research project. Chapter IV consists of the first article that was published in *GEOLOGY* (2020), titled: “Late Miocene contourite channel reveals intermittent overflow behaviour”. Chapter V contains the second article published in *SEDIMENTOLOGY* (2021), titled: “Contourite depositional system after the exit of a strait: case study from the late Miocene Rifian Corridor, Morocco”. Chapter VI consists of a discussion article to a paper published by Beelen et al. (2020), titled: “Tide-dominated deltas responding to high-frequency sea-level changes, pre-Messinian Rifian Corridor, Morocco: DISCUSSION”. The fourth article, chapter VII, consists of the third full article that in its current state is ready to be submitted. This article is titled: “Sedimentary facies distribution within erosional and depositional contourite channels”. These chapters are followed by Chapter VIII which contains a synthesis of the results.

# *Chapter IV*

*Late Miocene contourite channel system reveals  
intermittent overflow behavior*

# Late Miocene contourite channel system reveals intermittent overflow behavior

Wouter de Weger, F. Javier Hernández-Molina, Rachel Flecker, Francisco J. Sierro, Domenico Chiarella, Wout Krijgsman, M. Amine Manar (2020)

Geology, 48(12), 1194-1199. <http://doi.org/10.1130/G47944.1>

## Abstract

Palaeoceanographic information from submarine overflows in the vicinity of oceanic gateways is of major importance for resolving the role of ocean circulation in modulating Earth's climate. Earth System Models are currently the favored way to study the impact of gateways on global-scale processes, but studies on overflow-related deposits are more suitable to understand the detailed changes. Such deposits, however, had not yet been documented in outcrop. Here, we present a unique late Miocene contourite channel system from the Rifian Corridor (Morocco) related to the initiation of Mediterranean Outflow Water (MOW). Two channel branches were identified consisting of three vertically stacked channelized sandstone units encased in muddy deposits. Both branches have different channel fill characteristics. Our findings provide strong evidence for an intermittent behavior of overflow controlled by tectonic processes and regional climatic change. These fluctuations in paleo-MOW intermittently influenced global ocean circulation.

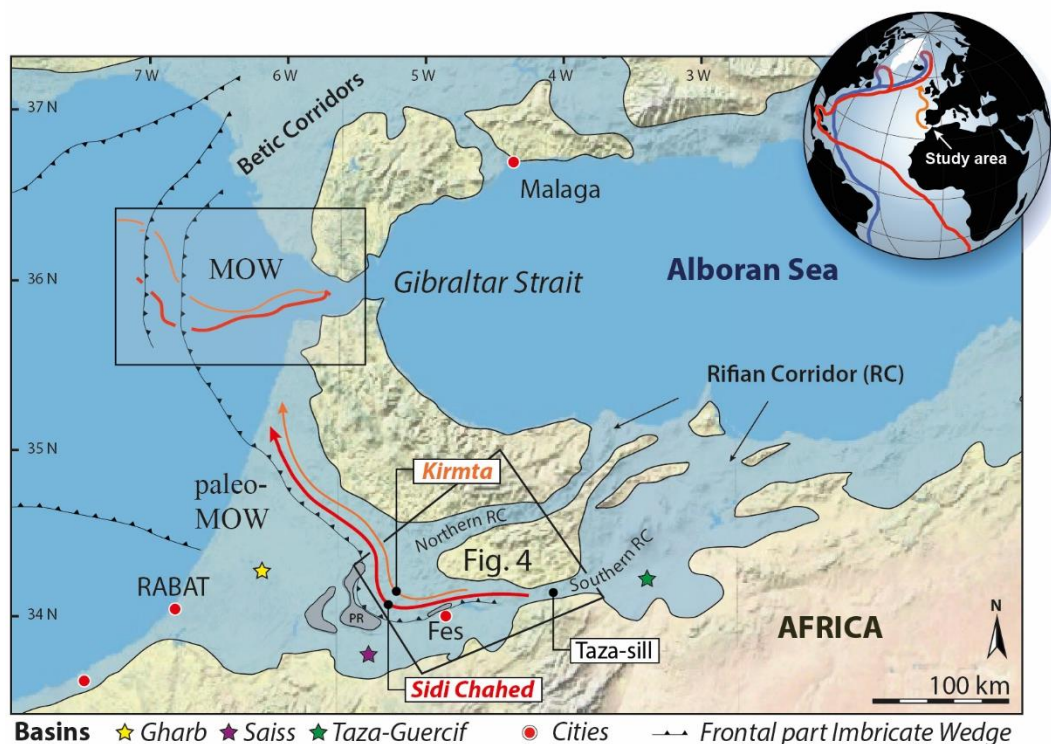
## Introduction

Plate-tectonic reconfiguration plays a major role in modifying global ocean circulation and poleward temperature gradients by opening and closing oceanic gateways (Knutz 2008). Changes in the transport of saline Mediterranean Outflow Water (MOW) to northern latitudes are no exception as the present-day MOW contributes to the Atlantic Meridional Overturning Circulation by as much as 15%, increasing the North Atlantic surface temperature by 1°C (Rogerson et al., 2012). The occurrence of a late Miocene paleo-MOW

therefore likely had an impact on global Ocean circulation and associated climate change. Recently, Capella et al. (2019) suggested that initiation of this paleo-MOW contributed to both the  $\delta^{13}\text{C}$  shift and global cooling.

General Circulation Models (GCMs) are regularly used to reconstruct the nature of changing connectivity between oceans and seas. However, these models are not suited to simulate hydraulic controls of narrow gateways, generating results which differ from observations (Ivanovic et al., 2013; Alhammoud et al., 2010). To reconstruct the detailed timing and nature of changing connectivity, a geological record is required. Critical information for reconstructing gateway overflows is most likely preserved in sediments accumulated at its exit, contourites (e.g. Toucanne et al. 2007).

Contourite features have been recognized in modern and ancient sedimentary records along continental margins and in deep-water. Despite growing scientific interest these deep marine systems remain relatively poorly understood (Rebesco et al, 2014; Stow and Smillie 2020), since very few ancient contourite deposits have been identified in outcrops and cores (Hüneke and Stow, 2008; Mutti et al. 2014). Here, we describe an unprecedented archive for unravelling the initial stages of MOW and the controls on overflow behavior based on two



**Figure 4.1.** Paleogeographic reconstruction of the late Miocene western Mediterranean (modified after Capella et al. 2017a). Grey – subaqueous Prerif Ridges (PR). Red (lower) and orange (upper) arrows depict Mediterranean Outflow Water (MOW) branches. Globe shows MOW (orange) and main surficial (red) and deep-water circulation pattern (blue). Map data are ©2018 Google™ with topographic overlay from U.S. Geological Survey topographic maps (<http://earthpoint.us/TopoMap.aspx>).

ancient contourite channels in the former Rifian Corridor, Morocco. These channels are associated to the late Miocene paleo-MOW that played an important role in water-mass exchange with the Atlantic Ocean (Seidenkrantz et al., 2000).

## Regional setting

The South Rifian Corridor is part of the Rif-Betic Cordillera, an arc shaped orogenic belt surrounding the Alborán Sea in the westernmost part of the Mediterranean (Fig. 4.1). This marine gateway evolved in the Tortonian as a SW-ward migrating foreland basin during the latest stage of Africa-Iberia collision (Sani et al., 2007). The main basins that recorded sedimentation are the Saiss-Gharb on the Atlantic side and the Taza-Guercif on the Mediterranean side of the paleo-Taza-Sill (Capella et al., 2017a) (Fig. 4.1). The studied sections were situated just north of the Saiss-Basin where the sea-floor morphology contained subaqueous highs formed by the Prerif Ridges ("PR" in Fig. 4.1) (Roldán et al., 2014) and the imbricate wedge (Prerifian Nappe in Capella et al. 2017a). The frontal part of this wedge formed the northern slope of the corridor which comprised intra slope sub-basins related to the main thrust faults.

## Sedimentary record

Eight facies (F1 -F8), associated to hemipelagic, gravitational and contourite deposits were identified (Table-4.I, supplementary material, p. 260). The Sidi Chahed section corresponds to "Ben Allou" studied by Capella et al. (2017a) while the Kirmta section is newly recognized. Both sections are composed of three vertically stacked sandstone units consisting of a compositional mix (sensu Chiarella et al., 2017) of bioclastic (dominantly shell-, echinoid-, bryozoan-fragments and foraminifera) and very fine- to coarse-grained siliciclastic sand. These sandstone units are encased in muddy sediments (F1 and F2) resulting in a sand/marl (N/G) ratio of 0.73 for Sidi Chahed and 0.42 for Kirmta.

In the Sidi Chahed section, the sandstone units form the infill of large (roughly 500 m wide), up to 40 m incised concave-up geometries (Fig. 4.2). Subordinate concave-up geometries (20 - 300 m wide) are filled (Fig. 4.2) by compound (up to m-scale) 3D-dunes (F5), 2D-dunes (F4) and slump deposits (F6).

Sandstone units in the Kirmta section are the infill of concave-up geometries that are wider (> 1 km) and less incised (5 – 15 m) compared to Sidi Chahed (Fig. 4.3). These units



consist of stacked 2D dunes (up to 60 cm in thickness, F4). The two lowermost units are preceded by bi-gradational (silt to fine sand sized) planar bed-sets (F3) with an average bed thickness of 10 cm and a lateral continuity exceeding 3 km (Fig. 4.3B). In both sections the

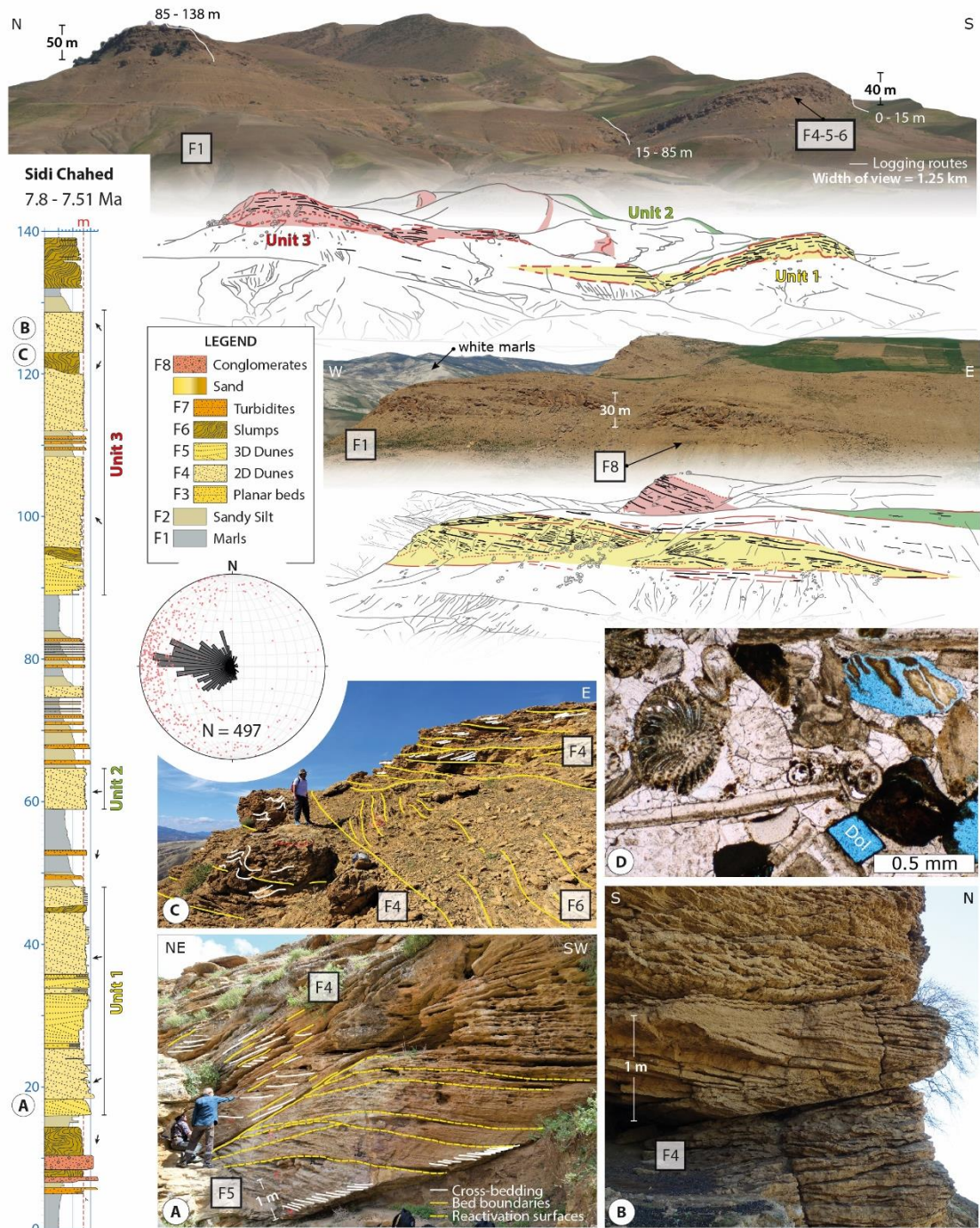


**Figure 4.2.** Sedimentary log, panoramic pictures, and interpretations for the Sidi Chahed section (Morocco; 34.101566°N, 5.301466°W). Three sand units (from old to young; yellow, green, and red) represent channel-fill sequences. Rosette diagram shows paleocurrent directions. (A) Basal fill sequence of sandstone unit 1. (B) Typical stacking pattern of facies F4. (C) Two bedsets of facies F4 separated by F6. Beds below F6 show soft-sediment deformation, and overlying beds are erosive. Note near-perpendicular difference in paleocurrent directions. (D) Thin section with mixed compositional sand of facies F4, and transported, exsolved dolomite (Dol) rhomb.



main sandstone intervals are bounded at the base and top by turbidite and occasionally by debris flow deposits (F7 and F8 respectively; Fig. 4.2, 4.3).

Paleocurrent measurements, mainly measured from crossbedding, indicate a dominant W-ward direction for Sidi Chahed, and NW-ward direction for the Kirmta sections (Fig. 4.2, 4.3). Gravity-driven deposits, such as turbidite (F7) and slump deposits (F6), show

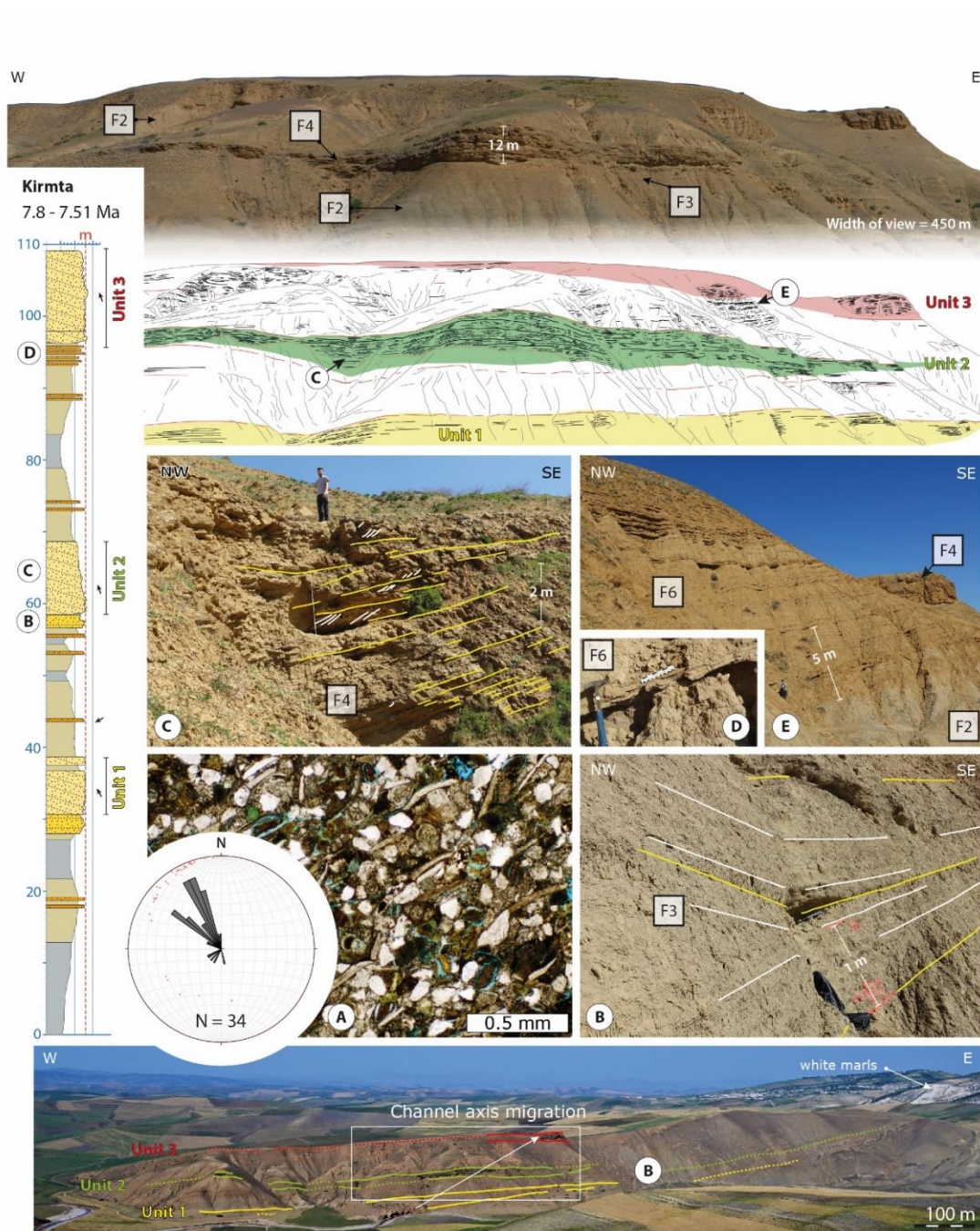


**Figure 4.3.** Sedimentary log (see Fig. 2 for legend), panoramic pictures, and interpretations for the Kirmta section (Morocco; 34.170855°N, 5.239288°W). Rosette diagram shows paleocurrent directions. (A-B) Facies F3. (C) Sandstone unit 2 with tabular cross-stratified beds (F4). (D-E) Facies F6, with turbidite deposits below the uppermost sand unit.

paleocurrent directions that are almost perpendicular to the main trends of the dunes (Fig. 4.2, 4.3) and are sub-parallel to the SW-directed paleo-slope.

Paleodepth estimates from benthic foraminifera indicate a physiographic domain between 150 – 400 m water depth, equivalent to an outer shelf to upper/middle continental slope (Capella et al., 2017a). The tectonically confined corridor and proximal location to the gateway resulted in steep margins (Longhitano, 2013), prone to gravitational depositional processes.

## Decoding the paleo-MOW

The investigation of the Kirmta outcrop allows us, for the first time, to analyze the spatial distribution and time variations between both sections. This new information enhances the paleogeographic reconstruction, sedimentological interpretation and understanding of the hydrodynamic setting.

Sidi Chahed and Kirmta, located 10 km apart, are situated ~120 km west of the paleo-Taza Sill (Fig. 4.1) where they occupy a position against the main thrust fault zone. The paleo-Taza Sill was a submerged high controlling Atlantic-Mediterranean water exchange in the late Miocene (Capella et al. 2017a). The system is thought to have acted in a similar way as the present-day MOW at the Camarinal Sill in the Strait of Gibraltar (Baringer and Price, 1999; Legg et al., 2009) where Mediterranean water was able to flow over and cascade down the sill into the Saiss Basin, generating a dense paleo-MOW that deflected to the right (N-NE) by the Coriolis force.

The main sandstone units are interpreted as contourite channels, part of an extensive Contourite Channel System. The interaction with partially incised interstratified slump deposits, the incorporation of these slump deposits in the overlying dunes (Fig. 4.2C) and the co-occurrence of shallow- and deep-marine bioclastic and foraminiferal assemblages that are subsequently reworked and accumulated within the along-slope channels by bottom currents, serve as evidence for an up-slope sediment source. Additional evidence of erosion and sediment supply lies in the presence of middle Miocene white marls (Sani et al. 2007; Fig. 4.2, 4.3) and Triassic bipyramidal quartz of the Keuper facies (Herrero et al. 2020) which was incorporated in the imbricate wedge. These sediments were sourced by both down- and along-slope processes as well as erosion induced by bottom currents.

Foraminifer assemblages, similar for both sites, indicate that deposition of the Sidi Chahed and Kirmta sections both occurred between 7.8 and 7.51 Ma (Capella et al., 2017a).

Despite coeval activity, both sections show morphological differences in channel geometry and channel fill related to different hydrodynamic properties (deeply incised, narrow channels filled by 3- and 2D dunes and interstratified slump deposits in Sidi Chahed, versus shallow, wide channels filled by 2D dunes in Kirmta). Hydrodynamic differences are also observed from the differences in sand/marl ratios. Based on bedforms types (F3, F4 and F5) and their characteristics (Table S4.1; Stow et al. 2009), Sidi Chahed was influenced by higher velocity bottom currents (up to  $1 \text{ ms}^{-1}$ ) compared to Kirmta ( $< 0.5 \text{ ms}^{-1}$ ).

By comparison with the present-day MOW through the Gibraltar Gateway, the proximal sector of the Gulf of Cádiz Contourite System (Fig. 4.1) (GoCCS) also has two main channels occupying the middle slope at different depths due to the circulation of the lower and upper branch of the MOW (Hernández-Molina et al., 2014). The similarities in geographic- and depositional-setting, channel distribution and large morphological elements between the GoCCS and the Rifian Corridor are indicative that hydrodynamic- and feedback processes associated to the MOW acted in a similar way. It is envisaged that bifurcation of the paleo-MOW, similarly to the flow bifurcation recognized in the Gulf of Cadiz (Hernández-Molina et al., 2014), took place in the Saiss basin, separating the paleo-MOW into two branches that occupied different depths along the slope of the Corridor. The lower branch (Sidi Chahed) occupied the deeper southern sub-basin, and the upper branch (Kirmta) the shallower northern sub-basin (Fig. 4.4).

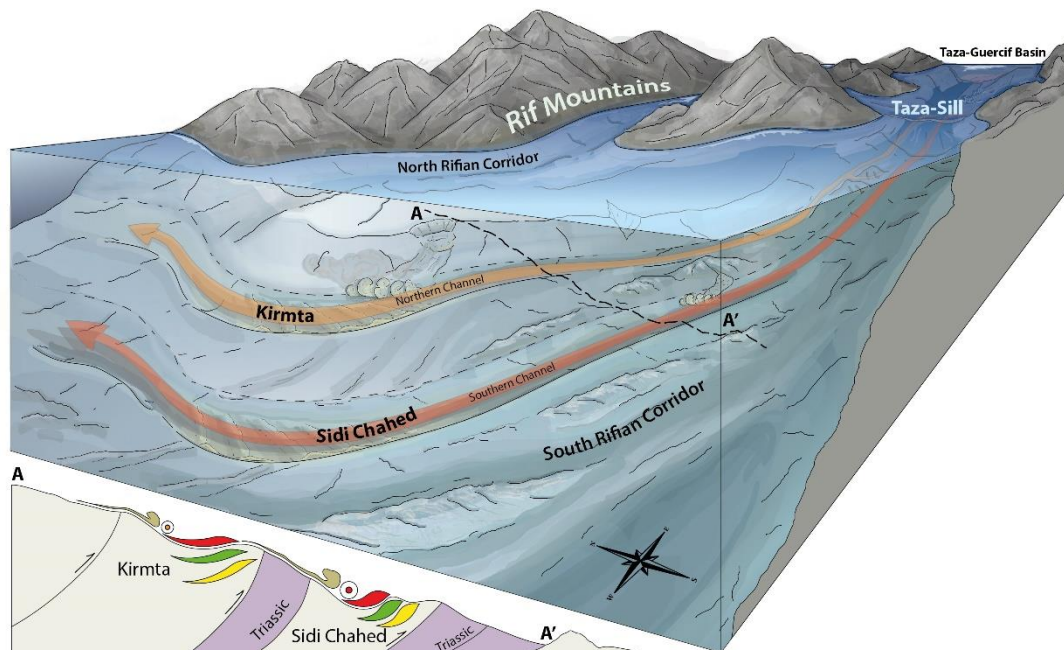


**Figure 4.4.** Paleogeographic model of the late Miocene Rifian Corridor (Morocco) with lower (red) and upper (orange) branches of paleo-Mediterranean Outflow Water (MOW). Cross section A-A' shows intraslope subbasins that act as fairways in the frontal part of the imbricate wedge and are filled by three vertically stacked, color-labeled (1-3) sand units. Circles depict location of core for each paleo-MOW branch.

Studies in the GoCCS (Baringer and Price, 1999; Legg et al., 2009) have also shown that the MOW consists of the vertical distribution of three Mediterranean water masses [Modified Atlantic Water, Levantine Intermediate Water and the Mediterranean Deep Water e.g. GRIDA 2013]. Bifurcation of the MOW into two branches, MU and ML (Hernández-Molina et al., 2014), is the result of partial mixing of intermediate and deep Mediterranean waters. Consequently, we can infer a similar vertical distribution of water masses in the Mediterranean during the late Miocene which agrees with numerical models proposed by de la Vara et al. (2016).

### Controls on overflow

The occurrence of two channel branches consisting of three vertically stacked sandstone units encased in muddy deposits with different channel fill characteristics for each branch, provides strong evidence for an intermittent behavior of the paleo-MOW during the late Tortonian. This intermittency is also evident from (i) subordinate erosional features which indicate migration and/or re-activation of the bottom current cores, (ii) alternating changes in dune morphology and sediment characteristics, and (iii) tidal signatures (Capella et al., 2017a). These different scales of changes in hydrodynamic properties indicate that intermittency of the paleo-MOW was controlled by a hierarchy of processes.

### *Tectonic processes*

Two important tectonic events are recorded in the late Miocene (Capella et al. 2017b): i) a regional compressional event around 8.4 – 7.8 Ma culminating in the emplacement of the imbricate wedge just before the onset of contourite deposition and, ii) the transition from thin- to thick-skinned contraction that happened around the Tortonian-Messinian boundary. Interestingly, between these two major tectonic events a period of relative tectonic quiescence occurred from ~7.8 to 7.25 Ma, coinciding with the development and preservation of the recognized Contourite Channel System. Nevertheless, the northeastward, up-slope migration of the three stacked contourite channels, observed from the channel axis distribution within the outcrops (Fig. 4.2, 4.3), indicates that the imbricate wedge migrated south-westward during this tectonically quiet period, intermittently affecting this system. These tectonic processes likely affected increased down-slope sediment supply by creating slope instability, but they might also have been accountable for



the channel migration, as a result of slope and sill reconfiguration and its effect on the behavior of the paleo-MOW.

### *Climatic processes*

A relationship between long- and short-term climatic processes and activity of the paleo-MOW is recognized at different scales but the lack of high-resolution age constraints hampers the ability to provide detailed evidence of the dynamics between the upper and lower paleo-channels. Observations from the GoCCS show that a stronger MOW in the deeper channel is linked to glacial periods which are associated to higher aridity in the Mediterranean and thus an increase in the density of Mediterranean Deep Water and intensification of the MOW (Llave et al., 2006). This implies that the MOW favors either the upper or lower channel based on its density characteristics because of tectonic and climatic induced effects on the Mediterranean water masses. The late Miocene was not severely influenced by eccentricity (glacial-interglacial) cycles but was dominated by precession (e.g. Sierro et al., 1999). Precessional cyclicity was therefore likely the driving force behind the intermittent behavior of the paleo-MOW. Smaller order changes in hydrodynamic characteristics of the overflow are likely related to millennial and seasonal changes in climatic conditions (e.g. Gladstone et al. 2007).

### Impact on thermohaline circulation

Late Miocene overflow is modulated by a complex hierarchy and interplay of processes. Studies across the Strait of Gibraltar have also demonstrated that the overflow processes are affected by a variety of control factors at different scales (e.g., Schonfeld, and Zahn, 2000; Llave et al., 2006). This indicates that understanding these late Miocene fossil contourite deposits can significantly help to better understand changes in behavior of overflows and their role in global ocean circulation.

In terms of consequences on the Atlantic circulation, a deeper input of MOW will reduce the upper ocean salinity in the Atlantic, while a shallower input increases it. Saltier near-surface Atlantic water is usually associated with stronger deep convection and overturning (Rahmstorf, 2006; Kuhlbrodt et al., 2007). This impact however also depends on the ambient stratification and mixing of the Atlantic, which we cannot infer from these records. Furthermore, as these sedimentary records represent an early stage of paleo-MOW formation, it is unclear how much time it took to fully establish the MOW in the Atlantic.

Despite these uncertainties, less input of salt and heat from the MOW would weaken the Atlantic Meridional Overturning Circulation, while the depth of the input impacts the connection with surface water properties, so impacting it in a less direct way.

The intermittency of overflows at precessional to seasonal time scales is currently not considered in models as proper sedimentary records are lacking. This record shows that intermittency is possible on such timescales and more evidence of such behavior should be obtained from similar systems such as the Denmark Straits, Faroe Bank Channel, Red Sea, and the Gulf of Cadiz.

## Acknowledgments

The authors would like to thank Sonya Legg (Princeton Univ., USA) for her review and contribution in improving the manuscript. Furthermore, we are very appreciative of the help and support given by ONHYM. This project is funded by the Join Industry Project supported by TOTAL, BP, ENI, ExxonMobil, Wintershal DEA and TGS and is done in the framework of “The Drifters Research Group” at Royal Holloway University of London (RHUL) and it is related to the projects CTM 2012-39599-C03, CGL2016-80445-R, and CTM2016-75129-C3-1-R.

## References cited

- Alhammoud, B., Meijer, P. T., & Dijkstra, H. A., 2010, Sensitivity of Mediterranean thermohaline circulation to gateway depth: A model investigation. *Paleoceanography*, 25(2).
- Baringer, M. O. N., and Price, J. F., 1999, A review of the physical oceanography of the Mediterranean outflow. *Marine Geology*, v. 155(1-2), p. 63-82.
- Capella, W., et al., 2017a, Sandy contourite drift in the late Miocene Rifian Corridor (Morocco): Reconstruction of depositional environments in a foreland-basin seaway. *Sedimentary geology*, v. 355, p. 31-57.
- Capella, W., Matenco, L., Dmitrieva, E., Roest, W. M., Hessels, S., Hssain, M., Chakor-Alami, A., Sierro, F.J., Krijgsman, W., 2017b, Thick-skinned tectonics closing the Rifian Corridor. *Tectonophysics*, v. 710, p. 249-265.
- Capella, W., Flecker, R., Hernández-Molina, F. J., Simon, D., Meijer, P. T., Rogerson, M., Sierro, F.J., and Krijgsman, W., 2019, Mediterranean isolation preconditioning the Earth System for late Miocene climate cooling. *Scientific reports*, v. 9(1), p. 3795.
- Chiarella, D., Longhitano, S. G., and Tropeano, M., 2017, Types of mixing and heterogeneities in siliciclastic-carbonate sediments. *Marine and Petroleum Geology*, v. 88, p. 617-627.
- De La Vara, A., Topper, R. P., Meijer, P. T., Kouwenhoven, T.J., 2015, Water exchange through the Betic and Rifian corridors prior to the Messinian Salinity Crisis: A model study. *Paleoceanography*, 30(5), 548-557.
- Flecker, R., et al., 2015, Evolution of the Late Miocene Mediterranean–Atlantic gateways and their impact on regional and global environmental change. *Earth-Science Reviews*, v. 150, p. 365-392.
- Gladstone, R., Flecker, R., Valdes, P., Lunt, D., & Markwick, P., 2007, The Mediterranean hydrologic budget from a Late Miocene global climate simulation.

- Palaeogeography, Palaeoclimatology, Palaeoecology*, 251(2), 254-267.
- Hernández-Molina, F. J., et al., 2016, Oceanographic processes and morphosedimentary products along the Iberian margins: A new multidisciplinary approach. *Marine Geology*, 378, 127-156.
- Hernández-Molina, F. J., et al., 2014, Contourite processes associated to the Mediterranean outflow water after its exit from the Gibraltar strait: global and conceptual implications. *Geology*, v. 42, p. 227-230.
- Herrero, M. J., Marfil, R., Escavy, J. I., Al-Aasm, I., & Scherer, M., 2020. Diagenetic Origin of Bipyrimal Quartz and Hydrothermal Aragonites within the Upper Triassic Saline Succession of the Iberian Basin: Implications for Interpreting the Burial-Thermal Evolution of the Basin. *Minerals*, 10(2), 177.
- Hüneke, H., Stow, D.A.V., 2008, Identification of ancient contourites: Problems and palaeoceanographic significance, in: Rebesco, M., Camerlenghi, A. (Eds.), Contourites. *Developments in Sedimentology*, v. 60, p. 323-344.
- Ivanovic, R. F., Valdes, P. J., Flecker, R., Gregoire, L. J., & Gutjahr, M., 2013, The parameterisation of Mediterranean-Atlantic water exchange in the Hadley Centre model HadCM3, and its effect on modelled North Atlantic climate. *Ocean Modelling*, 62, 11-16.
- Knutz, P.C., 2008, Paleooceanographic significance of contourite drifts. *Developments in Sedimentology*, v. 60, p. 511-535.
- Kuhlbrodt, T., Griesel, A., Montoya, M., Levermann, A., Hofmann, M., Rahmstorf, S., 2007. On the driving processes of the Atlantic meridional overturning circulation. *Reviews of Geophysics* 45, RG2001.
- Legg, S., et al., 2009, Improving oceanic overflow representation in climate models: the gravity current entrainment climate process team. *Bulletin of the American Meteorological Society*, v. 90(5), p. 657-670.
- Llave, E., Schönfeld, J., Hernández-Molina, F. J., Mulder, T., Somoza, L., Del Río, V. D., and Sánchez-Almazo, I., 2006, High-resolution stratigraphy of the Mediterranean outflow contourite system in the Gulf of Cadiz during the late Pleistocene: the impact of Heinrich events. *Marine Geology*, v. 227(3-4), p. 241-262.
- Longhitano, S. G., 2013. A facies-based depositional model for ancient and modern, tectonically-confined tidal straits. *Terra Nova*, 25(6), 446-452.
- Mutti, E., Cunha, R. S., Bulhoes, E. M., Arienti, L. M., & Viana, A. R., 2014, Contourites and turbidites of the Brazilian marginal basins. In *AAPG Annual Convention & Exhibition*.
- Nielsen, T., Kuijpers, A., Knutz, P., 2008. Seismic expression of contourite depositional systems. *Developments in Sedimentology*, v. 60, p. 301-322.
- Rahmstorf, S., 2006. Thermohaline ocean circulation. In: Elias, S.A. (Ed.), *Encyclopedia of Quaternary Science*. Elsevier, Amsterdam, pp. 739-750.
- Rebesco, M., Hernández-Molina, F. J., Van Rooij, D., and Wåhlin, A., 2014, Contourites and associated sediments controlled by deep-water circulation processes: state-of-the-art and future considerations. *Marine Geology*, v. 352, p. 111-154.
- Rogerson, M., Rohling, E. J., Bigg, G. R., and Ramirez, J., 2012, Paleooceanography of the Atlantic-Mediterranean exchange: Overview and first quantitative assessment of climatic forcing. *Reviews of Geophysics*, v. 50(2).
- Roldán, F. J., et al., 2014, Basin evolution associated to curved thrusts: The Prerif Ridges in the Volubilis area (Rif Cordillera, Morocco). *Journal of Geodynamics*, 77, 56-69.
- Sani, F., Del Ventisette, C., Montanari, D., Bendkik, A., and Chenakeb, M., 2007, Structural evolution of the Rides Prerifaines (Morocco): structural and seismic interpretation and analogue modelling experiments. *International Journal of Earth Sciences*, v. 96(4), p. 685-706.
- Schönfeld, J., Zahn, R., 2000, Late Glacial to Holocene history of the Mediterranean Outflow. Evidence from benthic foraminiferal assemblages and stable isotopes at the Portuguese margin. *Palaeogeography, Palaeoclimatology, Palaeoecology*, 159(1-2), 85-111.
- Seidenkrantz, M. S., Kouwenhoven, T. J., Jorissen, F. J., Shackleton, N. J., and Van der Zwaan, G. J., 2000, Benthic foraminifera as indicators of changing Mediterranean-Atlantic water exchange in the late Miocene. *Marine geology*, v. 163(1-4), p. 387-407.



- Sierro, F. J., et al., 1999, Messinian pre-evaporite sapropels and precession-induced oscillations in western Mediterranean climate. *Marine Geology*, 153(1-4), 137-146. Alger.
- Stow, D. A., Hernández-Molina, F. J., Llave, E., Sayago-Gil, M., Díaz del Río, V., Branson, A., 2009, Bedform-velocity matrix: the estimation of bottom current velocity from bedform observations. *Geology*, 37(4), 327-330.
- Toucanne, S., Mulder, T., Schönfeld, J., Hanquiez, V., Gonthier, E., Duprat, J., Cremer, M., Zaragosi, S., 2007, Contourites of the Gulf of Cadiz: a high-resolution record of the paleocirculation of the Mediterranean outflow water during the last 50,000 years. *Palaeogeography, Palaeoclimatology, Palaeoecology*, 246(2-4), 354-366.
- GRIDA, 2013, State the Mediterranean Marine and Coastal Environment: <http://www.grida.no/resources/5885>

# *Chapter V*

*Contourite depositional system after the exit of a  
strait: case study from the late Miocene South  
Rifian Corridor, Morocco*

## Contourite depositional system after the exit of a strait: case study from the late Miocene South Rifian Corridor, Morocco

W. de Weger, F.J. Hernández-Molina, O. Miguez-Salas, S. de castro, M. Bruno, D. Chiarella, F.J. Sierro, G. Blackbourn and M. Amine Manar (2021a)

doi:10.1111/sed.12882

### ABSTRACT

Idealized facies of bottom current deposits (contourites) have been established for fine-grained contourite drifts in modern deep-marine sedimentary environments. Their equivalent facies in the ancient record however are only scarcely recognized due to the weathered nature of most fine-grained deposits in outcrop. Facies related to the erosional elements (i.e., contourite channels) of contourite depositional systems (CDS) have not yet been properly established and related deposits in outcrop appear non-existent. To better understand the sedimentary facies, and facies sequences of contourites, the upper Miocene CDS of the South Rifian Corridor (Morocco) is investigated. This CDS formed by the dense palaeo-Mediterranean Outflow Water (palaeo-MOW). Foraminifera assemblages were used for age-constraints (7.51 to 7.35 Ma) and to determine the continental slope depositional domains. Nine sedimentary facies have been recognized based on lithology, grain-size, sedimentary structures and biogenic structures. These facies were subsequently grouped into five facies associations related to the main interpreted depositional processes (hemipelagic settling, contour currents and gravity flows). The vertical sedimentary facies succession records the tectonically induced, southward migration of the CDS and the intermittent behavior of the palaeo-MOW, which is mainly driven by precession and millennial-scale climate variations. Tides substantially modulated the palaeo-MOW on a sub-annual scale. This work shows exceptional examples of muddy and sandy contourite deposits in outcrop by which a facies distribution model from the proximal continental slope, the contourite channel to its adjacent contourite drift, is proposed. This model serves as a reference for contourite recognition both in modern environments and the ancient record. Furthermore, by establishing the hydrodynamics of overflow behavior a framework is provided that improves process-based interpretation of deep-water bottom current deposits.

**Keywords** Bottom currents, contourites, channels, deep-water sedimentation, Late Miocene, Morocco, Rifian Corridor, tides.

## 1. INTRODUCTION

Over the last decade there has been a significant increase in published evidence of deep-marine bottom current processes and associated deposits, contourites. Most of these works however are based on 2D and 3D seismic profiles (Faugères *et al.*, 1999; Paulat *et al.*, 2019), some from wells and cores (Gonthier *et al.*, 1984; de Castro *et al.*, 2020a, b; Hovikoski *et al.*, 2020), but there is still very little information from the exposed ancient record.

Sedimentation in deep-marine environments is predominantly controlled by pelagic, gravitational and contouritic processes, or their mixed occurrence (Fonnesu *et al.*, 2020; Shanmugam, 2020; Stow and Smillie, 2020). When bottom currents represent the dominant depositional process, a contourite depositional system (CDS) develops (Hernández-Molina *et al.*, 2008). Currently, there is no widely accepted model for such systems, but they are generally composed of a combination of depositional (related to low current velocities) and erosional (related to high current velocities) elements. Both elements result from the hydrodynamic behavior of water masses that reach and interact with the seafloor and are conditioned by bathymetry (Hernández-Molina *et al.*, 2006).

As a result of the differentiation between areas prone to low current and high current velocities, contourites deposits are generally divided into muddy contourites (fine-grained) or sandy contourites (coarse-grained) (Stow and Faugères, 2008). Most of the evidence used to identify contourites are based on the large morphological features of depositional elements (Faugères *et al.*, 1999; Hernández-Molina *et al.*, 2008), particularly on the large depositional contourite drifts, with less attention on the possible erosional contourite elements. Accordingly, the only generally accepted contourite facies model is the bi-gradational model (Faugères *et al.*, 1984; Gonthier *et al.*, 1984; Stow and Faugères, 2008) defined for fine-grained contourite drifts. Therefore, it is often wrongly assumed that bottom currents only generate muddy contourite deposits, disregarding the fact that some authors highlighted the occurrence of sandier sediments deposited or reworked by the action of bottom currents. These sandier sediments are mainly found within contourite erosional elements such as, channels (Hernández-Molina *et al.*, 2014b; Capella *et al.*, 2017a; Brackenridge *et al.*, 2018; de Weger *et al.*, 2020), contourite terraces (Viana and Faugères, 1998; Mutti *et al.*, 2014; Hernández-Molina *et al.*, 2009, 2016a, b, 2018; de Castro *et al.*,

2021) or in mixed turbidite and contourite depositional systems (Rebesco *et al.*, 2002; Creaser *et al.*, 2017; Sansom, 2018; Fonnessu *et al.*, 2020; Fuhrman *et al.*, 2020; Rodrigues *et al.*, 2021).

The natural evolution of a CDS comprises the lateral migration of both depositional and erosional elements. This implies that, for example, drifts develop on top of channels (Chen *et al.*, 2020) or channels erode into drifts (Llave *et al.*, 2001; Hernández-Molina *et al.*, 2008, 2014b; Chen *et al.*, 2020). This migration has been identified using seismic data, but the

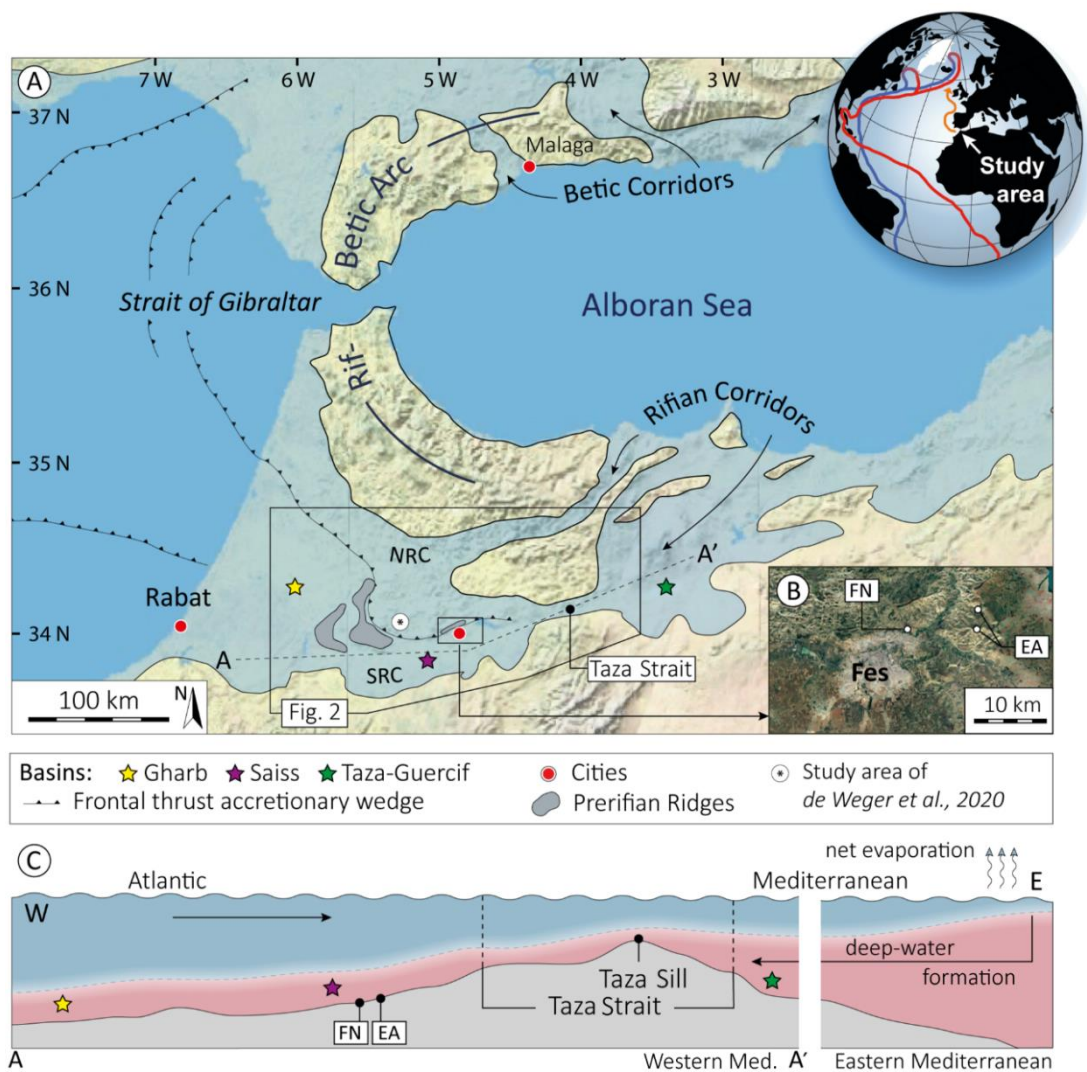


**Figure 5.1.** (A) Satellite terrain image of the western-most Mediterranean region, southern Spain and north-west Africa. The globe on the right-hand corner shows the location of the study area and depicts the thermohaline circulation pattern (red – shallow and blue – deep), the orange arrow indicates the pathway of the MOW. In transparent blue a late Miocene palaeogeographic overlay of the Betic and Rifian corridors, NRC = North Rifian Corridor and SRC = South Rifian Corridor, after de Weger *et al.* (2020). The location of the main geological features, such as the Gharb, Saiss and Taza-Guercif basins, the Prerifian Ridges and the Taza Strait are indicated. (B) Satellite image showing the location of the study areas. The abbreviations stand for the section names, FN = Fes-north and EA = El Adergha. (C) Late Miocene reconstruction through the SRC, cross-section A-A', of which the location is indicated in (A). The SRC accommodated Atlantic-Mediterranean exchange of surficial Atlantic and Mediterranean Deep Water.

sedimentary facies and facies sequences related to these migrating environments are currently not established. This is a partial consequence of the lack of recognized CDS in outcrop which show lateral and vertical facies variability.

Contourite outcrops, as mentioned earlier, have however only been scarcely recognized. This likely results from the lack of distinct diagnostic contourite features, hindering the scientific community to identify these deposits in outcrop (Hüneke and Stow, 2008; Rebesco *et al.*, 2014; Shanmugam, 2017). Furthermore, the problematic identifying of muddy contourites in outcrop, for which most diagnostic criteria (the bi-gradational model and morphological features) exists, results from their relatively homogeneous and their severely bioturbated nature (Gonthier *et al.*, 1984), but also because most fine-grained outcrops are usually severely weathered. The recognition of sandy contourites, for which no true diagnostic criteria exist, is mainly hindered by the process-based interpretation of deep-marine sediments. There is a general idea that sandy deposits only enter the deep-marine realm by gravitational processes, and it is regularly wrongly assumed that deep-marine bottom currents are only related to thermohaline circulation, not reaching current velocities capable of reworking, transporting and depositing sandy sediment. The poorly understood hydrodynamic properties of deep-marine water masses that reach and interact with the seafloor stand in the way of such process-based interpretation of bottom current deposits.

This paper investigates the sedimentary record of a well-exposed late Miocene CDS in the Saiss Basin, associated to the South Rifian Corridor of Morocco (Fig. 5.1). The main objective of this study is to: (i) determine the geometries, sedimentary facies and facies sequences

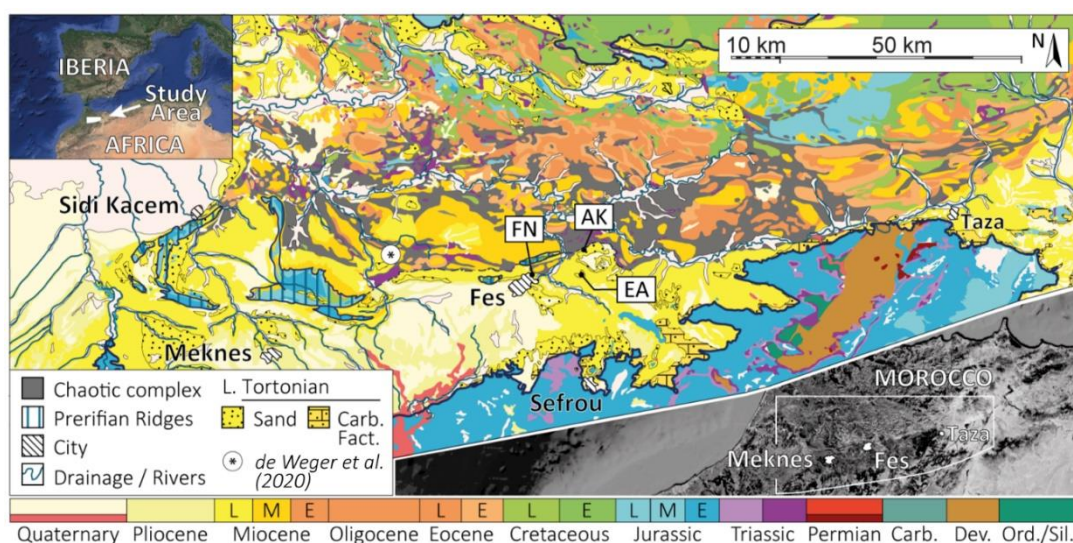


**Figure 5.2.** Regional geological map of the study area including the locations of the studied Upper Miocene outcrops; El Adergha (EA), Fes-north (FN) and Ain Kansera (EA) (modified after Saadi *et al.*, 1980). Carb. Fact = carbonate factory, L = late, M = middle and E = early. Satellite images are derived from GOOGLE Earth.



related to the lateral migration of the CDS; (ii) interpret its evolution; (iii) investigate the dynamics of overflow behavior in a confined basin; and (iv) provide the much-needed clarification on the role of bottom currents to improve process-based interpretation for deep-marine contourites. The results presented herein will thus also serve as a reference for the recognition of contourite deposits.

## 2. STUDY AREA AND GEOLOGICAL SETTING

The studied sections are exposed in the Saiss Basin in northern Morocco (Fig. 5.1). This basin is part of the external zone of the Rif-Betic Arc, or Gibraltar Arc which forms an arc-shaped orogenic belt surrounding the Alboran Sea in the westernmost Mediterranean region.

The Betic and Rifian corridors were late Miocene marine gateways that allowed Mediterranean-Atlantic water exchange (Fig. 5.1). The Rifian corridors evolved during the latest stage of Africa-Iberia collision in the late Tortonian (~ 8 Ma) as south-westward migrating foreland basins (Feinberg 1986; Wernli, 1988; Sani *et al.*, 2007). These foreland basins were limited northwards by the earlier exhumed Rif orogenic wedge (Iribarren *et al.*, 2009) and southwards by the Atlas Mountains (Barbero *et al.*, 2011). The corridor is generally divided into two strands (Fig. 5.1A), the North Rifian Corridor (NRC) related to the Rifian Intramontane basins, and the South Rifian Corridor (SRC) related to the Taza-Guercif and Saiss basins (Wernli, 1988). Both strands were separated by the chaotic complex of the accretionary wedge (Fig. 5.2), the emplacement of which over the African foreland started during the early Tortonian (Feinberg, 1986; Flinch 1993; Chalouan *et al.*, 2004; Michard *et al.*, 2008). Since the accretionary wedge is locally overlain by Upper Miocene marine sediments, the Rifian corridors were at times a single wide gateway westward of the Taza Strait (Fig. 5.1). The central portion of the Taza Strait was characterized by a sill (the Taza Sill) (Flecker *et al.*, 2015; Capella *et al.*, 2017a; de Weger *et al.*, 2020), which formed a submerged topographic high related to the E-W oriented thrust-front overlying the NE-SW oriented Middle Atlas. The Taza Strait separated the Taza-Guercif and the Saiss basins and the Taza Sill controlled the water mass exchange between the Mediterranean and the Atlantic during the late Miocene (Capella *et al.*, 2017a; de Weger *et al.*, 2020). The westernmost part of the Rifian corridors was in the Gharb Basin where both the Rifian Intramontane and Saiss basins merged (Sani *et al.*, 2007). The Gharb Basin was located just west of the Prerifian

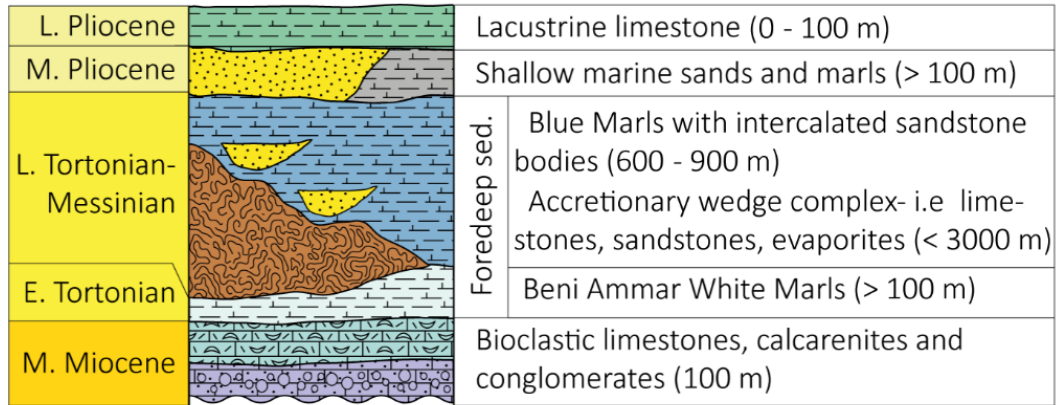


Figure 5.3. Middle Miocene to late Pliocene lithostratigraphy of the Saiss Basin. The intercalated sandstone bodies in the late Tortonian to Messinian Blue Marl Formation belong to the sections studied herein.

Ridges (Figs 5.1A and 5.2) which form the arcuate shaped southernmost leading edge of the Rif Chain.

The development of the Prerifian Ridges mainly took place during two phases (Roldán *et al.*, 2014). The initial development occurred during the middle to late Miocene, accompanied by the south-westward gravitational emplacement of the accretionary wedge (Capella *et al.*, 2017b). The second phase of compressional deformation happened during the late Tortonian to early Messinian during which the Prerifian Ridges were formed. These ridges represented a tectonically uplifting, likely subaqueous relief on the northern margin of the South Rifian Corridor during the Tortonian (Roldán *et al.*, 2014; de Weger *et al.*, 2020).

### 2.1 Lithostratigraphy of the Saiss Basin

The middle Miocene-late Pliocene Saiss Basin fill stratigraphy (Fig. 5.3) overlies a major angular unconformity. The basal foredeep sediments are mainly divided into two formations: (i) the Benni Ammar White Marl Formation, which pre-dates the emplacement of the accretionary wedge (Fig. 5.3); and (ii) the Blue Marl Formation, mainly post-dating its emplacement. Within the Blue Marl Formation up to 120 m thick sands were locally deposited (Capella *et al.*, 2017a; de Weger *et al.*, 2020). The accretionary wedge, consisting of Triassic to late Miocene tectono-stratigraphic units, developed in the study area during the late Tortonian to Messinian (Sani *et al.*, 2007) coinciding with the onset of Rifian Corridor sedimentation that started around 8 Ma (Wernli, 1988; Krijgsman *et al.*, 1999; Gelati *et al.*, 2000; Hilgen *et al.*, 2000; Barhoun and Bachiri Taoufiq, 2008; Achalhi *et al.*, 2016). On top of the Tortonian Blue Marls, mainly limited to the south Saiss Basin but also locally along the northern margin of the Saiss basin, early Messinian to middle Pliocene shelfal and nearshore



marine marls and sandstones are deposited (Capella *et al.*, 2018). These shallow-marine deposits are in turn locally truncated by an erosional unconformity and overlain by lacustrine limestones (Taltasse, 1953; Capella *et al.*, 2018).

### 3. PALAEOCEANOGRAPHIC SETTING

During the late Miocene, an Atlantic - Mediterranean connection existed through the Betic Corridor in southern Spain and the Rifian Corridors in northern Morocco (Fig. 1A). After subduction of the accretionary wedge, as well as of the external Betic and Rif fold-thrust belts largely came to a hold in the late Tortonian (van Hinsbergen *et al.*, 2014), tectonic uplift first took over in the Betic at  $\sim 7.8$  Ma (Betzler *et al.*, 2006; Krijgman *et al.*, 2006) and slightly later, by  $\sim 7$  Ma, in the Rif orogeny (Capella *et al.*, 2017b; Tulbure *et al.*, 2017). All the Betic-Atlantic – Mediterranean connections were closed due to Africa-Iberia convergence by the early Messinian (Spakman *et al.*, 2018). By  $\sim 7.2$  Ma the North Rifian Corridor was closed (Tulbure *et al.*, 2017) but the South Rifian Corridor was still open during the earliest Messinian recording a transition to continental and lacustrine deposits by  $\sim 6.9$  Ma (Capella *et al.*, 2017a). Since there is no evidence of a Mediterranean-Atlantic gateway through the Betic and Rifian corridors during the Messinian, the Gibraltar Corridor arguably became the sole Atlantic gateway during this period (Krijgman *et al.*, 2018). Between  $\sim 5.97$  Ma, the time of the onset of the Mediterranean Salinity Crisis (Hsü *et al.*, 1973; Ryan *et al.*, 1973), and  $\sim 5.6$  Ma, the Gibraltar Corridor accommodated a two-way connection (Simon and Meijer, 2017) after which it only facilitated Mediterranean inflow until  $\sim 5.33$  Ma (Krijgman *et al.*, 2018).

After the closure of all but one of the Betic corridors in the late Miocene, the North Rifian Corridor maintained the inflow of Atlantic water in the Mediterranean (Tulbure *et al.*, 2017) whereas the South Rifian Corridor maintained Atlantic-Mediterranean water exchange similar to what is currently occurring in the Strait of Gibraltar (de Weger *et al.*, 2020). The South Rifian Corridor likely accommodated inflow of the North Atlantic Surficial Water (NASW) and the Eastern North Atlantic Central Water (ENACW) into the Mediterranean, overriding a warm and highly saline water mass associated with the palaeo-Mediterranean Outflow Water (MOW). The water mass of the palaeo-MOW was formed due to net evaporation and cooling in the eastern Mediterranean (Fig. 5.1B). This net evaporation and cooling increased the density of Mediterranean surface water (Straume *et al.*, 2020) which was “continuously” replenished by cold and less saline Atlantic water. Subsequently, this increase in density forced this water to sink and ventilate the water column, a process known

as intermediate and deep-water formation (Millot, 1999; Candela, 2001). The formation of Mediterranean Deep Water (and thus the formation of water masses related to the palaeo-MOW) resulted in a significant density gradient, or water mass stratification, between the Mediterranean and the Atlantic. This density gradient drove water mass exchange by two-way flow (Rohling *et al.*, 2015; Simon *et al.*, 2017). During the late Miocene a dense palaeo-MOW flowed over the Taza Sill through the Taza Strait (Fig. 5.1) downwards into and through the South Rifian Corridor towards the Atlantic (de Weger *et al.*, 2020).

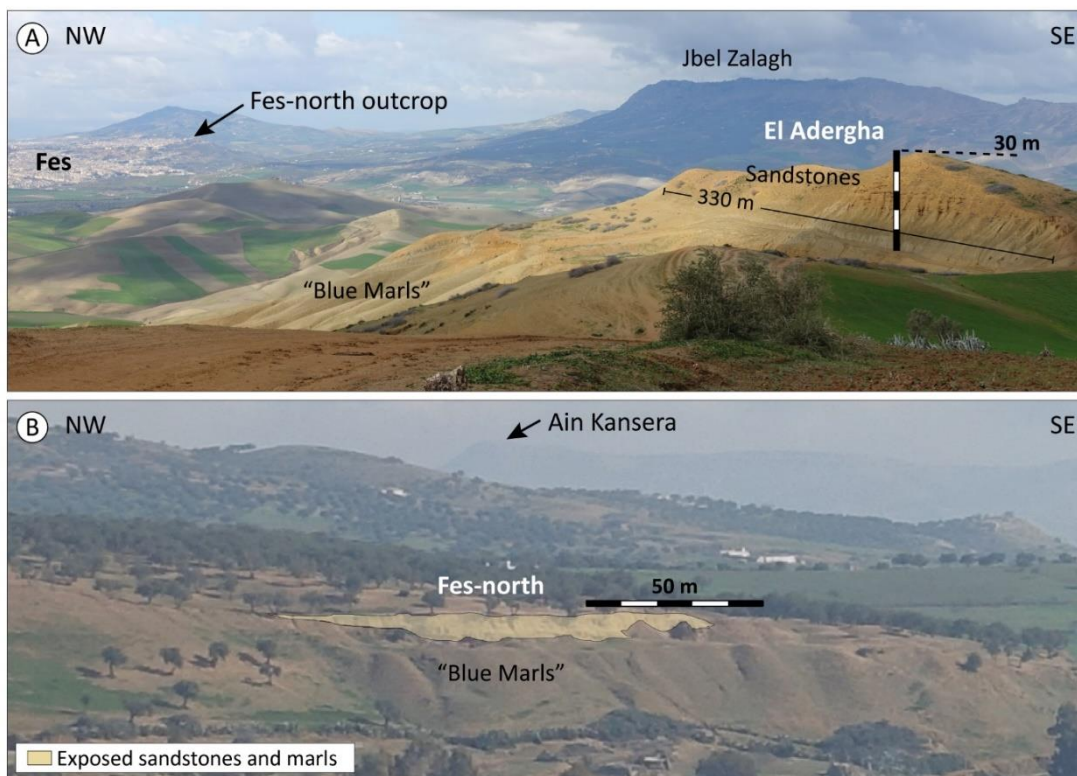


**Figure 5.4.** Panoramic view of the El Adergha (A) and Fes-north (B) outcrops. These pictures highlight the general exposed geometries and the scale of the outcrops. Due to the location of the Fes-north section being far away from the nearest vantage point no better pictures are currently available.

#### 4. METHODOLOGY

Two well-exposed late Miocene outcrops, El Adergha and Fes-north (Figs 5.1, 5.2, 5.4A and B), from the South Rifian Corridor are described in detail in this paper to unravel the facies successions and their vertical and lateral changes. The El Adergha section has previously partly been described by Capella *et al.* (2017a) and their results have been taken into consideration. The El Adergha section has been however re-interpreted and has been put in a new palaeogeographic framework based on the results of this study. A third section,

Ain Kansera (Fig. 5.2), previously studied by Capella *et al.* (2017a), has also been reviewed and considered for discussion. As present observations and interpretations do not significantly divert from those made previously, the Ain Kansera section is not described in detail in this work.

The sedimentary successions were studied by standard field techniques which include bed-scale characterization of sedimentological and stratigraphic elements. Two stratigraphic sections were measured at centimetre to metre-scale to document the key features such as lithology, grain-size and sorting, sedimentary structures, bedding thickness, nature of bed contacts and palaeocurrent indicators. These features form the basis for the facies analysis. Sixty-four palaeoflow indicators (cross-stratification, ripple lamination and sole marks) were recorded across both outcrops.

A bed-by-bed ichnological analysis was conducted. The distribution, types and abundance of trace fossils were characterized to describe stratigraphic trends throughout the sections. Ichnological observations focused on orientation, shape, length and diameter of individual burrow segments, configuration of burrow systems and taphonomy, allowing for ichnotaxonomical assignation.

Seven samples for petrographic analysis (Table S5.1; Figs S5.1 and S5.2) were derived from indurated sand beds. Two sets of thin sections were prepared for each sample, one of which was impregnated with dyed resin to highlight porosity. The samples were examined under a Nikon Optiphot-pol petrographic microscope (Nikon, Tokyo, Japan) with integral Canon EOS-50D camera system (Canon Inc., Tokyo, Japan). Modal analysis was carried out on 3 samples (EA3, FN1 and EA5) by determining the composition at 300 points using a stepping stage and associated PETROG software (Table S5.1).

Eight samples for biostratigraphy, derived from marls that were more than 50 cm below the rock's exposed surface, were analyzed. Tree samples for the El Adergha section were compared to what has been published by Capella *et al.* (2017a) to integrate their results. Five new samples from the Fes-north section were compared to the biostratigraphic framework published in Capella *et al.* (2017a) and Tulbure *et al.* (2017) to date these samples based on quantitative changes in abundance of keeled and unkeeled *Globorotalids*.

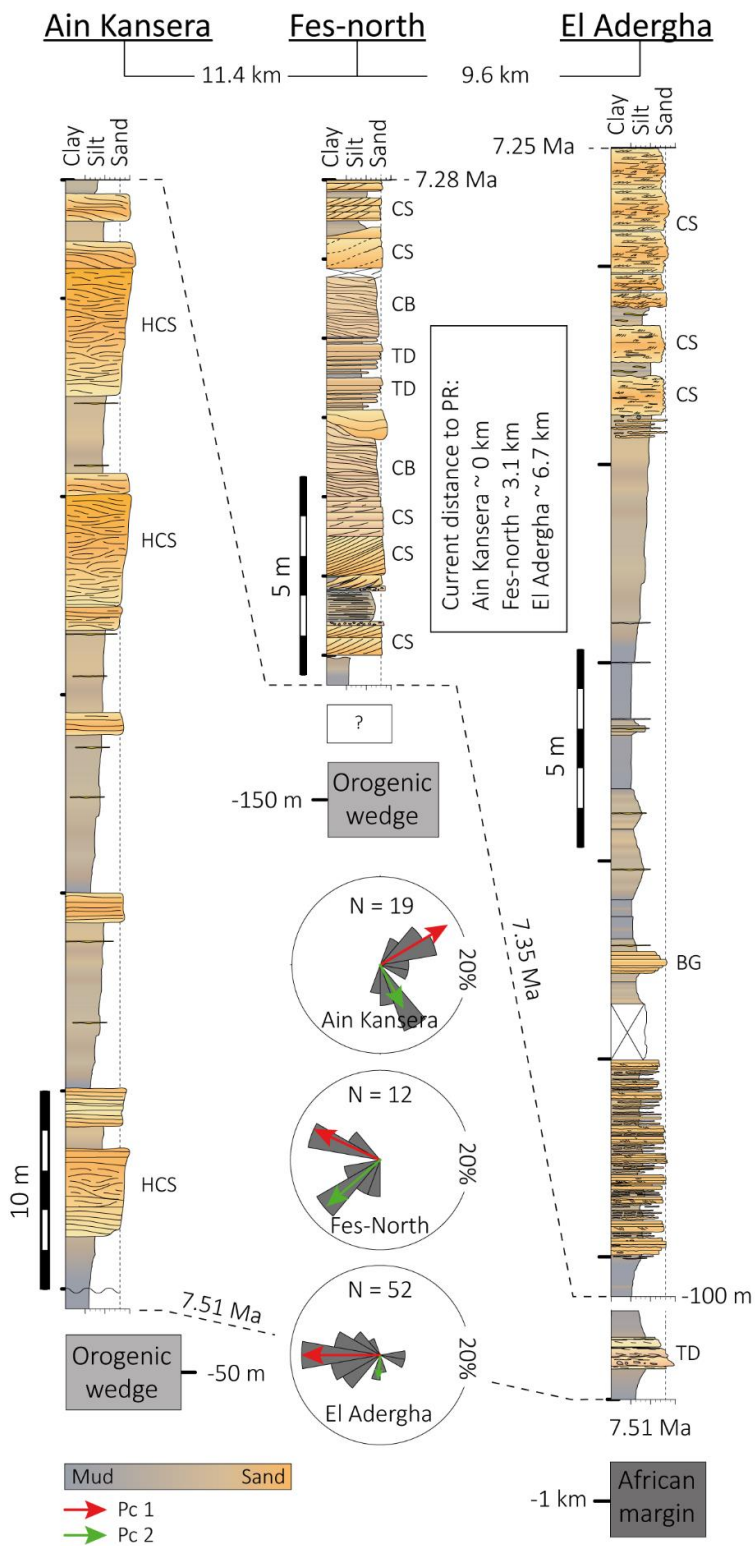


**Figure 5.5.** Sedimentary logs for the Ain Kansera (modified after Capella et al., 2017a), Fes-north and El Adergha sections. Their location is provided in Fig. 2, and their relative distance, and distance to the Prerifian Ridges is indicated. Palaeocurrents are divided in two major components, along-slope Pc 1 (red) and down-slope Pc 2 (green). The main sedimentary features are indicated next to the log. HCS = hummocky cross-stratification, CS = cross-stratification, BG = bi-gradational and TD = turbidite (see text for interpretation).

The palaeowater-depth was inferred from the benthic foraminifera assemblages of the biostratigraphic samples. The specific assemblages and relative abundance of benthic species were associated to depth ranges identified in the existing literature (Perez-Asensio *et al.*, 2012). The mixed occurrence of shallow-water and deep-water species is considered the result of downslope transport and hence, the deeper-water species are deemed most reliable in depositional depth estimates.

## 5. RESULTS

### *5.1 Studied sections*

The sections, El Adergha and Fes-north, comprise sandstone rich intervals intercalated within the Blue Marl Formation (Figs 5.4 and 5.5). The sections are located 9.6 km apart (Figs 5.2 and 5.5). The El Adergha outcrop (34.076402, -4.860522) is located on the northern flank of the Saiss Basin (Figs 5.1 and 5.2B), 10 km ENE of the city of Fes and 7.5 km SE of the western most expression of the Prerifian Ridges Jbel Zalagh. The section forms a topographic high with an up to 15 m thick sandstone body at its peak (Fig. 5.4A). Below the sandstone an up to 1000 m thick fine-grained succession related to the Blue Marl Formation occurs. The south-western flank is steeply inclined to near vertical whereas the north-eastern flank shows a much shallower inclination. The upper sandy part of the outcrop forms a gently sloping concave geometry which measures roughly 330 m (W-E) by 100 m (N-S) in a horizontal plane (Fig. 5.4A).

The Fes-north section (34.076337, -4.964840) is located north of the city of Fes, 3 km south of Jbel Zalagh and ~7 km west of the El Adergha section (Figs 5.2B and 5.4B). The Fes-north section forms a NE-SW striking topographic sandy ridge that is well exposed for roughly 100 m horizontally and 7 m vertically (Fig. 5.4B). The present-day shape of this outcrop is due to the soil and vegetation cover and does not represent the primary lithosome profile of the outcrop in cross-sectional view. The sandstone ridge overlies a succession of marlstone pertaining to the Blue Marl Formation.

### *5.2 Age and depositional domain*

The studied outcrops show a range of facies related to different depositional environments, as such, the age and depositional domain estimates will be treated individually for each section. The biostratigraphic results from the El Adergha section

indicate a depositional period between 7.51 Ma and 7.25 Ma for the uppermost 100 m of the section (Fig. 5.5). The sand-rich interval at the top, consisting of the uppermost 28 m (Figs 5.5 and 5.6) has been dated between 7.35 Ma and 7.25 Ma based on the common occurrence of *Globorotalia menardii* 5. This species appears frequently between its first common occurrence at 7.35 my and the replacement of *Globorotalia menardii* by *Globorotalia miotumida* at 7.25 Ma (Sierro, 1985; Sierro *et al.*, 1993, 2001; Hilgen *et al.*, 2000; Capella *et al.*, 2017a). Benthic foraminifer assemblages indicate a depositional domain in the slope for the blue marl package (250 to 400 m water depth) and an upper slope depositional domain (300 to 140 m water depth) for the sand package. These results are supported by the findings of Capella *et al.* (2017a).

Most of the collected samples in the Fes-north section contain abundant planktic foraminifers. In general, keeled globorotalid forms are scarce, but *Globorotalia menardii* 5 is common in some samples and *Globorotalia menardii* 4 is usually rarer. Based on this, this section is dated as being between the last common occurrence of *Globorotalia menardii* 4 at 7.51 Ma and the replacement of *Globorotalia menardii* by *Globorotalia miotumida* at 7.25 Ma (Sierro, 1985; Sierro *et al.*, 1993, 2001; Hilgen *et al.*, 2000; Capella *et al.*, 2017a; Tulbure *et al.*, 2017). The continuous presence of dominant sinistral specimen of *Globorotalia scitula*, including *Globorotalia suterae* led to a determination of an age older than 7.28 Ma, which is the age at which coiling in this group changed from sinistral to dextral (Sierro *et al.*, 1993). The benthic foraminifer assemblages indicate a depositional domain in the slope with abundant deeper water taxa such as *Lagena*, *Syphonina*, *Gyroidina*, *Melonis*, etc., mixed with shallow water benthic species such as *Elphidium*, *Ammonia*, *Nonion*, *Lobatula*, etc. The percentage of planktic foraminifers relative to benthic foraminifers is on average higher than 60%. Some samples contain reworked specimens from the Eocene to middle Miocene.

### *5.3 Palaeogeographic reconstruction based on obtained ages and depositional domains*

de Weger *et al.* (2020) recently described a contourite channel system and the intermittent behaviour of palaeo-Mediterranean Outflow Water (palaeo-MOW). The system described therein is located north of the Prerifian Ridges, compared to the outcrops described here (Figs 5.1 and 5.2). Furthermore, the deposits on which their interpretation is based are dated between 7.8 Ma and 7.51 Ma and are thus older than the deposits described in this study (7.51 to 7.25 Ma). Although attributed to a different stratigraphic interval, they



are thought to have likely been formed by similar deep-marine processes controlled by the overflow of the late Miocene palaeo-MOW.

The geographical offset between the contourite depositional system north of the Prerifian Ridges (de Weger *et al.*, 2020) and the El Adergha and Fes-north sections (Figs 5.1 and 5.2) has been related to the tectonic emplacement of these ridges. As described by Roldan *et al.* (2014), the Prerifian Ridges evolved since the late Miocene to the present. The northern channels were located on the frontal part of the accretionary wedge and recorded sedimentation until 7.51 Ma, however, once the Prerifian Ridges became more prominent during the late Tortonian, around 7.51 Ma, the main palaeo-MOW pathway was forced south of these ridges (Fig. 5.5), abandoning the northern channels. Further evidence for these changes is found in the Ain Kansera section described by Capella *et al.* (2017a). The Ain Kansera section, dated between 7.51 Ma and 7.35 Ma, consists of shallow-marine infralittoral deposits, and is located near the easternmost physical expression of the Prerifian Ridges, closer compared to the El Adergha and Fes-north sections (Fig. 5.5). The Ain Kansera section has previously been interpreted as a north-eastward prograding linear clastic coast with depositional water-depths ranging between 15 m and 100 m (Capella *et al.*, 2017a).

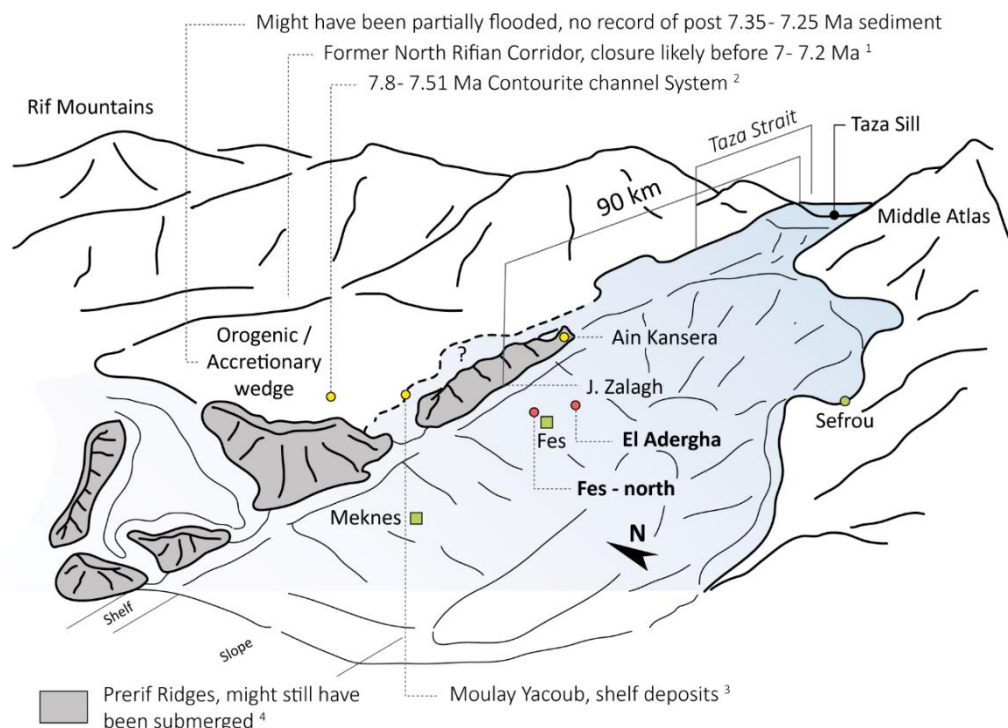


**Figure 5.6.** Palaeogeographic reconstruction of the late Miocene South Rifian Corridor (7.51 to 7.25 Ma). The Prerifian Ridges (grey) might still have been submerged at this time. Red dots indicate sections studied herein. Yellow dots indicate sections previously studied, publications of these sections studied previously are denoted by superscript numbers (<sup>1</sup> Tulbure *et al.*, 2017, <sup>2</sup> de Weger *et al.*, 2020, <sup>3</sup> Capella *et al.*, 2018). Green squares indicate the relative location of major cities in the area.

Based on the palaeogeographic reconstruction performed by Capella *et al.* (2017a), the thickness of underlying deposits for each section to the nearest expression of the orogenic/accretionary wedge and the African margin (Fig. 5.5) and the depositional domain obtained from benthic foraminifer assemblages, the Prerifian Ridges most likely formed a N-S oriented slope on the northern margin of the South Rifian Corridor (Fig. 5.6). The southern boundary of the South Rifian Corridor was located near the city of Sefrou (Capella *et al.*, 2018), roughly 30 km south of the Ain Kansera section, indicating that between 7.51 Ma and 7.25 Ma the corridor was approximately 30 km wide. The Taza Sill was located 90 km eastwards of the studied sections and the westernmost expression of the Prerifian Ridges is located roughly 85 km towards the west. This implies that the steeply flanked South Rifian corridor measured roughly 30 km in width and 175 km in length, westward of Taza Strait (Fig. 5.6).

#### *5.4 Sedimentary facies*

Nine different sedimentary facies (F1 to F9) have been distinguished in the two studied sections (Table 5.1; Figs 5.7 and 5.8). The sedimentary facies include: (i) F1 - fossil-rich blue marlstone; (ii) F2 - sandy marlstone; (iii) F3 - bi-gradational sandstone; (iv) F4 - heterolithic mudstone and sandstone; (v) F5 - heterolithic, cross-stratified and rippled sandstone; (vi) F6 – cross-stratified sandstone; (vii) F7 - sigmoidal, mud-draped sandstone; (viii) F8 - amalgamated, normal graded mudstone and sandstone; and (ix) F9 - deformed, heterolithic mudstone and sandstone.

##### *5.4.1 Facies F1 – fossil-rich blue marlstone*

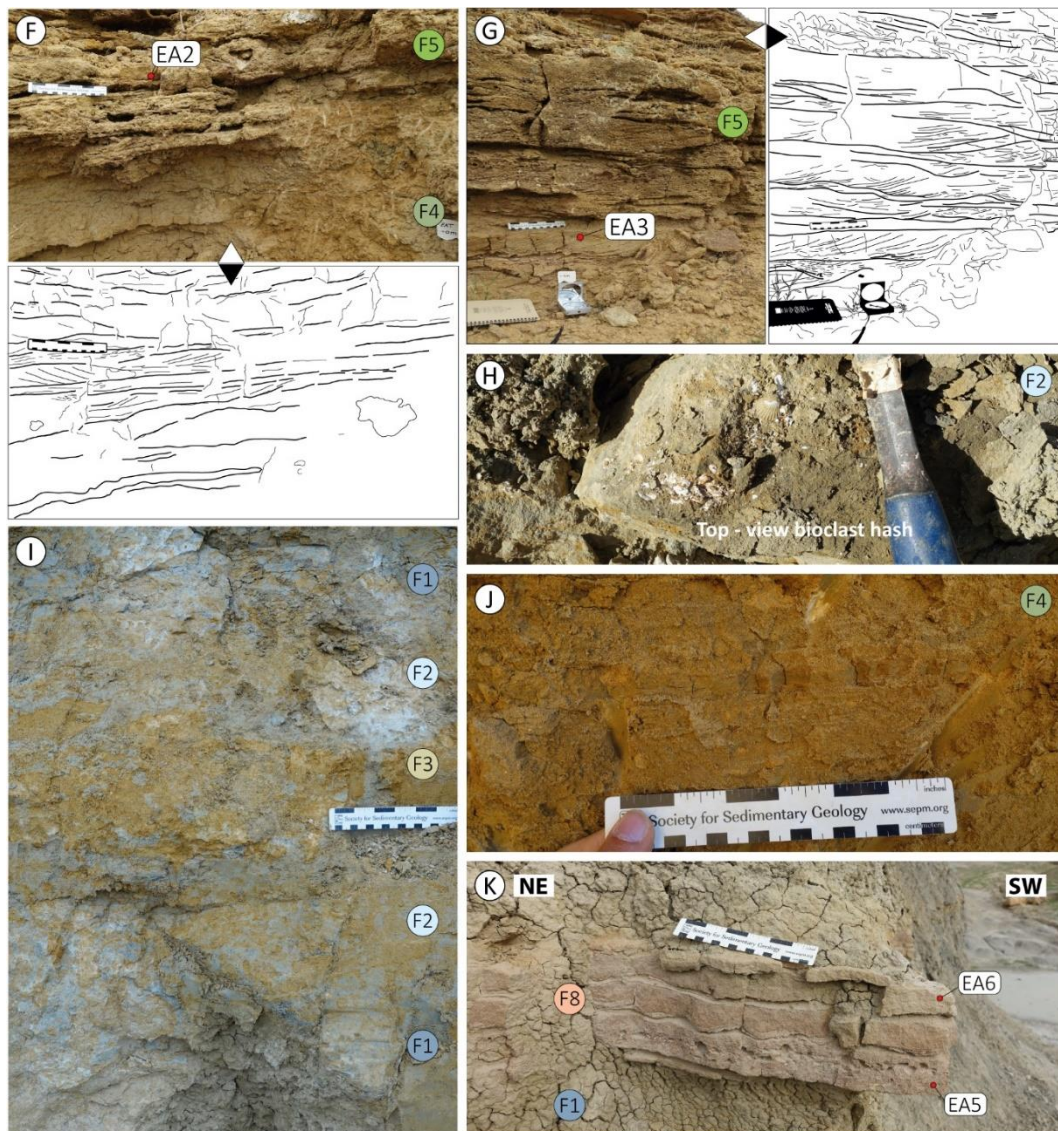
###### *Description.*

F1 consists of blueish marls, the sediments after which the Blue Marl Formation is named (Table 5.1; Fig. 5.7A to E). The intervals containing these dominantly structureless, fossil-rich marlstones (containing bivalves up to a centimetre in size) range in thickness from decimetres to hundreds of metres forming a continuous succession. Despite being dominantly blueish in colour, modest gradational changes ranging on average from 0.5 to 2 m in thickness from dark blueish-grey to more brownish-grey are common. This colour change results from slight increases in the biogenic and siliciclastic fraction consisting of up to fine-grained and very fine-grained sand, respectively. F1 only shows scarce discrete trace fossils.









(cont) Collage of examples of facies from the El Adergha outcrop. Picture letters correspond to those in (A) to (E). (F) Picture and line-drawing of the contact between facies F4 and F5 at 21 m in the log. Facies F4 is mottled, not easily captured by lines at this scale. (G) Picture and line-drawing of typical facies F5. The lowermost right corner is not well-exposed. (H) Top-view picture of bioclast (pecten) hash, imbrication bioclastic material not visible in picture. Note the 1 cm pecten shell in the middle top-view of the picture. (I) Bi-gradational stacking of facies F1-F2-F3-F2-F1. The F3 and F2 facies are intensely bioturbated leaving a mottled appearance. (J) Typical facies F4, consisting of laminated sandstone and mudstone and moderate bioturbation. (K) Turbidite deposits found roughly 100 m stratigraphically below the main studied interval, embedded in facies F1.

### Interpretation.

The late Miocene blue marls of F1, are widely recognized in northern Morocco and other parts of the Mediterranean region where they are generally associated with open deep-marine conditions (Di Geronimo *et al.*, 1981; Bernini *et al.*, 1992; Krijgsman *et al.*, 1999b; Mansour and Saint Martin, 1999; Barbieri and Ori, 2000; Gelati *et al.*, 2000; van Assen *et al.*, 2006; Muto *et al.*, 2017; Capella *et al.*, 2017a). F1 represents a low energy depositional

Facies	Lithology	Grading	Thickness	Sedimentary structures	Accessories	Ichnology
<b>F1</b> Fossil-rich blue marlstone	Fossil-rich marlstone occasionally enriched in silt to very fine-grained sand	None or subtle normal and inverse grading	cm-scale to 100's of m-scale	Structureless with occasional laminae of up to very fine-grained sand and shell debris		Scarce discrete trace fossils
<b>F2</b> Sandy marlstone	Fossil-rich sandy marlstone to marly, fine-grained sandstone	None, normal and inverse grading, or normal grading with sharp basal surface	dm-scale to 10's of m-scale	Structureless, occasional bioclast enriched traction carpets and remnants of starved, fine-grained sandy ripples		Abundant undifferentiated trace fossil and scarce <i>Planolites</i> -like and <i>Thalassinoides</i> -like
<b>F3</b> Bi-gradational sandstone	Up to medium-grained mixed compositional sand	Successive inverse and normal grading	Up to dm-scale	Planar parallel laminated to fully mottled		<b>EA:</b> scarce discrete trace fossils to abundant <i>Macaronichnus</i> and rare <i>Planolites</i> , <i>Thalassinoides</i> and <i>Rosselia</i> <b>FN:</b> low to moderate undifferentiated bioturbation and scarce <i>Planolites</i>
<b>F4</b> Heterolithic, thin-bedded mudstone and sandstone	Heterolithic mudstone and mixed compositional up to medium-grained sandstone	Normal grading with graded or sharp basal surfaces	1 to 15 cm	Wavy, lenticular, or discontinuous planar parallel sand laminae. Ripple laminae and mud flasers. Laminated silty/sandy claystone	Numerous detrital pellets of dark, glauconite and large planktonic foraminifers	Abundant discrete trace fossils; abundant <i>Macaronichnus</i> and <i>Parahaentschelinia</i> and rare <i>Planolites</i> and <i>Rosselia</i>
<b>F5</b> Heterolithic, cross-stratified mudstone and sandstone	Heterolithic mudstone and mixed compositional, moderately-sorted to well-sorted, up to coarse-grained sandstone	Normal graded with sharp basal surfaces and occasionally mud-draped foreset boundaries	2 to 20 cm	Undulatory and tabular cross stratified and rippled beds with occasional small (cm-scale) basal scours	Bed boundaries and sedimentary structures regularly encrusted with Fe and Mn	<b>EA:</b> abundant, increase of vertical burrows; abundant <i>Parahaentschelinia</i> and <i>Macaronichnus</i> , rare <i>Planolites</i> and <i>Thalassinoides</i> . <b>FN:</b> vertical traces that are <i>Ophiomorpha</i> -like and <i>Skolithos</i> -like
<b>F6</b> Cross-stratified sandstone	Mixed compositional up to medium-grained sandstone	None to normal grading	10 to 60 cm	Tabular, cross-stratified beds	High proportion of bioclasts and carbonate lithoclasts, muddy rip-up clasts are common	Moderate discrete trace fossils; abundant <i>Ophiomorpha</i> , occasional <i>Skolithos</i> and rare <i>Planolites</i> , <i>Rosselia</i> -like and <i>Thalassinoides</i>
<b>F7</b> Sigmoidal, mud draped sandstone	Up to granule grade mixed compositional sand "draped" by fluid muddy marls	Normal grading	Up to 30 cm	Sigmoidal, mud-draped sandstone bundles	Bed boundaries and burrow linings regularly show Fe and Mn crusting, rip-up clasts are common	Low to moderate undifferentiated bioturbation. Occasional <i>Planolites</i> -like and <i>Thalassinoides</i> -like.
<b>F8</b> Amalgamated, normal graded mudstone and sandstone	Up to medium-grained, well-to very well-sorted sandstone capped by mudstone	Normal grading	5 to 20 cm	Tabular, amalgamated, occasionally rippled beds with basal scour surfaces	Occasionally contain rip-up clasts	Low to moderate undifferentiated bioturbation. Scarce discrete trace fossils
<b>F9</b> Deformed, amalgamated mudstone and sandstone	Mixed compositional, up to coarse-grained sandstone capped by mudstone	Normal grading	4 up to 15 cm	Deformed, convolute and/or contorted beds with fluid escape structures	Remnants of original bedding	Low to moderate undifferentiated bioturbation. Scarce discrete trace fossils

**Table 5.1.** Sedimentary facies table (F1 to F9) showing the main sedimentological and ichnological characteristics and features of the studied deposits in the El Adergha (EA) and Fes-north (FN) outcrops.

environment where sedimentation is dominated by the vertical settling and lateral advection of both fine-grained biogenic and terrigenous particles through the water column, or hemipelagic sedimentation (Hesse, 1975; O'Brien *et al.*, 1980; Stow and Piper, 1984; Einsele, 2000).

The common increases in silt and sand content suggest fluctuations in carbonate productivity, terrigenous sediment supply and/or in the hydrodynamic regime. These alterations in silt and sand content might reflect the presence of low-density turbidity currents (Lowe, 1982), in which case they reflect Bouma divisions Td and Te (Bouma, 1962), diluted gravity flows and/or the activity of weak bottom currents (Stow and Faugères, 2008; Rebesco *et al.*, 2014; Stow and Smillie, 2020).

#### 5.4.2 Facies F2 – sandy marlstone

##### *Description.*

Facies F2 consists of fossil-rich sandy marlstone and very fine-grained muddy sandstone (Table 5.1; Fig. 5.7C, H and I). This facies occurs over intervals with thicknesses ranging from centimetres to tens of metres. The texture is homogeneous for the finest intervals that are more blueish-grey in colour. The coarser and more light-brownish grey intervals are regularly banded or laminated. Starved ripples of fine-grained sand are scarce. Changes in grain-size distribution are generally gradational, but sharp basal contacts have been observed between muddy and more sandy deposits. Laminae with sharp basal bounding surfaces and ripples coincide with an increased abundance of fine-grained, imbricated shell fragments (Fig. 5.7I) indicating palaeo-flow directions towards the west. The muddier intervals regularly contain well-preserved bivalves up to 1.5 cm in diameter. The trace fossil assemblage consists of abundant undifferentiated structures and scarce *Planolites*-like and *Thalassinoides*-like traces (Fig. 5.9A and C).

##### *Interpretation.*

Facies F2 represents a sand-enriched equivalent of facies F1, reflecting deposition under higher-energy conditions and/or a change in sediment supply. This facies generally lacks sharp bounding surfaces and traction structures, although the presence of the occasional bioclast enriched laminae may represent the remnants of traction carpets. Furthermore, the occasionally observed sharp lower bounding surfaces and sand lenses, which are likely remnants of starved ripples, rule out a pure hemipelagic origin.

Since sedimentary structures and other features related to turbiditic processes are lacking, it is likely that the change in sediment supply primarily resulted from hemipelagic settling of a turbidite suspension cloud also known as a hemiturbidite (Stow and Wetzel, 1990). However, the gradual (consecutive inverse and normal-graded) trends in grain-size distribution might reflect the presence of - and subtle changes in - bottom current velocities (Gonthier *et al.*, 1984; Hüneke *et al.*, 2020).

If hemiturbiditic processes were active, bottom currents, induced by the palaeo-MOW, likely deflected the turbidite suspension cloud down-current, changing the orientation from down-slope to along-slope. This deflection might be inferred from occasionally occurring imbrication patterns of shells and subtle ripple laminae. Furthermore, bottom currents might have been able to winnow and rework the sediment, preventing the settling of the finest particles in the coarsest intervals of facies F2. Winnowing and reworking can also be used to explain the occasional sharp bounding surfaces that are regularly interpreted to result from peak current velocities in most environments affected by bottom currents (Lucchi and Rebesco, 2007; Martín-Chivelet *et al.*, 2008; Rebesco *et al.*, 2014; de Castro *et al.*, 2020a, b).

Based on available data, it is hypothesized that the subtle compositional changes in facies F2 are the result of the interaction between hemipelagites, low-density turbidites and weak bottom currents. Fluctuations in the bottom current activity related to intensification and weakening of the palaeo-MOW might have reworked initial turbidite deposits and have caused fluctuations between contouritic and hemipelagic dominated periods. Based on grain-size, depositional texture and according to the bedform-velocity matrix proposed by Stow *et al.* (2009), bottom currents never exceeded 20 to 25 cm/s. Similar facies have recently been identified in the proximal and central sectors of the Gulf of Cadiz CDS, where muddy contourites are usually interbedded with hemipelagites and turbidites, forming metre-scale sedimentary deposits (de Castro *et al.* 2020b).

#### 5.4.3 Facies F3 – bi-gradational sandstone

##### *Description.*

Facies F3 consists of an inverse- to normal-graded sandstone with a thickness ranging from 10 to 60 cm (Table 5.1; Figs 5.7B, J and 5.8J). This bi-gradational pattern consists of very fine-grained, fine-grained and up to medium-grained sand. The sand is of mixed bioclastic-

siliciclastic composition (Chiarella *et al.*, 2017). Between the El Adergha and Fes-north section differences in this facies have been observed.

In the El Adergha section, facies F3 (Fig. 5.7B) is more bioclastic, contains glauconite and abundant bioturbation of *Macaronichnus* (Fig. 5.9A and B), rare *Planolites*, *Thalassinoides* and *Rosselia* (Fig. 5.9E), leaving a severely bioturbated appearance (Fig. 5.7J). However, despite the intense bioturbation, planar erosive surfaces between the inverse-graded and normal-graded division have been recognized in places. In the Fes-north section, F3 consists of distinct planar laminae with the thickest laminae (up to 1.5 cm) coinciding with the coarsest (medium-grained) sand fraction (Fig. 5.8J). Biogenic structures are limited to a low to moderate number of undifferentiated burrows, and scarce *Planolites* and *Thalassinoides*-like traces (Fig. 5.9H).

#### *Interpretation.*

The bi-gradational sandstone of facies F3 in the El Adergha section very closely resembles the C3 division of the bi-gradational contourite facies model proposed by Faugères *et al.* (1984), Gonthier *et al.* (1984), and Stow and Faugères (2008). The very close resemblance of this bi-gradational facies to the C3-division of the “diagnostic contourite facies model” favours the interpretation of a contouritic drift origin. This interpretation is supported by the findings of Capella *et al.* (2017a).

Bi-gradational sequences, however, might also be formed in different types of current-influenced depositional settings where waning/waxing currents are common, such as deltas with fluctuating river discharge. There is however no evidence of such current-influenced depositional systems in the surrounding area for the depositional period between 7.51 Ma and 7.25 Ma. Furthermore, the lack of distinct erosional surfaces both below and above facies F3 in the El Adergha section (Fig. 7I) indicates subtle changes in the depositional setting and thus the depositional domain did not significantly change to that inferred from the benthic foraminifer assemblage for facies F1 (i.e., the continental slope). This thus suggests that facies F3 was formed in the slope depositional domain, a common area for the formation of contourite drift deposits (Faugères *et al.*, 1999; Hernández-Molina *et al.*, 2008; Rebesco *et al.*, 2014).

Despite the slight differences in facies F3 observed between both outcrops, subtle breaks in sedimentation, indicated by the style of bioturbation and the relatively sharp bounding surfaces in the El Adergha and Fes-north sections respectively (Figs 5.7I and 5.8J), show that



the long-term flow fluctuation responsible for the bi-gradational sequence, was also affected by shorter scale flow variations. These shorter scale variations indicate that, at times, flow velocities were sufficiently high to cause a break in sedimentation, and/or there was a break in sediment supply. Omission surfaces in the central part of the bi-gradational sequence have

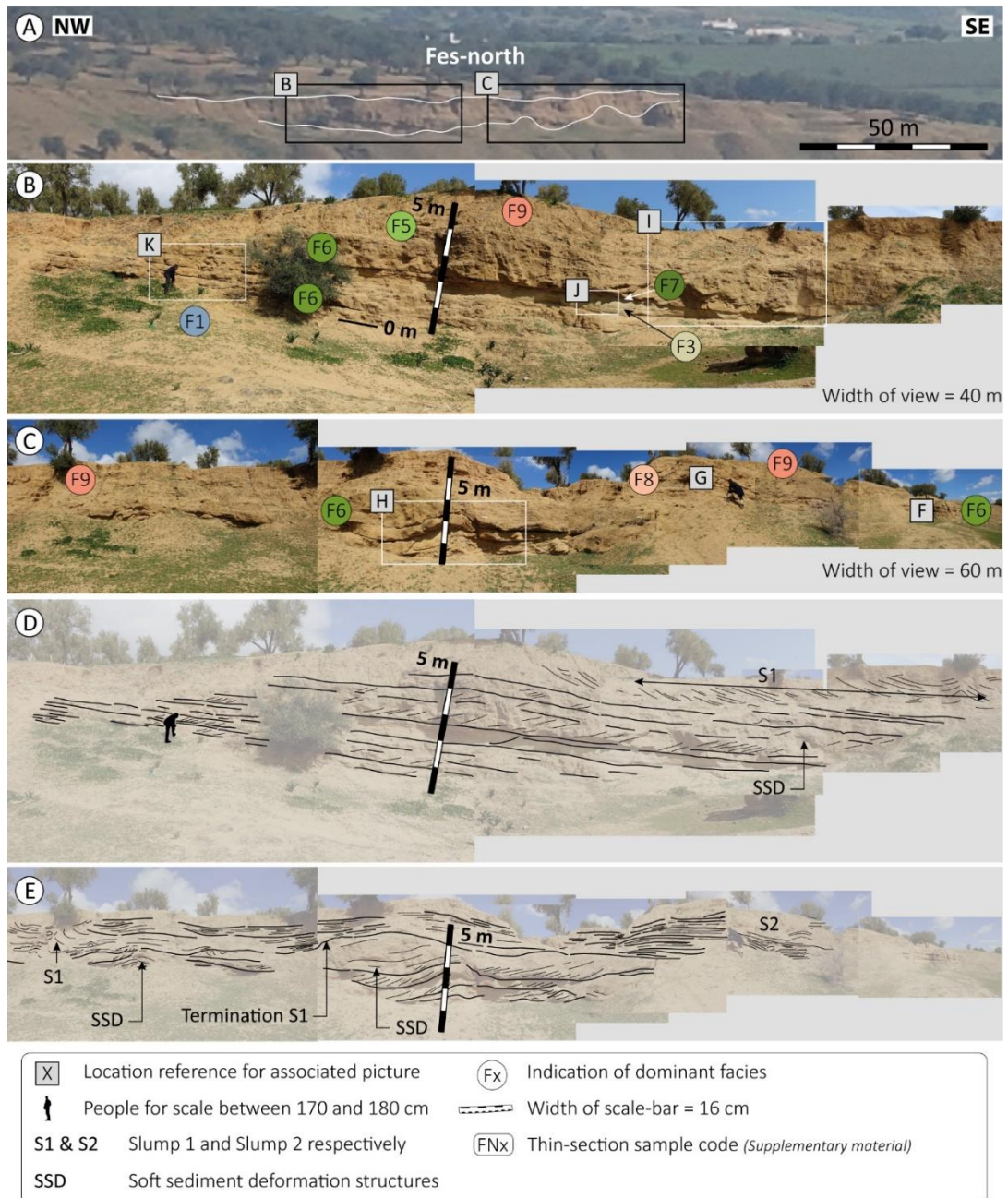


**Figure 5.8.** (A) Panoramic picture of the Fes-north outcrop with the panels indicating the locations of (B) to (E). (B) and (C) form a collage of the laterally (NW-SE) continuous section. Within these pictures the main facies distribution are indicated as well as locations for (F) to (K). (D) and (E) Line-drawings of (B) and (C) respectively. These line-drawings are made to emphasize bed-boundaries and internal structures. (D) Image clearly shows the tectonic tilt of the beds with respect to the near horizontal horizon. At the 5 m mark of the scale bar (4 m in the log) the mainly tabular beds with cross-stratification directed towards the left are overlain by S1 (slump 1) which is stratified mainly in the opposing direction. (E) This eastward lateral and upwards continuation of panel D (S1 for reference) shows that lateral facies changes are present. Furthermore, the termination of S1 against facies F6 (C) is visible. Within facies F6 SSD structures are visible. S2 overlies the more planar stratified facies F8 here.





(cont) Sedimentary log and picture collage of facies in the Fes-north outcrop. (F) Picture of facies F2 and F6, corresponding to 11 to 12 m in the log. Cross-stratification of facies F6 is directed towards the left (west). (G) Facies F8, alternating with facies F2. Facies F2 in this succession represents suspension fallout from a turbidity cloud. (H) Overview picture of the interval between 5.5 m and 8 m in the sedimentary log. The lower field of view shows facies F6 containing soft sediment deformation structures. This facies is overlain by facies F8. (I) Overview picture of the interval between 1 m and 5.5 m in the log. Here facies F3 and F6 are overlain by slump deposits of facies F9. (J) Picture showing both facies F3 and F7 and their stratigraphic relationship. On top of facies F7 a sharp basal contact with facies F6 is present. (K) Western-most expression of the exposed outcrop with stacked tabular beds of facies F6.



previously been reported in similar sequences, interpreted as contourite drift deposits, from the ancient record (Rodríguez-Tovar *et al.*, 2019; Hüneke *et al.*, 2020).

#### 5.4.4 Facies F4 – heterolithic, thin-bedded mudstone and sandstone

##### *Description.*

F4 consists of heterolithic orange to reddish-grey clay and marlstone and brownish to orangish-grey very fine-grained up to medium-grained sand (Table 5.1; Fig. 5.7J). The finely laminated to thinly bedded sands (<10 cm) are tabular (Fig. 5.7D) and occasionally show ripples. The base of the sandstone beds is sharp or gradational and occasionally shows an undulatory geometry. The sand component is of mixed siliciclastic-bioclastic composition, enriched in glauconite (< 10%). Muddy laminae that are interbedded with the sands, are often wavy, lenticular, or discontinuous parallel. Other features include silty mud flasers and muddy rip-up clasts (Fig. 5.7F and J). A mottled appearance, predominantly concentrated in the finest sediments, results from intense, often undifferentiated bioturbation. The trace fossil assemblage consists of abundant *Macaronichnus* (Fig. 5.8D), common *Parahentzschelinia* and rare *Planolites*, *Rosselia* (Fig. 5.8E) and *Thalassinoides*.

##### *Interpretation.*

Facies F4, in comparison to facies F1 and F2, due to its coarser medium grain-size and the presence of occasional traction structures, is related to higher peak current velocities. As this facies unconformably overlies facies F1 and F2 (Fig. 5.7D and B respectively), it indicates a change in hydrodynamic conditions related to an increase in maximum flow velocity. Like facies F3, the depositional domain was likely in the slope, ruling out a shallow-marine current-dominated setting. The rhythmical variations in grain-sizes and co-occurrence of fine-grained sand and mud laminae suggest deposition through alternating periods of bedload and suspension transport. Since facies F4 closely resembles the stacked sand sheets described by Martin-Chivelet *et al.* (2008), Rebesco *et al.* (2014), de Castro *et al.* (2020a) and Hovikoski *et al.* (2020) it might have a similar origin related to bottom currents with alternating flow conditions. During peak current velocities, the fine-grained sand can form ripples whilst the finest fraction of the sediment is winnowed or re-incorporated as aggregates and rip-up clasts (de Castro *et al.*, 2020a). Hüneke *et al.* (2020) suggest that fluctuating bottom currents characterize deposition for all contourite divisions even though the controlling mechanism behind the short-term fluctuation of flow strength is unknown.

Shanmugam (2008), however indicated that short-term oscillating energy conditions have been described from thermohaline and wind-driven bottom currents. Furthermore, climatic and tidal induced changes on the characteristics of the palaeo-MOW also affect variability in flow-conditions on shorter, millennial to sub-annual timescales (de Castro *et al.*, 2020b; de Weger *et al.*, 2020). These processes explain the development of heterolithic alternations as a consistent indicator of bottom current fluctuations. The preservation of primary sedimentary structures within the sandstone beds indicates that bottom currents remained sufficiently strong to winnow away fine-grained sediment and to prevent disruption due to bioturbation (de Castro *et al.*, 2020a).

#### 5.4.5 Facies F5 – heterolithic, cross-stratified mudstone and sandstone

##### *Description.*

Facies F5 typically consists of heterolithic, dominantly thin-bedded (< 10 cm) to medium-bedded (< 20 cm) sandstone draped by mud (Table 5.1; Fig. 5.7G and H) that are part of large westward migrating foresets (Fig. 5.7B). These beds, which thus likely present foresets, show unidirectionally westward verging cross-strata (Fig. 5.7C) with bundles of thickening and thinning foreset-laminae and angular to tangential toe-set geometries (Figs 5.7G and 5.10A; more clearly visible in 5.10A). Beds form 1 to 1.5 m thick sets, associated with the previously mentioned westward migrating foresets. Cross-sets have a planar parallel to undulatory erosive base and regularly show traction carpets of muddy rip-up clasts and small (cm-scale) scours at their base (Fig. 5.7G). The beds occasionally contain ripples showing opposing current directions (Fig. 5.7G). The sand consists of fine-grained up to coarse-grained sand of orangish-brown colour. Bed boundaries regularly show Fe-Mn crusting. Biogenic structures are dominantly vertically oriented and consist of an assemblage of abundant *Parahaentschelinia* (Fig. 5.9F) and *Macaronichnus*, common undifferentiated vertical structures, and rare traces such as *Ophiomorpha*-like and *Skolithos* vertical traces.

##### *Interpretation.*

The cross-stratified nature and general tabular bedding of these westward migrating deposits suggests them to be relics of deep-marine two-dimensional (2D) dunes. Based on the presence of thickening and thinning foreset-bundles (Allen, 1982; Longhitano and Nemec, 2005), gradual changes between angular to tangential toe-set geometries (Chiarella, 2016; Fig. 5.10) and sand-mud couplets (Nio and Yang, 1991; Longhitano *et al.*, 2012), the

formation of these deposits was influenced by oscillatory flow. As such, this facies can be related to a tidally modulated current.

Facies F5, based on dominant palaeocurrent directions indicating westward flow, is interpreted as a relic of westward migrating dunes. This interpretation is supported by the findings of Capella *et al.* (2017a). These dunes migrated under current velocities reaching more than 1 m/s (Stow *et al.*, 2009) in a late Tortonian channel in front of a strait. These conditions infer a depositional environment where energy is more concentrated than in other sectors, such as the contourite channel. Similar sandy deposits have also been identified in modern contouritic channels (Nelson *et al.*, 1993, 1999; Hernández-Molina *et al.*, 2006, 2014b; Stow *et al.*, 2013; Brackenridge *et al.*, 2018; Lozano *et al.*, 2020). The dominance of vertical biogenic structures in F5 supports the occurrence of energetic environmental conditions.

#### 5.4.6 Facies F6 – cross-stratified sandstone

##### *Description.*

Facies F6 consists of sandstones with unidirectionally westward verging cross-strata which include bundles of thickening and thinning foresets that show alternations between angular to tangential toe-set geometries (Fig. 5.8D, F and K). Bedding is generally 10 to 100 cm thick and has sharp basal boundaries with common muddy rip-up clasts. The thickest beds have a subtle concave-up geometry. Sediment is composed of moderately to well-sorted, medium-grained to coarse-grained sand represented by mixed bioclastic-siliciclastic grains. This facies is moderately bioturbated with *Ophiomorpha* (Fig. 5.9G), occasional *Skolithos* and rare *Planolites*, *Rosselia*-like and *Thalassinoides* trace fossils. Sometimes burrow linings as well as bed boundaries show Fe-Mn crusting.

##### *Interpretation.*

Like facies F5, the cross-stratified nature and the presence of tidal signatures of these westward migrating deposits (Fig. 5.5) suggests them to be relics of deep-marine 2D dunes of which their formation relies on a tidally modulated current near the seafloor. The lack of mud drapes indicates that despite the tidally modulated alternating flow conditions, flow velocities never dropped below the threshold value to deposits and/or preserve muddy sediment, indicating that deposition took place under flow velocities ranging from ~ 50 cm/s to over 1 m/s (Stow *et al.*, 2009). These conditions also infer a depositional environment in

the slope domain where energy is more concentrated than in other sectors, such as the contourite channel. Like facies F5, similar sandy deposits have also been identified in modern contouritic channels (Nelson *et al.*, 1993, 1999; Hernández-Molina *et al.*, 2006, 2014b; Stow *et al.*, 2013; Brackenridge *et al.*, 2018; Lozano *et al.*, 2020). The dominance of vertical biogenic structures in facies F6 also supports energetic environmental conditions.

#### 5.4.7 Facies F7 – sigmoidal, mud-draped sandstone

##### *Description.*

Facies F7 consists of sigmoidal cross-stratified sandstone alternating with mudstone (Table 5.1). The sandstone foresets are encapsulated in and draped by up to 1 cm thick, scarcely bioturbated mud forming distinct up to 30 cm thick bundles of thickening and thinning foresets (Fig. 5.8J). Muddy to marly rip-up clasts are common and mainly occur at the basal bounding surfaces. The sand fraction consists of up to granule-sized mixed siliciclastic-bioclastic sand. Biogenic structures are limited to scarce discrete trace fossils (e.g., *Thalassinoides*-like and *Planolites*-like).

##### *Interpretation.*

The sand-mud couplets recognized in the cross-strata of facies F7 suggest a fluctuation in the energy of the flow to form heterolithic bundles. The mud drapes and ripped-up muddy clasts are thought to represent fine particles originating from high suspended mud concentrations (Faas, 1991). Accordingly, the sandy intervals represent the record of current-dominated processes while the draping mud reflect a moment of reduced energy, favouring the decantation and drapes of the fine-grained material previously kept in suspension (Visser, 1980). According to Nio and Yang (1991), a bimodal grain-size with the muds interlayering medium-grained or coarse-grained sandstones is an indication of tide-modulated currents. The lack of sedimentary structures referable to wave action and high-energy environments suggest a depositional environment below the fair-weather-wave base in a current-dominated environment.

#### 5.4.8 Facies F8 – amalgamated, normal graded mudstone and sandstone

##### *Description.*

Facies F8 consists of heterolithic mud- and sandstone intervals (Table 5.1; Figs 5.7K and 5.8G). The tabular, generally thin-bedded, sandstones (up to 20 cm) are normal graded, and regularly have small (cm-deep) basal scours. Although a semi-gradational transition from sand to mud occurs, boundaries can be easily distinguished. This facies in El Adergha, consists of thin, amalgamated beds presenting basal rip-up clasts of up to pebble sized marls, plane-parallel lamination, and ripples, capped by a very thin marlstone. The sediment is of mixed siliciclastic-bioclastic composition. The sand is up to medium-grained and well-sorted to very well-sorted. The facies is bioturbated with scarce undifferentiated discrete trace fossils (Fig. 5.9I).

#### *Interpretation.*

Facies F8 generally shows basal scours and clear bounding surfaces. The well-sorted to very well-sorted, normal graded beds and internal structures typically represent a decelerating turbulent flow from the upper flow regime to suspension fallout (Bouma, 1962) and are, as such, interpreted as turbidites. The sediment composition of the sand fraction in this facies varies between both the El Adergha and Fes-north sections (Fig. 5.10B to D respectively). At the El Adergha section, facies F8 consists of very fine-grained, relatively mature siliciclastic sand whereas at the Fes-north section, it consists of medium-grained, immature siliciclastic sand (Table S5.1; Fig. S5.2). This implies that facies F8 at the El Adergha section represents a more distal sector in respect to the Fes-north section. The composition and stacking pattern of facies F8 in El Adergha (Fig. 5.7K) is most like those observed in base-of-slope or basin wedge settings (Stow, 1985). The tabular thin bedded nature of facies F8 recognized in the Fes-north section (Fig. 5.8C, G and H) might also suggest a basinal turbidite (silty-sandy distal lobe) depositional setting. However, here facies F8 more likely represents the tail of turbidity current deposits on the slope (Mutti, 1992; Mutti *et al.*, 2009; Mulder, 2011; Talling *et al.*, 2012) or very low-density turbiditic currents on the slope as recently discussed by de Castro *et al.* (2020a, b) and Hüneke *et al.* (2020).

#### *5.4.9 Facies F9 – deformed, amalgamated mudstone and sandstone*

##### *Description.*

Facies F9 consists of amalgamated, heterolithic, thin-bedded (up to 10 cm) strata of marlstone and sandstone up to medium-grained (Table S5.1; Fig. S5.2A). Strata are convolute and fluid escape structures are common (Fig. 5.8B, C and I). The primary sedimentary



structure is like facies F8, consisting of amalgamated normally graded tabular, thin-bedded mudstone and sandstone. The base is sharp, erosive and in many cases seems to have deformed the underlying facies (Fig. 5.8H). This facies appears wedge shaped, thinning out north-westwards. The preserved primary bedding is folded, indicating south to south-eastward deformational migration. Inclination of the modified but preserved primary strata varies laterally from high-angle (40°, westward dipping) to opposing angles (20°, eastward dipping) (Fig. 5.8D and I). Biogenic structures are scarce and discrete trace fossils are difficult to identify, a few *Planolites*-like traces were observed (Fig. 5.9J).

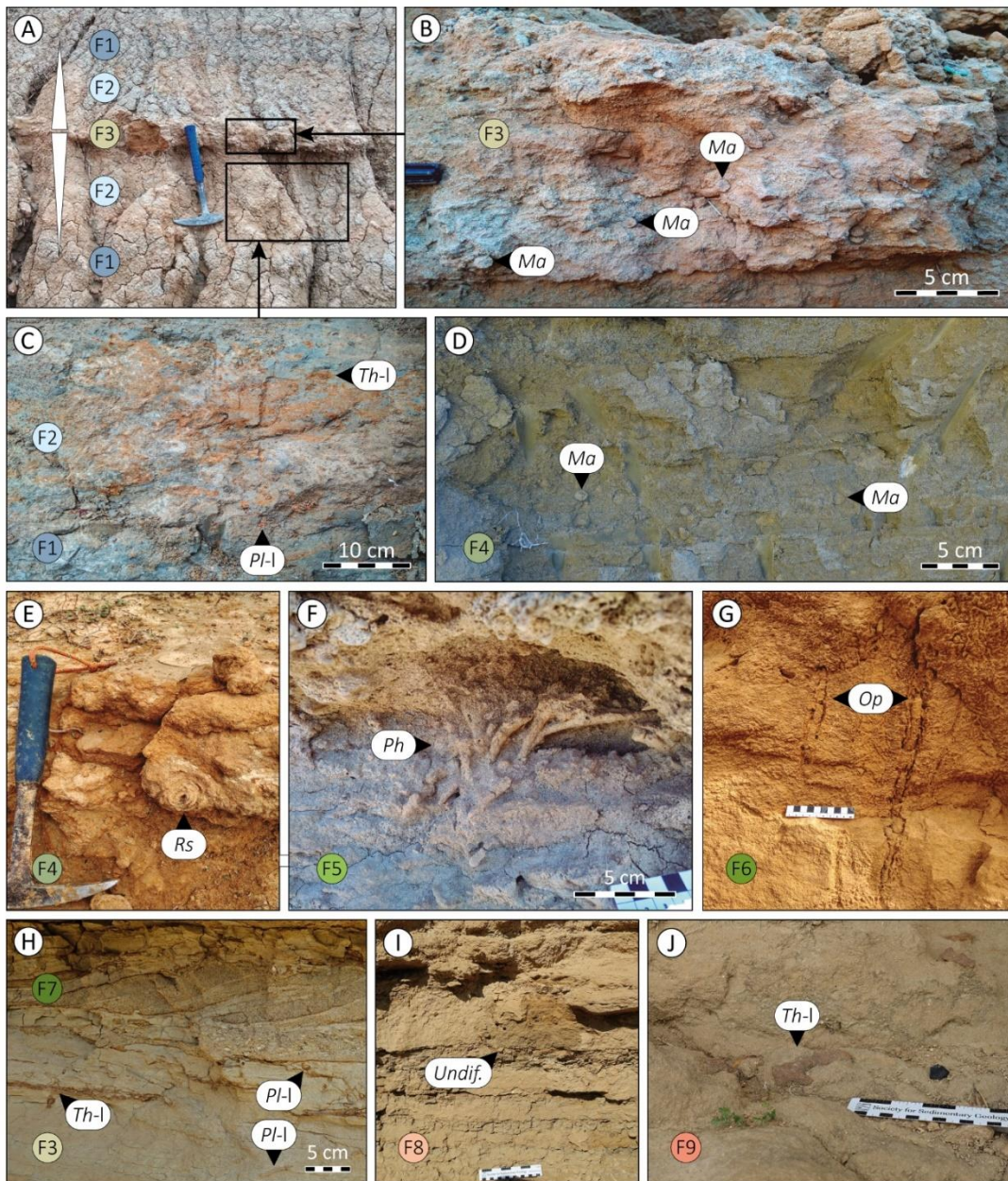


**Figure 5.9.** Overview of recognized ichnospecies: *Macaronichnus* (Mn), *Thalassinoides* (Th), *Planolites* (Pl), *Rosselia* (Rs), *Ophiomorpha* (Op) and undifferentiated (Undif.) traces. The addition of (l) stands for -like. Facies are indicated with the coloured and labelled circles. (A) to (F) are taken from the El Adergha sections and (G) to (J) from the Fes-north section.

### *Interpretation.*

The convolute and/or contorted nature, accompanied by the erosive basal surface recognized in facies F9 suggest that it represents the product of a slump (Leeder, 2009; Reading, 2009; Shanmugam, 2010). Additional evidence of the sudden displacement of large volumes of sediment is found in the fluid-escape structures locally present in the underlying sediment. Although slumps may occur over a wide range of depositional environments, their formation relies on slopes. Since the primary bedding of facies F9 is like F8, F9 represents down-slope, plastically deformed fine-grained turbidites.

### *5.5 Ichnofacies*

Ichnological analysis from the El Adergha and Fes-north sections reveals, in general, low ichnodiversity in assemblages. El Adergha has a higher abundance of traces which are dominantly horizontal whereas the structures in Fes-north are dominantly vertical. This difference is related to variable palaeoenvironmental conditions, especially with respect to hydrodynamic energy.

The trace fossil assemblages at the El Adergha section are characterized by low ichnodiversity and a high abundance of traces produced by deposit feeders. The two main ichnogenera (*Macaronichnus* and *Parahaentzschelinia*) are typical of proximal, shallow marine environments related to the *Skolithos* ichnofacies (MacEachern *et al.*, 2007, 2012; Buatois and Mángano, 2011; Knaust, 2017). However, being typified by dominantly horizontal traces allows the assignation to the *Cruziana* ichnofacies which is typical of deeper and more distal environments. In this context, the presence of vertical structures could be related to periods with stronger bottom currents creating higher energetic palaeological conditions like those in shallow marine environments (i.e., upper slope) at more distal and deeper settings (Miguez-Salas *et al.*, 2020).

In the Fes-north section, trace fossil assemblages record low ichnodiversity and a moderate to low abundance of traces of dominantly vertical forms. The main ichnogenus is *Ophiomorpha*. *Ophiomorpha* is generally, but not exclusively, characteristic of high-energy environments (i.e., shoreface) with well-sorted shifting sandy substrates, constituting a typical element of the *Skolithos* ichnofacies (MacEachern *et al.* 2007, 2012). However, the appearance of *Ophiomorpha* in deep-sea environments with gravity flow sediment supplies confirms the *Ophiomorpha rudis* ichnosubfacies (Uchman, 2009; and references therein). Thus, the presence of *Ophiomorpha* should not necessarily be related to the *Skolithos*



ichnofacies, but to higher energetic environments at Fes-north than that corresponding to El Adergha.

## 6. DEPOSITIONAL SUB-ENVIRONMENTS

### 6.1 Depositional elements and facies associations

The sedimentary facies are linked to form distinct facies associations (FA) and depositional elements (Table 5.2). The fine-grained sediments of facies F1 and F2 are grouped into FA1. FA1 occurs over intervals of one to hundreds of metres thick where both facies regularly grade into one-another. FA1 is generally coarsening upwards grading from facies F1 to F2. FA2 consists of the distinct bi-gradational stacking of facies F1, F2, F3, F2 and F1 (Fig. 5.7J) or F2, F3 and F2 (Fig. 5.8J). FA3 consists of facies F4, which, albeit heterolithic, is considered an individual facies based on the regular lack of bounding surfaces. However, the heterolithic occurrence of sandstone and marlstone could be considered the alternation between fine-grained facies (F1 and F2) and sand-rich facies somewhat similar in sedimentary composition as facies F3. FA4, consisting of facies F5, F6 and F7, typified by the presence of traction structures (mainly cross-stratification). FA5 is distinguished based on depositional features with palaeo-transport indicators perpendicular (downslope) to those observed in FA4.

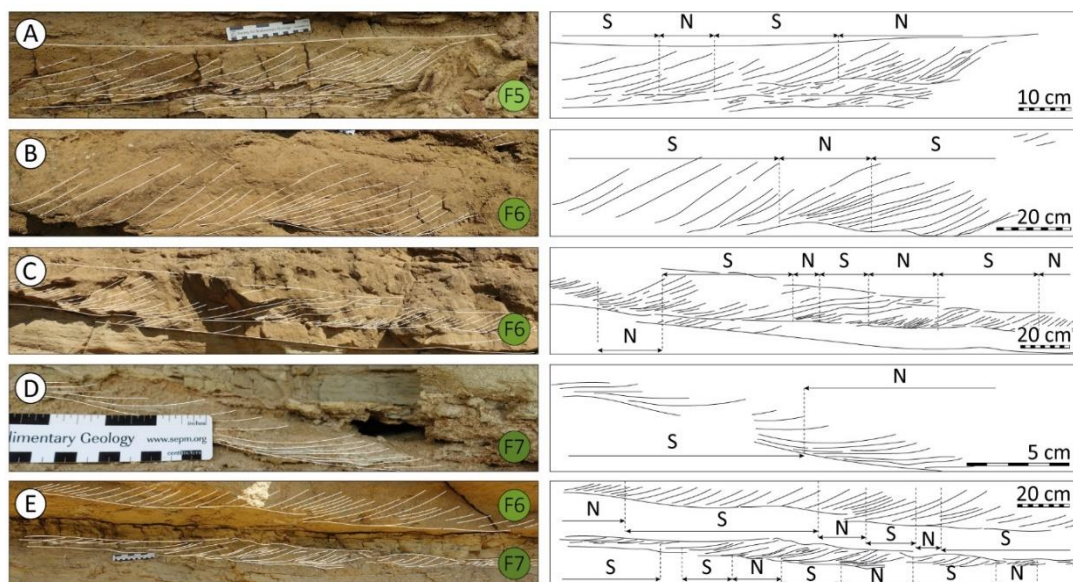


**Figure 5.10.** Examples of cyclic thickening and thinning foreset intervals and cyclic alterations between angular and tangential toe-sets. These alternations are associated with cross-stratification and interpreted as the record of sandy bedforms migrating under unidirectional, tidal-modulated accelerating/decelerating currents. N = neap tide and S = spring tides.

Based on the: (i) palaeogeographic reconstruction of the South Rifian Corridor; (ii) the topography of the Prerifian Ridges on the northern margin of this corridor (Fig. 5.6); (iii) the interpretation that the studied sections have been deposited in a slope depositional domain; and (iv) evidence suggesting the presence of a late Miocene unidirectionally westward migrating, tidal influenced bottom current (Fig. 5.10), it is suggested that the studied sedimentary successions were formed predominantly by the action of the late Miocene palaeo-MOW. As such, the facies associations and depositional domains are interpreted within this framework (Fig. 5.11).

### 6.1.1 Fine-grained marine sediment (FA1)

Based on the available data, the fine-grained marine sediment of facies association FA1 and its subtle changes in composition is interpreted to result from the interaction between hemipelagic, low-density turbiditic and bottom current induced sedimentation. Fluctuations in the bottom current activity, related to the intensification and deceleration of the palaeo-MOW have primarily caused fluctuations between contouritic and hemipelagic dominated

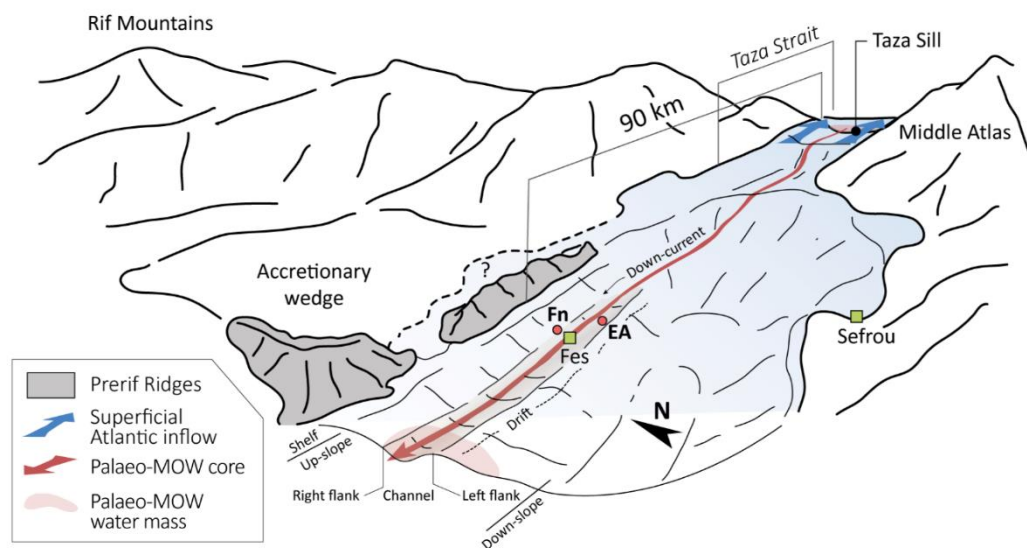


**Figure 5.11.** Palaeogeographic reconstruction of the late Miocene Rifian corridors between 7.51 Ma and 7.25 Ma. The palaeo-MOW cascaded over the Taza Sill, through the Taza Strait into the South Rifian Corridor where it was forced against the northern margin by the Coriolis force. The Atlantic surficial water flowed through the South Rifian Corridor and Taza Strait into the Mediterranean. The studied sections, Fes-north (FN) and El Adergha (EA) were located closely to or within the contourite channel changing over time. The red arrow, indicating the core of the palaeo-MOW depicts the trajectory of highest current-velocities confined within the channel, whereas the palaeo-MOW water mass was less confined.

**Table 5.2.** Sedimentary facies associations (FA) established for sedimentary deposits in the El Adergha (EA) and Fes-north (FN) outcrops.

Sediment size	Orientation	Facies association	FA	Dominant facies	Thickness (m)
Fine-grained sediment	Vertical settling, along-slope and down-slope	Contourite drift	<b>FA1</b>	<b>F1</b> – Hemipelagites <b>F2</b> – Fine-grained turbidites or contourites	up to 100's
		Drift/channel transition	<b>FA2</b>	<b>F3</b> – Fine-grained sandy contourites	0.6 to 1.5
		Channel/drift transition	<b>FA3</b>	<b>F4</b> – Bottom current reworked sands	0.1 to 5
Coarse-grained sediment	Along-slope	Contourite channel	<b>FA4</b>	<b>F5, F6 and F7</b> – Coarse-grained sandy contourites	0.2 to 5
		Down-slope	Upper slope	<b>FA5</b>	<b>F8</b> – Turbidites <b>F9</b> – Slumped deposits

periods. Similar facies have recently been identified in the proximal and central sectors of the Gulf of Cadiz CDS where muddy contourites, associated to the drift, are usually interbedded with hemipelagites forming m-scale sedimentary deposits (de Castro *et al.* 2020b). As such, facies association FA1 has been interpreted to represent the contourite drift or a zone that is located even more distally, further down the slope (Fig. 5.12).

### 6.1.2 Contourites: drift-channel transitional deposits (FA2 and FA3)

Both facies associations FA2 and FA3, due to their relative increase in grain-size and the presence of subtle indicators of bedload transport, are indicative of higher bottom current velocities compared to facies association FA1. This suggests an increase in the palaeo-MOW activity. However, the heterolithic occurrence of sand and mud indicates fluctuating energy conditions.

The strength or velocity of bottom currents associated to overflow water decreases both laterally and down current of the core of the bottom current which is generally confined to a contourite channel (Fig. 5.11) (McCave and Tucholke, 1986; Faugères *et al.*, 1999; Llave *et al.*, 2001; Rebesco *et al.*, 2014; de Castro *et al.*, 2020b). The core of the current is influenced by the Coriolis force. In the case of this study, the westward flowing palaeo-MOW was forced toward the right (north) against the N-S oriented palaeo-slope of the northern margin of the South Rifian Corridor (Fig. 5.11).

Since the highest bottom current velocities are associated with the contourite channel and the weakest bottom currents to the drift (Fig. 5.12), both facies associations FA2 and FA3 represent a transitional depositional environment with weaker currents compared to the core and stronger currents compared to the drift. Facies like those described in facies associations FA2 and FA3 have recently been ascribed to a drift-channel transitional domain where energy conditions are slightly higher than in the drift due to the increased influence of the more closely located core of the bottom current (de Castro *et al.*, 2020b). Also, areas closer to the core of the bottom current are more strongly receptive to changes in the palaeo-MOW activity, explaining the fluctuating energy conditions.

### 6.1.3 Contourites: channel fill deposits (FA4)

Facies pertaining to facies association FA4 (F5, F6 and F7) are characterized by a unidirectional trend of palaeo-current indicators showing a direction perpendicular to the N-S oriented palaeo-slope (Figs 5.11 and 5.12), indicating a roughly 90° offset compared to those measured in facies association FA5 (Fig. 5.5). As facies association FA4 shows a slope-parallel trend of dune migration related to high energetic conditions, this facies association is ascribed to the contourite channel.

The differences in sedimentary composition and structures between F5, F6 and F7 can be explained by their relative position within the contourite channel. As mentioned previously, the current velocity decreases away from the core of the bottom current which is also the case within the contourite channel. The palaeo-MOW core was forced northwards by the Coriolis force, against the palaeo-slope and therefore towards the slope side of the contourite channel (Figs 5.11 and 5.12). This implies that the strength of the bottom current weakens within the channel towards the distally/deeper located drift, but also towards the slope because of increased shear stress. In this case the coarsest sediment related to facies F6 and F7 would be expected in the section closest to the Prerifian Ridges, Fes-north (Fig. 5.11) if both the channel facies are related to the same channel. Furthermore, as mentioned in de Weger *et al.* (2020) the palaeo-MOW was intermittent on tectonic, orbital, climatic and tidal timescales. The explanation of processes behind changes in the modern MOW have recently been described by Sierro *et al.* (2020) who found that the MOW strength is mainly driven by precession cycles and the associated freshwater input in the Mediterranean. A decrease in Mediterranean freshwater input during precession maxima results in an increase in Mediterranean salinity and thus Mediterranean deep-water formation. Enhanced, dense

Mediterranean deep-water formation results in higher density gradients with Atlantic water and an enhanced, or stronger palaeo-MOW. On a millennial scale, the study found that Greenland stadials have a positive effect on buoyancy loss in the eastern Mediterranean which enhances the density gradient with Atlantic water. This results in a more vigorous palaeo-MOW. Similar controlling factors resulted in palaeo-MOW expansion (intensification) and collapse (deceleration) but also in its longer period (> seasonal) oscillatory flow behaviour. Expansion and collapse of the palaeo-MOW likely played an important role in the facies differences of FA4, where, during the deposition of facies F6 and F7, the palaeo-MOW was stronger compared to F5. However, during the deposition of facies F5 and F7 the palaeo-MOW intensity fluctuated considerably more on tidal timescales. The heterolithic nature within these facies, mudstone and sandstone, is likely related to tidally induced flow acceleration and deceleration where the flow velocity within the channel most significantly decreases towards the channel flanks (F5 and F7) with a decelerating bottom current core.

#### *6.1.4 Gravity-driven flow deposits (FA5)*

As mentioned previously, facies association FA5 is characterized by facies with a dominant down slope, N-S oriented, migration component. This down-slope migration is induced by gravitational processes, which, due to these facies occurring interbedded with facies association FA4, indicated that the sections have been deposited on the slope (Fig. 5.12).

## 7. Discussion

### *7.1 Required two-way exchange*

The South Rifian Corridor is regularly considered the last remaining gateway before the onset of the Mediterranean Salinity Crisis, yet the termination of Atlantic-Mediterranean connection through the Betic corridors is not fully constrained. Although the Atlantic-Mediterranean connection through the Betic corridors (Fig. 5.1) largely came to a hold in the late Miocene: (i) the North Betic Strait records continental deposits at ~7.6 Ma (Krijgsman *et al.*, 2000a); (ii) the Granada Basin demonstrates a phase of evaporite precipitation between 7.37 Ma and 7.24 Ma (Corbi *et al.*, 2012); and, (iii) the Guadix Basin was blocked by 7.8 Ma (Betzler *et al.*, 2006); (iv) the Guadalhorce Corridor might have accommodated Mediterranean outflow until 6.3 Ma (Martin *et al.*, 2001). Furthermore, the possible role of

the Strait of Gibraltar in late Miocene Atlantic-Mediterranean exchange should also be considered (Krijgsman *et al.*, 2018) but there is no evidence of its role in connecting both basins between 7.8 Ma and 7.25 Ma.

The Betic corridors were subject to tectonic uplift at around 7.8 Ma (Betzler *et al.*, 2006; Krijgsman *et al.*, 2006), roughly 800 ky earlier than in the Rifian corridors where tectonic uplift was initiated around 7 Ma (Capella *et al.*, 2017b; Tulbure *et al.*, 2017). This suggests that the Betic corridors were shallowing long before the Rifian corridors. By means of physical modelling, de la Vara *et al.* (2015), demonstrated that the exchange through the Betic - Guadalhorce Corridor and the South Rifian Corridor depends predominantly on the depth of each corridor with respect to the other. More specifically, both corridors present two-way flow unless the shallower gateway is shallower than about the mid-depth of the deeper corridor. Based on the Guadalhorce Corridor having been affected by tectonic uplift prior to the South Rifian Corridor, it is very likely that the South Rifian Corridor, or more specifically the Taza Sill, was twice as deep, only allowing two-way exchange through the Taza Sill. This allowed the overflow of the palaeo-MOW into the South Rifian Corridor, supporting the interpretation of the South Rifian Corridor having been subject to a palaeo-MOW, enabling the formation of a contourite depositional system like that described in the Gulf of Cadiz (Llave *et al.*, 2007; Hernández-Molina *et al.*, 2016).

## *7.2 The proposed facies model*

De Castro *et al.* (2020b) proposed the first inclusive contourite facies model for contourite channel systems to date. This facies model has been constructed based on a multiple core related dataset derived from the Gulf of Cadiz. However, the core material does not cover most of the sand-rich intervals related to the contourite channel. Despite not fully capturing the contourite channel deposits, the proposed model shows many similarities but is distinctly more inclusive of the coarse-grained channel deposits (Fig. 5.12). Since currently no other facies models for contourite channel deposits have been proposed results from this study cannot be compared any further.

The most challenging aspect of interpreting the deposits of facies association FA4 (contourite channel deposits) as having a contouritic origin arises from the tidal signatures observed (Fig. 5.10). The tidal signatures however can be explained by the tidal modulation of the palaeo-MOW as has been observed in the present-day MOW in the Strait of Gibraltar (Candela *et al.*, 1990).



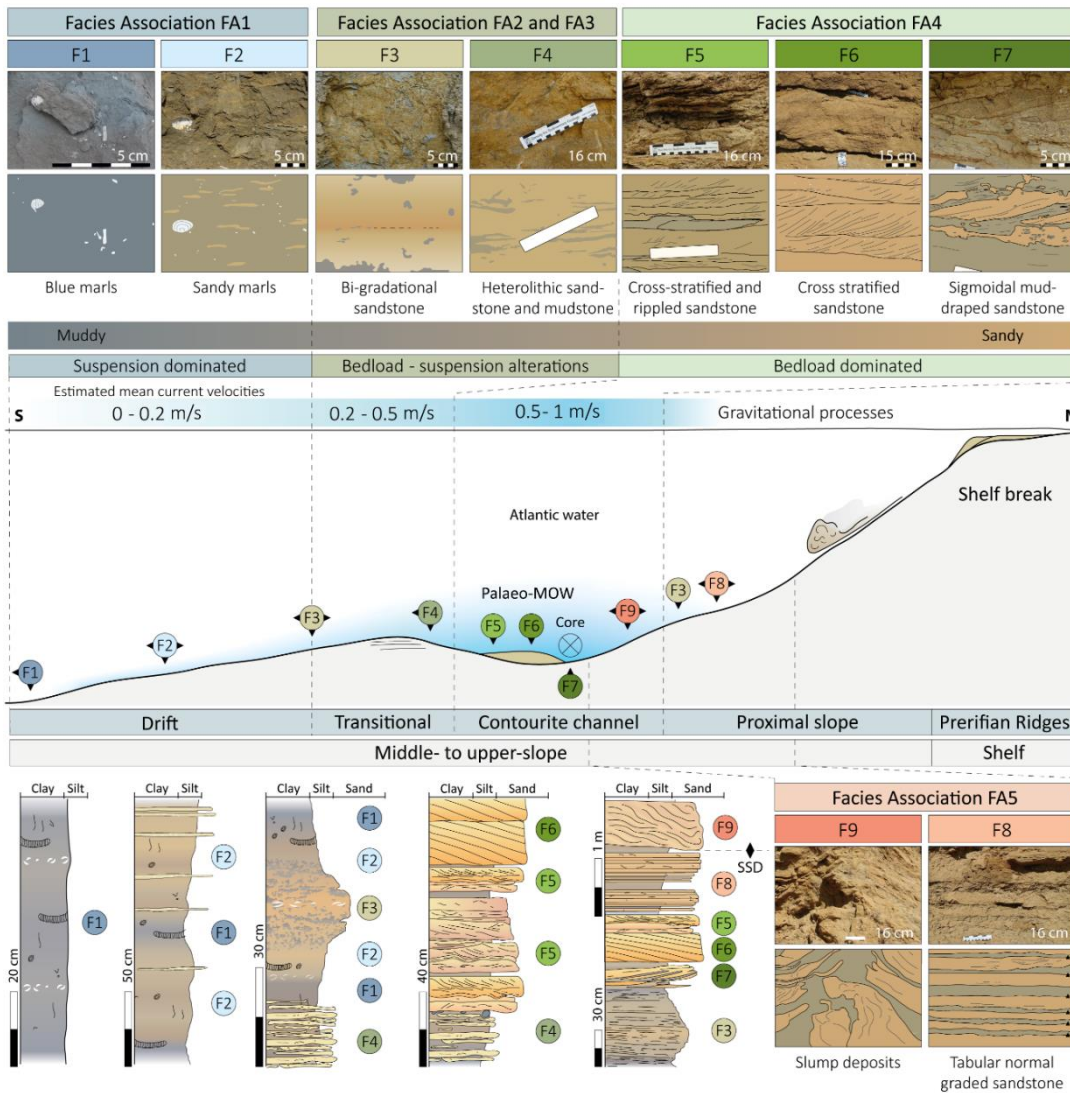


**Figure 5.12.** Sketch showing the relation between the facies (F1 to F9), facies associations and the different depositional and erosional elements from the proximal continental slope to the contourite drift. The facies associations are related to their dominant depositional process and associated current velocities. The panels in the bottom left corner show examples of observed facies stacking patterns. Soft sediment deformation structures (SSD) are regularly observed below facies F9.

### 7.3 Tidal modulation of the palaeo-MOW

The late Miocene Taza Strait in the South Rifian Corridor shows many similarities to the closely located modern Strait of Gibraltar (SoG) such as the Atlantic-Mediterranean connection, geometry, water-depths of a similar range and the presence of a sill (Camarinal Sill and Taza Sill respectively) located in the narrowest position of the strait. Due to these similarities flow variability through the South Rifian Corridor is expected to have behaved in a similar general fashion as the modern SoG. The flow variability through the modern SoG is herein discussed to explain the tidal signatures recognized in the Miocene Rifian deposits



(i.e., cyclically thickening and thinning foresets, cyclic alterations between angular and tangential toe-set geometries and sand-mud couplets observed in facies F5, F6 and F7; Fig. 5.10).

Lacombe and Richez (1982) categorized flow variability through the SoG into three distinct types: long-term, subinertial and tidal. The long-term flow variability relates to the double layer baroclinic exchange between the Atlantic and Mediterranean basins. The exchange, or circulation, consists of Atlantic waters flowing into the Mediterranean overriding the denser Mediterranean Outflow Water flowing westwards into the Atlantic (Armi and Farmer, 1988; Fig. 1B). This long-term flow variability is controlled by seasonal and interannual fluctuations in the evaporation-precipitation budget over the Mediterranean

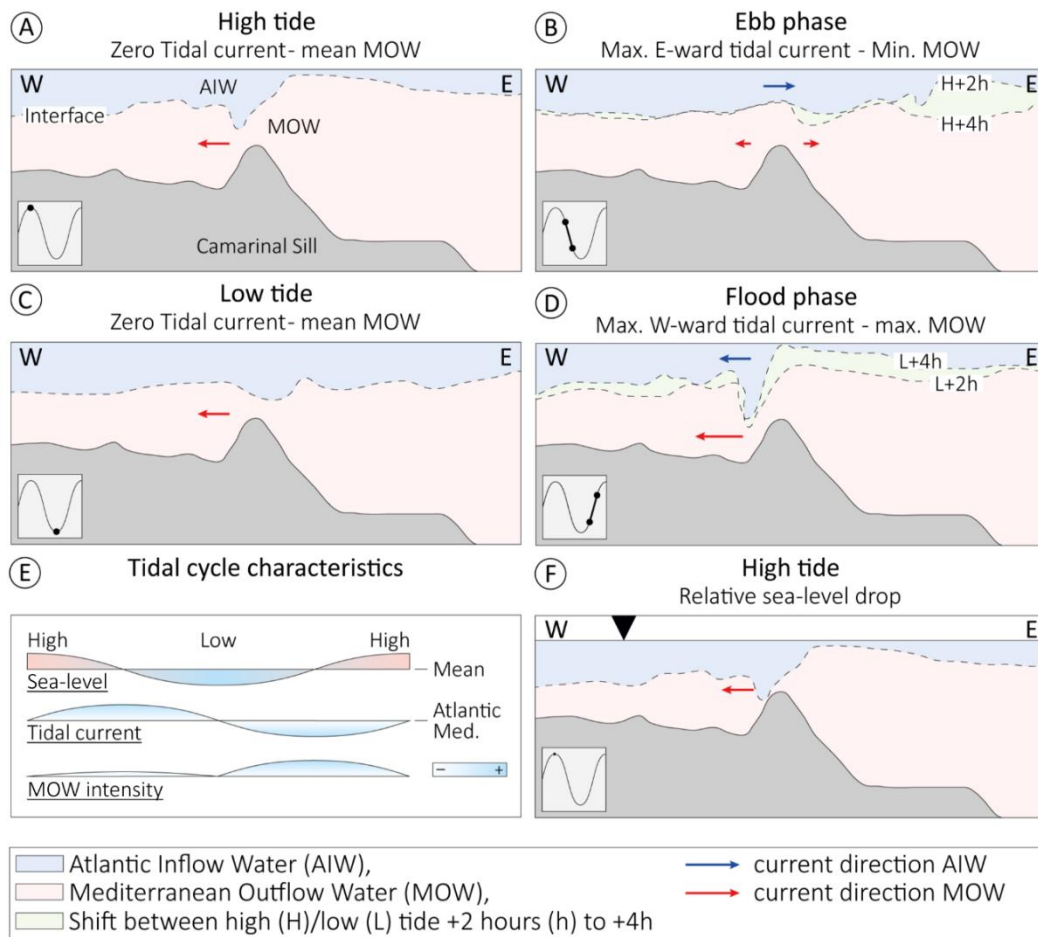


**Figure 5.13.** (A) to (D) Influence of a tidal cycle on Atlantic Inflow Water (AIW) and Mediterranean Outflow Water (MOW) and the interface between the two. At high tide and low tide (A and C respectively) the tidal current is zero and the MOW reaches its mean intensity. During the ebb phase (from high tide to low tide; B) the tidal current is directed towards the east and the MOW reaches its lowest velocity. Occasionally, the direction of the MOW can also be reversed. During the flood phase (from low tide to high tide; D) the tidal current is directed towards the west and the MOW reaches its highest velocity. (E) Summarizes the water mass characteristics during one tidal cycle. (F) Shows the long-term effect of a relative sea-level drop, by which the interface is located closer to the sill. The location of the interface to the sill affects the potential of Mediterranean Deep Water (MDW) to flow out of the Mediterranean.

Sea, affecting Mediterranean Deep Water formation. The two-layer exchange is interpreted to be hydraulically controlled at the Camarinal and Spartel sills (intensification of the MOW) on the western half and at the Tarifa narrow (intensification of the Atlantic inflow) on the eastern side of the strait (Bryden and Stommel, 1984; Armi and Farmer, 1986). The subinertial or interannual mostly barotropic flow variability, with periods ranging from days to months, is forced by the atmospheric pressure field over the Mediterranean (Candela *et al.*, 1989; Garcia Lafuente *et al.*, 2002). Tidal flows through the SoG are principally driven by the North Atlantic semidiurnal tide. Semidiurnal tides within the strait reach large amplitudes relative to subinertial flows, thus forming the dominant factor in flow variability (Candela *et al.*, 1990) and strongly modulating the long-term seasonal and interannual exchange pattern. On shorter, sub-daily timescales, modifications due to internal waves occur (Richez, 1994; Vazquez *et al.*, 2008).

As indicated by Rocha and Clarke (1987) the tidal wave arriving at a very narrow strait with a central sill is predominantly reflected, creating a standing tidal wave inside the strait. This standing wave, whose existence has been experimentally confirmed for the SoG (Candela *et al.*, 1990), generates barotropic tidal current peaks between high tide and low tide (Fig. 5.13B; ebb phase). The same authors indicated that due to the requirement of geostrophic adjustment in the across-strait direction maximum westward tidal currents are present between low tide and high tide (Fig. 5.13D; flood phase), diminishing the inflow of Atlantic water and intensifying the MOW. A maximum eastward tidal current is found in the ebb phase (Fig. 5.13B; between high tide and low tide), favouring Atlantic water inflow and diminishing or occasionally reversing the direction of the MOW. Both at high tide and low tide, the tidal current is zero, therefore, at both moments in the tidal cycle the MOW should approach its mean intensity (Fig. 5.13A and C).

Based on the analogies between the SoG and the Taza Strait it can be expected that during the late Miocene the Taza Strait was subjected to a similar hydrodynamic behavior responsible for the tidally modulated, pulsating behavior of the palaeo-MOW (Fig. 5.13E), recorded in the sedimentary successions of the El Adergha and Fes-north sections (Fig. 5.10). As the MOW/palaeo-MOW forms/formed a bottom current which is/was the dominant process responsible for the redistribution and deposition of sediment, hydraulically modulated by tides, its deposits are considered contourites.

The signature of cyclic deceleration (ebb phase) and acceleration (flood phase) of the palaeo-MOW is recognized in FA4 (Fig. 5.10). These facies are associated to the contourite

channel, the contourite element which is influenced most severely by hydrodynamic changes in the palaeo-MOW. Differences in the tidal signature between F5, F6 and F7 might be related to their position within the contourite channel. However, changes in the geometry and physiography of the strait margins (due to for example relative sea-level variations) and changes in water mass properties could potentially affect the tidal hydrodynamics of the palaeo-MOW as well.

The geometry of straits mainly controls the amplification of the tidal wave and the ability to transport water from one basin to another (Rocha and Clarke, 1987; Candela *et al.*, 1990). However, the Taza Strait is not expected to have changed geometry significantly over the period in which the sediments studied herein were deposited (7.35 to 7.25 Ma) as the main tectonic compressional event in the Rifian corridors took place around 7 Ma (Capella *et al.*, 2017b; Tubbore *et al.*, 2017). Mud drapes and heterolithic muddy and sandy beds are an indicator for significant changes in hydrodynamic conditions, bedload transport and suspension fallout. Such changes recorded on foreset-scale and laminae-scale suggest significant tidally induced fluctuations between “slack”- water and bottom currents with velocities up to 1 m/s.

The strength of the MOW is mainly a result of the density differences between the overriding Atlantic inflow water and the underlying MOW (Rogerson *et al.*, 2012; Sierro *et al.*, 2020). If the density difference between the two water masses is higher, a stronger MOW is expected because of an increased effect of acceleration due to gravity. Tidal effects on the MOW should also be significantly affected by the average depth of the Atlantic-Mediterranean water interface with respect to the sill. If the interface is closer to the sill (Fig. 5.13F) tidal effects on the MOW should be amplified, generating larger differences between flood and ebb phases. As overflow requires a minimum depth to the sill (de la Vara *et al.* (2016), at times, when the interface is near the sill, the MOW might have even completely stopped as the interface reached the Atlantic side of the sill during the ebb phase. Processes that would result in an interface close to the sill are likely related to relative sea-level changes. Miller *et al.* (2011) reported however that because of the development of a near-permanent East Antarctic Ice Sheet, the middle Miocene to early Pliocene glacio-eustatic sea-level changes were muted. This however does not mean that relative sea-level changes in the order of tens of metres would have had a profound effect on the interface-sill characteristics.

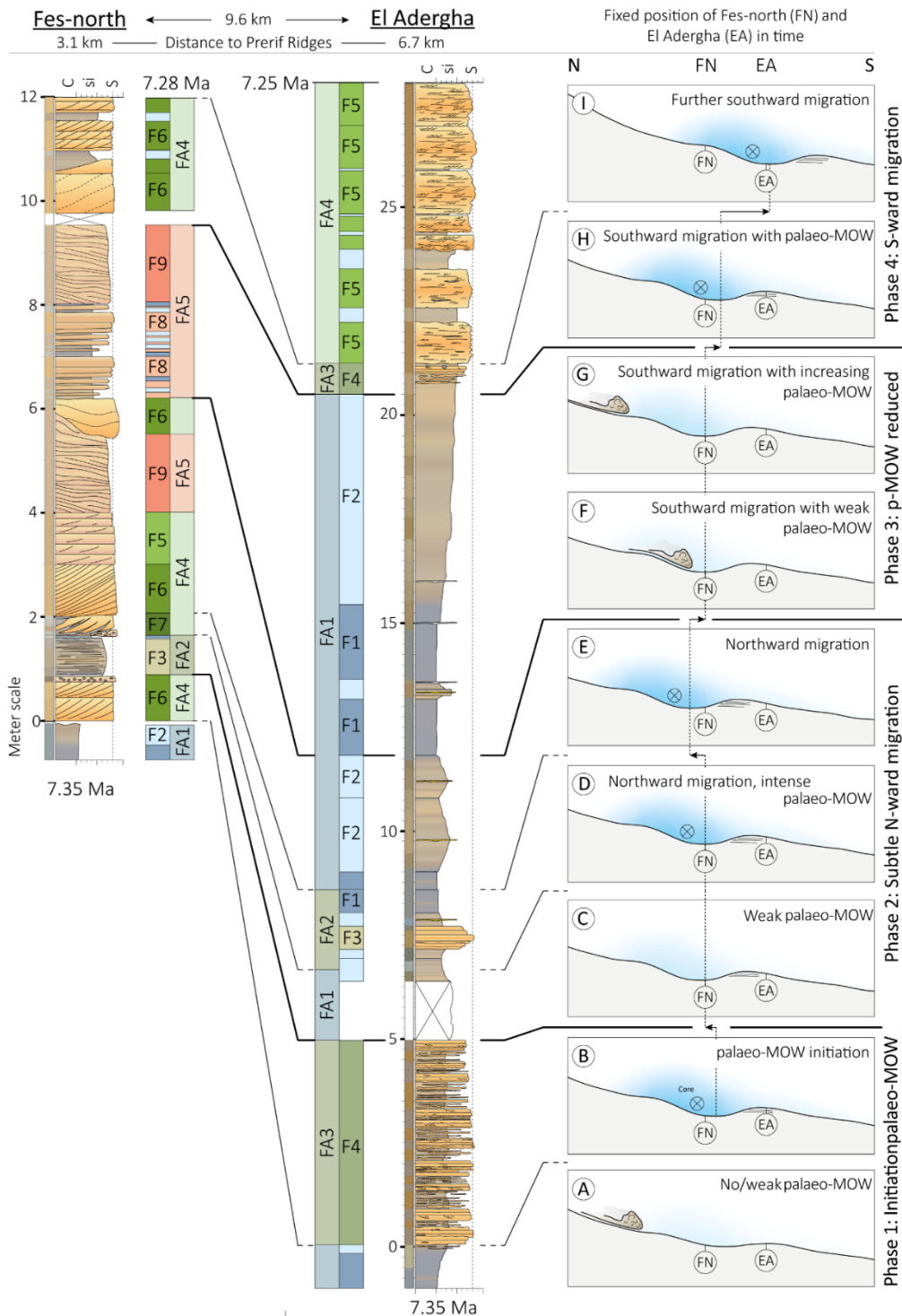


**Figure 5.14.** The logs of the late Miocene Fes-north (Fn) and El Adergha (EA) sections show vertical sedimentary facies changes. The vertical stacking of facies has been correlated based on their depositional ages (7.51 to 7.25 Ma) as well as on facies which, based on the herein proposed facies model, can be correlated in an across contourite channel system profile. (A) Depicts the transition from blue marls to more sand-rich marls which might indicate the initiation of a palaeo-MOW (p-MOW) in the area. (B) Shows the clear transition from FA1 to facies related to bottom current processes. By this time, the palaeo-MOW became the dominant depositional process. (C) to (E) Depicts the subtle northward migration of the contourite depositional system (CDS) and a possible intensification of the palaeo-MOW. (F) and (G) Depicts a period with low-velocity bottom currents associated with a weak palaeo-MOW. During this period, gravitational deposits could be preserved, as they were not being significantly affected by bottom currents. (H) and (I) Depicts the southward migration of the CDS, where the channel (FA4) migrated of the drift (FA1).

Here, it is assumed that during the deposition of facies F7, consisting of sigmoidal mud-draped sandstone, the Atlantic-Mediterranean interface was located close to the sill. This is explained by the strong tidally induced cyclic acceleration and deceleration changes inferred

from the studied facies. Facies F6, consisting of cross-stratified sandstones lacking any mud, is expected to have been deposited when the interface was located well above the sill, decreasing tidal amplification. However, the thick foresets and relatively coarse-grain sizes suggest that density differences between the Atlantic and Mediterranean were enhanced, allowing high velocity bottom currents. Facies F5, consisting of heterolithic cross-stratified mudstone and sandstone, is interpreted as an intermediate facies with relatively strong tidal fluctuations but lower-maximum current velocities.

#### *7.4 Evolution of the contourite channel system*

The vertical sedimentary facies stacking patterns observed in the Fes-north and El Adergha sections suggest that, over time, the depositional processes changed at the site at which the sections were located. The comparison and correlation between the two sections is used to explain the lateral migration of the contourite depositional system and the intermittent flow of the palaeo-MOW. As the Fes-north section is located north-westwards of the El Adergha section, it is assumed that it was located up-slope and down-current with respect to the westward flow-direction of the palaeo-MOW (Fig. 5.11). Since the down-current facies changes cannot be deduced from the vertical stacking of facies, this aspect will not be considered in the reconstruction of the system evolution. The relative distance between both sections has been considered constant over time. Based on the stratigraphic and facies (based on the proposed facies model) correlation, four main evolutionary phases have been identified (Fig. 5.14).

Phase 1 - The initiation or intensification of the palaeo-MOW related to a change from dominantly fine-grained deposits (FA1) to coarser grained deposits associated to FA3 and FA2 for the Fes-north and El Adergha sections, respectively (Fig. 5.14A and B). The initiation of an active palaeo-MOW in the study area is associated to the uplift of the accretionary wedge and the Prerifian Ridges. This tectonically driven event terminated the palaeo-MOW pathway north of these ridges that was active between 7.8 Ma and 7.51 Ma (de Weger *et al.*, 2020). As the palaeo-MOW was forced southward of the Prerifian Ridges this allowed the intensification of bottom current in this region. Over time this palaeo-MOW formed a contourite channel system in which the Fes-north section constituted the contourite channel and the El Adergha section the transitional channel-drift domain.

Phase 2 - The northward migration of the contourite depositional system is related to a facies stacking patterns that suggest decreasing flow-velocities. These decreasing flow velocities are associated to a northward shift of the contourite depositional system where, in El Adergha, the depositional setting changes from drift-channel transition to drift, and in Fes-north, the depositional setting changes from channel to channel-flank or slope deposits (Fig. 5.14C to E). As the palaeo-MOW is forced northwards by the Coriolis force, the system naturally migrates up-slope or northwards (Faugères *et al.*, 1999; Llave *et al.*, 2001). This migration is stimulated by active erosion on the right (up-slope) flank of the channel and highest rates of deposition over the left flank, the drift. However, since channel facies overly drift transitional facies (FA2) in the Fes-north section, FA2 in this section might be, although highly speculative, related to up-slope overbank deposits. These overbank deposits could be drift deposits associated to another water mass as similar features have been identified along the middle and upper slope of the Gulf of Cadiz at the exit of the SoG (Brackenridge *et al.*, 2018; García *et al.*, 2020). In the SoG these deposits are related to a different, shallower water-mass compared to that of the contourite channel (García *et al.*, 2020).

Phase 3 - Reduction of the palaeo-MOW intensity is indicated by the disappearance of contourite facies related to high-velocity bottom currents. This allowed the preservation of turbidites (F8) in Fes-north and the deposition of fine-grained contourites or hemipelagites (FA1) in El Adergha (Fig. 5.14F and G). In the facies stacking pattern of this interval in El Adergha, minor fluctuations related to flow velocities have been observed, suggesting the intermittent behavior of the palaeo-MOW. The reduction of the palaeo-MOW intensity is most likely associated to a decrease in the density gradient between Atlantic inflow and Mediterranean outflow water (Rogerson *et al.*, 2012). This decrease in density could be related to subduction of the Taza Strait, enabling increased inflow of less-saline Atlantic water, and reducing the formation of Mediterranean Deep Water (MDW). Since no evidence was found of eastward flow related to the inflow of Atlantic water, the palaeo-MOW was likely still present. This stratigraphic interval being dominated by gravitational deposits furthermore suggests that the slope was tectonically unstable. This tectonic instability was a precursor to the tectonically induced southward migration of the system as indicated in phase 4.

The final phase, Phase 4 - is marked by a significant southward migration of the contourite depositional system (Fig. 5.14H and I). This southward shift is recognized by the emplacement of contourite channel facies (FA4) over the drift facies (FA1) in El Adergha. The southward migration of the contourite channel system could be related to intensification of

the density gradient between the Atlantic and the palaeo-MOW, supporting a deeper settling depth of the palaeo-MOW. Rogerson *et al.* (2012) however suggest that the negative feedback process of enhanced ambient water entrainment with a denser palaeo-MOW plume counteract deeper settlement of this plume. As such, it is more likely that the palaeo-MOW was forced southward by tectonic uplift resulting in the southward migration of the contourite channel. Ongoing tectonic uplift since 7.25 Ma closed the Atlantic-Mediterranean connection leading to the Mediterranean Salinity Crisis (Capella *et al.*, 2020b).

### *7.5 Implications*

The main controls on depositional style of contourite features are flow-velocity and the characteristics of sediment availability. Taking this into account, the resulting morphology and depositional style should not be drastically different between the studied sections and other contourite systems. Current velocities generated by overflow are however high in comparison to thermohaline circulation. Accordingly, the ability of the flow to transport and deposit sandy sediment is a function of flow-velocity and sediment particle characteristics [e.g., the Hjulström curve (Hjulström, 1935)], and thus sandy contourite deposits independent of the style of bottom current generation should show similar features. As such, the contourite channel system and the erosional and depositional features are unique due to the morphology of the gateway and the effects of this morphology on flow characteristics. The gateway however was sufficiently wide (~30 km) not to restrict the palaeo-MOW allowing it to “freely” flow along the slope, controlled only by seafloor morphology, density gradients and the Coriolis force. The morphology of the gateway however amplified tidal forces generating a tidal control on overflow behavior. Accordingly, it can be deduced that in other contourite systems characterized by similar flow-velocities and not related to gateway systems, should likely show less pronounced tidal signatures.

## 8. CONCLUSIONS

The main findings described and discussed in this manuscript relate to the discovery and description of sandy contourites and their first ever recognition as being relics of a contourite channel system, outcropping in the ancient record. As such, they represent a valuable analogue for modern contourite depositional systems and ancient subsurface exploration and research targets.



The findings presented herein elaborate on the evolution of this system and emphasizes the occurrence of different facies associated to bottom currents. Facies and facies associations have been interpreted as representing the “full-spectrum” of contourite depositional and erosional environments, the drift, drift-channel transition and the contourite channel. The facies changes are predominantly related to changes in the intensity of the palaeo-MOW which decreases away from its core. The contourites are interstratified with hemipelagites, turbidites and slump deposits where their preservation is related to a decrease in palaeo-MOW intensity.

The vertical sedimentary facies stacking pattern records the tectonically induced, southward migration of the contourite depositional system (CDS) and the intermittent behavior of the palaeo-MOW which is mainly driven by precessional-scale and millennial-scale climate variations. The tidal signature in the sandy contourite deposits shows that tides played a key factor in modulating the palaeo-MOW on a sub-annual timescale.

The results of this study indicate that bottom currents, their hydrodynamic conditions and their effect on deep-marine depositional processes and environments are controlled by: (i) the intermittent behavior of flow (on-off); (ii) flow acceleration and deceleration; and (iii) tidal modulation. All these factors should be considered in the process-based interpretation of all deep marine deposits possibly affected by bottom currents.

Keeping in mind, the well-known expression of “the past is the key to the future”, contourite research, such as this study, could significantly attribute to the understanding of processes leading to changes in global ocean circulation and associated climate change. As this manuscript provides information regarding mechanisms that affect the overflow of dense Mediterranean water and gateway evolution, which impacts global ocean circulation, this work provides information on processes that contribute to climate change.

## ACKNOWLEDGEMENTS

We are very appreciative of the help and support given by the Office National des Hydrocarbures et des Mines (ONHYM), Morocco. This project was funded by the Joint Industry Project supported by TOTAL, BP, ENI, ExxonMobil, Wintershal DEA, and TGS, executed in the framework of “The Drifters Research Group” at Royal Holloway University of London (RHUL), related to projects CTM 2012039599-C03, CGL2016-80445-R, and CTM2016-75129-C3-1-R. The research contribution of O. Salas-Miguez was funded through

a pre-doctoral grant from the Ministerio de Educacion, Cultura y Deporte (Gobierno Espana). Journal reviews by A.R. Viana and S.G. Longhitano are greatly appreciated, and their comments helped us to improve the clarity of the manuscript.

## References

- Achalhi, M., Münch, P., Cornée, J.J., Azdimousa, A., Melinte-Dobrinescu, M., Quillévéré, F., Drinia, H., Fauquette, S., Jiménez-Moreno, G., Merzeraud, G., Moussa, A. B., El Kharim, Y. and Feddi, N. (2016). The late Miocene Mediterranean-Atlantic connections through the north Rifian corridor: new insights from the Boudinar and Arbaa Taourirt basins (northeastern Rif, Morocco). *Palaeogeogr. Palaeoclimatol. Palaeoecol.*, 459, 131-152.
- Allen, J.R.L. (1982) Mud drapes in sand-wave deposits: a physical model with application to the Folkestone Beds (early Cretaceous, southeast England). *Phil. Trans. Roy. Soc. London. Series A, Math. Phys. Sci.*, 306, 291-345.
- Armi, L. and Farmer, D.M. (1988) The flow of Mediterranean water through the Strait of Gibraltar. *Prog. Oceanogr.* 21, 1–105.
- Barbero, L., Jabaloy, A., Gómez-Ortiz, D., Pérez-Peña, J.V., Rodríguez-Peces, M.J., Tejero, R., Estupiñán, J., Azdimousa, A., Vázquez, M. and Asebriy, L. (2011) Evidence for surface uplift of the Atlas Mountains and the surrounding peripheral plateaux: Combining apatite fission-track results and geomorphic indicators in the Western Moroccan Meseta (coastal Variscan Paleozoic basement). *Tectonophysics*, 502, 90-104.
- Barbieri, R. and Ori, G.G. (2000) Neogene palaeoenvironmental evolution in the Atlantic side of the Rifian Corridor (Morocco). *Palaeogeogr. Palaeoclimatol. Palaeoecol.*, 163, 1-31.
- Barhoun, N. and Taoufio, N.B. (2008) Biostratigraphic and environmental events recorded in the Rifian southern corridor (Northern Morocco) in late Miocene before the Messinian salinity crisis. *Geodiversitas*, 30, 21-40.
- Bernini, M., Boccaletti, M., El Mokhtari, J., Gelati, R., Iaccarino, S., Moratti, G. and Papani, G. (1992) Données stratigraphiques nouvelles sur le Miocène supérieur du bassin de Taza-Guercif (Maroc nord-oriental). *Bulletin de la Société géologique de France*, 163, 73-76.
- Betzler, C., Braga, J.C., Martín, J.M., Sanchez-Almazo, I.M. and Lindhorst, S. (2006) Closure of a seaway: stratigraphic record and facies (Guadix basin, Southern Spain). *International Journal of Earth Sciences*, 95, 903-910.
- Bouma, A.H. (1962). Sedimentology of some flysch deposits. *A graphic approach to facies interpretation*, 168.
- Brackenridge, R.E., Stow, D.A.V., Hernández-Molina, F.J., Jones, C., Mena, A., Alejo, I., Ducassou, E., Llave, E., Ercilla, G., Nombela, M.A., Perez-Arlucea, M. and Frances, G. (2018) Textural characteristics and facies of sand-rich contourite depositional systems. *Sedimentology*, 65, 2223-2252. doi:[10.1111/sed.12463](https://doi.org/10.1111/sed.12463)
- Bryden, H.L. and Stommel, H.M. (1984) Limiting processes that determine basic features of the circulation in the Mediterranean Sea, *Oceanol. Acta*, 7, 289–296.
- Buatois, L.A. and Mángano, M.G. (2011) *Ichnology: Organism-substrate interactions in space and time*. Cambridge University Press., 358.
- Candela, J., Winant, C.D. and Ruiz, A., (1989) Meteorologically forced subinertial flows through the Strait of Gibraltar. *J. Geophys. Res.*, 94, 12667–12674.
- Candela, J., Winant, C. and Ruiz, A. (1990) Tides in the Strait of Gibraltar, *J. Geophys. Res.*, 95, 7313–7335.
- Candela, J. (2001) Mediterranean water and global circulation. In *Int. Geophys.*, Academic Press. 77, 419-488.
- Capella, W., Hernández-Molina, F.J., Flecker, R., Hilgen, F.J., Hssain, M., Kouwenhoven, T.J., van Oorschot, M., Sierro, F.J., Stow, D.A.V., Trabucho-Alexandre, J., Tulbure, M.A., de Weger, W., Yousfi and M.Z., Krijgsman, W. (2017a) Sandy contourite drift in the late Miocene Rifian Corridor (Morocco): Reconstruction of depositional

- environments in a foreland-basin seaway. *Sed. Geol.*, 355, 31-57.
- Capella, W., Matenco, L., Dmitrieva, E., Roest, W. M., Hessels, S., Hssain, M., Chakor-Alami, A., Sierro, F.J. and Krijgsman, W. (2017b) Thick-skinned tectonics closing the Rifian Corridor. *Tectonophysics*, 710, 249-265.
- Capella, W., Barhoun, N., Flecker, R., Hilgen, F. J., Kouwenhoven, T., Matenco, L.C., Sierro, F.J., Tulbure, M.A., Yousfi, M.Z., and Krijgsman, W. (2018) Palaeogeographic evolution of the late Miocene Rifian Corridor (Morocco): reconstructions from surface and subsurface data. *Earth-Science Reviews*, 180, 37-59.
- Chalouan, A. and Michard, A. (2004) The Alpine Rif Belt (Morocco): a case of mountain building in a subduction-subduction-transform fault triple junction. *Pure and Applied Geophysics*, 161, 489-519.
- Chen, Y., Yao, G., Wang, X., Lv, F., Shao, D., Lu, Y., Cao, Q. and Tang, P. (2020) Flow processes of the interaction between turbidity flows and bottom currents in sinuous unidirectionally migrating channels: An example from the Oligocene channels in the Rovuma Basin, offshore Mozambique. *Sed. Geol.*, 105680.
- Chiarella, D. (2016) Angular and tangential toeset geometry in tidal cross-strata: An additional feature of current-modulated deposits. *Contributions to Modern and Ancient Tidal Sedimentology: Proceedings of the Tidalites 2012 Conference, First Edition*. Edited by Bernadette Tessier and Jean-Yves Reynaud. International Association of Sedimentologists. John Wiley & Sons, Ltd.
- Chiarella, D., Longhitano, S.G. and Tropeano, M. (2017) Types of mixing and heterogeneities in siliciclastic-carbonate sediments. *Mar. Petrol. Geol.*, 88, 617-627.
- Corbí, H., Lancis, C., García-García, F., Pina, J. A., Soria, J.M., Tent-Manclús, J.E., and Viseras, C. (2012) Updating the marine biostratigraphy of the Granada Basin (central Betic Cordillera). Insight for the Late Miocene palaeogeographic evolution of the Atlantic–Mediterranean seaway. *Geobios*, 45, 249-263.
- Creaser, A., Hernández-Molina, F.J., Badalini, G., Thompson, P., Walker, R., Soto, M. and Conti, B. (2017) A Late Cretaceous mixed (turbidite-contourite) system along the Uruguayan Margin: Sedimentary and palaeoceanographic implications. *Mar. Geol.*, 390, 234-253.
- de Castro, S., Hernández-Molina, F.J., Rodríguez-Tovar, F.J., Llave, E., Ng, Z.L., Nishida, N. and Mena, A. (2020a) Contourites and bottom current reworked sands: Bed facies model and implications. *Mar. Geol.*, 428, 106267.
- de Castro, S., Hernández-Molina, F.J., de Weger, W., Jiménez-Espejo, F.J., Rodríguez-Tovar, F.J., Mena, A., Llave, E. and Sierro, F.J. (2020b) Contourite characterisation and its discrimination from other deep-water deposits in the Gulf of Cadiz contourite depositional system. *Sedimentology*. doi.org/10.1111/sed.12813.
- de Castro, S., Miramontes, E., Dorador, J., Jouet, G., Cattaneo, A., Rodríguez-Tovar, F.J. and Hernández-Molina, F.J. (2021) Siliciclastic and bioclastic contouritic sands: textural and geochemical characterisation. *Marine and Petroleum Geology*. In press
- De La Vara, A., Topper, R.P., Meijer, P.T., and Kouwenhoven, T.J. (2015) Water exchange through the Betic and Rifian corridors prior to the Messinian Salinity Crisis: A model study. *Paleoceanography*, 30, 548-557.
- de Weger, W., Hernández-Molina, F.J., Flecker, R., Sierro, F.J., Chiarella, D., Krijgsman, W. and Manar, M.A. (2020) Late Miocene contourite channel system reveals intermittent overflow behavior. *Geology*, 48, 1194-1199.
- DiGeronimo, I., Grasso, M. and Pedley, H.M. (1981) Palaeoenvironment and palaeogeography of Miocene marls from Southeast Sicily and the Maltese Islands. *Palaeogeogr. Palaeoclimatol. Palaeoecol.*, 34, 173-189.
- Einsele, G. (2000) *Sedimentary basins: evolution, facies, and sediment budget*. Springer Science & Business Media.
- Faas, R.W. (1991) Rheological boundaries of mud: where are the limits?. *Geo-Marine Letters*, 11, 143-146.
- Farmer, D. and Armi, L. (1986) Maximal two-layer exchange over a sill and through the combination of a sill and contraction with barotropic flow. *J. Fluid Mech.*, 164, 53-76.
- Faugères, J.C., Gonthier, E. and Stow, D.A.V. (1984) Contourite drift molded by deep Mediterranean outflow. *Geology*, 12, 296-300.

- Faugères, J.C., Stow, D.A.V., Imbert, P. and Viana, A. (1999) Seismic features diagnostic of contourite drifts. *Mar. Geol.*, *162*, 1-38.
- Feinberg, H. (1986) Les séries tertiaires des zones externes du Rif (Maroc): biostratigraphie, paléogéographie et aperçu tectonique. *Éditions du Service géologique du Maroc*, (No. 315).
- Flecker, R., Krijgsman, W., Capella, W., de Castro Martins, C., Dmitrieva, E., Mayser, J.P., Marzocchi, A., Modestou, S., Ochoa, D., Simon, D., Tulbure, M., van den Berg, B., van der Schee, M., de Lange, G., Ellam, R., Govers, R., Gutjahr, M., Hilgen, F., Kouwenhoven, T., Lofi, J., Meijer, P., Sierro, F. J., Bachiri, N., Barhoun, N., Alami, A. C., Chacon, B., Flores, J.A., Gregory, J., Howard, J., Lunt, D., Ochoa, M., Pancost, R., Vincent, S. and Yousfi, M.Z. (2015) Evolution of the Late Miocene Mediterranean–Atlantic gateways and their impact on regional and global environmental change. *Earth-Sci. Rev.*, *150*, 365–392.
- Flinch, J. (1993) Tectonic evolution of the Gibraltar arc [Ph. D. thesis]: Houston. *Rice University*.
- Fonnesu, M., Palermo, D., Galbiati, M., Marchesini, M., Bonamini, E. and Bendias, D. (2020) A new world-class deep-water play-type, deposited by the syndepositional interaction of turbidity flows and bottom currents: The giant Eocene Coral Field in northern Mozambique. *Mar. and Petrol. Geol.*, *111*, 179-201.
- Fuhrmann, A., Kane, I.A., Clare, M.A., Ferguson, R.A., Schomacker, E., Bonamini, E. and Contreras, F.A. (2020) Hybrid turbidite-drift channel complexes: An integrated multiscale model. *Geology*, *48*, 562-568.
- García, M., Llave, E., Hernández-Molina, F.J., Lobo, F.J., Ercilla, G., Alonso, B., Casas, D., Mena, A. and Fernández-Salas, L. M. (2020) The role of late Quaternary tectonic activity and sea-level changes on sedimentary processes interaction in the Gulf of Cadiz upper and middle continental slope (SW Iberia). *Mar. Petrol. Geol.*, *121*, 104595.
- García Lafuente, J., Álvarez, E., Vargas, J.M. and Ratsimandresy, W. (2002) Subinertial variability in the flow through the Strait of Gibraltar. *J. of Geophys. Res.*, *107*, 32.1–32.9.
- Gelati, R., Moratti, G. and Papani, G. (2000) The Late Cenozoic sedimentary succession of the Taza-Guercif Basin, South Rifian Corridor, Morocco. *Mar. Petrol. Geol.*, *17*, 373-390.
- Gonthier, E.G., Faugères, J.C. and Stow, D.A.V. (1984) Contourite facies of the Faro drift, Gulf of Cadiz. *J. Geol. Soc. London, Special Publications*, *15*, 275-292.
- Hernández-Molina, F.J., Llave, E., Stow, D.A.V., García, M., Somoza, L., Vázquez, J.T., Lobo, F.J., Maestro, A., Diaz del Rio, V., Leon, R., Medialdea, T. and Gardner, J. (2006) The contourite depositional system of the Gulf of Cadiz: a sedimentary model related to the bottom current activity of the Mediterranean outflow water and its interaction with the continental margin. *Deep Sea Research Part II: Topical Studies in Oceanography*, *53*, 1420-1463.
- Hernández-Molina, F.J., Llave, E. and Stow, D.A.V. (2008) Continental slope contourites. *Dev. Sedimentol.*, *60*, 379-408.
- Hernández-Molina, F.J., Paterlini, M., Violante, R., Marshall, P., de Isasi, M., Somoza, L. and Rebesco, M. (2009) Contourite depositional system on the Argentine Slope: An exceptional record of the influence of Antarctic water masses. *Geology*, *37*, 507-510.
- Hernández-Molina, F.J., Llave, E., Preu, B., Ercilla, G., Fontan, A., Bruno, M., Serra, N., Gomiz, J.J., Brackenridge, R.E., Sierro, F.J., Stow, D.A.V., Garcia, M., Juan, C., Sandoval, N. and Mrnaliz, A. (2014a) Contourite processes associated with the Mediterranean Outflow Water after its exit from the Strait of Gibraltar: Global and conceptual implications. *Geology*, *42*, 227-230.
- Hernández-Molina, F.J., Stow, D.A.V., Alvarez-Zarikian, C.A., Acton, G., Bahr, A., Balestra, B., Ducassou, E., Flood, R., Flores, J.A., Furota, S., Grunert, P., Hodell, D., Jimenez-Espejo, F., Kim, J.K., Krissek, L., Kuroda, J., Li, B., Llave, E., Lofi, J., Lourens, L., Miller, M., Nanayama, F., Nishida, N., Richter, C., Roque, C., Pereira, H., Sanchez Goñi, M.F., Sierro, F.J., Singh, A.D., Sloss, C., Takashimizu, Y., Tzanova, A., Voelker, A.H.L., Williams, T. and Xuan, C. (2014b) Onset of Mediterranean outflow into the North Atlantic. *Science*, *344*, 1244-1250.
- Hernández-Molina, F.J., Soto, M., Piola, A.R., Tomasini, J., Preu, B., Thompson, P., Badalini, G., Creaser, A., Violante, R.A.,

- Morales, E., Paterlini, M. and De Santa Ana, H. (2016a) A contourite depositional system along the Uruguayan continental margin: sedimentary, oceanographic and paleoceanographic implications. *Mar. Geol.*, 378, 333-349.
- Hernández-Molina, F.J., Wåhlin, A., Bruno, M., Ercilla, G., Llave, E., Serra, N., Roson, G., Puig, P., Rebesco, M., Van Rooij, D., Roque, D., Gonzalez-Pola, C., Sanchez, F., Gomez, M., Preu, B., Schwenk, T., Hanebuth, T.J.J., Sanchez Leal, F.S., Garcia-Lafuente, J., Brackenridge, R.E., Juan, C., Stow, D.A.V. and Maria Sanchez-Gonzalez, J.M. (2016b) Oceanographic processes and morphosedimentary products along the Iberian margins: A new multidisciplinary approach. *Mar. Geol.*, 378, 127-156.
- Hernández-Molina, F.J., Campbell, S., Badalini, G., Thompson, P., Walker, R., Soto, M., Conti, B., Preu, B., Thieblemont, A., Hyslop, L., Miramontes, E. and Morales, E. (2018) Large bedforms on contourite terraces: Sedimentary and conceptual implications. *Geology*, 46, 27-30.
- Hesse, R. (1975) Turbiditic and non-turbiditic mudstone of Cretaceous flysch sections of the East Alps and other basins. *Sedimentology*, 22, 387-416.
- Hilgen, F.J., Bissoli, L., Laccarino, S., Krijgsman, W., Meijer, R., Negri, A. and Villa, G. (2000) Integrated stratigraphy and astrochronology of the Messinian GSSP at Oued Akrech (Atlantic Morocco). *Earth Planet. Sci. Lett.*, 182, 237-251.
- Hjulstrom, F. (1935) Studies of the morphological activity of rivers as illustrated by the river fyris, bulletin. Geological Institute Upsala, 25, 221-527.
- Hovikoski, J., Uchman, A., Weibel, R., Nøhr-Hansen, H., Sheldon, E., Ineson, J., Bjerager, M., Therkelsen, J., Olivarius, M., Larsen, M., Alsen, P. and Bojesen-Koefoed, J. (2020) Upper Cretaceous bottom current deposits, north-east Greenland. *Sedimentology*. <https://doi.org/10.1111/sed.12764>
- Hüneke, H., and Stow, D.A.V. (2008) Identification of ancient contourites: problems and palaeoceanographic significance. *Dev. Sedimentol.*, 60, 323-344.
- Hüneke, H., Hernández-Molina, F., Rodríguez-Tovar, F., Llave, E., Chiarella, D., Mena, A. and Stow, D. (2020) Diagnostic criteria using microfacies for calcareous contourites, turbidites and pelagites in the Eocene–Miocene slope succession, southern Cyprus. *Sedimentology*. doi:[10.1111/sed.12792](https://doi.org/10.1111/sed.12792)
- Hsü, K.J., Ryan, W.B. and Cita, M.B. (1973) Late Miocene desiccation of the Mediterranean. *Nature*, 242, 240-244.
- Iribarren, L., Vergés, J. and Fernández, M. (2009) Sediment supply from the Betic–Rif orogen to basins through Neogene. *Tectonophysics*, 475, 68-84.
- Knaust, D. (2017) Atlas of trace fossils in well core: appearance, taxonomy and interpretation. Springer International, 209
- Krijgsman, W., Langereis, C.G., Zachariasse, W.J., Boccaletti, M., Moratti, G., Gelati, R., Laccarino, S., Papani, G. and Villa, G. (1999) Late Neogene evolution of the Taza–Guercif Basin (Rifian Corridor, Morocco) and implications for the Messinian salinity crisis. *Mar. Geol.*, 153, 147-160.
- Krijgsman, W., Garcés, M., Agusti, J., Raffi, I., Taberner, C., and Zachariasse, W.J. (2000) The ‘Tortonian salinity crisis’ of the eastern Betics (Spain). *Earth and Planetary Science Letters*, 181, 497-511.
- Krijgsman, W., Leewis, M.E., Garcés, M., Kouwenhoven, T.J., Kuiper, K.F., and Sierro, F. J. (2006) Tectonic control for evaporite formation in the Eastern Betics (Tortonian; Spain). *Sedimentary Geology*, 188, 155-170.
- Krijgsman, W., Capella, W., Simon, D., Hilgen, F.J., Kouwenhoven, T.J., Meijer, P.T., Sierro, F.J., Tulbure, M.A., van den Berg, C., van der Schee, M. and Flecker, R. (2018) The Gibraltar corridor: Watergate of the Messinian salinity crisis. *Mar. Geol.*, 403, 238-246.
- Kuhlbrodt, T., Griesel, A., Montoya, M., Levermann, A., Hofmann, M. and Rahmstorf, S. (2007) On the driving processes of the Atlantic meridional overturning circulation. *Reviews of Geophysics*, 45.
- Lacombe, H. and Richez, C. (1982) The regime of the Strait of Gibraltar. In: Nihoul, J.C.J. (Ed.), *Hydrodynamics of Semi-Enclosed Seas. Elsevier Sci. Publ. Comp.*, New York, 13–73.
- Leeder, M.R. (2009) *Sedimentology and sedimentary basins: from turbulence to tectonics*. John Wiley & Sons, 784 pp.
- Llave, E., Hernández-Molina, F.J., Somoza, L., Díaz-del-Río, V., Stow, D.A.V., Maestro, A. and Dias, J.A. (2001) Seismic stacking pattern of the Faro-Albufeira contourite system (Gulf of Cadiz): A Quaternary

- record of paleoceanographic and tectonic influences. *Mar. Geophys. Res.*, 22, 487-508.
- Llave, E., Hernández-Molina, F.J., Somoza, L., Stow, D.A.V. and Del Río, V.D. (2007) Quaternary evolution of the contourite depositional system in the Gulf of Cadiz. Geological Society, London, Special Publications, 276, 49-79.
- Longhitano, S.G. and Nemec, W. (2005) Statistical analysis of bed-thickness variation in a Tortonian succession of biocalcarenic tidal dunes, Amantea Basin, Calabria, southern Italy. *Sed. Geol.*, 179, 195-224.
- Longhitano, S.G., Mellere, D., Steel, R.J. and Ainsworth, R.B. (2012) Tidal depositional systems in the rock record: a review and new insights. *Sed. Geol.*, 279, 2-22.
- Lowe, D.R. (1982) Sediment gravity flows; II, Depositional models with special reference to the deposits of high-density turbidity currents. *J. Sed. Res.*, 52, 279-297.
- Lozano, P., Fernández-Salas, L.M., Hernández-Molina, F.J., Sánchez-Leal, R., Sánchez-Guillamón, O., Palomino, D., Farias, C., Mateo-Ramírez, A., López-González, N., García, M., Vázquez, J.T., Vila, Y. and Rueda, J.L. (2020) Multiprocess interaction shaping geoforms and controlling substrate types and benthic community distribution in the Gulf of Cádiz. *Mar. Geol.*, 423, 106139.
- Lucchi, R.G. and Rebesco, M. (2007) Glacial contourites on the Antarctic Peninsula margin: insight for palaeoenvironmental and palaeoclimatic conditions. *Geol. Soc. London Spec. Publ.*, 276, 111-127.
- MacEachern, J.A., Pemberton, S.G., Gingras, M.K. and Bann, K.L. (2007) The ichnofacies paradigm: a fifty-year retrospective. In *Trace fossils*, 52-77. Elsevier.
- MacEachern, J.A., Bann, K.L., Gingras, M.K., Zonneveld, J.P., Dashtgard, S.E. and Pemberton, S.G. (2012) The ichnofacies paradigm. In *Dev. Sedimentol.*, 64, 103-138. Elsevier.
- Mansour, B. and Saint-Martin, J.P. (1999) Conditions de dépôt des diatomites messiniennes en contexte de plateforme carbonatée d'après l'étude des assemblages de diatomées: Exemple du Djebel Murdjadjo (Algérie). *Geobios*, 32, 395-408.
- Martín, J.M., Braga, J.C. and Betzler, C. (2001) The Messinian Guadalhorce corridor: the last northern, Atlantic–Mediterranean gateway. *Terra Nova*, 13, 418-424.
- Martín–Chivelet, J., Fregenal–Martínez, M.A. and Chacón, B. (2008) Traction structures in contourites. *Dev. Sedimentol.*, 60, 157-182.
- McCave, I.N. and Tucholke, B.E. (1986) Deep current-controlled sedimentation in the western North Atlantic. *Geol. Soc. Am.*
- Michard, A., Saddiqi, O., Chalouan, A. and de Lamotte, D.F. (Eds.). (2008) Continental evolution: The geology of Morocco: Structure, stratigraphy, and tectonics of the Africa-Atlantic-Mediterranean triple junction, 116. Springer.
- Miguez-Salas, O., Rodríguez-Tovar, F.J. and de Weger, W. (2020) Macaronichnus and contourite depositional settings: Bottom currents and nutrients as coupling factors. *Palaeogeogr. Palaeoclimatol. Palaeoecol.*, 545, 109639.
- Miller, K.G., Mountain, G.S., Wright, J.D., and Browning, J.V. (2011) A 180-million-year record of sea level and ice volume variations from continental margin and deep-sea isotopic records. *Oceanography*, 24, 40-53.
- Millot, C. (1999) Circulation in the western Mediterranean Sea. *Journal of Marine Systems*, 20, 423-442.
- Mulder, T. (2011) Gravity processes and deposits on continental slope, rise and abyssal plains. In *Dev. Sedimentol.*, 33, 25-148. Elsevier.
- Mutti, E. (1992) *Turbidite sandstones*. Agip, Istituto di geologia, Università di Parma. 722.
- Mutti, E., Bernoulli, D., Lucchi, F.R. and Tinterri, R. (2009) Turbidites and turbidity currents from Alpine 'flysch' to the exploration of continental margins. *Sedimentology*, 56, 267-318.
- Mutti, E., Cunha, R.S., Bulhoes, E.M., Arienti, L. M. and Viana, A.R. (2014) Contourites and turbidites of the Brazilian marginal basins. *AAPG Search and Discovery Article*, 51069, 1-46.
- Nelson, C.H., Baraza, J. and Maldonado, A. (1993) Mediterranean undercurrent sandy contourites, Gulf of Cadiz, Spain. *Sed. Geol.*, 82, 103-131.
- Nelson, C.H., Baraza, J., Maldonado, A., Rodero, J., Escutia, C. and Barber Jr, J.H. (1999) Influence of the Atlantic inflow and Mediterranean outflow currents on Late Quaternary sedimentary facies of the Gulf

- of Cadiz continental margin. *Mar. Geol.*, 155, 99-129.
- Nio, S.D. and Yang, C.S. (1991) Diagnostic attributes of clastic tidal deposits: a review.
- O'Brien, N.R., Nakazawa, K. and Tokuhashi, S. (1991) Use of clay fabric to distinguish turbiditic and hemipelagic siltstones and silts. *Deep-Water Turbidite Systems*, D.A.V. Stow (Ed.), 271-271.
- Paulat, M., Lüdmann, T., Betzler, C. and Eberli, G.P. (2019) Neogene palaeoceanographic changes recorded in a carbonate contourite drift (Santaren Channel, Bahamas). *Sedimentology*, 66, 1361-1385.
- Pérez-Asensio, J.N., Aguirre, J., Schmiedl, G. and Civis, J. (2012) Messinian paleoenvironmental evolution in the lower Guadalquivir Basin (SW Spain) based on benthic foraminifera. *Palaeogeogr. Palaeoclimatol. Palaeoecol.*, 326, 135-151.
- Rahmstorf, S. (2006) Thermohaline ocean circulation. *Encyclopedia of quaternary sciences*, 5.
- Reading, H.G. (Ed.). (2009) *Sedimentary environments: processes, facies and stratigraphy*. John Wiley & Sons. 704 pp.
- Rebesco, M., Pudsey, C.J., Canals, M., Camerlenghi, A., Barker, P.F., Estrada, F. and Giorgetti, A. (2002) Sediment drifts and deep-sea channel systems, Antarctic Peninsula Pacific Margin. *Geol. Soc. London, Mem.*, 22, 353-371.
- Rebesco, M., Hernández-Molina, F.J., Van Rooij, D. and Wåhlin, A. (2014) Contourites and associated sediments controlled by deep-water circulation processes: state-of-the-art and future considerations. *Mar. Geol.*, 352, 111-154.
- Richez, C. (1994) Airborne synthetic aperture radar tracking of internal waves in the Strait of Gibraltar. *Prog. Oceanogr.*, 33, 93-159.
- Rocha, C.C.A. and Clarke, A.J. (1987) Interaction of ocean tides through a narrow single strait and narrow multiple straits. *J. Phys. Oceanogr.*, 17, 2203-2218.
- Rodrigues, S., Hernández-Molina, F.J. and Kirby, A. (2021) A Late Cretaceous hybrid (turbidite-contourite) system along the Argentine Margin: Paleooceanographic and conceptual implications. *Mar. and Petrol. Geol.*, 123, 104768.
- Rodríguez-Tovar, F.J., Hernández-Molina, F.J., Hüneke, H., Llave, E. and Stow, D.A.V. (2019) Contourite facies model: Improving contourite characterization based on the ichnological analysis. *Sed. Geol.*, 384, 60-69.
- Rogerson, M., Rohling, E.J., Bigg, G.R. and Ramirez, J. (2012) Paleooceanography of the Atlantic-Mediterranean exchange: Overview and first quantitative assessment of climatic forcing. *Rev. Geophys.*, 50, RG2003.
- Rohling, E.J., Marino, G. and Grant, K.M. (2015) Mediterranean climate and oceanography, and the periodic development of anoxic events (sapropels). *Earth Sci. Rev.*, 143, 62-97.
- Roldán, F.J., Galindo-Zaldívar, J., Ruano, P., Chalouan, A., Pedrera, A., Ahmamou, M., Ruiz-Constan, A., Sanz de Galdeano, C., Benmakhlouf, M., Lopez-Garrido, A.C., Anahnah, F. and Gonzalez-Castillo, L. (2014) Basin evolution associated to curved thrusts: The Prerifian Ridges in the Volubilis area (Rif Cordillera, Morocco). *J. Geodynamics*, 77, 56-69.
- Ryan, W.B.F. and Hsü, K.J. (1973) Initial reports of the deep-sea drilling project, 13, US Govt. Printing Office, Washington, D.C.
- Sani, F., Del Ventisette, C., Montanari, D., Bendkik, A. and Chenakeb, M. (2007) Structural evolution of the Rides Prerifaines (Morocco): structural and seismic interpretation and analogue modelling experiments. *Int. J. Earth Sci.*, 96, 685-706.
- Sansom, P. (2018) Hybrid turbidite–contourite systems of the Tanzanian margin. *Petrol. Geosci.*, 24, 258-276.
- Sierro, F.J. (1985) The replacement of the “Globorotalia menardii” group by the Globorotalia miotumida group: An aid to recognizing the Tortonian-Messinian boundary in the Mediterranean and adjacent Atlantic. *Mar. Micropaleontol.*, 9, 525-535.
- Sierro, F.J., Flores, J.A., Civis, J., Gonza, J.A. and France, G. (1993) Late Miocene globorotaliid event-stratigraphy and biogeography in the NE-Atlantic and Mediterranean. *Mar. Micropaleontol.*, 21, 143-167.
- Sierro, F.J., Hilgen, F.J., Krijgsman, W. and Flores, J.A. (2001) The Abad composite (SE Spain): a Messinian reference section for the Mediterranean and the APTS. *Palaeogeogr. Palaeoclimatol. Palaeoecol.*, 168, 141-169.
- Sierro, F.J., Hodell, D.A., Andersen, N., Azibeiro, L.A., Jimenez-Espejo, F.J., Bahr, A., Flores, J.A., Ausin, B., Rogerson, Lozano-



- Luz, R., Lebreiro, S. and Hernandez-Molina F.J. (2020) Mediterranean Overflow over the last 250 ky. Freshwater forcing from the tropics to the ice sheets. *Paleoceanography and Paleoclimatology*, e2020PA003931.
- Simon, D. and Meijer, P.T. (2017) Salinity stratification of the Mediterranean Sea during the Messinian crisis: A first model analysis. *Earth Planet. Sci. Lett.*, 479, 366-376.
- Simon, D., Marzocchi, A., Flecker, R., Lunt, D. J., Hilgen, F.J. and Meijer, P.T. (2017) Quantifying the Mediterranean freshwater budget throughout the late Miocene: New implications for sapropel formation and the Messinian Salinity Crisis. *Earth and Planetary Science Letters*, 472, 25-37.
- Shanmugam, G. (2008) Deep-water bottom currents and their deposits. *Developments in sedimentology*, 60, 59-81.
- Shanmugam, G. (2010) Slides, slumps, debris flow, and turbidity currents. *Ocean Currents: A Derivative of the Encyclopedia of Ocean Sciences*, 20, 418.
- Shanmugam, G. (2017) The contourite problem. In *Sediment provenance*, 183-254. Elsevier.
- Shanmugam, G. (2020). Mass transport, gravity flows, and bottom currents: Downslope and alongslope processes and deposits. *Elsevier*. 608.
- Spakman, W., Chertova, M.V., van den Berg, A., and van Hinsbergen, D.J. (2018) Puzzling features of western Mediterranean tectonics explained by slab dragging. *Nature Geoscience*, 11, 211-216.
- Stow, D.A.V. and Piper, D.J.W. (1984) Deep-water fine-grained sediments: facies models. *Geol. Soc. London, Spec. Publ.*, 15, 611-646.
- Stow, D.A.V. (1985) Fine-grained sediments in deep water: An overview of processes and facies models. *Geo-Mar. Lett.*, 5, 17-23.
- Stow, D.A.V. and Wetzel, A. (1990) Hemiturbidite: a new type of deep-water sediment. In *Proceedings of the ocean drilling program, scientific results*, 116, 25-34. College Station, TX: Ocean Drilling Program.
- Stow, D.A.V. and Faugères, J.C. (2008) Contourite facies and the facies model. *Dev. Sedimentol.*, 60, 223-256.
- Stow, D.A.V., Hernández-Molina, F.J., Llave, E., Sayago-Gil, M., Díaz del Río, V. and Branson, A. (2009) Bedform-velocity matrix: the estimation of bottom current velocity from bedform observations. *Geology*, 37, 327-330.
- Stow, D.A.V., Hernández-Molina, F.J., Llave, E., Bruno, M., García, M., del Río, V.D., Somoza, L. and Brackenkridge, R.E. (2013) The Cadiz Contourite Channel: Sandy contourites, bedforms and dynamic current interaction. *Mar. Geol.*, 343, 99-114.
- Stow, D.A.V. and Smillie, Z. (2020) Distinguishing between Deep-Water Sediment Facies: Turbidites, Contourites and Hemipelagites. *Geosci.*, 10, 68.
- Straume, E.O., Gaina, C., Medvedev, S. and Nisancioglu, K.H. (2020) Global Cenozoic Paleobathymetry with a focus on the Northern Hemisphere Oceanic Gateways. *Gondwana Research*.
- Talling, P.J., Masson, D.G., Sumner, E.J. and Malgesini, G. (2012) Subaqueous sediment density flows: Depositional processes and deposit types. *Sedimentology*, 59, 1937-2003.
- Taltasse, P. (1953) Recherches géologiques et hydrogéologiques dans le Bassin lacustre de Fès-Moknès, &c.
- Tulbure, M.A., Capella, W., Barhoun, N., Flores, J.A., Hilgen, F.J., Krijgsman, W., Kouwenhoven, F.J., Sierro, F.J. and Yousfi, M. Z. (2017) Age refinement and basin evolution of the North Rifian Corridor (Morocco): No evidence for a marine connection during the Messinian Salinity Crisis. *Palaeogeogr. Palaeoclimatol. Palaeoecol.*, 485, 416-432.
- Uchman, A. (2009) The Ophiomorpha rudis ichnosubfacies of the Nereites ichnofacies: characteristics and constraints. *Palaeogeogr. Palaeoclimatol. Palaeoecol.*, 276, 107-119.
- Van Assen, E., Kuiper, K.F., Barhoun, N., Krijgsman, W. and Sierro, F.J. (2006) Messinian astrochronology of the Melilla Basin: stepwise restriction of the Mediterranean–Atlantic connection through Morocco. *Palaeogeogr. Palaeoclimatol. Palaeoecol.*, 238, 15-31.
- van Hinsbergen, D.J., Vissers, R.L. and Spakman, W. (2014) Origin and consequences of western Mediterranean subduction, rollback, and slab segmentation. *Tectonics*, 33, 393-419.
- Vázquez, A., Bruno, M., Izquierdo, A., Macías, D. and Ruiz-Cañavate, A. (2008) Meteorologically forced subinertial flows and internal wave generation at the main

- sill of the Strait of Gibraltar, Deep-Sea Research Part I: *Oceanogr. Res. Pap.*, 55, 1277-1283.
- Viana, A.R. (2008) Economic relevance of contourites. *Dev. Sedimentol.*, 60, 491-510.
- Visser, M.J. (1980) Neap-spring cycles reflected in Holocene subtidal large-scale bedform deposits: a preliminary note. *Geology*, 8, 543-546.
- Wernli, R. (1988) Micropaléontologie du Néogène post-nappes du Maroc septentrional et description systématique des foraminifères planctoniques. *Notes et Mémoires du Service géologique*, 331.

# Chapter VI

## *Tide-dominated deltas responding to high-frequency sea-level changes, pre-Messinian Rifian Corridor, Morocco: DISCUSSION*

### Chapter VI

This article has been written as a discussion reply to:

*Beelen, D., Wood, L., Zaghoul, M. N., Haissen, F., Arts, M., Ouahbi, I., Redouan, M., & Cardona, S. (2020). Tide-dominated deltas responding to high-frequency sea-level changes, Pre-Messinian Rifian Corridor, Morocco. Journal of Sedimentary Research, 90(11), 1642-1666.*

Their original manuscript is can be found at: <https://doi.org/10.2110/jsr.2020.010>

Pictures referred to in the text are provided in the appendices of Chapter VI



# Tide-dominated deltas responding to high-frequency sea-level changes, pre-Messinian Rifian Corridor, Morocco: DISCUSSION

Wouter de Weger, Domenico Chiarella, Francisco J. Rodríguez Tovar, Francisco J. Sierra,  
Olmo Miguez-Salas, M. Amine Manar, F. Javier Hernández-Molina

Accepted

## Introduction

Beelen et al. re-interpreted the late Miocene contourite depositional system of the Saiss Basin in the Rifian Corridor, Morocco (*Capella et al., 2017a; de Weger et al., 2020*), as a tide-dominated delta environment that responded to high-frequency sea-level changes. Despite the authors stimulating a valuable discussion on the interpretation of the studied deposits, their proposed depositional system seems largely based on erroneous interpretations of the data that are misleading for the reader that is unfamiliar with the geological framework of the study area. Based on (i) issues with spatial location of the outcrops they interpreted relative to known tectonic structures, (ii) poor or contradictory age control that suggest the studied outcrops are not all the same age, (iii) faunal and sedimentary structures evidence that better supports a deep-water setting, and (iv) a lack of evidence to support the necessarily high-amplitude relative or eustatic sea-level changes, we consider that the balance of evidences recognized in these outcrops better supports a deep-water setting. With this comment we would like to address these inconsistencies and express our concerns about the train-of-thought used by Beelen et al. for their interpretation of shallow- rather than deep-marine depositional settings for the studied intervals.

## Spatiotemporal location of the outcrops

Beelen et al. provided a geological and paleogeographic framework that is mostly in line with the existing literature, reporting that a series of partially connected foreland basins formed the Rifian Corridor connection between the Atlantic Ocean and the Mediterranean Sea during the late Miocene. Furthermore, the authors address that the Rifian Corridor was probably divided into a narrower North

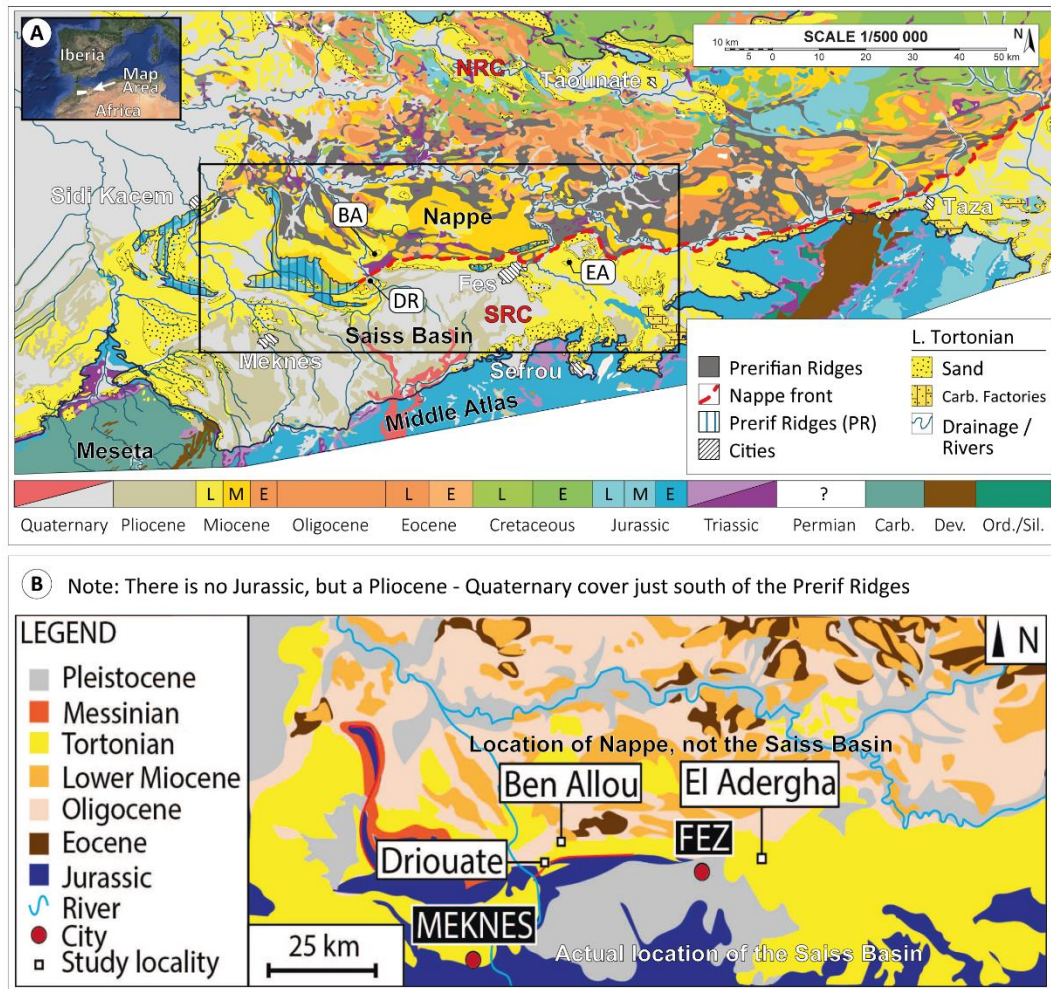


**Figure 6.1** (herein). **A**) Regional geological map of the study area including the locations of the studied Upper Miocene outcrops; Ben Allou (BA) and El Adergha (EA), as well as the Pliocene Driouate (DR) outcrop. The South Rifian Corridor (SRC) was limited northwards by the Nappe and southwards by both the Moroccan Meseta in the southeast, and the Middle Atlas towards the south. The North Rifian Corridor (NRC) is located north of the Nappe. The square outlines the location of figure **B**. Carb. Factories is short for Carbonate factories, L = late, M = middle and E = early. (modified after Saadi. et al., 1980). **B**) Shows the geological map wrongly modified by Beelen et al. after Chankeb, 2004. Note that the Jurassic cover south of Fes and Meknes, or south of the Prerif Ridges is not present in the Saiss Basin but is related to the Middle Atlas.

Rifian Corridor (NRC) and a wider South Rifian Corridor (SRC), separated by an up-thrusted nappe belonging to the African continent (Capella et al, 2018). The Saiss foredeep Basin, the main conduit of the SRC, is positioned in the front of this SW-ward emplaced nappe, bounded in the south, roughly 30 km south of the cities of Fes and Meknes, by the Moroccan Meseta and the Middle Atlas (Fig. 6.1A herein). Accordingly, Capella et al. (2017) and de Weger et al. (2020) argued that the frontal part of the nappe, which was already mostly emplaced by 7.8 Ma, formed the slope of the northern margin of the SRC. However, based on a misinterpretation of the geological map (Fig. 6.1B), Beelen et al. have erroneously considered the nappe as the Saiss Basin, and as such, assumed the main conduit of the SRC was located on top of the nappe with its southern margin being located just north of the cities of Fes and Meknes.

Beelen et al. considered for their reinterpretation of the depositional environment three outcrops: *Ben Allou*, *El Adergha* and *Driouate*. In the paper, Beelen et al. state that these outcrops are “broadly similar and contemporaneous”. However, the deposits of the Ben Allou outcrop were deposited between 7.8 and 7.51 Ma, the El Adergha deposits between 7.35 – 7.25 Ma (*Capella et al., 2017*) and the Driouate deposits have not been dated by Beelen et al. but Beelen et al. considered them to be time equivalent to both Ben Allou and El Adergha. Strikingly, based on the original geological map (*Chankeb, 2004*) used by the Authors, as well as in figure 1A reported here, the Driouate deposits are of Middle Pliocene to Upper Pleistocene in age (3.56 – 1.78 Ma). As such, the outcrops considered (Fig. 6.2) do not belong to the same stratigraphic interval and can thus not be used for a time equivalent paleogeographic reconstruction.

The paleogeographic reconstruction provided by Beelen et al. (Fig. 15 - Appendix), based on the argumentation addressed above, not only places the SRC north of the foredeep basin and on top of the nappe, but it also contains discrepancies with respect to their Figure 1 (Appendix). Figure 1 by Beelen et al. (Appendix) correctly shows the relative location of the Driouate outcrop with respect to the Ben Allou outcrop in the south-west, geographically located west of the city of Fes. However, in Figure 15 (Appendix) the Driouate system is positioned south-east with respect to the Ben Allou system and south-west compared to the city of Fes to support their interpretation. Furthermore, the authors also used paleo-current data derived from *Capella et al. (2017)* for other nearby located outcrops to support their interpretations. These data from *Capella et al. (2017)* however, are derived from outcrops of which the interpretation does not fit with the interpretation of Beelen et al., the authors fail to discuss these deviating interpretations. For example, the Sidi Harazem outcrop has been interpreted by *Capella et al. (2017)* as turbidite deposits in the axial foredeep of the SRC whilst in the Beelen et al. proposed reconstruction, this outcrop is located on the southern margin of their corridor. Moreover, the Ain Kansera outcrop is used by Beelen et al. as an argument to support the presence of wave action and a shallow marine setting after the interpretation by *Capella et al. (2017)*, However, Beelen et al. placed this outcrop in the axis of the SRC in their reconstruction (Fig. 15 in Beelen et al. - Appendix), not fitting within their interpretation of a shallow marine setting.

## Shallow- vs Deep-water

Based on the dominant occurrence of benthic foraminiferal genera indicative for shallow water environments; *Ammonia*, *Elphidium* and *Cibicides*, Beelen et al. indicate deep-middle to inner-neritic water depths for the fine-grained deposits and inner-neritic to littoral water depths for the calcarenites. The presence of these genera is indeed consistent with inner neritic settings, but the Authors fail to explain how genera indicative for deeper settings (*Pullenia*, *Dentalina*, *Oolina*, *Planulina* and others) were transported to the interpreted coastal environments. *García-Gallardo et al. (2017)* and *van der Schee et al. (2016)* have observed the abundant presence of shelf foraminifera in sandy

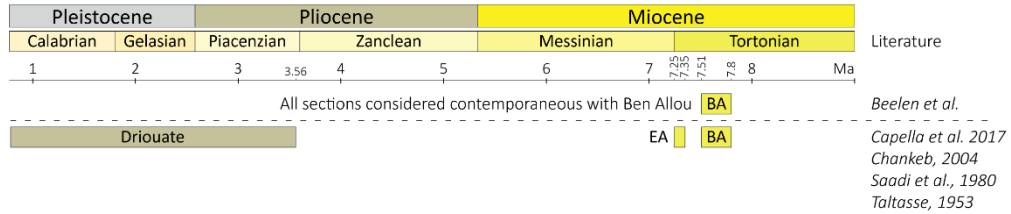


**Figure 6.2** (herein). Temporal distribution of the studied outcrops used by Beelen et al. and based on other sources such as Capella et al. (2017); Chankeb (2004); Saadi et al. (1980) and Taltasse (1953). BA = the Ben Allou outcrop and, EA = El Adergha.

deposits associated to the early Pliocene contourite deposits in the Gulf of Cadiz, in water-depths exceeding 400 m. These allochthonous assemblages contain similar specimens as reported by Beelen et al., containing also abundant *Ammonia* and *Elphidium*. Garcia-Gallardo et al. (2017) and van der Schee et al. (2016) argued that these shelfal foraminifera were transported down the slope by turbidity currents to be redistributed, along-slope by contour currents, similarly as was proposed by Capella et al. (2017). This all suggests that a shallow depositional setting cannot be affirmed by the foraminiferal assemblages. Furthermore, the Driouate section was interpreted as a lagoon deposit, however, most of the species found are incompatible with a lagoon setting. Although *Ammonia* and *Elphidium* can be found in lagoons, as well as in the inner shelf, *Pullenia*, *Oolina*, *Amphicoryna*, *Dentalina*, *Planulina* and the planktonic genera, referred to in table 2 (by Beelen et al. - Appendix) of the supplementary information, are characteristic of open, deeper-marine waters.

Contourites are associated with bottom currents that transport and accumulate sedimentary particles. The type of particles transported by the currents depends on the geological setting, but only a minority of these particles are formed in the slope. The vast majority is siliciclastic, supplied by for example rivers, or bioclastic (mostly calcareous fossils) formed on the shelf or coming from pelagic settling (planktonic foraminifers, coccoliths) (e.g., Hüneke et al., 2021; de Castro et al., 2021b). The presence of largely fragmented macrofossils, such as barnacles, bryozoan, mollusks, calcareous algae, and others, which live in shallow water environments, as such, cannot be considered as indicators of paleobathymetry. Bioclasts derived from these macrofossils are very commonly the main components of deposits associated to bottom currents (e.g., Longhitano et al., 2014; de Castro et al., 2021a, b). Ostracods have for example been identified in the upper continental slope (at water depths of 501 m) and were used to evaluate their relationship with bottom water condition variability and the control of the Levantine Intermediate Water current benthic faunas (Angue Minto'o et al., 2015). Beelen et al. particularly regard the abundant occurrence of barnacles as an indicator of the shallow-water origin of the calcarenites as they argue that some of them appear to be in life position. Barnacles, however, are sessile crustaceans living attached to a substrate. We never found barnacles in life position and apparently neither have the Authors as they did not find the hard substrates where these barnacles were fixed on. To support their ideas, Beelen et al. speculated that these barnacles were probably attached to tidewrack or wood that was not preserved.



Beelen et al. furthermore mentioned that trace fossils recognized in the Ben Allou and El Adergha outcrops are indicative of the *Glossifungites* ichnofacies. However, two of the most abundant trace fossils recorded by Beelen et al. (*Scolicia* and *Macaronichnus*) are not included in this archetypical ichnofacies (MacEachern et al., 2007, 2012). Moreover, the ichnological information (i.e., *Rhizocorallium*, *Skolithos* and *Phytoplasma*) presented to justify the *Glossifungites* ichnofacies, is poorly documented. As such, any interpretation based on the recognition of the *Glossifungites* ichnofacies is weak and should be reconsidered. Additionally, *Rosalina* is not an ichnogenus *per se* as this term only refers to small foraminiferans that produce small boreholes (Bromley, 1981; Neuman and Wisshak, 2006). Thus, the appearance of “*Rosalina*” ichnogenus cannot be used to support that El Adergha was deposited in shallower waters compared to the grey marlstones in Ben Allou.

Beelen et al. explain the alternating occurrence of “shallow-marine” and “deep-marine” fine grained deposits by roughly 70 - 80 m fluctuations of high-frequency eustatic sea-level rise to support their interpretation of a tide dominated delta. Although the Authors claim these high-magnitude sea-level fluctuations are supported by previous work, the references cited either do not cover the studied interval (Liebrand et al., 2011) or do not support such high-magnitude and high-frequency sea-level variations (Kominz et al., 2008; Westerhold et al., 2005). Westerhold et al. (2005) and Kominz et al. (2008) reported sea-level fluctuations for the late Tortonian of not more than 30 meters. Consequently, sea-level fluctuations with a magnitude sufficient to explain shallow- to deep-marine transitions are not supported, and in fact are contradicted by the references cited, making the interpretation of a deep-water depositional setting more suitable.

## Depositional setting: Sedimentological data and interpretation

Beelen et al. mention the presence of bidirectional sedimentary structures eleven times throughout the manuscript, but do not provide any data to support the interpretation of bidirectional tidal flow. Furthermore, the authors stated: “Overall, our combined measurements of paleocurrent directions across the calcarenite layers agree with those published by Capella et al. (2017) and show a dominance of southwestward-oriented, omnidirectional flow”. However, the Authors failed to provide their own paleocurrent data; the data used (Fig. 16 in Beelen et al. - appendix) is derived from Capella et al. (2017) which does not show a bidirectional trend. Moreover, what has been reported as bidirectional cross stratification and potentially herringbone cross stratification (Fig. 4C in Beelen et al. - Appendix) is an example of “false herringbones” showing a section which is not parallel to the paleo-flow. As such, we found the interpretation of the existence of bidirectional currents a somewhat “forced” interpretation.

Beelen et al. mention that hummocky cross-stratification was found in the El Adergha outcrop (p. 1652) but this is not supported by any evidence. Moreover, the Authors even mention a lack of

sedimentary structures associated to waves, such as symmetrical ripples, hummocks, and swales (p. 1655).

The presence of mudcracks, highly relevant for the interpretation of subaerial exposures, has been mentioned but is not strongly supported by evidence in the manuscript (Fig. 6C - Appendix). Furthermore, dewatering structures are used to support a periodic subaerial exposure (p. 1656), not considering that these structures are usually related to loosely packed and rapidly deposited sediment, independent of water depth. Plant rootlets (Fig. 10B - Appendix) have also been used to support the interpretation that the deposits have been subaerially exposed. However, the supporting material (Fig. 10A and B - Appendix) suggests that they are just as likely to be Anthropocene rather than Miocene roots growing in the strata and forcing them to break apart producing the photographed exposure (Fig. 10B - Appendix). Furthermore, insect-larva burrows reported for the Driouate outcrop (Fig. 10G - Appendix), despite this outcrop not being relevant for their interpretation of the late Miocene, are also more probably the product of recent biological activities.

Finally, the Ben Allou and El Adergha outcrops are composed of marls and sand bodies that, particularly in the Ben Allou outcrop, show large concave-up features. Although Beelen et al. argue to have found facies related to depositional sub-environments of a tide-dominated deltas, evidence for a delta plain and a time-equivalent (7.8 – 7.25 Ma) proximal fluvial feeder system have not been documented.

## Conclusion

In conclusion, based on issues with spatial locations of the outcrops and the use of erroneous data, we find that the observations and interpretations provided by Beelen et al. are not adequate to challenge the current interpretations of the studied deposits as being formed in deep-water by the paleo-Mediterranean Outflow Water.

## References

- Bromley, R.G., 1981, Concepts in ichnotaxonomy illustrated by small round holes in shells. *Acta Geologica Hispanica*, v. 16, p. 55-64.
- Capella, W., Hernández-Molina, F.J., Flecker, R., Hilgen, F.J., Hssain, M., Kouwenhoven, T.J., van Oorschot, M., Sierro, F.J., Stow, D.A.V., Trabucho-Alexandre, J., Tulbure, M.A., de Weger, W., Yousfi, M.Z. and Krijgsman, W. 2017a, Sandy contourite drift in the late Miocene Rifian Corridor (Morocco): reconstruction of depositional environments in a foreland-basin seaway: *Sedimentary Geology*, v. 355, p. 31–57.
- Capella, W., Barhoun, N., Flecker, R., Hilgen, F.J., Kouwenhoven, T., Matenco, L.C., Sierro, F.J., Tulbure, M.A., Yousfi, M.Z., and Krijgsman, W., 2018, Palaeogeographic evolution of the late Miocene Rifian Corridor (Morocco): reconstructions from surface and subsurface data: *Earth-Science Reviews*, v. 180, p. 37–59.
- Chenakeb, M., 2004, Carte Géologique du Maroc, Feuille Beni Ammar, échelle 1:

- 50,000: Notes et Memoires Service Géologique du Maroc, v. 428.
- de Castro, S., Hernández-Molina, F.J., de Weger, W., Jiménez-Espejo, F.J., Rodríguez-Tovar, F.J., Mena, A., Llave, E., Sierro, F.J., 2021a, Contourite characterization and its discrimination from other deep-water deposits in the Gulf of Cadiz contourite depositional system. *Sedimentology*, v. 68, p. 987-1027.
- de Castro, S., Miramontes, E., Dorador, J., Jouet, G., Cattaneo, A., Rodríguez-Tovar, F.J. and Hernández-Molina, F.J., 2021b, Siliciclastic and bioclastic contouritic sands: textural and geochemical characterisation. *Marine and Petroleum Geology*, v. 128, 105002.
- de Weger, W., Hernández-Molina, F.J., Flecker, R., Sierro, F. J., Chiarella, D., Krijgsman, W., and Manar, M.A., 2020, Late Miocene contourite channel system reveals intermittent overflow behavior. *Geology*, v. 48, p. 1194-1199.
- García-Gallardo, Á., Grunert, P., van der Schee, M., Sierro, F.J., Jiménez-Espejo, F.J., Zariqian, C.A.A., and Piller, W.E., 2017, Benthic foraminifera-based reconstruction of the first Mediterranean-Atlantic exchange in the early Pliocene Gulf of Cadiz. *Palaeogeography, Palaeoclimatology, Palaeoecology*, v. 472, p. 93-107.
- Hüneke, H., Hernández-Molina, F.J., Rodríguez-Tovar, F.J., Llave, E., Chiarella, D., Mena, A., and Stow, D.A.V., 2021, Diagnostic criteria using microfacies for calcareous contourites, turbidites and pelagites in the Eocene–Miocene slope succession, southern Cyprus. *Sedimentology*, v. 68, p. 557-592. <https://doi.org/10.1111/sed.12792>
- Kominz, M.S., Browning, J.V., Miller, K.G., Dugarman, P.J., Mizintseva, D., and Dcotese, C.R., 2008, Late Cretaceous to Miocene sea level estimates from the New Jersey and Delaware coastal plain coreholes: an error analysis: *Basin Research*, v. 20, p. 211–226.
- Liebrand, D., Lourens, L.J., Hodell, D.A., de Boer, B., van de Wal, R.S.W., and Pälike, H., 2011, Antarctic ice sheet and oceanographic response to eccentricity forcing during the early Miocene: *Climate of the Past*, v. 7, p. 869–880.
- Longhitano, S.G., Chiarella, D., and Muto, F., 2014, Three-dimensional to two-dimensional cross-strata transition in the lower Pleistocene Catanzaro tidal strait transgressive succession (southern Italy). *Sedimentology*, v. 61, p. 2136-2171.
- Maceachern, J.A., Pemberton, S.G., Gingras, M.K. and Bann, K.L., 2007, The ichnofacies paradigm: a fifty-year retrospective. In *Trace fossils*, p. 52-77. Elsevier.
- Maceachern, J.A., Bann, K.L., Gingras, M.K., Zonneveld, J.P., Dashtgard, S.E., Pemberton, S.G., 2012, The ichnofacies paradigm. In *Dev. Sedimentol.*, v. 64, p. 103-138. Elsevier.
- Minto'o, S.A., Bassetti, M.A., Morigi, C., Ducassou, E., Toucanne, S., Jouet, G., and Mulder, T., 2015, Levantine intermediate water hydrodynamic and bottom water ventilation in the northern Tyrrhenian Sea over the past 56,000 years: New insights from benthic foraminifera and ostracods. *Quaternary International*, v. 357, p. 295-313.
- Neumann, C. and Wisshak, M., 2006, A Foraminiferal Parasite on the Sea Urchin *Echinocorys*: Ichnological Evidence from the Late Cretaceous (Lower Maastrichtian, Northern Germany), *Ichnos*, v. 13, p. 185-190,
- Saadi, S.E., Hilali, E.A., and Boudda, A., 1980, ROAYME DU MAROC. Ministère de l'énergie et des mines. Direction de la géologie. Editions du Service Géologique du Maroc. Notes et Mémoires N° 245b (Maquette achevée en 1975).
- Taltasse, P., 1953, Recherches géologiques et hydrogéologiques dans le bassin lacustre de Meknès-Fès. *Notes & M. Serv. géol. Maroc*, v. 115, p. 78-81.
- Van der Schee, M., Sierro, F.J., Jiménez-Espejo, F.J., Hernández-Molina, F.J., Flecker, R., Flores, J.A., Acton, G., Gutjahr, M., Grunert, P., García-Gallardo, Á., and Andersen, N., 2016, Evidence of early bottom water current flow after the Messinian Salinity Crisis in the Gulf of Cadiz. *Marine Geology*, v. 380, p. 315-329.
- Westerhold, T., Bickert, T., and Rohl, U., 2005, Middle to late Miocene oxygen isotope stratigraphy of ODP site 1085 (SE Atlantic): new constrains on Miocene climatevariability and sea-level fluctuations: *Palaeogeography, Palaeoclimatology, Palaeoecology*, v. 217, p. 205–222.

# *Chapter VII*

# Contourite channels: sedimentary facies and depositional sequences

de Weger, W., Hernández-Molina, F.J., Chiarella, D., Fedele, J.J., Llave, E., Rodriguez-Tovar, F.J., Miguez-Salas, O. and Manar, M.A.

ARTICLE READY FOR SUBMISSION:

## ABSTRACT

Sedimentary deposits are generally recognized, interpreted, and classified based on depositional processes. However, many depositional processes in the deep-marine realm are not well understood. This regularly leads to a bias in assumptions towards processes that gained more scientific attention. Despite the rise in published evidence of deep-marine bottom current processes and associated deposits there are still very few documented outcrop examples. Outcrop examples however play a pivotal role in understanding deep-marine sedimentary systems as they represent the record of otherwise poorly accessible deposits. Herein we report results of a contourite channel system related to the late Miocene paleo-Mediterranean Outflow Water (MOW) in the Rifian Corridor, Morocco. This work aims to unravel the sedimentary evolution and facies distribution based on the study of large morphological features related to contourite channels and their subsequent sandstone dominated infill sequences. It was found that the channel evolution and facies distribution are related to spatiotemporal changes in flow characteristics of the paleo-MOW. The recognized inter-channel facies distribution correlates well with previously established bedform stability diagrams. Erosion and upper-stage flow regime bedforms are associated to the most vigorous bottom currents, generally related to its core. Laterally, following the decrease in flow velocity towards the adjacent drift, bedforms comprise dunes, lower-stage plane bedforms and more heterolithic facies. Similar facies changes are also observed down-channel, related to a decrease in flow velocities resulting from turbulent mixing of water masses, its associated decrease in density gradients and the subsequent deceleration due to gravity. Results of this work have been used to propose a 3D facies model for channelized sandy contourites. In addition, this study contributes to increase our understanding of contourite systems, thus benefitting oceanographic and climatic reconstructions as well as aiding the predictability of contourite channel systems for industry geoscience applications.

**Keywords:** Deep-water sedimentation, Contourite channel system, Drifts, Bottom Currents, Tides, Facies Models, Late Miocene, Rifian Corridor, Morocco

## 1. INTRODUCTION

Deep-marine deposits are generally interpreted based on depositional processes. Many depositional processes in the deep-marine realm, particularly with regards to bottom currents, are however not well understood. This has led to a bias in assumptions towards processes that gained more scientific attention. As such, the poorly understood hydrodynamic behavior of bottom currents and their depositional processes hinders the recognition of contourites (*de Weger et al., 2021*), further hampering their scientific attention.

Over the last decade there has been a significant rise in published evidence of deep-marine bottom current processes and associated deposits. Most of these works are based on seismic data (*e.g. Faugères et al., 1999; Paulat et al., 2019*), some from wells and cores (*e.g. Gonthier et al., 1984; de Castro et al., 2020a, b; Hovikoski et al., 2020*), but there is still very little information from the outcrop record (*e.g. Duan et al., 1992; Hüneke et al., 2020*). This is particularly true for deep-water contourite channels.

Significant advances in the sedimentological understanding of deep-water channels and their sedimentary features have been made in recent years. These advances have mainly focused on channel belts and channel belt systems formed by down-slope gravity driven processes. These channels comprise architectural elements such as lateral-accretion packages, channel-bend mounds, levees, non-turbiditic mass-transport deposits and last-stage channel-fills (*e.g. Walker, 1978; Weimer et al., 2006; Kolla et al., 2007; Wynn et al., 2007; Harris and Whiteway, 2011; Janocko et al., 2013*). Contrastingly, contourite channels (*Hernández-Molina et al., 2006; García et al., 2009*) have received much less scientific attention. Moreover, these erosional elements received much less scientific attention compared to the large depositional features, the contourite drifts. Contourite channels, however, might contain most information on past ocean circulation and thus climate. Furthermore, their coarse-grained nature makes them valuable targets for hydrocarbon reservoirs.

Attempts to better understand the sedimentological features of modern contourite channel systems by studying cores have generally failed as the sediment proved too unconsolidated for acquisition (*Expedition 339 scientists, 2012; Brackenridge et al., 2018; de Castro et al., 2021*). As a result, the information from these features are generally limited to bathymetric imaging and bottom photographs (*e.g. Stow et al., 2009, 2013*). Observations

from the ancient rock record are predominantly based on seismic data, cores, and logs (Hernández-Molina et al., 2014a; Gong et al., 2017). Because of the extreme differences in scale and resolution between these, comprehensive understanding and testing of process hypotheses relating the evolution of contourite erosive features and their associated infill deposits have remained elusive.

Herein, we report the results of an extensive field outcrop study of an exposed late Miocene contourite channel system in northern Morocco (Capella et al., 2017a; Capella et al., 2018; de Weger et al., 2020, 2021). De Weger et al. (2020, 2021) recently described the occurrence and the regional evolution of these channels, but the lateral and vertical sedimentary facies and depositional sequences within the channels had not yet been considered in detail. Therefore, the aims of this work are to: (1) improving our general understanding of contourite channel systems, (2) better understand the detailed hydrodynamic behavior of channelized bottom currents, (3) identify recognition criteria for sandy contourites, and (4) propose a facies model for these systems. Finally, this contribution will address some of the implications for climatic studies and industry resource and exploration potential.

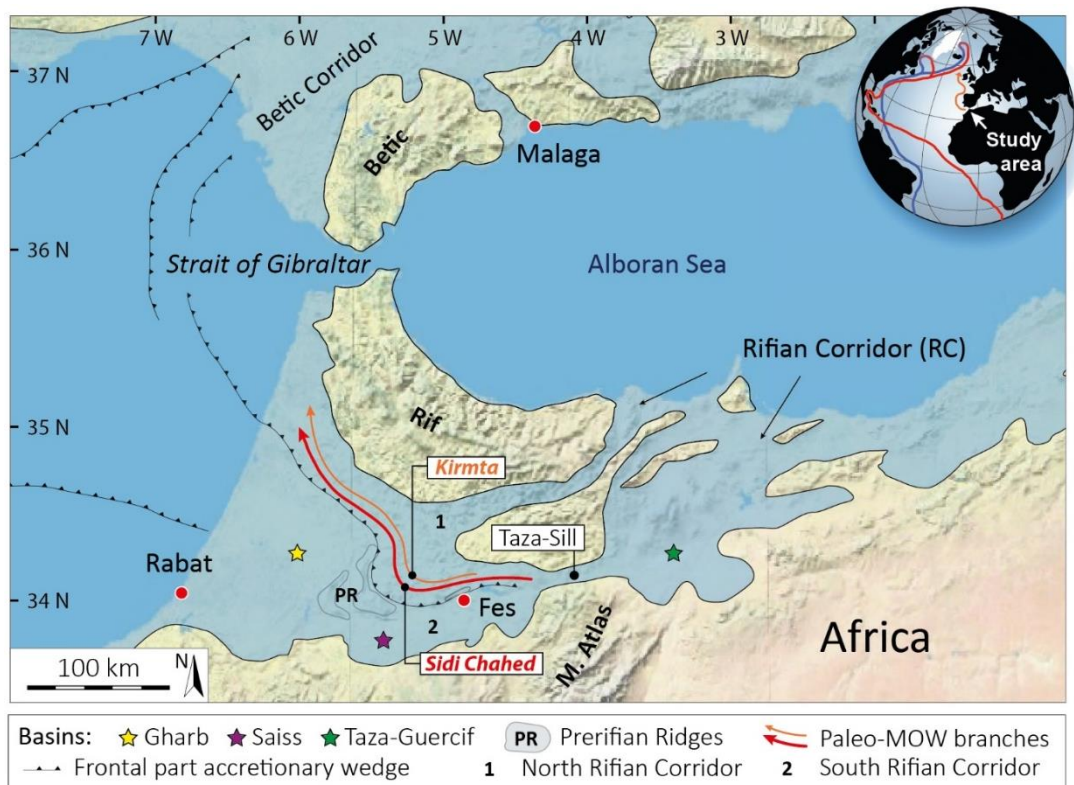


**Figure 7.1.** Paleogeographic reconstruction of the late Miocene Rifian Corridor, Morocco (modified after de Weger et al., 2020, 2021). The Betic and Rif, Middle Atlas, Prerif Ridges, and the Taza-Sill form the main geological features. The studied outcrops (Kirmta and Sidi Chahed) are related to different branches of the paleo-Mediterranean Outflow Water (MOW). The small globe depicts the location of the study area, the general ocean circulation pattern and in orange, the trajectory of the present-day MOW.



## 2. STUDY AREA AND GEOLOGICAL SETTING

The studied rock outcrops (i.e., *Sidi Chahed* and *Kirmta*) are in the Rifian Corridor of northern Morocco (Fig. 7.1). This corridor is part of the external zone of the Rif-Betic-, or Gibraltar-Arc which forms an arc-shaped orogenic belt surrounding the Alboran Sea in the westernmost Mediterranean region. The Rifian Corridor formed a late Miocene marine gateway that allowed Mediterranean-Atlantic water exchange (e.g. *Capella et al., 2017a; Krijgsman et al., 2018*). The corridor evolved as a south-westward migrating foreland basin during the Tortonian (~ 8 Ma) (*Feinberg, 1986; Wernli, 1988; Sani et al., 2007*), limited northwards by the earlier exhumed Rif orogenic wedge (*Iribarren et al., 2009*) and southwards by the Middle Atlas Mountains (*Barbero et al., 2011*). The Rifian Corridor was previously divided into two strands (Fig. 7.1), the North Rifian Corridor related to the Intramontane Basins, and the South Rifian Corridor related to the Taza-Guercif and Saiss Basins (e.g. *Wernli, 1988*). Both strands were separated by the chaotic complex of the accretionary wedge, emplaced over the African foreland since the early Tortonian (e.g. *Feinberg, 1986; Flinch, 1993; Chalouan et al., 2008; Michard et al., 2008*). Since the accretionary wedge is locally overlain by Upper Miocene marine sediments the Rifian Corridor, at times, was a single wide gateway (Fig. 7.1) westward of the Taza Strait (*Flecker et al., 2015; Capella et al., 2017a; de Weger et al., 2020*). During the late Tortonian to early Messinian the Prerif Ridges were formed, constituting a subaqueous relief (Fig. 7.1) in the South Rifian Corridor, (*Roldan et al., 2014; de Weger et al., 2020*). By roughly 7.5 Ma these

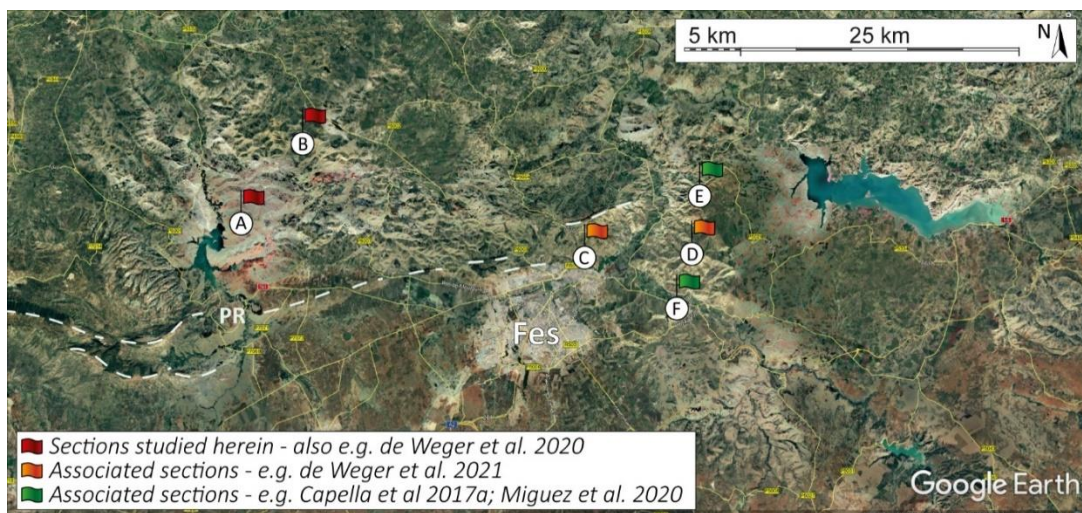


**Figure 7.2.** Satellite image of the study area near the city of Fes. The main sections described herein, (A) *Sidi Chahed* and (B) *Kirmta* are located north of the Prerif Ridges (PR). The locations of Fes-north (C), *El Adergha* (D), *Ain Kansera* (E) and, *Sidi Harazem* (F) sections, located south of the PR, are provided as a reference to previous work (see white box for references).

ridges were sufficiently uplifted to terminate the contourite channel system described herein (*de Weger et al., 2021*).

The Taza-Sill, located in the Taza Strait (*de Weger et al., 2021*), formed a submerged topographic high related to the E-W oriented thrust-front overlying the NE-SW oriented Middle-Atlas (Fig. 7.1). The Taza Strait separated the Taza-Guercif- and the Saiss-basins and the Taza-Sill controlled the water-mass exchange between the Mediterranean and the Atlantic (*Capella et al., 2017a; de Weger et al., 2020, 2021*). The westernmost part of the Rifian Corridor, just west of the Prerif Ridges, was in the Gharb Basin (Fig. 7.1) where both the Intramontane and Saiss basins merged (*Sani et al., 2007*).

### 3. PALEOCEANOGRAPHIC SETTING

During the late Miocene an Atlantic - Mediterranean connection existed through the Betic Corridors in southern Spain and the Rifian Corridors in northern Morocco (Fig. 7.1). The Rifian Corridor likely represented the last remaining connection before the onset of the Mediterranean Salinity Crisis (MSC; 5.97 – 5.33 Ma, *e.g. Hsü et al., 1973; Ryan et al., 1973*). The MSC is associated to the restriction and closure of the Miocene Atlantic-Mediterranean connections which resulted in extreme salinity fluctuations in the Mediterranean. The opening of the Strait of Gibraltar (5.33 Ma) brought the MSC to an end (*e.g. Hsü et al., 1973, 1977; Blanc, 2002; García-Castellanos et al., 2009; Krijgsman et al., 2018*).

After the restriction and closure of the Betic Corridors in the late Miocene (*e.g. Flecker et al., 2015*), the Rifian Corridor maintained Atlantic-Mediterranean water exchange in a similar fashion as the present-day Strait of Gibraltar (*de Weger et al., 2020, 2021*). The Rifian Corridor accommodated inflow of the North Atlantic Surficial Water and likely the Eastern North Atlantic Central Water into the Mediterranean, overriding the warm and highly saline paleo-Mediterranean Outflow Water (MOW). The water mass of the paleo-MOW was formed by net evaporation in the eastern Mediterranean, which increased the density of Mediterranean surface water (*Straume et al., 2020*). This surface water was “continuously” replenished by the inflow of cold and less saline Atlantic water. Subsequently, the increase in density forced this water to sink and ventilate the water column, a process known as intermediate and deep-water formation (*Millot, 1999; Candela, 2001*). The formation of these relatively dense water masses resulted in a density gradient between the Mediterranean and the Atlantic which drives two-way exchange (*Rohling et al., 2015; Simon*

et al., 2017). During the late Miocene, a dense paleo-MOW flowed over the Taza-Sill (Fig. 7.1), through the Rifian Corridor, towards the Atlantic (de Weger et al., 2020, 2021).

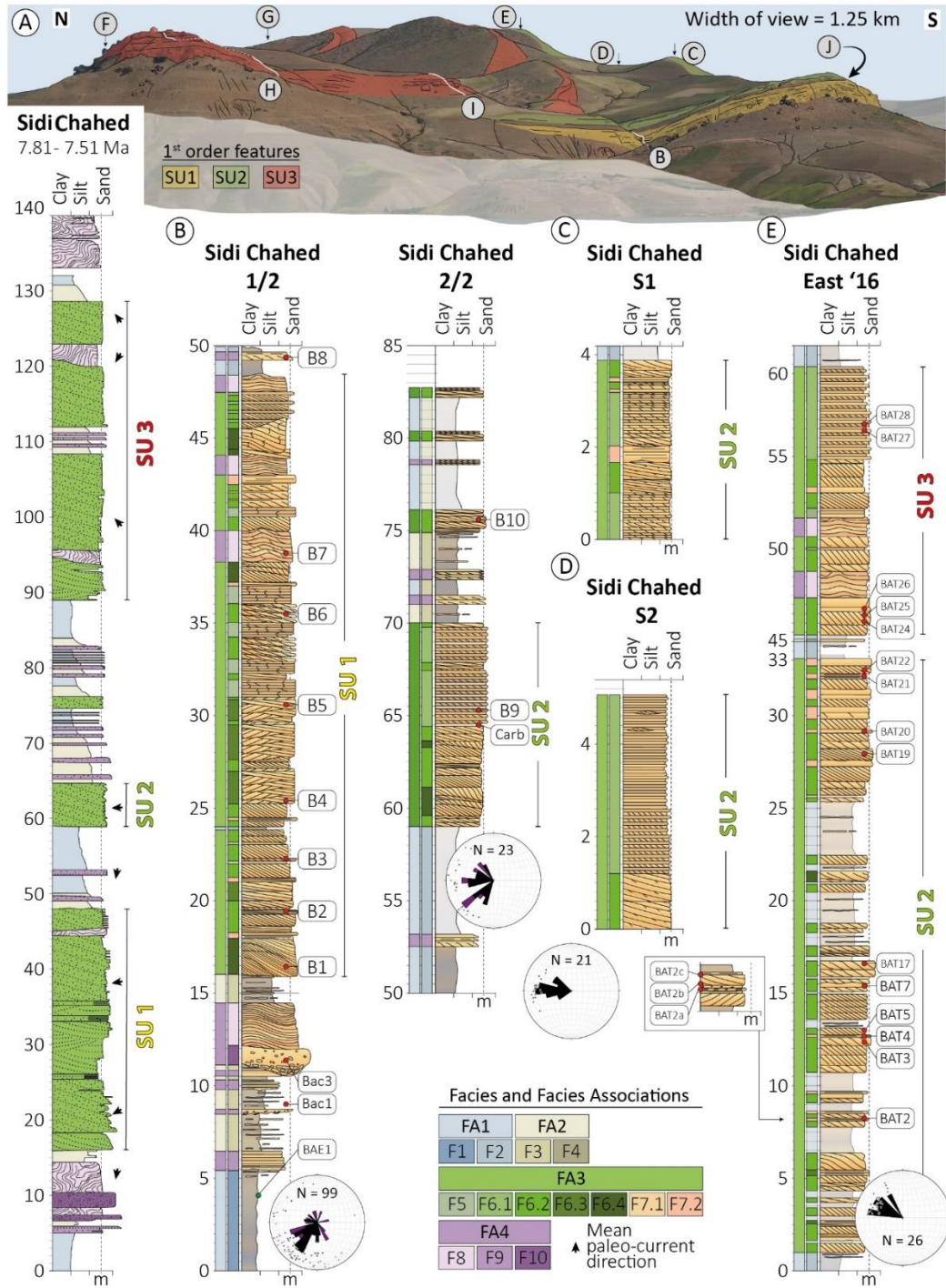
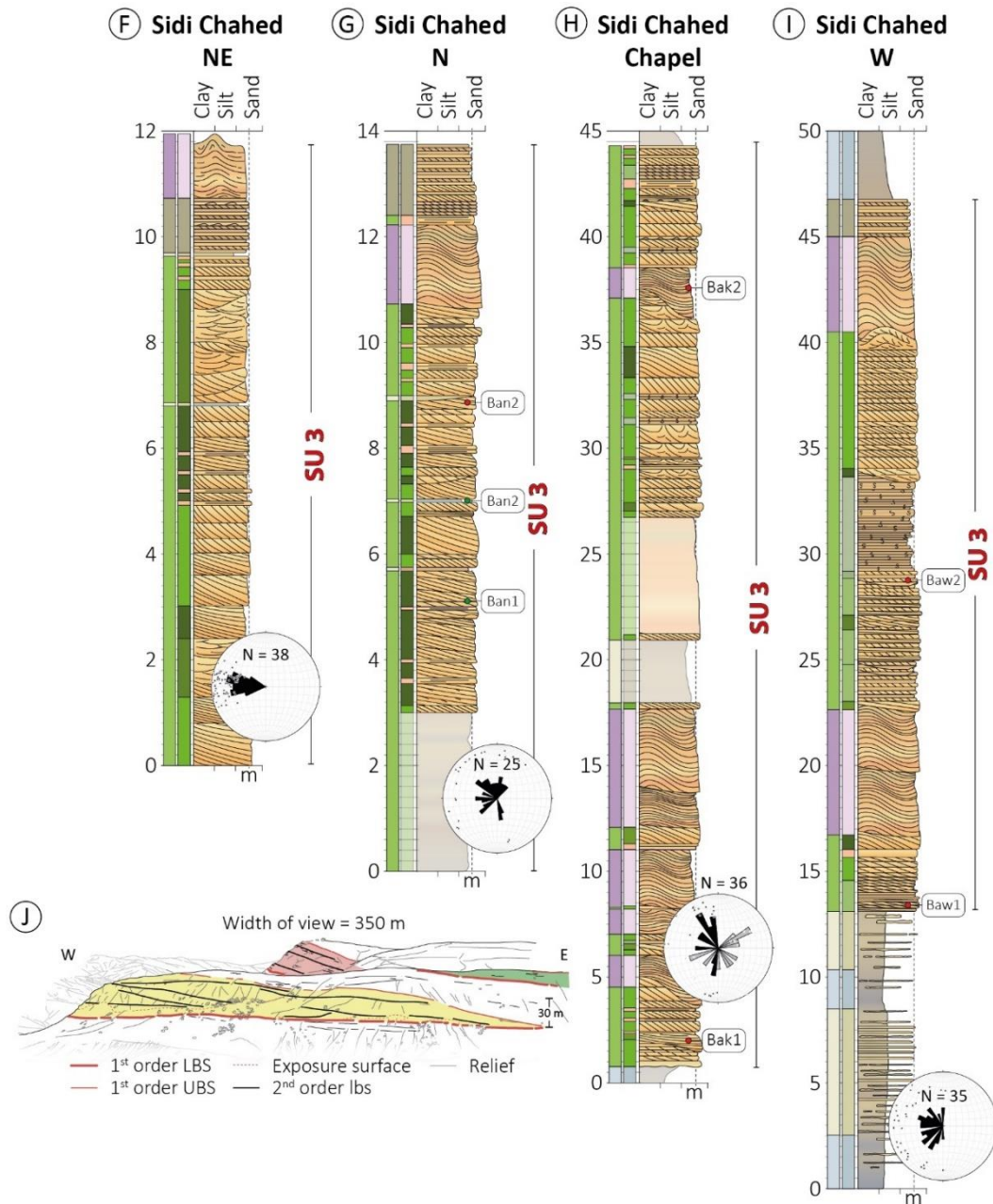


**Figure 7.3.** (Above) Overview figure of the Sidi Chahed outcrop (A) and associated sections (B – E). The log on the left represents a generalized composite log through the three main 1<sup>st</sup> order sand units (SU), the black arrows indicate mean paleocurrent directions with respect to the north (up). (A) Panoramic picture of the outcrop. In yellow, green, and red respectively the paleochannels SU1, SU2 and SU3. The small grey circles depict the location of the sections (B-I) and the location of figure J.

>>> (Right) Sections F – I of the Sidi Chahed outcrop. (J) Drawing of the south western flank of the outcrops as indicated in (A). This sketch shows the 1<sup>st</sup> order lower- (LBS) and upper-bounding surfaces (UBS) as well as the 2<sup>nd</sup> order bounding surfaces.





#### 4. METHODOLOGY

Two well-exposed outcrops from the Rifian Corridor; *Sidi Chahed* and *Kirmta* (Figs. 7.1 and 7.2), are studied herein. These outcrops were previously documented and interpreted as being relics of contourite channels (*de Weger et al., 2020*). Here, we studied these contourite channels in more detail to unravel erosional events that led to channel formation, their evolution, and the vertical and lateral facies variability of their infill sequences.

The sedimentary record was studied by standard field techniques which include bed-scale characterization of sedimentological and stratigraphic elements. Twelve stratigraphic

sections were measured at centimetre-to-meter-scale to document key features used in facies analyses. These features include lithology, grain-size and sorting, sedimentary structures, bedding thickness, nature of bed contacts and paleocurrent indicators. The sand fraction predominantly consists of a mixed bioclastic-siliciclastic composition for which the terminology of *Chiarella et al. (2017)* is applied. A total of 323 observations of paleoflow indicators (e.g., cross-stratification, ripple-lamination, and sole-marks) were recorded across both outcrops. In addition, high resolution pictures taken during different seasons (winter and fall of 2018 and spring of 2019) were used for detailed analyses of morphologies and facies distributions.

Fifteen samples for biostratigraphic determinations, derived from marls that were more than 50 cm below the rock's exposed surface, have been analyzed and compared to the findings of *Capella et al. (2017a)*. The paleo-water depth has been inferred from the benthic foraminifera assemblages of the biostratigraphic samples. The observed mixed occurrence of shallow- and deep-water species is considered here the result of downslope transport and hence, the deeper-water species are deemed most reliable in depositional depth estimates.

Ichnological analysis was primarily conducted in the sand rich facies of the studied sections. Ichnotaxonomy, distribution, and abundance of trace fossils were characterized to describe stratigraphic trends and lateral and vertical variability to decode the environmental conditions during or after sedimentation. Ichnological observations focussed on orientation, shape, length and diameter of individual burrow segments, configuration of burrow systems, relationship with facies and bed surfaces, and taphonomy.

Thirty-nine samples for petrographic analysis were collected from indurated sand beds. Two sets of thin sections were prepared for each sample, one of which was impregnated with dyed resin to highlight porosity. The samples were examined under a petrographic microscope with integral camera system. Modal analysis was carried out on five samples (BAT2a, b, c, BAT4 and BAT14) by determining the composition at 300 points using a stepping stage and associated PETROG software.

## 5. STUDIED SECTIONS

Both outcrops, *Sidi Chahed* (Fig. 7.3) and *Kirmta* (Fig. 7.4), formed in wedge top basins on the northern flank of the Saiss Basin. The outcrops are located 9 km apart (Fig. 7.2). The *Sidi Chahed* outcrop (34.102693, -5.299355) is located roughly 25 km WNW of the city of Fes and

5 km north of the Prerif Ridges. The *Kirmta* outcrop (34.171445, -5.239184) is located 22 km NW of the city of Fes and 12 km N of the Prerif Ridges (Fig. 7.2).

The Sidi Chahed section forms a topographic high composed of, in a horizontal plane, three arcuate shaped, indurated sandstone ridges which measure 2 km (E-W) by 1 km (N-S). The southern, western, and eastern flanks are typically steeply sloped to near vertically inclined. The northern flanks are much less inclined to near horizontal in places. The total thickness of the section, consisting of three concave-up sandstone units (SU1, SU2 and SU3) encased in marls and sandy marls belonging to the Blue Marl Fm. is roughly 140 m (Fig. 7.3).

The Kirmta outcrop is roughly 110 meters thick, forming a topographic high with three distinct sandstone units (SU1, SU2 and SU3) encased in marl and sandy marls belonging to the Blue Marl Fm (Fig. 7.4). The southern flank of the outcrop, which is exposed for well over 3 km, is steeply inclined whereas the northern flank hardly shows any inclination.

## 6. RESULTS

### *6.1 Distribution of channelized sandstone bodies and internal architectures*

Both the Sidi Chahed and Kirmta outcrops consist of three sandstone units (SU1 – SU3) which are encased in fine-grained marl deposits. Each of these sandstone units have concave-up geometries (Figs. 7.3 and 7.4). The concave-up lower bounding surface of each Sand Unit, herein referred to as 1<sup>st</sup> order channel, is in unconformable contact with fine-grained marl deposits. In the Sidi Chahed outcrop these 1<sup>st</sup> order channels are 750 – 1000 m wide and up to 35 m thick (Fig. 7.3), whereas in the Kirmta outcrop these 1<sup>st</sup> order channels are up to 2 km wide and 5 – 15 m thick (Fig. 7.4). The 1<sup>st</sup> order channels, most clearly observed in the Sidi Chahed outcrop, subsequently contain smaller concave-up sandstone bodies (Fig. 7.3J), herein referred to as 2<sup>nd</sup> order channels. These 2<sup>nd</sup> order channels are incised into previously deposited sandstones. The width of these 2<sup>nd</sup> order channels ranges between 30 and 300 m and their thickness does not exceed 15 m.

### *6.2 Age and paleo-water depth*

The biostratigraphic results from the Sidi Chahed section indicate that the section was deposited within the *Globigerinoides obliquus extremus/Globorotalia suterae* biozone MMi-12a of *Lirer et al. (2019)*. The lowermost part of the section, below the first sand unit (SU1), is dominated by sinistrally coiled *Neogloboguadrina acostaensis* and *Globorotalia scitula*,

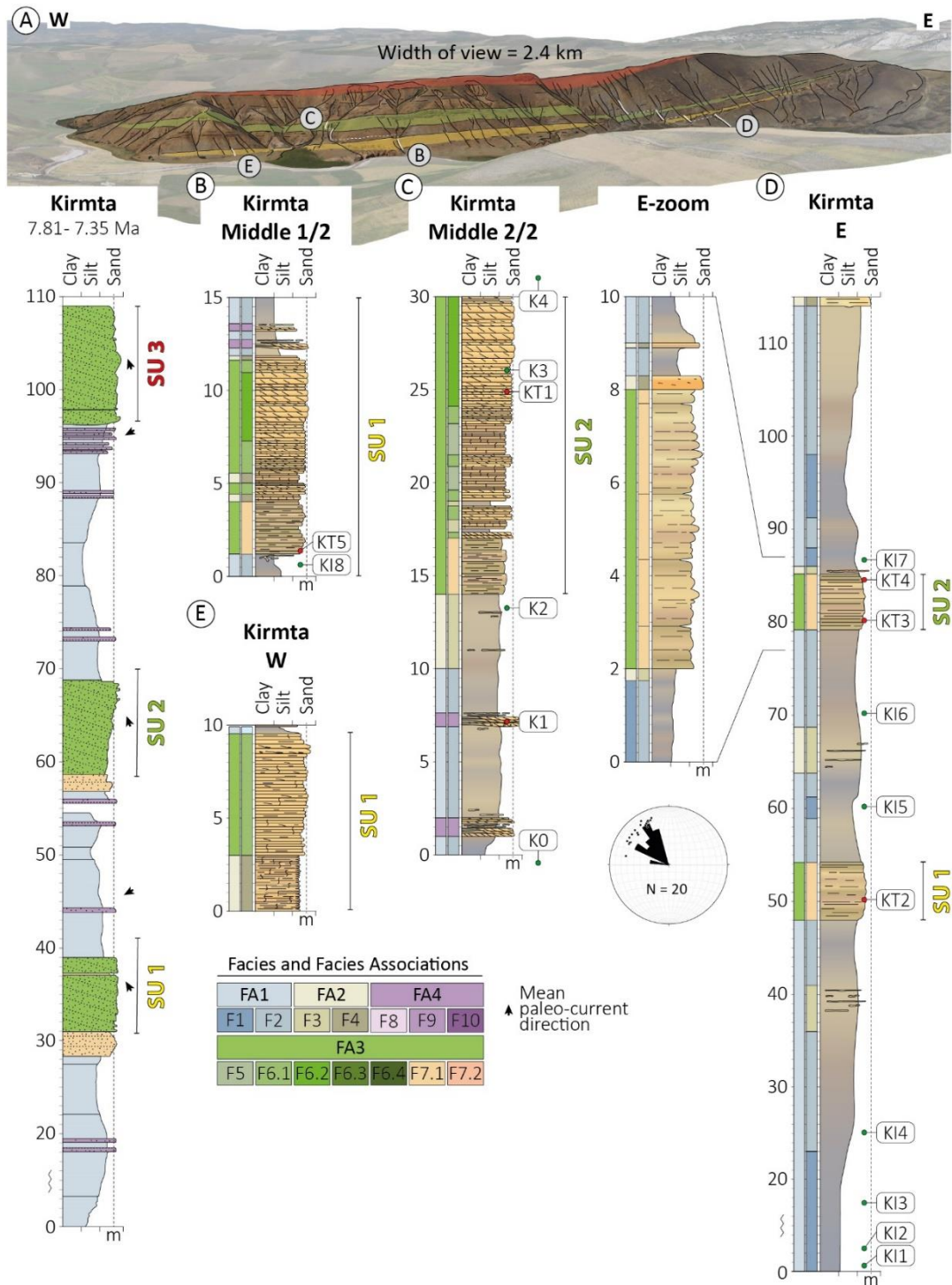


**Figure 7.4.** Overview figure of the Kirmta outcrop (A) and associated sections (B–E). The log on the left represents a generalized log through the three 1<sup>st</sup> order sand units, the black arrows indicate the mean paleocurrent directions with respect to the north (up). (A) Panoramic picture of the outcrop photographed towards the north. In yellow, green, and red respectively the paleochannels SU1, SU2 and SU3. The small grey circles depict the location of the sections.

including specimens of *G. suterae* and *Globorotalia menardii* 4. This foraminifer assemblage suggests a late Tortonian age, younger than 7.80 Ma. The uppermost marlstones derived stratigraphically above the uppermost sand unit (SU3), showed an abundant presence of *G.*



*menardii* 4 and no presence of *G. menardi* 5, indicating that the whole succession was deposited prior to 7.51 Ma.

The benthic foraminiferal assemblages of the Sidi Chahed outcrop consist of mixed shallow- and deep-water species. The species *Planulina ariminensis*, *Sphaeroidina bulloides*, *Uvigerina semiornata* and *U. peregrina* are present throughout (including samples obtained from marlstone interbedded within the sandstone units), and *Cibicidoides kullenbergi* occurs in about half of the samples, indicating upper bathyal environments roughly equivalent to the upper slope physiographic domain (250 – 400 m water depth). The upper part of the section contains less slope taxa, indicating a slightly shallower depth range (upper slope-outer shelf physiographic domain, 150 – 300 m water depth).

The Kirmta section, based on the foraminiferal assemblage of 12 samples has been assigned to *Globigerinoides obliquus extremus*/*Globorotalia suterae* biozone MMi-12b of *Lirer et al. (2019)*. The marls contain abundant planktic and benthic foraminifers, but the proportion of benthic foraminifers is always lower (20 - 40%). Based on the common occurrence of *Globorotalia merardii* 4, whose last common occurrence was at 7.51 Ma (*Sierro, 1985; Sierro et al., 1993, 2001; Hilgen et al., 2000; Capella et al., 2017a*) and the presence of *Globorotalia suterae* whose first occurrence has been proven at 7.8 Ma (*Lirer et al., 2019*), the section was dated between 7.8 and 7.51 Ma. In all samples the assemblages of planktic foraminifers are similar, showing scarce keeled Globorotalids, more abundant *Globorotalia scitula* (sinistral and dextral) and abundant *Globigerinoides extremus*, *Globigerina bulloides*, Neogloboquadrinids (mainly sinistral) and in some samples common *Dentoglobigerina altispira*.

The benthic foraminifer assemblages of the samples contain rare shallow-water species: *Ammonia*, *Nonion* and more frequent deep-water species: *Uvigerina peregrina*, *Uvigerina semiornata*, *Pullenia bulloides*, *Martinottiella communis*, *Cibicidoides pachyderma*, *Sphaeroidina bulloides*, *Marginulina costata*, *Buliminids*, *Trifarina*, *Gyroidina*, *Lenticulina*, etc. Based on these assemblages and the high percentages of planktic foraminifers in most of the samples, we infer that the depositional environment was most likely the outer shelf and/or upper slope, with the common presence of shallow benthic foraminifers living in the shelf that were probably transported downslope through the shelf-slope break.

**Table 7.1.** Sedimentary facies and facies associations table including the colour codes used throughout the chapter, sedimentary structures, thickness, grain-size, percentage of bioclastic component for the coarse grained sediments (Bc%, note: 0% bioclasts on the left side of the column, 100% bioclastic on the right side. Dotted line represents 50%), biogenic structures, estimated current velocities in cm/s ( $v \text{ cms}^{-1}$ ) and microfacies (MF).

FA	Picture	Sed. facies	Sed. structures	Thickness	Grain-size	Bc%	Bioturbation	$v \text{ cms}^{-1}$	MF
FA1. Hemipelagic/Drift		F1. Fossil-rich blue marlstone	Massive to gradational	Up to 1 km	Clay, silt & very-fine sand < 0.125 mm		Scarce discrete trace fossils	< 5	-
		F2. Sandy marlstone	Massive, gradational or sharp basal surfaces	Up to 10's of meters	Clay, silt & fine sand < 0.25 mm		Ab. undiff. scarce <i>Planolites</i> - and <i>Thalassinoides</i> -like	5 - 15	-
FA2. Transitional		F3. Sandstone laminae	Lenticular laminae	< 1.5 cm	Fine sand 0.125- 0.25 mm		Scarce <i>Planolites</i> - and <i>Thalassinoides</i> -like	10 - 20	-
		F4. Heterolithic sandstone	Tabular bedding with remnants of ripples	1- 5 cm	Sand & marl < 0.5 mm		Ab. undiff. <i>Macaronichnus</i> <i>Planolites</i> - and <i>Thalassinoides</i> -like	10 - 40	I
FA3. Contourite channel		F5. Fully bioturb. sandstone	Remnants of parallel lamination	10- 15 cm	Coarse sand 0.5 - 1.2 mm		<i>Macaronichnus</i> , scarce <i>Scolicia</i> , <i>Planolites</i> and <i>Thalassinoides</i> -like	35- 50	III
		F6. Cross-strat. sandstone	F6.1 Thin-bedded	5- 15 cm	Medium sand 0.25- 0.5 mm		Abundant <i>Macaronichnus</i> and <i>Scolicia</i> , common undiff. hor. biogenic structures, rare <i>Planolites</i> and <i>Thalassinoides</i> -like	40 - 60	II- III
			F6.2 Medium- to thick-bedded	0.1- 1 m	Medium sand 0.25- 0.5 mm			40 - 60	II- III
			F6.3 Trough cross-bedded	0.5- 1 m	Medium sand 0.25- 0.5 mm			60 - 100	II- III
			F6.4 Tangentially cross-bedded	~ 2 m	Medium sand 0.25- 0.5 mm			80 - 120	I- II
FA4. Gravitational		F7. Planar lam. sandstone	F7.1 Bi-gradational silty sandst.	5- 20 cm	very fine to fine sand 0.062- 0.25 mm		Abundant undiff. biogenic structures, scarce <i>Macaronichnus</i> , <i>Planolites</i> and <i>Thalassinoides</i> -like	60 - 100	I
			F7.2 Planar laminated sandst.	10 - 40 cm	Medium sand 0.25- 0.6 mm			100 - 180	III
FA4. Gravitational		F8. Convolute sandstone	Convolute, contorted and soft-sediment deformation	Up to 3 m	Sand < 0.6 mm		Difficult to appreciate		II- III
		F9. Amalgamated normal graded sandstone	Massive, planar laminae, ripples and basal scours	< 40 cm	Sand to silt occasional up to pebble sized rip-up clasts		Scarce undiff., occasional <i>Planolites</i>		II- III
		F10. Conglomerate	Monomictic, deeply incised lower bounding surface	< 3 m	Up to cobble sized clasts in arenitic matrix		None		-

### 6.3 Sedimentary facies description and interpretation

Ten different sedimentary facies (F1 to F10) have been distinguished between the fine-grained deposits (marls) and the sandstone units (channels) in the two studied sections (Table 7.1, Fig. 7.5). The sedimentary facies include: F1) Fossil-rich blue marlstone, F2) sandy marlstone, F3) sandstone laminae, F4) heterolithic sandstone, F5) fully-bioturbated sandstone, F6) cross-stratified sandstone, F7) planar-laminated sandstone, F8) convolute sandstone, F9) amalgamated normal-graded sandstone, and F10) conglomerate.

#### 6.3.1 F1 – Fossil-rich blue marlstone

Facies F1 (*like in de Weger et al., 2020, 2021*) consists of blueish marls - the sediments after which the Blue Marl Formation is named (Table 6.1, Fig. 6.5A, B). These mainly structureless, fossil-rich marlstones (containing bivalves up to cm-scale) occur as laminae interbedded with sandstone or continuous sequences of up to 100's of meters in thickness. Despite being dominantly blueish in colour, gradational changes from dark blueish grey to more brownish grey are common. This colour change results from slight increases in the siliciclastic fraction consisting of up to very fine-grained sand. F1 only shows scarce discrete trace fossils.

#### 6.3.2 F2 – Sandy marlstone

Facies F2 (*like in de Weger et al., 2020, 2021*) consists of fossil-rich sandy marlstones and very fine-grained muddy sandstones (Table 7.1, Fig. 7.5A, C). This facies regularly occurs in gradational alternation with the fossil rich blue marlstone (F1) consisting of continuous sequences of up to meter-scale thickness. The texture is homogeneous for the finest intervals that are more blueish grey in colour (like F1). The coarser and more light-brownish grey intervals are regularly banded or laminated. Changes in grain-size distribution are generally gradational, but sharp basal contacts have been observed between more muddy and more sandy deposits. Starved ripples of fine-grained sand are scarce. Laminae with sharp basal bounding surfaces and ripples coincide with an increased abundance of fine-grained shell fragments whereas the muddier intervals regularly contain well preserved bivalves up to 1.5 cm in diameter. The trace fossil assemblage consists of abundant undifferentiated structures and scarce *Planolites*-like and *Thalassinoides*-like traces.

#### 6.3.3 F3 – Sandstone laminae

Facies F3 consists of discontinuous slightly undulatory, lenticular, up to fine-grained sand laminae that only rarely exceed 1 cm in thickness (Table 7.1, Fig. 7.5A, D). The sand consists



of a mixed siliciclastic-bioclastic composition and are encased by facies F2. These laminae or sand lenses occur over short (up to 1 m) intervals where the sand (facies F3) / silt (facies F2) ratio is approximately 1:4. The trace fossil assemblage consists of abundant undifferentiated structures and scarce *Planolites*-like and *Thalassinoides*-like traces.

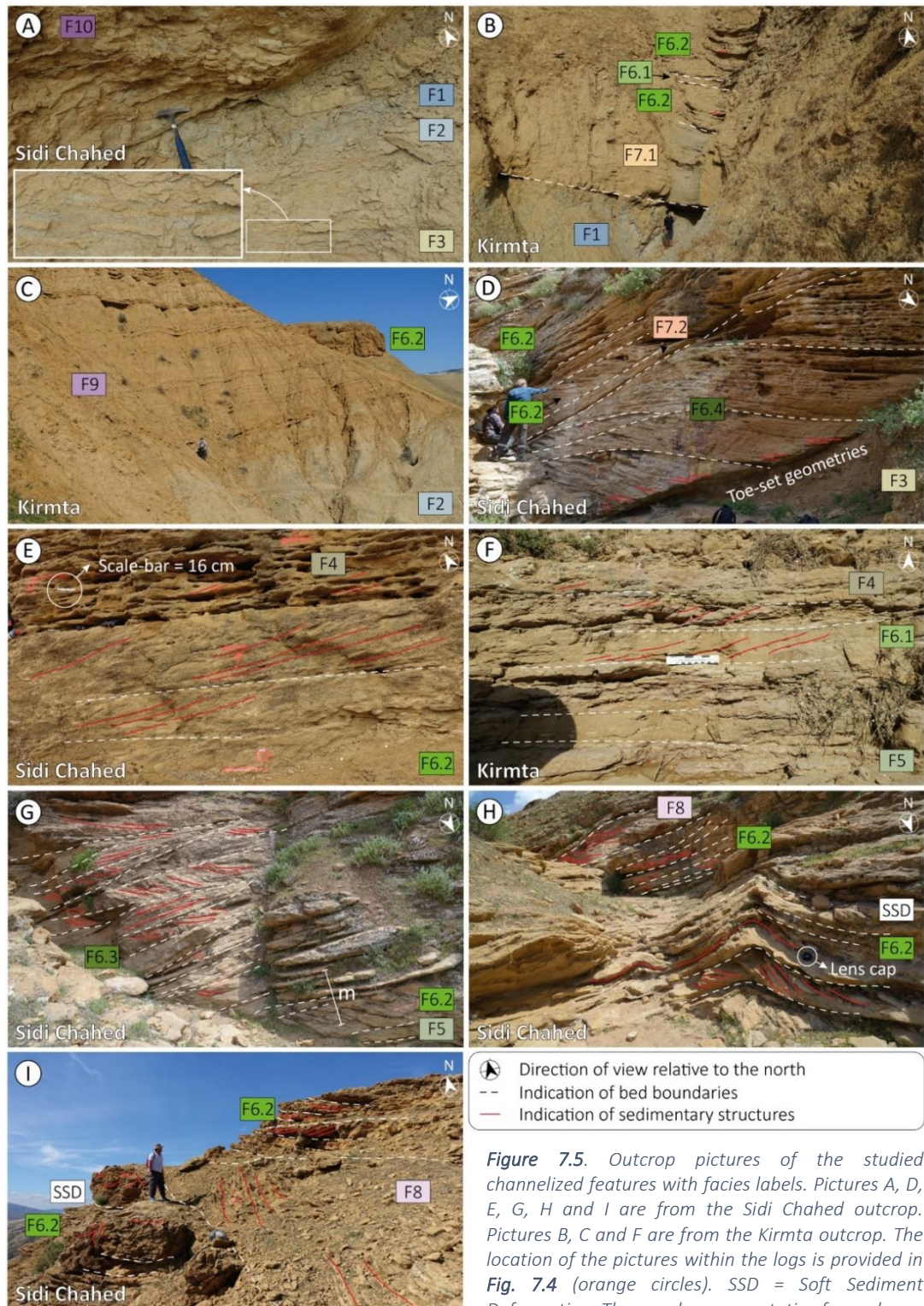


**Figure 7.5.** Outcrop pictures of the studied channelized features with facies labels. Pictures A, D, E, G, H and I are from the Sidi Chahed outcrop. Pictures B, C and F are from the Kirmta outcrop. The location of the pictures within the logs is provided in Fig. 7.4 (orange circles). SSD = Soft Sediment Deformation. The people representative for scale are

#### 6.3.4 F4 – Heterolithic sandstone

Facies F4 typically consists of heterolithic, tabular, dominantly very thin to thin bedded (< 5 cm), compositionally mixed (bioclastic dominated), up to fine-grained sandstone and siltstone with an average ratio of 3:1 (Table 7.1, Fig. 7.5E, F). The sandstone hosts remnants of dominantly unidirectional, along-slope oriented cross-lamination. The trace fossil assemblage consists of abundant undifferentiated structures and scarce *Macaronichnus*, *Planolites*-like and *Thalassinoides*-like traces.

#### 6.3.5 F5 – Fully bioturbated sandstone

Facies F5, consisting of coarse-grained mixed compositional siliciclastic-bioclastic sand is fully reworked by *Macaronichnus* (Fig. 7.5F). The sandstone, dark brown in color, shows remnants of tabular bedding (10 – 15 cm) and parallel lamination (Table 7.1, Fig. 7.5F, G). Besides being dominated by *Macaronichnus*, the trace fossil assemblage consists of scarce *Scolicia*, *Planolites* and *Thalassinoides*-like traces.

#### 6.3.6 F6 – Cross-stratified sandstone

Facies F6 consists of compositionally mixed, siliciclastic–bioclastic, unidirectionally cross-stratified sandstones (Table 7.1). Due to the occurrence of a variety of sedimentological characteristics this facies has been divided into four sub-facies; (1) (F6.1) thin-bedded cross-stratified sandstone (Fig. 7.5B and F), (2) (F6.2) medium- to thick-bedded cross-stratified sandstone (Fig. 7.5B, D and G), (3) (F6.3) trough cross-stratified sandstone and (Fig. 7.5G), and (4) (F6.4) tangentially cross-stratified sandstone (Fig. 7.5D). This facies commonly shows a pale/dark cm-scale banding within foresets (Fig. 7.5). The paler bands are dominated by bivalve fragments up to several mm long, together with a variety of other bioclast types, and are cemented by sparry calcite (Fig. 7.6). The darker bands also contain bioclasts that are smaller (sand-grained). Furthermore, these bands contain numerous rounded pellets of dark claystone, usually contain brownish glauconite, and are cemented by sparry calcite albeit less prominent as porosity is lower. The trace fossil assemblage consists of abundant *Scolicia* and *Macaronichnus*, and rare *Planolites* and *Thalassinoides* with common undifferentiated horizontal biogenic structures.

##### *F6.1 – Thin-bedded sandstone*

Sub-facies F6.1 consists of tabular, medium-grained sandstone beds with unidirectional top-cut cross-strata (Table 7.1, Fig. 7.5B, F). Bed thicknesses range from 5 to 15 cm. Due to weathering; it is apparent that this facies regularly is interbedded with more easily erodible

sediment forming alterations between indurated and eroded beds. These alterations are related to foreset banding as described above, where the finer-grained, darker band of each foreset was more prone to erosion.

#### *F6.2 – Medium- to thick-bedded sandstone*

Sub-facies F6.2 consists of tabular, medium- to thick-bedded (15 to 100 cm), moderately- to well- sorted, up to coarse-grained sandstone with unidirectional cross-strata (Table 7.1). The cross-strata regularly reflect bundles of thickening and thinning foresets that show modest alternations between angular to tangential toe-set geometries (Fig. 7.5D, E). Toesets are commonly enriched in bioclastic material. Basal boundaries are sharp (Fig. 7.5) and occasionally contain muddy rip-up clasts. Soft sediment deformation structures are most common in this sub-facies, regularly being present as overturned folds (Fig. 7.5G) and fluid escape structures (Fig. 7.5I).

#### *F6.3 – Trough cross-stratified sandstone*

Sub-facies F6.3 is typified by trough cross-stratified, medium-grained, sandstone (Table 7.1, Fig. 7.5G). Foresets are convex and alternate between more orange and darker brownish colors that reflect changes in the abundance of bioclastic material. The concave-up bedform geometries are typically between 5 to 10 m wide and up to a meter in thickness.

#### *F6.4 – Tangential cross-bedded sandstone*

Sub-facies F6.4 consists of very thick (~2 m), cross-stratified, up to coarse-grained sandstones with toe-set geometries that cyclically change from tangential to angular (Table 7.1, Fig. 7.5D). Toe-sets are enriched in bioclastic material and show a higher intensity of bioturbation. Internally, erosional sigmoidal bounding surfaces are common.

#### *6.3.7 F7 – Planar-laminated sandstone*

Facies F7 is typified by the presence of planar-laminated, tabular beds of compositionally mixed siliciclastic - bioclastic, up to coarse grained sandstone (Table 7.1). Since the lithology varies between fine- and coarse-grained sand this facies has been divided into two sub-facies (F7.1 and F7.2 respectively). The trace fossil assemblage consists of abundant undifferentiated structures and scarce *Macaronichnus*, *Planolites*-like and *Thalassinoides*-like traces.

#### *F7.1 – Bi-gradational silty sandstone*

Sub-facies F7.1, only present in the Kirmta outcrop, consists of stacked, tabular, planar parallel laminated, subsequently inverse- and normal-graded (bi-gradational) sandstone beds with thicknesses ranging from 5 to 20 cm (Table 7.1, Fig. 7.5B). A bi-gradational pattern has also been observed on a bed-set scale (0.5 to 1.2 m). This facies typically consists of very fine- to fine-grained sand of dominantly siliciclastic composition. Furthermore, this facies is rich in sand-sized pellets of mudstone and brownish glauconite.

#### *F7.2 – Planar-laminated sandstone*

Sub-facies F7.2 consists of tabular, planar-laminated sandstone beds that range in thicknesses between 10 and 40 cm (Fig. 7.5D). The sandstone beds generally consist of coarse-grained sand and the abundance of bioclastic material determines the differentiation between laminae. This facies generally lacks or shows a very low abundance of trace fossils.

#### *6.3.8 F8 – Convolute sandstone*

Facies F8 consists of thin bedded (up to 10 cm) convolute strata. Fluid escape structures are common in the underlying sandstone (Table 7.1, Fig. 7.5H, I). The primary beds are either like cross-stratified sandstones (F6) or amalgamated, normal graded sandstones (F9). The lower bed bounding surface is sharp and erosive (Fig. 7.5H). This facies appears wedge shaped, thinning out perpendicular to the dominant paleocurrent direction of facies F6, in an inferred up-slope direction. Inclination of the preserved primary strata varies laterally from high- angle to opposing angles (-20°) down-dip with respect to the inferred paleo-slope. Trace fossils are difficult to identify.

#### *6.3.9 F9 – Amalgamated, normal-graded sandstone*

Facies F9 consists of dominantly tabular, heterolithic, normal graded, amalgamated sand- and mudstone with bed thicknesses averaging 5 - 10 cm, never exceeding 40 cm (Table 7.1, Fig. 7.5C). Although a semi-gradational transition from sand to mud occurs, boundaries can be easily distinguished. This facies regularly shows plane-parallel lamination and ripples, capped by a very thin siltstone grading to marlstone. Basal scours and marly rip-up clasts are common. The well- to very-well sorted, up to medium-grained sand predominantly consists of siliciclastic material but has a bioclastic component. This facies is bioturbated with scarce undifferentiated discrete trace fossils, and only occasional *Planolites* can be recognized (Fig.7.6).

#### *6.3.10 F10 – Matrix-supported conglomerate*



This monomictic conglomerate changes upwards from an ortho- to para-conglomerate (Fig. 7.5A). The clasts are poorly sorted, rounded and disc shaped, dominantly consisting of arenitic cobbles and boulders. The matrix consists of silty sand and the basal bounding surface is deeply incised in the underlying sandy marls belonging to facies F3. No biogenic structures were observed.

#### 6.4 Petrographic analysis

The petrographic samples examined are derived from indurated sandstones related to facies F4, F6, F7, F8 and F9 (Table 7.1; Figs. 7.3 and 7.4). All samples contain the same range of detrital components, but their proportions and rock fabric vary. Examples based on modal

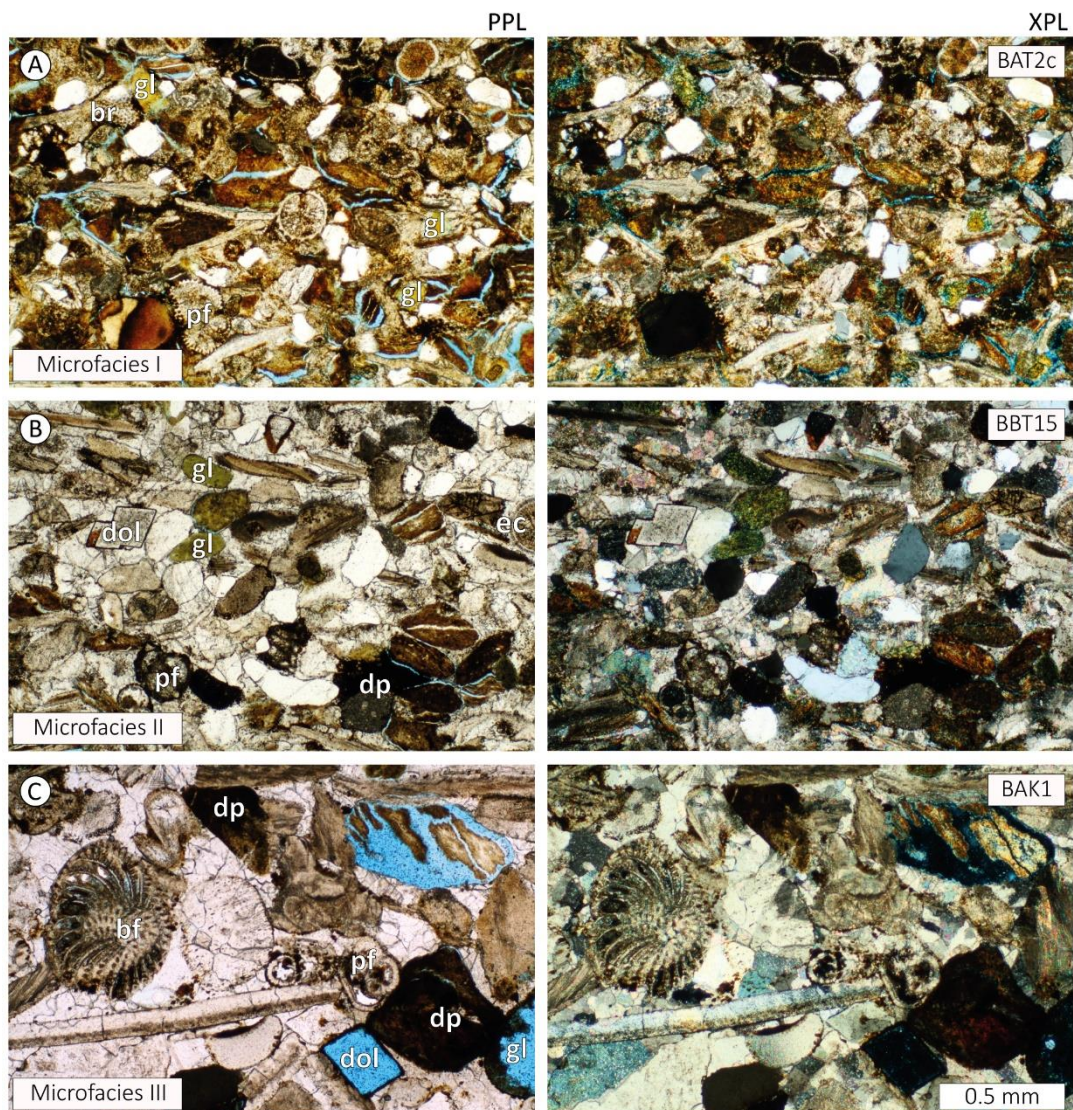


**Figure 7.6.** Thin-section images of the three microfacies identified: (A) Microfacies I, (B) Microfacies II and, (C) Microfacies III. The pictures on the left-hand side are in plane polarized light whereas the pictures on the right hand side are in cross polarized light. The scale of the pictures is provided in the lower left corner. Abbreviations in the pictures stand for: gl – glauconite, br – bryozoan fragments, ec – echinoderm fragments, pf – planktonic foraminifers, bf – benthic foraminifers, dp – detrital pellets, commonly consisting of mud and, dol – dolomite.

analysis of five samples are provided in Table 7.2. The detrital components include bioclasts, of which bivalve fragments are usually most common, together with fragments of echinoids, benthonic and planktonic foraminifera, calcareous algae, occasional bryozoa and other forms. Bivalves and other elongate fragments are often aligned horizontally to the bedding (e.g., Fig. 7.6A, B). Many of the bioclasts are fragmented and display signs of transport. Individual bioclasts typically occur as sand-grade fragments, and their small size and common recrystallisation often impedes their identification. The bioclasts within the coarsest-grained samples seldom exceed 5 mm. Rounded sand-sized grains of limestone, usually comprising variably recrystallized calcite, are common, and large dolomite rhombs which often display signs of erosion and transport also occur. The crystal mould (Fig. 7.6A) and the rhombohedral crystal (Fig. 7.6B) represent secondary replacement dolomite.

Quartz grains, typically sub-rounded and consisting of fine- to medium-grained sand, are almost always present, but usually form a subordinate component of the sample. Pellets of glauconite are also recognized in almost all samples (Fig. 7.6), usually brown or olive-yellow and reworked, but fresher green pellets have also been observed. Feldspar grains and mica flakes occur in small proportions. Heavy minerals are uncommon – several grains of tourmaline, rutile and possible small zircons have been observed. There is sometimes a brown argillaceous matrix, commonly silty, which may be patchily distributed or form thin irregular laminae which may be deformed. A pervasive argillaceous matrix is uncommon. Sand-sized pellets of brown claystone are common, some apparently partially glauconitised. Most samples are cemented by sparry calcite, or sometimes a more finely crystalline calcite, although the cement (together with other carbonate components of a sample) has often suffered dissolution.

Three main “microfacies” have been defined, forming a spectrum along which almost all the samples examined can be placed, others contain several microfacies. Microfacies I (MF1) (Fig. 7.6A) is relatively fine-grained and contains abundant argillaceous components such as clay pellets and glauconite. Microfacies III (MF3) (Fig. 7.6C) is a relatively coarse bioclastic limestone. Microfacies II (MF2) (Fig. 7.6B) is intermediate in composition and grain-size. In most cases the boundary between one microfacies and another observed in thin section is gradational. Both fining- and coarsening-up trends are observed in thin section.

Overall, most samples of facies F4 and F7.1 are microfacies I. Most samples of facies F6 are transitional between MF1 and MF3, and most samples of facies F5 and F7.2 are MF3. The samples of the Kirmta sections, on average, are finer grained compared to the samples of

the Sidi Chahed sections, with half of the samples being assigned to microfacies I and the other half dominantly consisting of MF2.

**Table 7.2.** Modal analysis data based on 300-point modal analysis in thin section. Proportions of solid rock components (all but porosity) are renormalised to a total of 100%. Component abbreviations, from left to right: MF = micro facies, Qm = Monocrystalline Quartz, Qp = Polycrystalline Quartz, Qt = Quartz total, F = Feldspar, Gg = Green glauconite, Gb = Brownish/yellowish glauconite, Gt = Glauconite total, L = Lithic fragments; c = carbonate, d = dolomite, cp = claystone pellets, fa = feldspar aggregates, qm = quartz-mica aggregates, Lt = Lithic total, B = Bioclastic; b = bivalves, f = foraminifera, e = echinoderm, ca = calcareous algae, u = undifferentiated, Bt = Bioclast total, Cc = Calcite cement, Fe = Iron Oxides/Hydroxides, P% = porosity percentage, GS = Mean grain-size (ms = medium-grained sand, fs = fine grained sand), S = Sorting (w = well, vw = very well).

Sample	MF	Qm	Qp	Qt	F	Gg	Gb	Gt	Lc	Ld	Lcp	Lfa	Lqm	Lt	Bb	Bf	Be	Bca	Bu	Bt	Cc	Fe	P%	GS	S
BAT2a	II	7.2	0.0	<b>7.2</b>	0.0	0.0	2.1	<b>2.1</b>	12	0.0	14	0.0	0.0	<b>26</b>	20.9	2.7	1	Tr	14.1	<b>38.7</b>	25.3	0.7	2.7	Fs	w
BAT2b	I-II	14.3	0.7	<b>15</b>	0.3	Tr	5.9	<b>5.9</b>	11.8	0.3	16	0.7	0.0	<b>28.8</b>	12.9	2.8	0.3	1.3	21.7	<b>39</b>	10.1	0.7	4.3	Fs	w
BAT2c	I	12.2	2.2	<b>14.4</b>	0.4	0.0	3.6	<b>3.6</b>	14.7	0.7	24.7	0.0	0.4	<b>40.5</b>	5.4	5.0	0.0	0.0	20.8	<b>31.2</b>	9.3	0.4	7.0	Fs	w
BAT4	II	9.7	1.8	<b>11.5</b>	0.9	0.0	3.1	<b>3.1</b>	18.1	0.0	11.9	0.0	0.0	<b>30</b>	21.4	1.8	0.0	2.0	16.1	<b>41.3</b>	11.9	1.3	24.3	Ms	w-vw
BAT14	II	12.0	2.1	<b>14.1</b>	0.0	0.0	7.9	<b>7.9</b>	14.9	0.0	4.6	0.0	0.0	<b>19.5</b>	15.4	2.5	0.7	1.3	20	<b>39.9</b>	17.8	0.8	19.7	Ms	w-vw



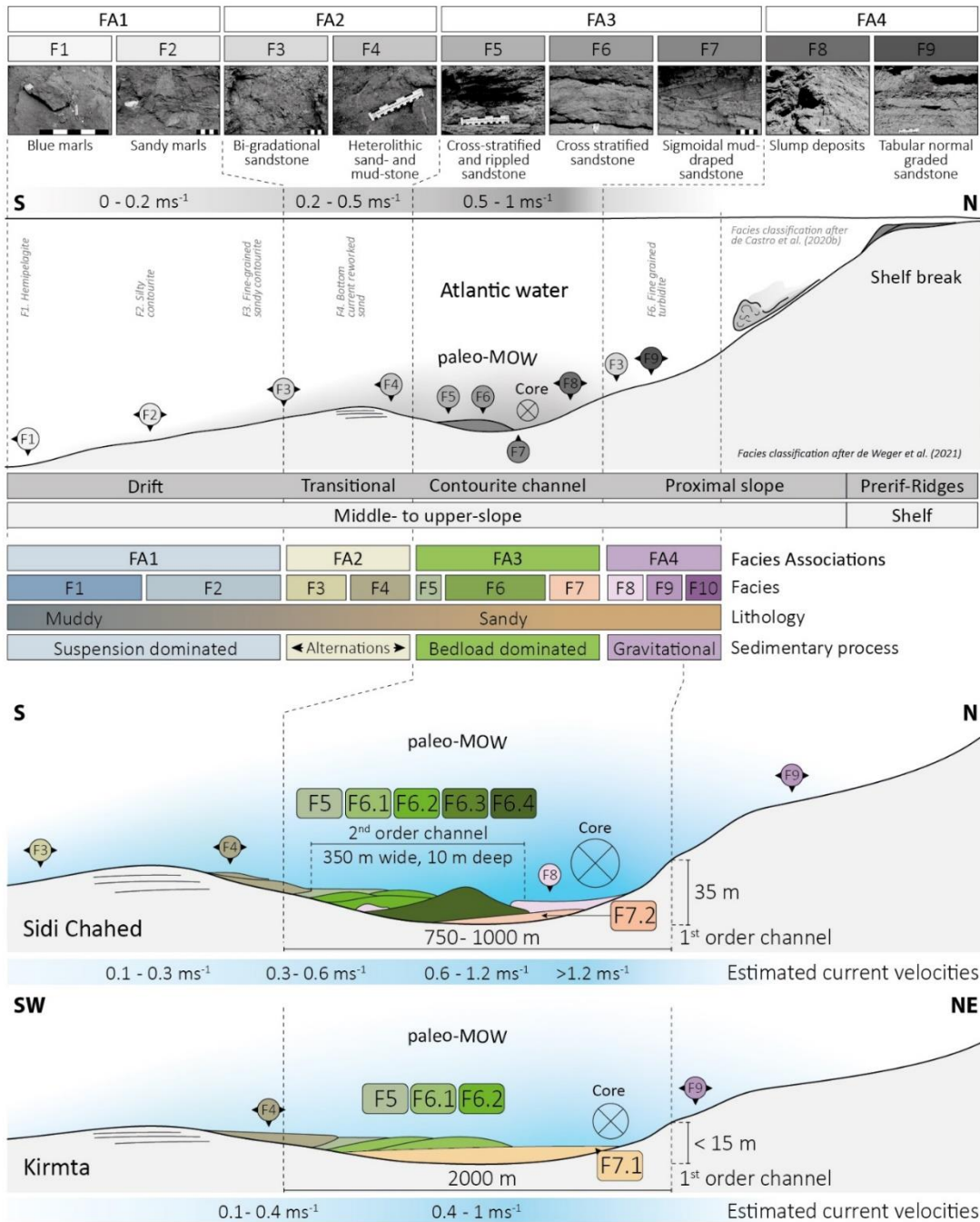


**Figure 7.7.** The top panel is derived from de Weger et al. (2021) and shows the relation between facies F1-F9 defined therein. This facies model is used for comparison to the newly proposed facies model made herein (two bottom panels, one for the Sidi Chahed and one for the Kirmta outcrop at the bottom). This facies model shows the relation between facies and facies associations within the 1<sup>st</sup> order contourite channel, which transitions towards the drift (S/SW or left). The estimated current velocities for each depositional domain is included.

### 6.4 Facies associations and interpretations

The sedimentary facies are linked to form distinct facies associations and depositional elements (Table 7.1, Fig. 7.7). The finest-grained sediments are grouped into FA1 and consist

of both fossil rich blue marls (F1) and sandy marlstones (F2) which regularly grade into one another. FA1 occurs over intervals upwards of 10's to 100's of meters in thickness. FA1 is generally coarsening upwards grading from F1 to F2 towards the base of the sand units (Figs. 7.3 and 7.4). Facies association FA2, consisting of sandstone laminae (F3) and heterolithic sandstone (F4), contains transitional facies between FA1 and FA3. This facies association is marked by the presence of heterolytically co-occurring sand and fine-grained sediment for which, in part, they are similar and always associated to the facies of FA1. In facies association FA3, occurring within the channels, all facies (F5 to F7) are found interbedded with one-another. However, they generally grade both upwards and laterally from planar laminated sandstone (F7) to cross-stratified sandstone (F6) and fully bioturbated sandstone (F5). FA4, consisting of convolute sandstone (F8), amalgamated normal graded sandstone (F9) and conglomerates (F10), is typified by the presence of sedimentary structures that are directed parallel to the inferred paleo-slope and perpendicular to those observed in FA3. The convolute sandstones (F9) are regularly found interbedded within FA3, occurring within the channels. Facies F9 is always found in association and amalgamated with facies association FA1 (Figs. 7.3 and 7.4) and is only recognized outside the channels. Conglomerates (F10) are only present at one location in the Sidi Chahed section, interbedded between F3 and F8.

#### *6.4.1. Fine-grained marine sediment (FA1) - Interpretation*

The fine-grained sediment of FA1, the blue marls (Table 7.1), are the same as previously described in *de Weger et al. (2020, 2021)*. Since the facies (F1 and F2) of this facies association are not the focal point of this work and they are like FA1 as previously described in *de Weger et al. (2020, 2021)*, their interpretation is directly applied. Facies association FA1 is thus interpreted to represent a low energy depositional environment dominated by the vertical settling and lateral advection of both fine-grained biogenic and terrigenous particles (hemipelagic sedimentation) and the activity of weak bottom currents resulting in drift deposits (Fig. 7.7). Furthermore, there was a likely presence of occasional low-density turbidity currents.

#### *6.4.2. Contourite channel-drift transition (FA2)*

Within FA2, the sandstone laminae (F3) represent the lowest energy conditions within FA2. As F3 is closely associated to FA1, its origin is also dominantly related to bottom current processes. As such, the lenticular sand laminae of facies F3 represent starved ripples formed by increased flow-conditions in an environment otherwise dominated by suspension fallout

related to weaker current velocities. This indicates that flow conditions alternated between low to moderate current strengths and associated periods of winnowing (*Martín-Chivelet et al., 2008*). Similar facies were also recognized by *de Castro et al. (2020a, b)* and *de Weger et al. (2021)* who interpreted these deposits as bottom current reworked sands formed by moderate but intermittent bottom currents capable of reworking gravity driven flow deposits which supplied sediment to the system. This facies is ascribed to a channel-drift transition environment, marked by stronger/weaker current activity compared to the drift/channel (Fig. 7.7).

The heterolithic sandstones (F4) are more closely related to facies association FA3 compared to FA1, where facies F4 often represents the lateral equivalent of the larger cross-stratified bedforms of F6.1 and F6.2. In comparison to F3, the cross-laminated sandstone beds are better developed, and the sand/mud ratio is higher, indicating higher mean-current velocities and a possible increase in sediment supply. With respect to the findings of *de Weger et al. (2021)* (Fig. 7.7), this facies forms an intermediate between F4 (Heterolithic sandstone and mudstone) and F5 (cross-stratified and rippled sandstone) described therein, allowing for an assignation in the channel-drift transitional domain. The heterolithic nature of the beds suggest alternating flow conditions between bedload transport and suspension fallout. These alterations might have been induced by the tidal modulation of the paleo-MOW (*de Weger et al., 2021*) or have resulted from other, longer time-scale control on overflow behavior responsible for the expanse and collapse of the bottom-current core.

The undifferentiated biogenic structures together with *Macaronichnus* and *Planolites*-like burrows indicated that benthic food was concentrated on the seafloor and within the upper centimeters of the substrate. The higher abundance and diversity of trace fossils in facies F4 with respect to F3 can be related to the increased availability of benthic food, which in turn is likely associated to an increase in sediment supply.

#### 6.4.3. *Contourite channel (FA3)*

The commonality of the facies ascribed to facies association FA3 (Table 7.1) is that they show traction structures in the form of planar- and unidirectional cross-stratification (F5, F6 and F7). This facies association occurs over thick intervals (generally over 5 m in thickness) where related facies occur both stacked and in lateral transition. Only minor intervals (facies F3 and F4) indicative of weaker current velocities are present (Figs. 7.3 and 7.4). These characteristics indicate that flow conditions were relatively persistent and of high flow velocities. The alternation of sedimentary facies and the presence of erosive surfaces

however indicates that current velocities fluctuated but, in general, remained high enough to erode and redistribute medium- to coarse-grained sand. The erosive, or reactivation surfaces, could also indicate periods of decreased sediment supply. The presence of tidal signatures, such as thickening and thinning foreset-bundles (e.g. Allen, 1982; Longhitano and Nemec, 2005), gradual changes between angular to tangential toe-set geometries (sensu Chiarella, 2016), and foreset composition couplets (e.g. Ichnas and Dalrymple, 2009; Longhitano et al., 2012) indicate that the formation of the cross-stratified beds took several tidal cycles (months – years), ruling out a turbiditic origin of these deposits. De Weger et al. (2021) argued that these tidal signatures in deep-water environments of the Rifian Corridor resulted from tidal modulation of the paleo-MOW, most prominently observed within contourite channel deposits. This combined with the strong energy conditions required for the deposition of these sediments allows the assignment of this facies association to the contourite channel (Fig. 7.7). The general scarcity of trace fossils agrees with persistent high energy conditions hindering bioturbation trace makers.

Facies F5, although fully bioturbated, shows remnants of parallel lamination. Unlike the planar laminated sandstone of facies F7, the fully bioturbated nature suggests bottom-current velocities that sustained environmental conditions suitable for burrowing organisms. As such, and since the sand fraction is generally coarse-grained, the planar lamination and tabular bedding are more likely associated to the lower stage plane bed flow-regime with current velocities between 0.4 and 0.6 ms<sup>-1</sup> (e.g. Southard and Boguchwal, 1990). Like the heterolithic sandstones of facies F4, this facies often forms the lateral equivalent of sub-facies F6.1 and F6.2, albeit associated to lower current velocities. As the flow velocity within bottom currents decreases laterally away from the core (e.g. de Weger, 2021) this facies represents a lateral facies change related to an inter channel depositional environment away from the core, towards the southern (left) channel flank and the drift (Fig. 7.7), or it was deposited at a time when the paleo-MOW was diminished. *Macaronichnus*, the ichnogenus responsible for the fully bioturbated appearance of this facies, typically occurs in sand-rich shallow-marine (up to foreshore) high-energy settings (e.g. Seike, 2007) but it has also, albeit scarcely, been identified in deeper environments (Rodríguez-Tovar and Aquirre, 2014). Based on the same outcrops Miguez-Salas and Rodríguez-Tovar (2020) explained the *Macaronichnus* trace maker activity in this deep environment by high-energy and nutrient-rich influxes related to strong bottom currents, generating similar environmental conditions as those in shallow-marine settings. The presence of *Scolicia*, usually associated with coarse silty to fine sandy sediment, supports the availability of benthic food. The abundance and



size of this trace, produced by irregular echinoids, increases with the amount and nutritious value of benthic food (Kröncke, 2006; Wetzel, 2008).

The cross-stratified nature and general tabular bedding of the unidirectionally migrating deposits of facies F6 suggests they most likely constitute relics of deep-marine dunes. Based on the depositional domain in the slope and the evidence of a tidally modulated paleo-MOW in the late Miocene (e.g. Capella et al., 2017a; de Weger et al., 2020, 2021), these deposits are interpreted as sandy contourite dunes. Previously facies F6 had been interpreted as 2-D (F6.1 and F6.2) and 3-D dunes (F6.3 and F6.4) by de Weger et al. (2020, 2021) related to vigorous bottom currents along the contourite channel. We do not divert from this interpretation. Based on grain-size, sedimentary structures, and the bedform-velocity matrix of Stow et al. (2009) these bedforms have formed as unidirectionally migrating dunes under bottom current velocities reaching up to  $1 \text{ ms}^{-1}$  (Table 7.1, Fig. 7.7). The regularly observed soft sediment deformation structures (Fig. 7.5G, I) consisting of overturned cross-strata (*Type 1 sensu Allen and Banks 1972*) and fluid escape structures indicate disturbance whilst the sediments still contained water. According to Mckee et al. (1962), Brenchley and Newall (1977) and Owen (1996), tangential shearing drag on liquefied sand may produce these kinds of overturned folds. The fold-style of overturned cross-strata suggests that the deforming force was unidirectional in its action. The fluid escape structures with upwards directed water-escape porphologies can be described as internally ruptured fluid-escape structures (*sensu Owen, 1995*). Since the water escape processes hardly involve foreset laminae but affected bedsets, they likely did not originate during the migration of the sand dunes (Chiarella et al., 2016).

The thinner-bedded, tabular, cross-stratified sandstones of F6.1 are more heterolithic in nature compared to F6.2 as foresets more distinctly alternate between more and less indurated sand. This alteration is the result of fining-upward foresets that are upward depleted in bioclastic material, likely resulting from alternating flow conditions induced by tides (e.g. de Weger et al., 2021).

The medium- to thick-bedded cross stratified sandstones of F6.2 represent higher energy- , and more stable conditions of the paleo-MOW compared to sub-facies F6.1 as they are thicker and more uniform in composition. Based on the bedform-velocity matrix by Stow et al. (2009), the bedform stability diagram by Southard and Boguchwal (1990), and the sedimentary structures of contourite deposits by Martín-Chivelet et al. (2008), flow velocities likely ranged between  $0.4$  and  $1 \text{ ms}^{-1}$ .

The 3-D dunes related to sub-facies F6.3 and F6.4 are, based on the bedform stability diagram by *Southard and Boguchwal (1990)*, deposited by higher current velocities compared to the 2D-dunes of sub-facies F6.1 and F6.2. The cyclic changes from angular to tangential toe-set geometries in F6.4 indicate cyclically changing, tidally modulated bottom current velocities.

The increasingly dominant occurrence of *Macaronichnus* and *Scolicia* between sub-facies 6.1 to 6.4 supports the increase in bottom current velocities between these facies (*Kröncke, 2006; Wetzel, 2008; Miguez-Salas and Rodríguez-Tovar, 2020*). The intense bioturbation by these trace makers likely hampered bioturbation by other trace makers such as *Planolites* and *Thalassinoides*-like producers.

The planar laminated sandstones of facies F7 are always found below facies F6, regularly forming the lateral, towards the right channel flank, equivalent of facies F6. Due to its association with facies F6 and its inter channel position, facies F7 is associated to the contourite channel and has a contouritic origin. Thin-section analysis on samples from F7.1 (KT1, KT2, KT3 and KT5) revealed that the very-fine to fine-grained sand contains a significant number of pellets of reworked mudstone and glauconite, fine-grained shell fragments and predominantly planktonic foraminifers. The claystone pellets are likely sourced as rip-up clasts due to strong bottom current activity and the composition of this sand indicates winnowing. The elongated bioclasts are oriented sub-parallel to the bedding, indicating primary current lamination. The planar parallel laminated beds with the presence of primary current lamination also suggest strong bottom currents, likely in the upper stage plane bed flow regime. *Martín-Chivelet et al. (2008)* reported similar facies in contourite deposits associated to current speeds ranging from 0.6 to 2 ms<sup>-1</sup>. Based on the bedform stability diagram by *Southard and Boguchwal (1990)*, flow velocities for the very-fine to fine-grained sand in facies F7.1 were likely in the range of 0.6 to 1 ms<sup>-1</sup>, whereas flow velocities for the medium-grained sand in facies F7.2 were likely in the range of 1 to 1.6 ms<sup>-1</sup>. The bi-gradational nature of the beds and on a larger scale the bed-sets, most clearly observed in facies F7.1, suggest gradual changes in flow strength.

Like facies F5, this facies contains abundant trace fossils, however traces are predominantly undifferentiated, indicating benthic food is mainly available on the seafloor, decreasing downwards within the sediment. The scarcity of benthic food available within the sediment might have resulted from winnowing, depleting the sediment of nutrients. The presence of benthic food at the seafloor also indicates changes in flow strength, where

during times of decreased flow velocities nutrients were preserved at the seafloor, favoring trace maker activity.

#### 6.4.4. Gravity-driven flow deposits (FA4)

The convolute and/or contorted nature and the erosive basal surfaces of facies F8 (Table 7.1) suggest that it represents the product of a slump (*e.g. Leeder, 2009; Reading, 2009; Shanmugam, 2010*). The regular presence of fluid escape structures recognised directly below facies F8, most often occurring in facies F6, attests to the sudden displacement of sediment creating overpressure in the still water-bearing cross-stratified sandstones (F6). Although slumps may occur over a wide range of depositional environments, their formation relies on slopes. Since the primary bedding of facies F8 is like facies F6.3/F6.4 and F9, F8 might represent down-slope, plastically deformed dunes and fine-grained turbidites, respectively. As facies F8 with a primary composition like facies F6.3/F6.4 is predominantly found interbedded with facies association FA3, these slumps might represent collapsed dunes. As facies F8 with a primary composition like facies F9 is primarily found on the right flank of the channel, here facies F8 likely represents slope deposits that slumped into the channel (Fig. 7.7), either due to oversteepening of the slope and/or tectonic instability or due to undercutting of the slope by the core of the bottom current. *Mézerais et al. (1993)* also observed that local sediment slumps occur on flanks of contourite channels and that sedimentation on these flanks was likely disrupted by slumps.

Facies F9 (Table 7.1) generally shows basal scours and clear bounding surfaces. The well- to very well-sorted, normal graded beds and internal structures typically represent a decelerating turbulent flow from the upper flow regime to suspension fallout (*e.g. Bouma, 1962*). Facies F9, predominantly consisting of thin bedded turbidites might suggest a basinal (silty-sandy distal lobe) depositional setting. However, they more likely represent the tail of turbidity current deposits on the slope (*Mutti, 1992; Mutti et al., 2009; Mulder, 2011; Talling et al., 2012*) or very low-density turbiditic currents on the slope as recently discussed by *de Castro et al. (2020a, b)* and *Hüneke et al. (2020)* (Fig. 7.7).

The deeply incised erosional surface of facies F10 indicates high shear stresses likely related to very high flow velocities or dense flow. The nature of deposition suggests a clastic flow most likely resulting from slope instability. Some conglomerates enriched in quartzose clasts may be first-cycle deposits that formed by erosion of a quartzite, quartz arenite, or chert-

nodule limestone source (Boggs, Jr. 2009). The accretionary wedge, actively uplifting around the time of deposition and slope formation prior to the deposition of the studied sections, is composed of imbricates, blocks of different lithologies (limestones, sandstones and evaporites among others, Sani et al., 2007) and was thus likely the source of the debris-flow conglomerate.

### 6.5. Facies distribution within the contourite channels (FA3)

The 2<sup>nd</sup> order channels and their sedimentary facies distribution within the 1<sup>st</sup> order channels (sand units), is referred to with respect to the position within the 1<sup>st</sup> order channels. Terminology applied for both the 1<sup>st</sup> and 2<sup>nd</sup> order channels is provided in Figure 7.8. In the Sidi Chahed outcrop the across channel direction is roughly N-S, whereas the across channel direction in Kirmta is oriented NE-SW (Figs. 7.9 and 7.10).

Besides the vertical facies stacking pattern logged in throughout both outcrops (Figs. 7.3 and 7.4), picture analysis and field sketches allow for the recognition and distribution of 2<sup>nd</sup> order channels as well as both vertical and lateral sedimentary facies changes (Figs. 7.9 and 7.10). The detailed assignation of sub-facies from pictures proved difficult and as such we mainly deal with the facies F6 and F7. This does not significantly change the outcome of the interpretations. The 1<sup>st</sup> order channels are dominantly encased by facies association FA1. For all 1<sup>st</sup> order channels the lower bounding surfaces are erosive (concave-up). The 2<sup>nd</sup> order channels with erosional, concave-up lower bounding surfaces, most clearly identified in the Sidi Chahed outcrop (Fig. 7.9), are mainly filled by facies association FA3 but show a strong correlation to facies F8.

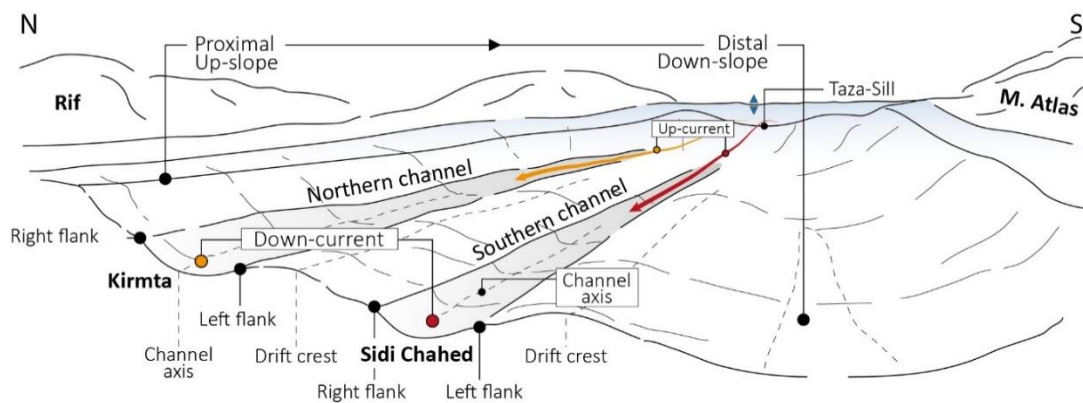
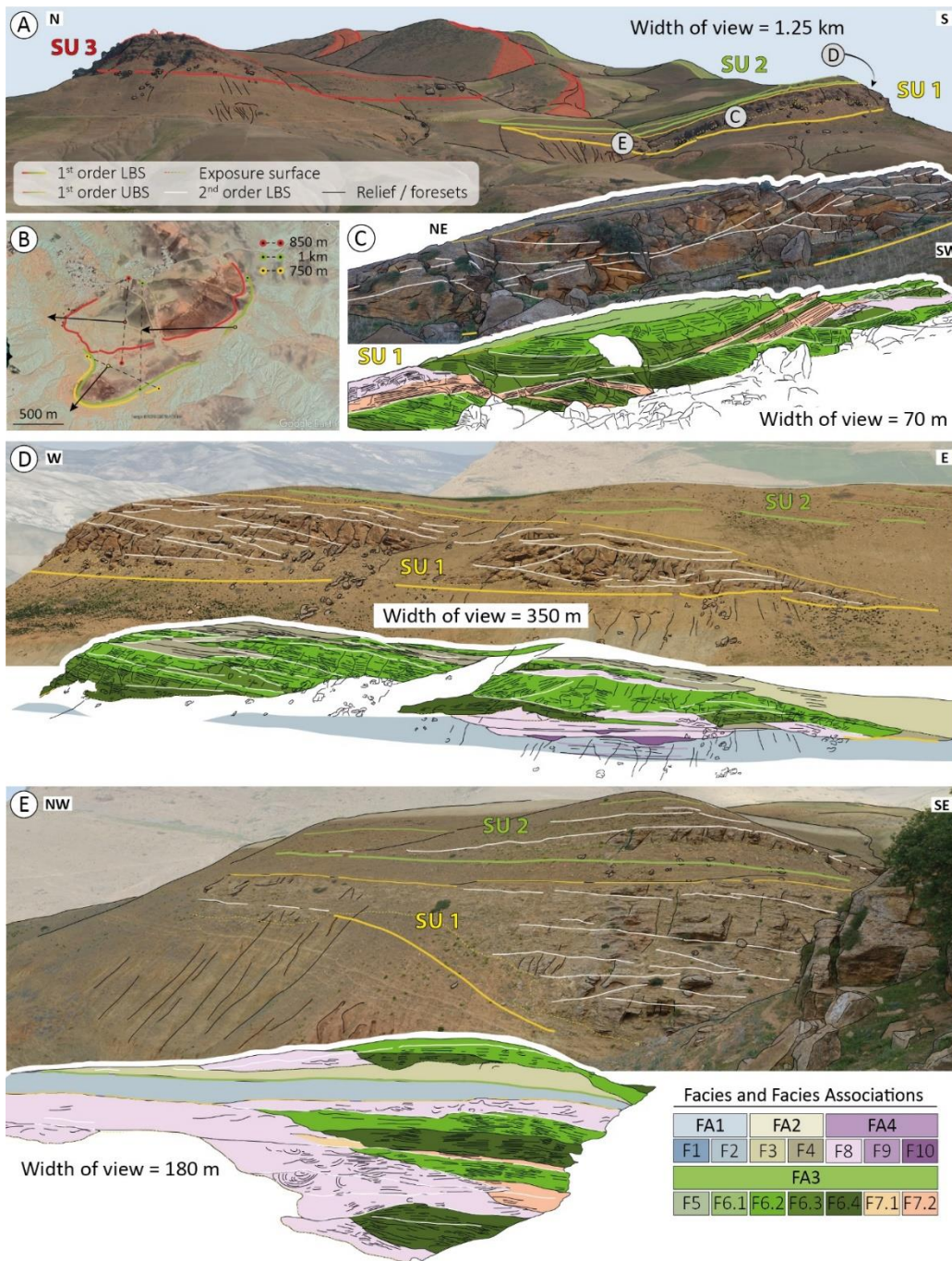
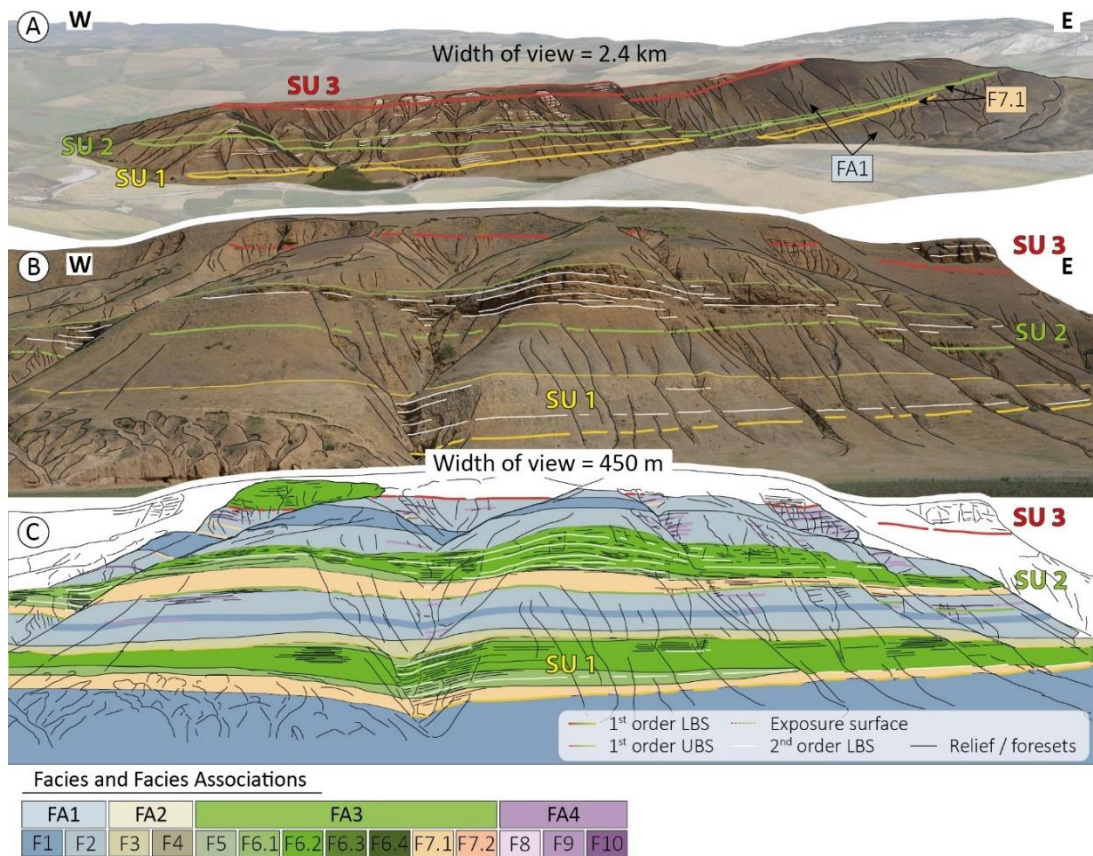


Figure 7.8. Simplified paleogeographic setting and terminology of the late Miocene, South Rifian Corridor contourite channel system.



**Figure 7.9.** Facies distribution within main sand-units (SU1-3) of the Sidi Chahed outcrop. **(A)** Panoramic picture with the main, concave-up sand units, indicated (from old to young), by the yellow (SU1), green (SU2) and red (SU3) lines. This color-scheme is also applied to the remaining figures. **(B)** Top-view of the outcrop with the black arrows indicating the main paleo-current direction and the dotted lines indicating the width of each sand unit. **(C)** Panoramic picture and interpretation of part of Sand-Unit 1 as indicated in **(A)**. **(D)** The southern flank of Sand-unit 1 and its interpretation. **(E)** The northern flank of Sand-Unit 1 and its interpretation.





**Figure 7.10.** Facies distribution within main sand-units (SU1-3) of the Kirmta outcrop. **(A)** Panoramic picture with the main, gently concave-up sand units, indicated (from old to young), by the yellow (SU1), green (SU2) and red (SU3). Facies in the east consist of laterally extensive F7.1 encased by facies association FA1. **(B)** Panoramic of the middle part of the outcrop with **(C)** the facies distribution interpretation below.

### 6.5.1. Sidi Chahed

In the Sidi Chahed section, the best visualization of the 2<sup>nd</sup> order channels and its sedimentary facies distribution is applied for SU-1 (Fig. 7.9), however, similar trends were observed in SU-2 and SU-3. Figure 7.9E represents the right-, most proximal, flank of the channel whereas Figure 7.9D represents the left (more distal) flank of the channel. Figure 7.9C represents a location in the channel close to its axis.

The right channel flank is dominated by turbidites (F8), which have a similar primary petrographic composition as the slump deposits (F9). This facies transitions laterally (towards the axis of the channel) towards planar laminated sandstones (F7.2) and cross-stratified sandstones (F6.4/F6.3 and F6.2) (Fig. 7.9E). The vertical facies signature in the right flank consists of the subsequent stacking of convolute sandstones (F8), separated by erosive bounding surfaces. In the direction towards the channel axis the vertical facies distribution consists of the subsequent stacking of F7.2, F6.3/F6.4 and F6.2. The overall vertical facies

trend in the 2<sup>nd</sup> order channels is fining upwards, related to changes in facies with complex to more simple architectures and internal structures, grading from facies F8, F7 to F6.

The axis area of the channel (Fig. 7.9C) is marked by extensive 2<sup>nd</sup> order erosional surfaces with distinct changes in bedding orientation of the infill sequences. Similar as for the right flank, the overall trend is fining-upwards related to a vertical facies distribution that, in general, consists of the subsequent stacking of F7.2, F6.3/F6.4 and F6.2. The lateral facies changes (towards the left flank) are marked by a modest change from dominantly higher, to lower order facies (F7 – F6).

The left flank of the channel (Fig. 7.9D) is marked by 2<sup>nd</sup> order channels with clear erosional lower bounding surfaces. Although these unconformities can also be identified in the previously discussed parts of the channel, here they are most prominent. The vertical facies distribution in this flank is marked by a change from dominantly higher- to lower order facies (F6.4 – F3). The lateral facies changes are marked by a similar distribution (fining towards the left) albeit directed in a more distal direction, outside of the channel.

Below the left flank of the channel facies F8, F9 and F10 can be found as individual bodies encased in facies association FA1 (Fig. 7.9D), not showing any process related lateral facies changes. Within the left flank of the channel, facies F8, which occurs interbedded with F6, shows internal features more like facies F6 than F9.

### 6.5.2. *Kirmta*

Within the Kirmta outcrop the three 1<sup>st</sup> order channels (SU's) show good lateral and vertical exposure (Fig. 7.10). The direction of view is roughly parallel to the flow direction and thus to the axis of the 1<sup>st</sup> order channels. The erosive lower channel bounding surface is incised into facies association FA1. This erosive bounding surface is overlain by sub-facies F7.1 which, in the axis of the channel is overlain by another erosive bounding surface. On top of facies F7.1 we find stacked intervals of facies F6 (predominantly sub-facies F6.2) which are separated by laterally extensive, near vertical erosional surfaces. Facies F6 grades, quite rapidly to the facies of FA2 and FA1, where FA1 is regularly interbedded by facies F9 (Fig. 7.10).

Below the left channel flank of the 1<sup>st</sup> order channel, facies association FA1 is coarsening upwards, followed by the erosional lower bounding surface of the channel. At this location, the channel fill sequence consists of the stacking of facies F7.1, F6.1, F6.2 (erosive lower bounding surface) and F6.1 after which a fining upwards transition occurs from facies F4, F3,



F2 to F1. Towards the axis of the channel the main lateral facies change consists of a thicker interval of facies F6.2, which, towards the left flank grades to FA3 (Fig. 7.10C). The right flank in the east (Fig. 7.10A) is less complex, only consisting of slightly coarsening upwards facies association FA1, followed by the presence of cyclically stacked bed-sets of F7.1 (Fig. 7.4D).

## 7. DISCUSSION

*De Weger et al. (2020)* investigated the spatial distribution and time variations between sand units in the Sidi Chahed and Kirmta sections which were interpreted as two separate contourite channels related to the late Miocene Contourite Channel system. Similarities have been observed in analog channels which have developed in the Gulf of Cádiz since the opening of the Strait of Gibraltar (*Hernández-Molina et al., 2014a; Llave et al., 2020*). In the Strait of Gibraltar, the contourite depositional system consists of a succession of deeply incised valleys/channels, channel fills, and mounded drifts (Fig. 7.11). This system is formed by the present MOW circulation (*Hernández-Molina et al., 2014a*). *De Weger et al. (2020)* recognized that the paleo-MOW acted in a similar way as the present-day MOW, which also consisted of two branches, the upper, shallower northern channel/branch related to the Kirmta outcrop and the lower, deeper southern channel/branch related to the Sidi Chahed outcrop. Both branches of the paleo-MOW were deflected towards the right (north) by the Coriolis force. The upper branch results from the partial mixing of intermediate and deep Mediterranean waters, whereas the lower branch consists of deep Mediterranean waters (*sensu Hernández-Molina et al., 2014b*), resulting in relatively lower/higher density gradients and lower/higher flow velocities for the upper/lower branches. Because the interpretation of the large morphological features is adopted herein, most sedimentary facies are associated to the contourite channel or adjacent drift (Fig. 7.8).

### 7.1. 1<sup>st</sup> order contourite channels

The 1<sup>st</sup> order contourite channels are large concave-up, purely erosional features in the frontal part of the accretionary wedge. *De Weger et al. (2020)* suggested that these 1<sup>st</sup> order contourite channels migrated up-slope from SU1 to SU3, driven by tectonic activity. Based on the study case of the Gulf of Cadiz, the southern channel is influenced by the present-day lower core of the MOW, conditioned both by tectonics and glacioeustatic changes in sea-level. In the Gulf of Cadiz, the 1<sup>st</sup> order channels are on average 3 – 4 km wide, about 160 km long and are, like in the ancient record (35 m), between 30 – 50 m incised. In the Gulf of

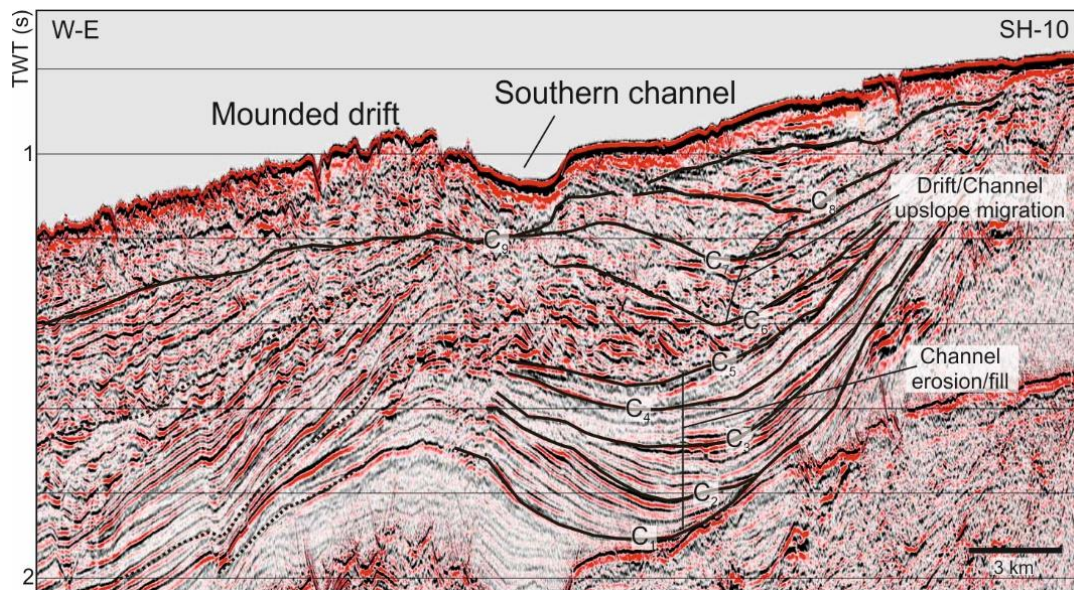


**Figure 7.11.** Multichannel (west-east oriented) seismic profile from the Gulf of Cadiz contourite depositional system showing the distribution of the erosive base of contourite channels developed coeval with regional discontinuities (from old to young;  $C_1 - C_9$ ). This profile is oriented in the direction of flow, roughly towards the North. Seismic line provided by REPSOL.

Cadiz, several channel erosive discontinuities ( $C_1$  to  $C_9$  in Fig. 7.11) and their respective smaller incisions with sedimentary infill units (2<sup>nd</sup> order channels?) are described since their onset in the early Pliocene. Five of these channels ( $C_1 - C_3$ ) have developed in the central depression between two structural highs, the western high being the hanging wall of a thrust fault. During the early Quaternary to late Pleistocene, there is a clear displacement of three erosive channels ( $C_5$  to  $C_8$ ) as well as the formation of adjacent smooth mounded drifts on their western side (Fig. 7.11). These channels and associated mounded drifts have migrated upslope until their present-day location. This mode of up-slope migration is similar as observed in the Kirmta and Sidi Chahed outcrops (SU1 – SU3). The youngest channel ( $C_9$ ) has been laterally displaced towards the northwest during the Late Pleistocene to present, reaching its present location and morphosedimentary characteristics (Fig. 7.11).

Besides a tectonic origin for channel migration, it is also assumed that tectonism is intimately related to the behavior of the paleo-MOW due to the formation and control of the Taza-Sill. The purely erosive nature of the paleo-MOW in its phase of 1<sup>st</sup> order contourite channel formation is related to very vigorous bottom currents. Since the 1<sup>st</sup> order contourite channels are larger than the 2<sup>nd</sup> order channels, the core of the paleo-MOW during this stage was larger and likely more confined (Fig. 7.12). The initiation of bottom currents is believed to have coincided with large density differences between the paleo-MOW and the ambient water due to enhanced Mediterranean deep-water formation as a result of increased restriction of water-mass exchange. Furthermore, the density gradient was thought to be

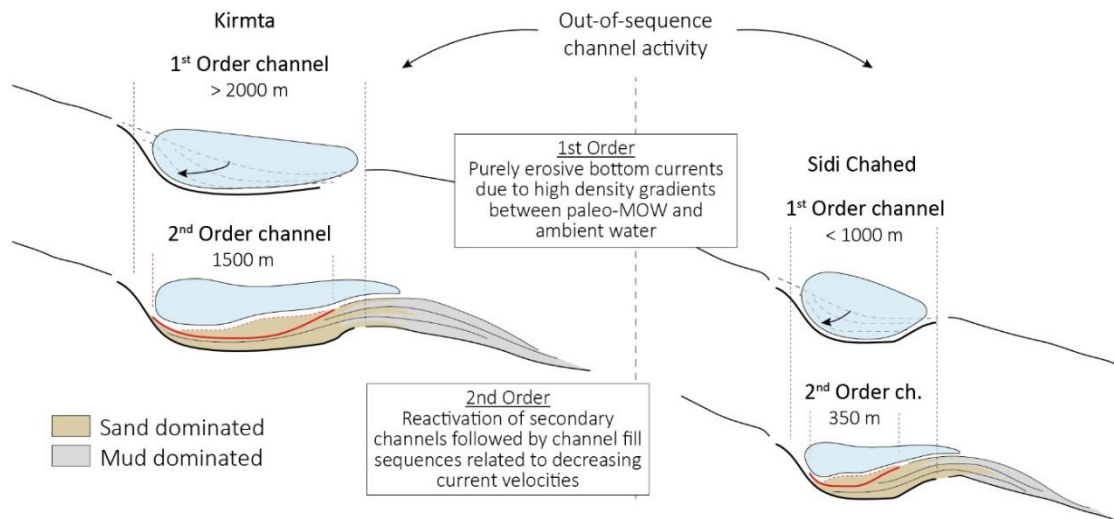


**Figure 7.12.** Sketch of the Sidi Chahed and Kirmta sections within the slope. This sketch furthermore depicts the 1<sup>st</sup> and 2<sup>nd</sup> order channels, their morphologies and their interrelationship.

very high as the ambient water mass and the paleo-MOW were not yet diluted by turbulent mixing. This high-density gradient not only resulted in very vigorous currents, but it also resulted in a large, confined core. These factors are likely the reason why the initial phase of contourite channels is usually marked by large erosive surface (e.g. Fauquères et al., 1999; Llave et al., 2006; García et al., 2009; Hernández-Molina et al., 2014b; Gong et al., 2017).

In the literature it is well established that the current velocities of overflow water are highest near the point of overflow, decelerating due to turbulent mixing and topographic gradient changes down current (e.g. Sánchez-Leal et al., 2017). This indicates that both the Sidi Chahed and Kirmta outcrops were in proximity to the sill.

The transition from a purely erosive, towards a more depositional system is most likely primarily related to a decrease in flow velocities resulting from turbulent mixing with the ambient water masses. Furthermore, upon establishment of two-way exchange, related to the initiation of overflow water associated to the formation of the 1<sup>st</sup> order channel, the density of the paleo-MOW decreased as it became less restricted. Sediment supply should not have been a controlling factor as tectonic activity, a major constituent for down-slope sediment supply, is thought to have played an important role during this phase of contourite channel formation.

Reconfiguration of the Taza-Sill, its effect on the behavior of the paleo-MOW and the southward migration of the accretionary wedge are all primarily deemed responsible for the step-wise formation of the six identified 1<sup>st</sup> order contourite channels (de Weger et al., 2020).

Observations from the Gulf of Cadiz Contourite System have shown that a stronger MOW in the deeper channel is linked to glacial periods, associated to higher aridity in the Mediterranean and thus an increase in the density of Mediterranean Deep Water (*Llave et al., 2006*). *De Weger et al. (2020)* implied from this that the MOW favors either the upper or lower channel, out-of-sequence, due to changes in density characteristics of the paleo-MOW. Thus, all these changes are induced by tectonic- and climatic- processes and their effects on the Mediterranean water masses. The late Miocene however was not severely affected by glacial-interglacial (eccentricity) cycles but was more dominantly affected by precession (*e.g. Sierra et al., 1999*). Precessional cyclicity was therefore likely a secondary driving force behind the 1<sup>st</sup> order intermittent behavior of the paleo-MOW and the out-of-sequence behavior of the channel branches, or it controlled the 2<sup>nd</sup> order contourite channel features. Smaller-order changes in the hydrodynamic characteristics of the paleo-MOW are related to millennial and seasonal changes in climatic conditions (*e.g. Gladstone et al., 2007*) and due to the short time-scales that primarily affected channel fill sequences.

### 7.2. 2<sup>nd</sup> order contourite channels

The 2<sup>nd</sup> order contourite channels are filled by sediment, making them both erosional and depositional. The formation of these 2<sup>nd</sup> order channels is initiated by erosive reactivation events after which deposition takes place. This change from erosional to depositional is mainly due to a decrease in flow velocity of the paleo-MOW and/or increased down-slope sediment supply to the channel. The reason why these 2<sup>nd</sup> order channels are more easily identified in the Sidi Chahed section might be because, in general, this section was influenced by more vigorous bottom currents and thus also stronger erosive events.

As mentioned previously, prior to deposition, vigorous bottom currents shaped the slope, creating wedge top sub basins in the form of 1<sup>st</sup> order channels. With decelerating current velocities, the purely erosional system transformed to a depositional setting with secondary channel geometries. The spatiotemporal infill of these secondary channels is primarily related to the velocity distribution of bottom-current water masses. Highest bottom current velocities are found in the core of the bottom current with decreasing current velocities towards the left flank (dependent on the deflection caused by the Coriolis Force) and the drift (Figs. 7.7). Depending on sediment availability, its sediment characteristics and the velocity of the current, bedforms are identified to have been developed following the bedform stability diagram (*e.g. Southard and Boguchwal, 1990*). The full range of across channel facies/bedforms identified in the Sidi Chahed outcrop (Fig. 8), from the right to the

left flank, consist of slope erosion, upper-stage plane bedforms (or part of larger wavelength bedforms in upper stage) (F7), 3-dimensional dunes (F6.4 and F6.3), 2-dimensional dunes (F6.2 and F6.1), lower-stage plane bedforms, and heterolithic, transitional facies (F4). The channel-drift transitional facies of F4 cover both the left flank of the channel and the adjacent drift. The channel-drift transitional facies F3 is located closely to the drift and transitions to pure drift facies F2 and F1 in a distal direction (Figs. 7.7 and 7.12).

The panoramic pictures of the Sidi Chahed outcrop (Fig. 7.9) clearly show the stepwise reactivation of the bottom current, recognized by 2<sup>nd</sup> order channel migration. The secondary channels are recognized to either prograde or retrograde with respect to the paleo-slope.

Progradation is usually associated with large slump deposits in the right flank. These slump deposits, by occupying the right flank area of the channel, likely forced the core of the current in the direction of the left flank, forcing progradation or southward channel migration (Fig. 7.13C). These slumps were either triggered by tectonic instability or undercutting by the core of the bottom current. Progradation could also be stimulated by

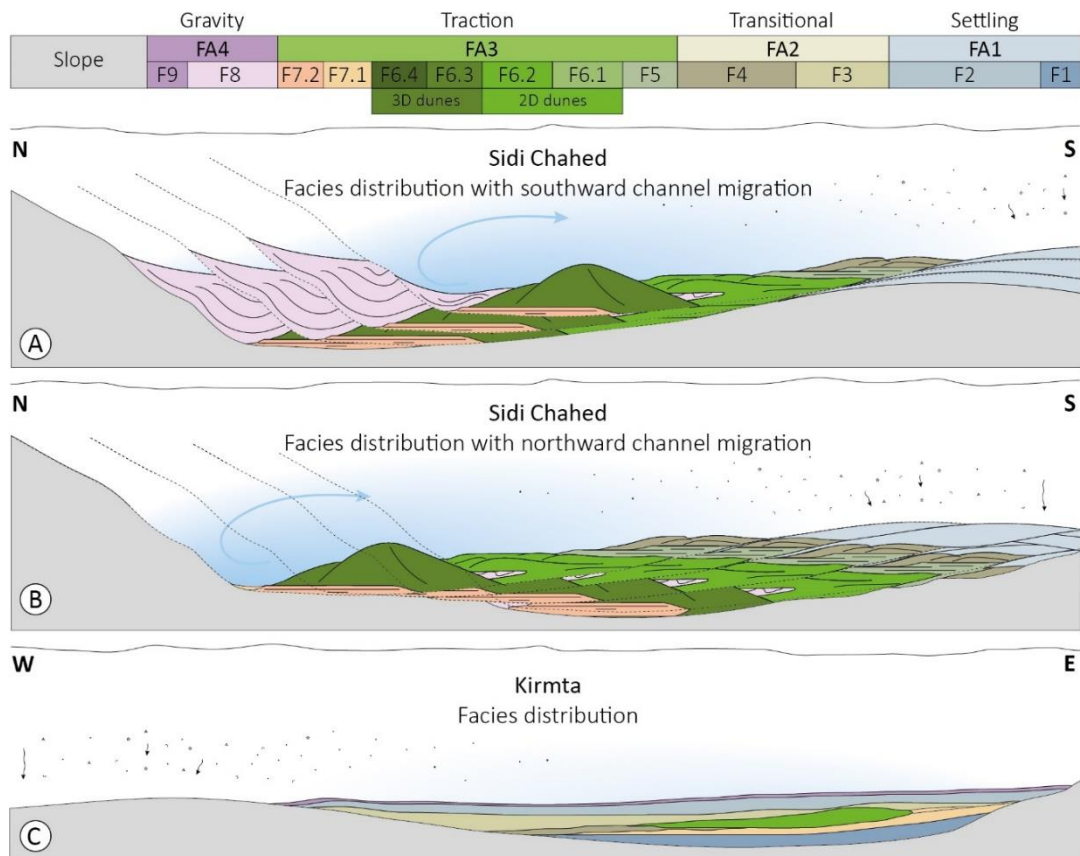


**Figure 7.13.** Evolution of 2<sup>nd</sup> order channels and their related infill deposits. The secondary channels within the Sidi Chahed section (**A and B**) either prograde (**A**) or retrograde (**B**). The channel fill sequence in the Kirmta section is less complex due to weaker bottom currents and smaller bottom current velocity fluctuations.



higher density contrasts between the bottom current and the ambient water-mass, allowing the core to flow deeper, down slope. Retrogradation represents the normal evolution of contourite channel systems (*e.g. Faugeres and Stow, 2008*), where erosion occurs in the right flank and deposition is focused on the left flank and the adjacent drift, forcing the system to migrate towards the right or up-slope. The observed secondary channel distribution comprises the subsequent progradation and retrogradation of the contourite channel. This evolution indicates that, if the slumps were triggered by tectonic induced instability, the system was initially affected by stronger/more frequent tectonic activity. These tectonic pulses decreased roughly half-way during the evolution of the channel, decreasing sediment slumping, and causing the system to prograde. The final stages of channel fill are marked by the presence of relatively fine-grained and thinner bedded deposits, indicating a decrease in flow velocity (Figs. 7.3 and 7.4). This decrease in flow velocity likely resulted from a decrease in the density gradient between the paleo-MOW and the ambient water masses.

The facies distribution in the Kirmta outcrop is distinctly different from that in the Sidi Chahed outcrop and 2<sup>nd</sup> order channels are hardly recognized. Despite the lack of distinct 2<sup>nd</sup> order channels, within the facies distribution several laterally extensive and near horizontal reactivation surfaces have been recognized. These reactivation surfaces are expected to have resulted from either a decrease in sediment transported to the system or temporary flow velocities exceeding that required for sediment deposition. These features were triggered by similar processes as those described for the Sidi Chahed outcrop.

### *7.3 Mechanics of dense gravity flows*

A slightly different approach for the flow estimates is also explored, considering now the mechanics of dense gravity flows and their sedimentologic impacts. The MOW flowing down the Taza Sill and through the channels can be regarded as a dense (saline) gravity flow driven not only by the density gradient established with the water mass above, but also the topographic gradient down the sill. The energetic bottom dense flow will entrain water from above due to the increased friction and turbulent mixing at the interface and develop a lower boundary layer in contact with the seabed, the thickness of which is controlled by the relative importance between bed and interface friction. It is important to keep in mind that, although some of the hydrodynamic and sediment transport processes associated to dense bottom flows might not be fully analogous to the subaerial (fluvial) case, some fundamental behaviour related to particularities of bedform dynamics remain common to many different flow types, such as for example the relationship between dune and turbulent boundary layer

mechanics (Fedele et al., 2016). We estimate the thickness of the lower boundary layer of the MOW flowing through the channels within the range 8-14 m, using scaling from the observed dune properties (wavelength, height, grain size; Kennedy 1969; Engelund, 1970; Yalin, 1977; Raudkivi 1976; Fedele et al, 2016). Assuming well-developed dunes, dune heights of about 2-3 m and sediments ranging 250-500 microns, would indicate dune wavelengths on the order of 40-70 m. In addition, estimates of shear velocities and thus dimensionless shear stresses (Shields –or mobility parameter)  $\tau^*$  of about 0.4-0.6 (Liu, 1957; van den Berg and van Gelder, 1993; van Rijn, 1993; Parker, 2008) lead to a range of bed-related friction coefficients  $C_f$  of the flows in the range 0.007-0.01. Bed-related friction coefficients are then increased appropriately to account for the contribution of interfacial friction and mixing in the dense gravity flow (Ellison and Turner, 1959; Streeter and Kestin, 1961), to obtain estimates of the current average velocity, thus found in the range 0.6-0.9 m/s.

Although very similar to previous estimates described above using dimensioned bedform diagrams (e.g. Boguchwal and Southard, 1990), the latter are derived and consistent with a more realistic flow setting. Finally, using these average flow velocities and thickness of the boundary layer, along with a range of fractional density differences between the dense lower cascading flow in the MOV and the water mass above of the order of 0.001-0.005,

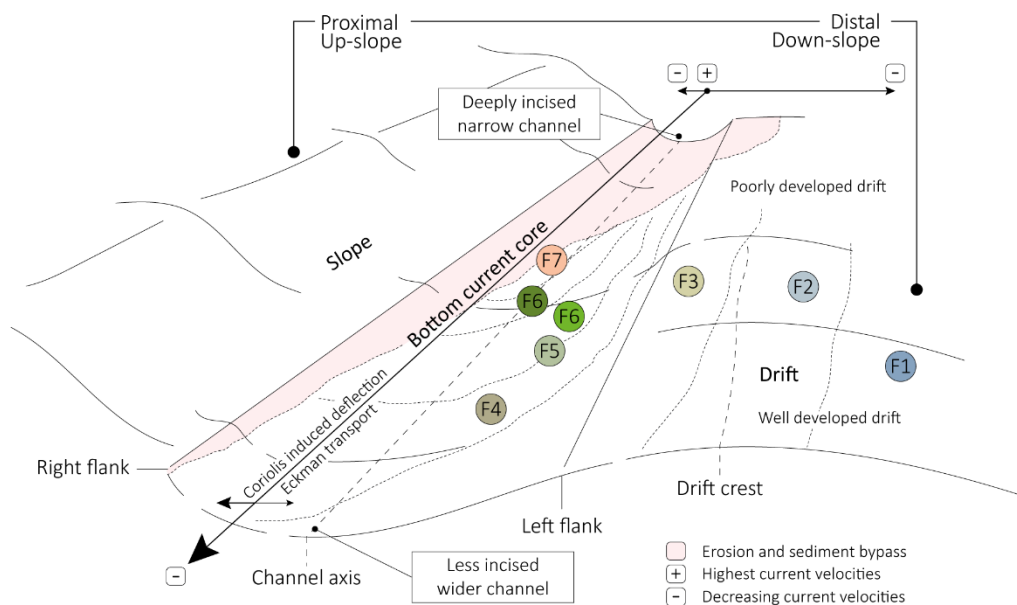


**Figure 7.14.** Three-dimensional sandy contourite facies model showing the contourite channel and drift. Up current, or at the site of overflow, bottom current velocities are highest. Down-current bottom current velocities decrease. The bottom current core is the most energetic part within contourite systems, with decreasing current velocities away from the core. This model represents an idealized facies model where the facies distribution is a product of both sediment characteristics and current velocities.



densimetric Froude numbers applicable to the lower boundary layer are computed and found in the order of 1.5-1.9 (supercritical). The Froude estimates and grain sizes observed place the observed bedforms in the appropriate field of stability of dunes created by dense gravity flows, reported in *Fedele et al., (2016)*.

#### *7.4. Facies model*

Based on our findings the sedimentary facies model for sandy contourites, previously proposed by *de Weger et al. (2021)* requires the addition of a down-current dimension (Fig. 7.14). The range of erosional morphologies and depositional sedimentary facies both depend on, as stated previously, (i) the sediment availability, (ii) the characteristics of the available sediment and, (iii) the hydrodynamic characteristics of the water-mass that forms a bottom current with respect to the hydrodynamic characteristics of the ambient water-mass.

In general, the velocity of bottom currents decreases in two directions, both down current and away from the core of the current in the opposite direction to which the core is deflected by the Coriolis force (Fig. 7.14). The formation of bedforms follows this down-current and core-perpendicular trend in decrease in flow velocities depending on the grain-size and current velocity. Despite bedform stability diagrams being deduced from tank-experiments, the evolution of bedform formation correlates well to the bedforms formed and the decrease in flow velocities, limited by the availability of sediment and its characteristics.

If current velocities and sediment availability are all appropriate, the full range of bedforms might develop in contourite channels. If flow velocities are lower, either due to a decrease in the density difference between the water mass of the bottom current and the ambient water mass, turbulent mixing of the water-masses, or other processes affecting a decrease in flow velocities, the depositional regime changes. An example of this change is recorded between the Sidi Chahed and Kirmta outcrops, where the Kirmta outcrop was affected by weaker current velocities. On the other hand, morphological features such as obstacles and confinement can increase current velocities, causing a shift in bedforms related to higher flow velocities.

#### *7.5. Facies model applicability*

Published evidence of sandy contourite deposits, primarily located in the Gulf of Cadiz (*e.g. Hernández-Molina et al., 2006, 2014a; Stow et al., 2013; Brakenridge et al., 2018; de*

*Castro et al., 2020b*) but also in Faero Bank Channel area (*Akhmetzhanov, et al., 2007*), the South China Sea (*Gong et al., 2017*), onshore in the Yangtze region of China (*Zhang et al., 2020*) and in the southern Brasil Basin (*Mézeris et al., 1993*), reveals that contourite channel deposits are primarily found in areas in which the contourite channel changes its orientation, forming a bend. The studied sections, due to the obstruction of the Prerif Ridges (*Fig. 7.1, de Weger et al., 2020*), were likely also located in an area where the contourite channel formed a bend. The scarcity of recognized contourite channel deposits and the fact that, where recognized, the contourite channel depositional features are located in bends of the channel suggest that sedimentation in contourite channels might primarily take place within these bends, and/or that the preservation potential is highest in these areas. Consequently, contourite channels in outcrop might only be scarcely recognized as depositional features might only be present in bends. The factors behind this phenomenon are likely related to changes in flow characteristics. *Piper & Normark (1983)* mentioned that flow stripping happens mostly in the bends of turbidite channels and otherwise most of the flow is concentrated within the channel. Similar as for turbidite channels, flow stripping might be responsible for the change in flow characteristics in the bends of contourite channels and its associated deposits. Thus far, the processes behind the change in flow characteristics responsible for preferred deposition in bends (such as cross-flows resulting from the combined action of coriolis, slope gradient, and bottom Ekman layers) can only be hypothesised and thus need to be investigated further. The proposed facies model however is still viable as it is primarily related to down-current and core lateral decreases in flow velocity. It is possible though that the coarsest grained sedimentary facies are only found in areas of the contourite channel where it changes its orientation.

## 8. IMPLICATIONS

### *8.1. Climate reconstruction*

Contourite systems are controlled by climatic processes. These climatic processes are captured in the sedimentary record. Particularly sandstone contourite facies are prone to capturing even small-scale changes in flow-characteristics induced by climatic change (*e.g. de Weger et al., 2021*). By unraveling these signatures in the ancient record, the information contained within can help understanding changes in global ocean circulation. Inversely, as is the case for the paleo-MOW, bottom-currents in gateways, or overflows, can significantly contribute to the thermohaline circulation (*e.g. Rahmstorf, 2006; Kuhlbrodt et al., 2007*;

Rogerson et al., 2012), significantly affecting global climate. By studying contourite deposits we can improve the detailed resolution of fluxes of dense overflow water and its contribution to global ocean circulation (de Weger et al., 2020).

## 8.2. Reservoir potentiality

Contourite channels and terraces have been recognized to contain large amounts of well-sorted sands in contourite depositional systems (Viana, 2008; Mutti and Carminatti, 2012; Stow et al., 2013; Hernández-Molina et al., 2016a; Brackenridge et al., 2018; de Weger et al., 2021). These systems however were, as of yet, not well understood and the inter-channel and down-channel facies distribution had not yet been documented. This facies distribution however plays a vital role in the characterization and appraisal of sandy contourite reservoirs. Based on our findings, porosities within the inter channel sandstone facies range between 2% and 25% (Table 7.2), albeit that porosity estimates might be enhanced by dissolution. These values however are based on microfacies MF1 and MF2, not including the coarser grained MF3 which has shown porosities up to 35%. Despite these preliminary results of reservoir quality, extensive petrophysical analysis on fresh rock samples should be executed.

One of the most promising features from the prospective of hydrocarbon system's potential is the association of the sand prone contourite channel fill and the adjacent mud prone contourite drift. The contourite drift has a high mud-to-sand ratio which likely has good characteristics to act as seal (Viana et al., 2007; Viana, 2008). Based on the findings of this study, the 1<sup>st</sup> order contourite channels, filled by sandstone facies (F5, F6 and F7), are encapsulated by muddy drift deposits (F1, F2, F3 and F4), indicating that the system is self-sealing.

## 9. CONCLUSIONS

This contribution focusses on the description and interpretation of relics of late Miocene contourite channels in outcrop that have formed by the action of overflow of the paleo-Mediterranean Outflow Water (MOW). These channels consist of 1<sup>st</sup> order contourite channels that range in width between 750 – and 2000 m and are up to 35 m deep. These 1<sup>st</sup> order channels have formed by vigorous, erosive bottom currents associated to the tectonically induced initial phase of overflow formation. Subsequently, the 1<sup>st</sup> order channels, that formed intra slope sub-basins, are filled by up to 300 m wide and up to 15 m

deep 2<sup>nd</sup> order channels. These 2<sup>nd</sup> order channels comprise a phase of erosion, followed by the deposition of sediment associated to a relative decrease in flow velocity. Migration of the 2<sup>nd</sup> order channels is partly controlled by tectonic instability, evidenced by slumps in the proximal part of the channel. The emplacement of slump deposits might have forced the core of the bottom current (or 2<sup>nd</sup> order channel) to migrate down-slope. The natural migration of contourite channels is up-slope, forced against the slope by the Coriolis Force and migrating up-slope because of erosion and down slope accretion.

The depositional phase of the 2<sup>nd</sup> order channels is marked by sandstone deposits with traction structures associated to tidally modulated bottom currents generated by the paleo-MOW. Changes in sedimentary facies are primarily related to short-term, tidally, seasonally and orbitally induced changes in the overflow characteristics and the resulting changes in the velocity of the paleo-MOW. Both down-current and across-channel facies changes from planar laminated sandstones (F7), 3D-dunes (F6.4 and F6.3), 2D-dunes (F6.2 and F6.1) to fully bioturbated sandstones with remnants of planar lamination (F5) are ascribed to a decrease in flow-velocity resulting from a decrease in acceleration due to gravity and the across-channel velocity profile respectively. As such, the inter-channel sandstone facies correlate well to bedform stability diagrams. Despite these diagrams having been established based on sub-areal flume experiments, fundamental behaviour related to particularities of bedform dynamics remain common to turbulent boundary layer mechanics.

This work comprises a novel, detailed study of an exposed contourite channel system from which we proposed a facies model for contourite channels. Although much evidence is provided to support this model, this work needs to be carefully compared to other modern and ancient contourite depositional systems to increase its validity. From this work it is now established that contourite channel deposits contain valuable, high resolution information regarding the evolution of overflow-processes and their effect on changes in global ocean circulation. Furthermore, the coarse-grained nature of contourite channels makes them valuable targets for exploration geosciences.

## 10. ACKNOWLEDGEMENTS

We are very appreciative of the help and support given by the Office National des Hydrocarbures et des Mines (ONHYM), Morocco. Furthermore, we thank REPSOL for kindly providing us with the seismic line from the Gulf of Cadiz. This project was funded by the Joint Industry project supported by Total, BP, ENI, ExxonMobil, Wintershall DEA and TGS, executed

in the framework of “The Drifters Research Group” at Royal Holloway University of London (RHUL). The research contribution of O. Miguez-Salas was funded through a pre-doctoral grant from the Ministerio de Educacion, Cultura y Deporte (Gobierno Espana).

## References

- Akhmetzhanov, A., Kenyon, N.H., Habgood, E., Van Der Mollen, A.S., Nielsen, T., Ivanov, M., & Shashkin, P. (2007). North Atlantic contourite sand channels. Geological Society, London, Special Publications, 276(1), 25-47.
- Allen, J.R.L. (1982). Mud drapes in sand-wave deposits: a physical model with application to the Folkestone Beds (early Cretaceous, southeast England). *Phil. Trans. Roy. Soc. London. Series A, Math. Phys. Sci.*, 306(1493), 291-345.
- Allen, J.R.L., & Banks, N.L. (1972). An interpretation and analysis of recumbent-folded deformed cross-bedding. *Sedimentology*, 19(3-4), 257-283.
- Barbero, L., Jabaloy, A., Gómez-Ortiz, D., Pérez-Peña, J.V., Rodríguez-Peces, M.J., Tejero, R., Estupiñán, J., Azdimousa, A., Vázquez, M., Asebriy, L. (2011). Evidence for surface uplift of the Atlas Mountains and the surrounding peripheral plateaux: Combining apatite fission-track results and geomorphic indicators in the Western Moroccan Meseta (coastal Variscan Paleozoic basement). *Tectonophysics*, 502(1-2), 90-104.
- Blanc, P.L. (2002). The opening of the Plio-Quaternary Gibraltar Strait: assessing the size of a cataclysm. *Geodin. Acta*, 15(5-6), 303-317.
- Boggs Jr, S., & Boggs, S. (2009). *Petrology of sedimentary rocks*. Cambridge university press.
- Boguchwal, L.A., & Southard, J.B. (1990). Bed configurations in steady unidirectional water flows; Part 1, Scale model study using fine sands. *Journal of Sedimentary Research*, 60(5), 649-657.
- Bouma, A.H. (1962). Sedimentology of some flysch deposits. *Agraphic approach to facies interpretation*, 168.
- Brackenridge, R.E., Stow, D.A.V., Hernández-Molina, F.J., Jones, C., Mena, A., Alejo, I., Ducassou, E., Llave, E., Ercilla, G., Nombela, M.A., Perez-Arlucea, M. Frances, G. (2018), Textural characteristics and facies of sand-rich contourite depositional systems. *Sedimentology*, 65, 2223-2252. doi:[10.1111/sed.12463](https://doi.org/10.1111/sed.12463)
- Brenchley, P.J., & Newall, G. (1977). The significance of contorted bedding in upper Ordovician sediments of the Oslo region, Norway. *Journal of Sedimentary Research*, 47(2), 819-833.
- Candela, J. (2001). Mediterranean water and global circulation. In *Int. Geophys*, Academic Press. 77, 419-XLVIII.
- Capella, W., Hernández-Molina, F.J., Flecker, R., Hilgen, F.J., Hssain, M., Kouwenhoven, T.J., van Oorschot, M., Sierro, F.J., Stow, D.A.V., Trabucho-Alexandre, J., Tulbure, M.A., de Weger, W., Yousfi, M.Z., Krijgsman, W. (2017a). Sandy contourite drift in the late Miocene Rifian Corridor (Morocco): Reconstruction of depositional environments in a foreland-basin seaway. *Sed. Geol.*, 355, 31-57.
- Chalouan, A., Michard, A., El Kadiri, K., Negro, F., de Lamotte, D.F., Soto, J.I., & Saddiqi, O. (2008). The Rif Belt. In *Continental evolution: the geology of Morocco* (pp. 203-302). Springer Berlin Heidelberg.
- Chiarella, D. (2016). Angular and tangential toset geometry in tidal cross-strata: An additional feature of current-modulated deposits.
- Chiarella, D., Moretti, M., Longhitano, S.G., & Muto, F. (2016). Deformed cross-stratified deposits in the Early Pleistocene tidally-dominated Catanzaro strait-fill succession, Calabrian Arc (Southern Italy): triggering mechanisms and environmental significance. *Sedimentary Geology*, 344, 277-289.
- Chiarella, D., Longhitano, S.G., Tropeano, M. (2017). Types of mixing and heterogeneities in siliciclastic-carbonate sediments. *Mar. Petrol. Geol.*, 88, 617-627.
- de Castro, S., Hernández-Molina, F.J., Rodríguez-Tovar, F.J., Llave, E., Ng, Z.L., Nishida, N., Mena, A. (2020a). Contourites and bottom current reworked sands: Bed

- facies model and implications. *Mar. Geol.*, 428, 106267.
- de Castro, S., Hernández-Molina, F.J., de Weger, W., Jiménez-Espejo, F.J., Rodríguez-Tovar, F.J., Mena, A., Llave, E., Sierro, F.J. (2020b). Contourite characterisation and its discrimination from other deep-water deposits in the Gulf of Cadiz contourite depositional system. *Sedimentology*.
- de Weger, W., Hernández-Molina, F.J., Flecker, R., Sierro, F.J., Chiarella, D., Krijgsman, W., Manar, M.A. (2020). Late Miocene contourite channel system reveals intermittent overflow behavior. *Geology*, 48(12), 1194-1199.
- de Weger, W., Hernández-Molina, F.J., Miguez-Salas, O., de Castro, S., Miguel, B., Chiarella, D., Sierro, F.J., Blackburn, G., Manar, M. (2021). Sedimentary evolution of a laterally migrating contourite depositional system – a case study from the late Miocene Rifian Corridor, Morocco. *Sedimentology*. In review.
- Duan, T., Gao, Z., Zeng, Y., & Stow, D. (1993). A fossil carbonate contourite drift on the Lower Ordovician palaeocontinental margin of the middle Yangtze Terrane, Jiuxi, northern Hunan, southern China. *Sedimentary Geology*, 82(1-4), 271-284.
- Ellison, T.H., & Turner, J.S. (1959). Turbulent entrainment in stratified flows. *Journal of Fluid Mechanics*, 6(3), 423-448.
- Engelund, F. (1970). Instability of erodible beds. *Journal of Fluid Mechanics*, 42(2), 225-244.
- Expedition 339 Scientists, 2012. Site U1389 Summary. In: IODP Expedition 339: Mediterranean Outflow. Site Summaries. International Ocean Discovery Program.
- Faugères, J.C., Stow, D.A.V., Imbert, P., Viana, A. (1999). Seismic features diagnostic of contourite drifts. *Mar. Geol.*, 162(1), 1-38.
- Faugères, J.C., & Stow, D.A.V. (2008). Contourite drifts: nature, evolution and controls. *Developments in sedimentology*, 60, 257-288.
- Fedele, J.J., Hoyal, D., Barnaal, Z., Tulenko, J., & Awalt, S. (2016). Bedforms created by gravity flows. *Autogenic dynamics and self-organization in sedimentary systems*, 106, 95-121.
- Feinberg, H. (1986). Les séries tertiaires des zones externes du Rif (Maroc): biostratigraphie, paléogéographie et aperçu tectonique. *Éditions du Service géologique du Maroc*, (No. 315).
- Flecker, R., Krijgsman, W., Capella, W., de Castro Martins, C., Dmitrieva, E., Maysers, J.P., Marzocchi, A., Modestou, S., Ochoa, D., Simon, D., Tulbure, M., van den Berg, B., van der Schree, M., de Lange, G., Ellam, R., Govers, R., Gutjahr, M., Hilgen, F., Kouwenhoven, T., Lofi, J., Meijer, P., Sierro, F.J., Bachiri, N., Barhoun, N., Alami, A.C., Chacon, B., Flores, J. A., Gregory, J., Howard, J., Lunt, D., Ochoa, M., Pancost, R., Vincent, S., Yousfi, M.Z. (2015). Evolution of the Late Miocene Mediterranean–Atlantic gateways and their impact on regional and global environmental change. *Earth-Sci. Rev.*, 150, 365–392.
- Flinch, J. (1993). Tectonic evolution of the Gibraltar arc [Ph.D. thesis]: Houston. *Rice University*.
- García, M., Hernández-Molina, F.J., Llave, E., Stow, D.A.V., León, R., Fernández-Puga, M.C., ... & Somoza, L. (2009). Contourite erosive features caused by the Mediterranean Outflow Water in the Gulf of Cadiz: Quaternary tectonic and oceanographic implications. *Marine Geology*, 257(1-4), 24-40.
- García-Castellanos, D., Estrada, F., Jiménez-Munt, I., Gorini, C., Fernández, M., Vergés, J., De Vicente, R. (2009). Catastrophic flood of the Mediterranean after the Messinian salinity crisis. *Nature*, 462(7274), 778-781.
- Gladstone, R., Flecker, R., Valdes, P., Lunt, D., & Markwick, P. (2007). The Mediterranean hydrologic budget from a Late Miocene global climate simulation. *Palaeogeography, Palaeoclimatology, Palaeoecology*, 251(2), 254-267.
- Gong, C., Peakall, J., Wang, Y., Wells, M.G., Xu, J. (2017). Flow processes and sedimentation in contourite channels on the northwestern South China Sea margin: A joint 3D seismic and oceanographic perspective. *Mar. Geol.*, 393, 176-193.
- Gonthier, E.G., Faugères, J.C., Stow, D.A.V. (1984). Contourite facies of the Faro drift, Gulf of Cadiz. *J. Geol. Soc. London, Special Publications*, 15(1), 275-292
- Harris, P.T., and Whiteway, T., 2011. Global distribution of large submarine canyons: geomorphic differences between active and passive continental margins. *Marine Geology* 285, 69–86.
- Hernández-Molina, F.J., Llave, E., Stow, D.A.V., García, M., Somoza, L., Vázquez, J.T., ... & Gardner, J. (2006). The contourite depositional system of the Gulf of Cadiz: a



- sedimentary model related to the bottom current activity of the Mediterranean outflow water and its interaction with the continental margin. *Deep Sea Research Part II: Topical Studies in Oceanography*, 53(11-13), 1420-1463.
- Hernández-Molina, F.J., Llave, E., Preu, B., Ercilla, G., Fontan, A., Bruno, M., Serra, N., Gomiz, J.J., Brackenridge, R.E., Sierro, F.J., Stow, D.A.V., Garcia, M., Juan, C., Sandoval, N., Mrnaliz, A. (2014a). Contourite processes associated with the Mediterranean Outflow Water after its exit from the Strait of Gibraltar: Global and conceptual implications. *Geology*, 42(3), 227-230.
- Hernández-Molina, F.J., Stow, D.A.V., Alvarez-Zarikian, C.A., Acton, G., Bahr, A., Balestra, B., Ducassou, E., Flood, R., Flores, J.A., Furota, S., Grunert, P., Hodell, D., Jimenez-Espejo, F., Kim, J.K., Krissek, L., Kuroda, J., Li, B., Llave, E., Lofi, J., Lourens, L., Miller, M., Nanayama, F., Nishida, N., Richter, C., Roque, C., Pereira, H., Sanchez Goñi, M.F., Sierro, F.J., Singh, A.D., Sloss, C., Takashimizu, Y., Tzanova, A., Voelker, A.H.L., Williams, T., Xuan, C. (2014b). Onset of Mediterranean outflow into the North Atlantic. *Science*, 344(6189), 1244-1250.
- Hernández-Molina, F.J., Soto, M., Piola, A.R., Tomasini, J., Preu, B., Thompson, P., Badalini, G., Creaser, A., Violante, R.A., Morales, E., Paterlini, M., De Santa Ana, H. (2016a). A contourite depositional system along the Uruguayan continental margin: sedimentary, oceanographic and paleoceanographic implications. *Mar. Geol.*, 378, 333-349.
- Hilgen, F.J., Bissoli, L., Iaccarino, S., Krijgsman, W., Meijer, R., Negri, A., Villa, G. (2000). Integrated stratigraphy and astrochronology of the Messinian GSSP at Oued Akrech (Atlantic Morocco). *Earth Planet. Sci. Lett.*, 182(3-4), 237-251.
- Hovikoski, J., Uchman, A., Weibel, R., Nøhr-Hansen, H., Sheldon, E., Ineson, J., Bjerager, M., Therkelsen, J., Olivarius, M., Larsen, M., Alsen, P., Bojesen-Koefoed, J. (2020). Upper Cretaceous bottom current deposits, north-east Greenland. *Sedimentology*. <https://doi.org/10.1111/sed.12764>
- Hsü, K.J., Ryan, W.B., Cita, M.B. (1973). Late Miocene desiccation of the Mediterranean. *Nature*, 242 (5395), 240-244.
- Hsü, K.J., Montadert, L., Bernoulli, D., Cita, M.B., Erickson, A., Garrison, R.E., Kidd, R.B., Mèlières, F., Müller, C., Wright, R. (1977). History of the Mediterranean salinity crisis. *Nature*, 267(5610), 399-403.
- Hüneke, H., Hernández-Molina, F., Rodríguez-Tovar, F., Llave, E., Chiarella, D., Mena, A. and Stow, D. (2020), Diagnostic criteria using microfacies for calcareous contourites, turbidites and pelagites in the Eocene–Miocene slope succession, southern Cyprus. *Sedimentology*. Accepted Author Manuscript. doi:[10.1111/sed.12792](https://doi.org/10.1111/sed.12792)
- Ichaso, A.A., Dalrymple, R.W. (2009). Tide- and wave-generated fluid mud deposits in the Tilje Formation (Jurassic), offshore Norway. *Geology*, 37(6), 539-542.
- Iribarren, L., Vergés, J., Fernández, M. (2009). Sediment supply from the Betic–Rif orogen to basins through Neogene. *Tectonophysics*, 475(1), 68-84.
- Janocko, M., Nemeč, W., Henriksen, S., & Warchol, M. (2013). The diversity of deep-water sinuous channel belts and slope valley-fill complexes. *Marine and Petroleum Geology*, 41, 7-34.
- Kennedy, J.F. (1969). The formation of sediment ripples, dunes, and antidunes. *Annual review of fluid mechanics*, 1, 147-168.
- Kolla, V., Posamentier, H.W., & Wood, L.J. (2007). Deep-water and fluvial sinuous channels—Characteristics, similarities and dissimilarities, and modes of formation. *Marine and Petroleum Geology*, 24(6-9), 388-405.
- Krijgsman, W., Capella, W., Simon, D., Hilgen, F.J., Turbure, M.A., van den Berg, C., van der Schee, M., Flecker, R. (2018). The Gibraltar corridor: Watergate of the Messinian salinity crisis. *Mar. Geol.*, 403, 238-246.
- Kröncke, I. (2006) Structure and function of macrofaunal communities influenced by hydrodynamically controlled food availability in the Wadden Sea, the open North Sea, and the deep-sea. A synopsis. *Senckenbergiana maritima*, 36, 123–164.
- Kuhlbrodt, T., Griesel, A., Montoya, M., Levermann, A., Hofmann, M., & Rahmstorf, S. (2007). On the driving processes of the Atlantic meridional overturning circulation. *Reviews of Geophysics*, 45(2).
- Llave, E., Schönfeld, J., Hernández-Molina, F.J., Mulder, T., Somoza, L., Del Río, V.D., &

- Sánchez-Almazo, I. (2006). High-resolution stratigraphy of the Mediterranean outflow contourite system in the Gulf of Cadiz during the late Pleistocene: the impact of Heinrich events. *Marine Geology*, 227(3-4), 241-262.
- Llave, E., Hernández-Molina, F.J., García, M., Ercilla, G., Roque, C., Juan, C., ... & Stow, D. (2020). Contourites along the Iberian continental margins: conceptual and economic implications. *Geological Society, London, Special Publications*, 476(1), 403-436.
- Leeder, M. R. (2009) *Sedimentology and sedimentary basins: from turbulence to tectonics*. John Wiley & Sons.
- Lirer, F., Foresi, L.M., Iaccarino, S.M., Salvadorini, G., Turco, E., Cosentino, C., ... & Caruso, A. (2019). Mediterranean Neogene planktonic foraminifer biozonation and biochronology. *Earth-Science Reviews*, 196, 102869.
- Liu, H.K. (1957). Mechanics of sediment-ripple formation. *Journal of the Hydraulics Division*, 83(2), 1197-1.
- Longhitano, S.G., Nemeč, W. (2005). Statistical analysis of bed-thickness variation in a Tortonian succession of biocalcarenic tidal dunes, Amantea Basin, Calabria, southern Italy. *Sed. Geol.*, 179(3-4), 195-224.
- Longhitano, S.G., Mellere, D., Steel, R.J., Ainsworth, R.B. (2012). Tidal depositional systems in the rock record: a review and new insights. *Sed. Geol.*, 279, 2-22.
- Martín-Chivelet, J., Fregenal-Martínez, M.A., Chacón, B. (2008). Traction structures in contourites. *Dev. Sedimentol.*, 60, 157-182.
- McKee, E.D., Reynolds, M.A., & Baker Jr, C.H. (1962). 164. Laboratory studies on deformation in unconsolidated sediment. *US Geological Survey Professional Paper*, 151.
- Mézerai, M.L., Faugères, J.C., Figueiredo Jr, A.G., & Massé, L. (1993). Contour current accumulation off the Vema Channel mouth, southern Brazil Basin: pattern of a "contourite fan". *Sedimentary Geology*, 82(1-4), 173-187.
- Michard, A., Saddiqi, O., Chalouan, A., & de Lamotte, D.F. (Eds.). (2008). *Continental evolution: The geology of Morocco: Structure, stratigraphy, and tectonics of the Africa-Atlantic-Mediterranean triple junction* (Vol. 116). Springer.
- Miguez-Salas, O., & Rodríguez-Tovar, F.J. (2020). Trace fossil analysis of sandy clastic contouritic deposits in the late Miocene Rifian Corridor (Morocco): Ichnotaxonomical and palaeoenvironmental insights. *Journal of African Earth Sciences*, 104054.
- Miguez-Salas, O., Rodríguez-Tovar, F.J., & De Weger, W. (2020). Macaronichnus and contourite depositional settings: Bottom currents and nutrients as coupling factors. *Palaeogeography, Palaeoclimatology, Palaeoecology*, 545, 109639.
- Millot, C. (1999). Circulation in the western Mediterranean Sea. *Journal of Marine Systems*, 20(1-4), 423-442.
- Mulder, T. (2011). Gravity processes and deposits on continental slope, rise and abyssal plains. In *Dev.Sedimentol.*, (Vol. 63, pp. 25-148). Elsevier.
- Mutti, E. (1992). *Turbidite sandstones*. Agip, Istituto di geologia, Università di Parma.
- Mutti, E., Bernoulli, D., Lucchi, F. R., Tinterri, R. (2009). Turbidites and turbidity currents from Alpine 'flysch' to the exploration of continental margins. *Sedimentology*, 56(1), 267-318.
- Mutti, E., & Carminatti, M. (2012). Deep-water sands of the Brazilian offshore basins: Search and Discovery.
- Owen, G. (1996). Experimental soft-sediment deformation: structures formed by the liquefaction of unconsolidated sands and some ancient examples. *Sedimentology*, 43(2), 279-293.
- Owen, G. (1995). Soft-sediment deformation in upper Proterozoic Torridonian sandstones (Applecross Formation) at Torridon, northwest Scotland. *Journal of Sedimentary Research*, 65(3a), 495-504.
- Paulat, M., Lüdmann, T., Betzler, C., Eberli, G. P. (2019). Neogene palaeoceanographic changes recorded in a carbonate contourite drift (Santaren Channel, Bahamas). *Sedimentology*, 66(4), 1361-1385.
- Parker, G. (2008). Transport of gravel and sediment mixtures. In *Sedimentation engineering: Processes, measurements, modeling, and practice* (pp. 165-251).
- Piper, D. J., & Normark, W. R. (1983). Turbidite depositional patterns and flow characteristics, Navy submarine fan, California Borderland. *Sedimentology*, 30(5), 681-694.

- Rahmstorf, S. (2006). Thermohaline ocean circulation. *Encyclopedia of quaternary sciences*, 5.
- Reading, H.G. (Ed.). (2009). *Sedimentary environments: processes, facies and stratigraphy*. John Wiley & Sons.
- Rebesco, M., Hernández-Molina, F.J., Van Rooij, D., Wåhlin, A. (2014). Contourites and associated sediments controlled by deep-water circulation processes: state-of-the-art and future considerations. *Mar. Geol.*, 352, 111-154.
- Rodríguez-Tovar, F.J., & Aguirre, J. (2014). Is Macaronichnus an exclusively small, horizontal and unbranched structure? *Macaronichnus segregatis degiberti* subsp. nov. *Spanish Journal of Palaeontology*, 29(2), 131-142.
- Rogerson, M., Rohling, E.J., Bigg, G.R., Ramirez, J. (2012). Paleoceanography of the Atlantic-Mediterranean exchange: Overview and first quantitative assessment of climatic forcing. *Rev. Geophys.*, 50(2), RG2003.
- Rohling, E.J., Marino, G., Grant, K.M. (2015). Mediterranean climate and oceanography, and the periodic development of anoxic events (sapropels). *Earth Sci. Rev.*, 143, 62-97.
- Roldán, F.J., Galindo-Zaldívar, J., Ruano, P., Chalouan, A., Pedrera, A., Ahmamous, M., Ruiz-Constan, A., Sanz de Galdeano, C., Benmakhlof, M., Lopez-Garrido, A.C., Anahnah, F., Gonzalez-Castillo, L. (2014). Basin evolution associated to curved thrusts: The Prerif Ridges in the Volubilis area (Rif Cordillera, Morocco). *J. Geodynamics*, 77, 56-69.
- Raudkivi, A.J. (1976). *Loose Boundary Hydraulics* Pergamon.
- Ryan, W.B.F., Hsü, K.J. (1973). Initial reports of the deep-sea drilling project, 13, US Govt. *Printing Office, Washington, D. C.*
- Sánchez-Leal, R.F., Bellanco, M.J., Fernández-Salas, L.M., García-Lafuente, J., Gasser-Rubinat, M., González-Pola, C., ... & Sánchez-Garrido, J.C. (2017). The Mediterranean Overflow in the Gulf of Cadiz: A rugged journey. *Science advances*, 3(11), eaao0609.
- Sani, F., Del Ventisette, C., Montanari, D., Bendkik, A., Chenakeb, M. (2007). Structural evolution of the Rides Prerifaines (Morocco): structural and seismic interpretation and analogue modelling experiments. *Int. J. Earth Sci.*, 96(4), 685-706.
- Seike, K., Yanagishima, S.I., Nara, M., & Sasaki, T. (2011). Large Macaronichnus in modern shoreface sediments: Identification of the producer, the mode of formation, and paleoenvironmental implications. *Palaeogeography, Palaeoclimatology, Palaeoecology*, 311(3-4), 224-229.
- Shanmugam, G. (2010). Slides, slumps, debris flow, and turbidity currents. *Ocean Currents: A Derivative of the Encyclopedia of Ocean Sciences*, 20, 418.
- Shanmugam, G. (2017). The contourite problem. In *Sediment provenance*, 183-254. Elsevier.
- Sierro, F.J., Flores, J.A., Civis, J., Gonza, J.A., France, G. (1993). Late Miocene globorotaliid event-stratigraphy and biogeography in the NE-Atlantic and Mediterranean. *Mar. Micropaleontol.*, 21(1-3), 143-167.
- Sierro, F.J., Flores, J.A., Zamarreno, I., Vázquez, A., Utrilla, R., Francés, G., ... & Krijgsman, W. (1999). Messinian pre-evaporite sapropels and precession-induced oscillations in western Mediterranean climate. *Marine Geology*, 153(1-4), 137-146.
- Sierro, F.J., Hilgen, F.J., Krijgsman, W., Flores, J.A. (2001). The Abad composite (SE Spain): a Messinian reference section for the Mediterranean and the APTS. *Palaeogeogr. Palaeoclimatol. Palaeoecol.*, 168(1-2), 141-169.
- Simon, D., Marzocchi, A., Flecker, R., Lunt, D. J., Hilgen, F.J., & Meijer, P.T. (2017). Quantifying the Mediterranean freshwater budget throughout the late Miocene: New implications for sapropel formation and the Messinian Salinity Crisis. *Earth and Planetary Science Letters*, 472, 25-37.
- Southard, J.B., & Boguchwal, L.A. (1990). Bed configuration in steady unidirectional water flows; Part 2, Synthesis of flume data. *Journal of Sedimentary Research*, 60(5), 658-679.
- Stow, D.A.V., Hernández-Molina, F.J., Llave, E., Sayago-Gil, M., Díaz del Río, V., Branson, A. (2009). Bedform-velocity matrix: the estimation of bottom current velocity from bedform observations. *Geology*, 37(4), 327-330.
- Stow, D.A.V., Hernández-Molina, F.J., Llave, E., Bruno, M., García, M., del Río, V.D., Somoza, L., Brackenridge, R.E. (2013). The Cadiz Contourite Channel: Sandy contourites, bedforms and dynamic

- current interaction. *Mar. Geol.*, 343, 99-114.
- Stow, D.A.V, Hernández-Molina, F.J., Llave, E., Sayago-Gil, M., Díaz del Río, V., Branson, A. (2009). Bedform-velocity matrix: the estimation of bottom current velocity from bedform observations. *Geology*, 37(4), 327-330.
- Straume, E.O., Gaina, C., Medvedev, S., Nisancioglu, K.H. (2020). Global Cenozoic Paleobathymetry with a focus on the Northern Hemisphere Oceanic Gateways. *Gondwana Research*.
- Streeter, V.L., & Kestin, J. (1961). Handbook of fluid dynamics. *Journal of Applied Mechanics*, 28(4), 640.
- Talling, P.J., Masson, D.G., Sumner, E.J., Malgesini, G. (2012). Subaqueous sediment density flows: Depositional processes and deposit types. *Sedimentology*, 59(7), 1937-2003.
- Van den Berg, J.H., & Van Gelder, A. (1993). A new bedform stability diagram, with emphasis on the transition of ripples to plane bed in flows over fine sand and silt. *Special Publications of the International Association of Sedimentologists*, 17, 11-21.
- van Rijn, L.C. (1984). Sediment transport, part III: bed forms and alluvial roughness. *Journal of hydraulic engineering*, 110(12), 1733-1754.
- Viana, A.R., Almeida, W., Nunes, M.C.V., & Bulhões, E.M. (2007). The economic importance of contourites. *Geological Society, London, Special Publications*, 276(1), 1-23.
- Viana, A.R. (2008). Economic relevance of contourites. *Developments in Sedimentology*, 60, 491-510.
- Walker, R.G. (1978). Deep-water sandstone facies and ancient submarine fans: models for exploration for stratigraphic traps. *AAPG Bulletin*, 62(6), 932-966.
- Weimer, P., Slatt, R.M., Bouroullec, R., Fillon, R., Pettingill, H., Pranter, M., Tari, G., 2006. Deepwater-Reservoir Elements: Channels and Their Sedimentary Fill, Introduction to the Petroleum Geology of Deepwater Setting. *American Association of Petroleum Geologists*, v. 5. <https://doi.org/10.1306/St571314>
- Wernli, R. (1988). Micropaléontologie du Néogène post-nappes du Maroc septentrional et description systématique des foraminifères planctoniques. *Notes et Mémoires du Service géologique*, 331.
- Wetzel, A. (2008) Recent bioturbation in the deep South China Sea: a uniformitarian ichnologic approach. *Palaios*, 23, 601–615.
- Wynn, R.B., Cronin, B.T., Peakall, J., 2007. Sinuous deep-water channels: Genesis, geometry and architecture. *Marine and Petroleum Geology*, v24 (6–9): 341-387. <https://doi.org/10.1016/j.marpetgeo.2007.06.001>.
- Yalin, M.S.(1977). *Mechanics of sediment transport*. Pergamon. and early results. *Sediment. Geol*, 15, 1-53.

# *Chapter VIII*

## *General Discussion and Conclusions*

(i) What are the main contributions of this research project?

The foremost contribution of this research project is the first ever recognition and detailed description of a Contourite Channel System in outcrop. The recognition of this late Miocene contourite channel system in the Rifian Corridor allowed for subsequent and more detailed studies regarding climatic, oceanographic, sedimentological, and economical implications. Furthermore, the processes that control contourite erosional and depositional systems could be deducted. The synthesis of all results allowed for the proposal of new contourite facies models which provides a conceptual framework for contourite recognition and understanding the behavior and sedimentological evolution of sand prone contourite channel systems.

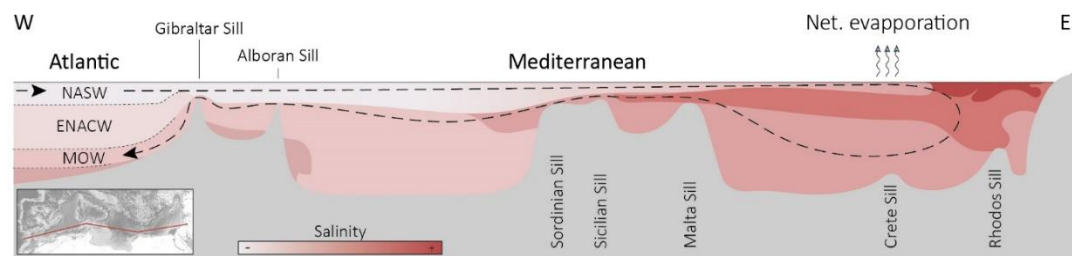


**Figure 8.1.** Zonal section of the salinity (“density”) distribution along the axis of the Levantine intermediate current (simplified after Wüst, 1961; Pinardi et al., 2019). ENACW stands for Eastern North Atlantic Central Water. Note that this section is based on data from the winter season. The salinity distribution differs slightly during the summer season.

(ii) How are contourite channel systems formed?

The Rifian Corridor and the Gulf of Cadiz contourite systems are formed by the overflow of dense Mediterranean Outflow Water. The restricted Atlantic-Mediterranean connections allow for the two-way exchange between the water masses occurrent on both sides. This exchange is hindered by the presence of a submerged topographic high, the Taza-Sill (Capella et al., 2017a) and the Camarinal Sill (Baringer and Price, 1999; Legg et al., 2009) for the Rifian Corridor and the Strait of Gibraltar, respectively. The sills particularly affect the exchange of water-masses with thermoclines that are deeper than the top of the sill, trapping them on either side of the sill. At times when the net loss of water in the Mediterranean region is higher compared to the Atlantic, inflow of the surficial water-mass from the Atlantic, the North Atlantic Surficial Water (NASW), is forced through the corridors into the Mediterranean. This NASW thus “continuously” replenished the Mediterranean. Net evaporation and cooling in the eastern Mediterranean increases the density of Mediterranean surface water (Straume et al., 2020), forcing this water to sink trough, and

ventilate the Mediterranean water column (Fig. 8.1), a process known as intermediate and deep-water formation (*Millot, 1999; Candela, 2001*) or Mediterranean Overturning Circulation (*e.g. Wüst, 1961; Armi and Farmer, 1988; Pinardi et al., 2019*). The formation of these deeper water-masses resulted in increased density gradients between the Mediterranean and the Atlantic waters which drives anti-estuarine exchange (*Rohling et al., 2015; Simon et al., 2017*). If the sill falls below the resulting thermocline (Fig. 8.2), a concentrated, dense MOW cascades over the sill. This MOW follows the bathymetry of the seafloor downwards, deflected towards the right (north) in the northern hemisphere by the Coriolis Force, until the water-mass of the MOW reaches a depth coinciding with a water-mass of a higher density. When the MOW reaches this depth, the water mass of the MOW starts to override this denser water-mass, no longer being attached to the seafloor. In the area where the MOW water-mass, or other over-flow related water-mass, flows over the seafloor as a semi-permanent, semi-unidirectional bottom current it can generate a contourite channel system. A contourite channel system results from the pathways and transformations of dense water overflow which depends on small-scale interactions between flow dynamics and erosional and depositional processes (*Sánchez-Leal et al., 2017*).

### (iii) What are the main control factors of overflow induced contourite channel systems?

As briefly introduced in the previous paragraph, the main element which controls the formation of overflow water is the presence of a submerged barrier, or sill, which separates two bodies of water. The morphology of this sill and its depth with respect to thermoclines controls the initiation and behavior of overflow (Fig. 8.2, *Chapter IV; de Weger et al., 2020*). When the interface of the overriding water-mass and the overflow water is well above the sill this intensifies the inflow of Atlantic water which hampers the formation of a significant density gradient between the two water-masses, decelerating the current velocity of overflow water. When the interface of the overriding water-mass and the overflow water is below the sill, overflow is brought to a halt. An intermediate elevation of the interface above the sill allows for the acceleration of overflow water (*Chapter V; de Weger et al., 2021a*). The morphology of the sill, and in part the depth of the sill, are controlled by tectonic processes, making them the primary control factor of overflow induced contourite channel systems. Furthermore, tectonic activity and reorganization of the slope likely triggers the migration of



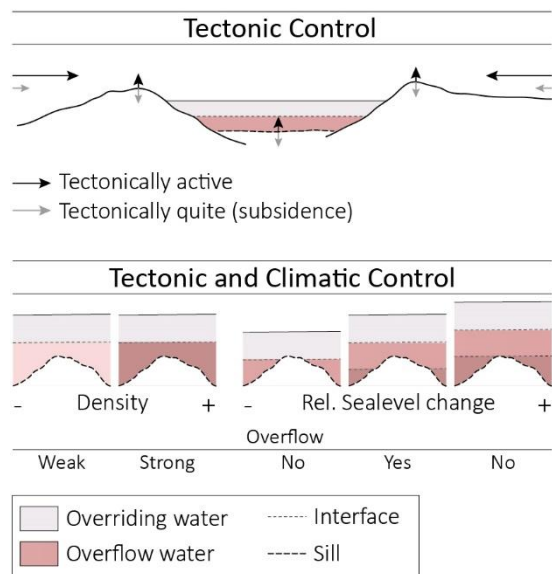


**Figure 8.2.** Schematic diagrams of the primary effects on overflow induced by tectonic activity and climate

aridity increases the density of Mediterranean Deep Water (Llave et al., 2006). A higher density contrast between overriding- and overflow-water intensifies overflow. Furthermore, due to increased/decreased densities of the overflow-water this water settles deeper/shallower in the Atlantic as the interface with Atlantic water-masses becomes deeper/shallower. Not only does this affect the behavior of overflow, but it is also responsible for the migration of contourite elements (Chapter IV, V and VII; de Weger et al., 2020, 2021a, 2021c?). These climatic induced changes in overflow behavior range from (ky) orbitally controlled to seasonal changes (yr) in climatic conditions (e.g. Llave et al., 2006; Gladstone et al., 2007; Pinardi et al., 2019). Furthermore, like tectonically induced changes in the elevation of the sill, climatic induced sea-level changes also affect the elevation of the interface between water-masses with respect to the sill, controlling the overflow behavior in a similar fashion.

Primarily based on the findings of this research project, the observation of tidal signatures in outcrop, tides have been identified to play a role in controlling overflow behavior (Chapter V; de Weger et al., 2021a). Semidiurnal tides within the strait reach large amplitudes forming the dominant factor in flow variability, strongly modulating the long-term exchange pattern, more significantly than atmospheric pressure fields and internal waves (Candela et al., 1991). The tidal forcing and its effects on overflow water have been extensively studied and analyzed for the Strait of Gibraltar (e.g. Farmer and Armi, 1986; Bryden and Kinder, 1988; Candela et al., 1989, 1990; Wang, 1993; Bryden et al., 1994; Helfrich, 1995; Bruno et al., 2000; Lafuente et al., 2000; Tsimplis and Bryden, 2000; Bascheck et al., 2001; Sannino et al., 2004).

contourite channel systems. Tectonically induced slope instability likely resulted in enhanced sediment supply (Chapters IV, V and VII; de Weger et al., 2020, 2021a, 2021c?).

Besides tectonic activity controlling the behavior of overflow, climatic processes also play a significant role. Observations from the Gulf of Cadiz Contourite Channel System (GoCCS) have shown that stronger overflow is associated to higher aridity in the Mediterranean region. This increase in

Tides accelerate and decelerate the overflow water between high- and low-tide and between low – and high-tide respectively (*Chapter V; de Weger et al., 2021a*).

All main processes responsible for controlling overflow as described above are interrelated, influencing one-another. Because of this it is hard to pin-point the dominant process based on sedimentological characteristics.

#### (iv) Which features make up a contourite system?

The Gulf of Cadiz contourite depositional system, the modern analogue for the sections studied in the Rifian Corridor, is composed of both depositional and erosive features which have a specific location along the margin. The main depositional features of this contourite systems are characterised by sedimentary wave fields, sedimentary lobes and contourite drifts. The main erosional features are contourite channels, furrows, moats, and marginal valleys, which are the product of both gravitational currents and bottom currents (Fig. 8.4). Based on these features, five morphosedimentary sectors have been identified within the contourite depositional system, from east to west: (1) proximal scour and sand ribbons; (2) overflow sedimentary lobe; (3) channels and ridges; (4) active contourite drifts; and (5) submarine canyons. The distribution of these features is primarily related to the systematic deceleration of the MOW as it flows westwards (*Llave et al., 2001, 2006; Habgood et al., 2003; Hernández-Molina et al., 2003, 2006*).

The systematic deceleration of overflow water is a result of four main factors (*Johnson et al., 1994*): (1) turbulent stresses arising from bottom friction and entrainment, (2) a decreasing density anomaly which reduces the pressure force of the outflow, (4) the deflection by the Coriolis force, deflecting the current along the slope rather than directly down-slope and, (4) the frictional effect of the channel floor. The local velocity of overflow is conditioned by bathymetry, a key factor in the development of different elements of the contourite depositional system (*Hernández-Molina et al., 2006*). As the morphosedimentary sectors identified in the Gulf of Cadiz, are primarily a remnant of the overflow characteristics since the quaternary, their location was likely different under the overflow water characteristics during the late Miocene. Their distribution however, for a large part, still reflects the down current changes in sector evolution related to the generalized down-current deceleration of overflow water. With respect to the overflow characteristics of the modern GoCCS, increased overflow activity, because of a higher density gradient, would shift the depositional sectors further away from the point of overflow as flow velocities are higher.

The system would shift down slope due to the overflow water being of higher specific density. With decreased overflow activity the depositional sectors would migrate closer to the point of overflow and the system would shift up-slope.

The Gulf of Cadiz hosts a very pronounced contourite depositional system related to very strong, vigorous bottom currents as density gradients of overflow water are extremely high. Contourite features however have been described, in increasing intensity, for other areas in the Atlantic Ocean, the Mediterranean, Indian, Pacific, Arctic, and Antarctic realms as well (*Rebesco et al., 2014 and references therein*). Most of the described large contourite depositional and erosional features extend from the upper slope/outer shelf, continental rises, abyssal plains and around banks, seamounts, etc (*Hernández-Molina et al., 2008a, b*). Contourite features are significantly controlled by the physiographic and geological setting in which they develop and by different water masses and their differing characteristics, flowing at different depths, different velocities and in the same or opposite directions (*Rebesco et al., 2014 and references therein*). Like in the Gulf of Cadiz, systems that are persistently affected by bottom-currents and associated oceanographic processes show erosional and depositional features. These features can be isolated but are more likely to be part of contourite depositional systems, consisting of various drifts and related erosional features where along-slope processes dominate (*Hernández-Molina et al., 2003, 2008a, 2009*). The erosional and depositional features produced by bottom-currents range in scale from small bedforms to large, more than 100 km wide, up to kilometres long and up to 2 km thick features. Contourite systems however can also be influenced by other deep-water processes and therefore do not necessarily form individual sedimentary bodies.

The best compilation of contourite features, associated sediments, and deep-water circulation processes for the entire spectrum of contourite systems can be found in *Rebesco et al., 2014*. New insights in mixed systems and associated sedimentary features are best described in the works of *Fonessu et al. (2020)*, *Fuhrmann et al. (2020)* and the dissertation of *Rodrigues et al. (2020, 2021 - thesis)*.

#### (v) What characterizes contourite channels and moats?

Contourite channels are part of the erosional features of contourite depositional systems. Erosional features typically occur in association with contourite drifts (*Faugères et al., 1999; Stow and Mayall, 2000; Rebesco et al., 20014*) but can mainly be found in continental slopes (*Viana, 2001; Hernández-Molina et al., 2003, 2006a, 2009; Ercilla et al., 2011; Rebesco et al.,*

20014). Two main types of large-scale erosional features are classified: areal and linear (Hernández-Molina et al., 2008b; García et al., 2009).

Contourite channels, like moats and marginal valleys (Fig. 8.3) are erosional types related to large scale linear erosional features (Hernández-Molina et al., 2008b). Contourite channels are erosional features trending parallel to the margin (or obliquely) that are formed mainly by the action of bottom currents. These channels are characterised by the presence of truncated reflections. Contourite moats are channels trending parallel to the slope. They differ from contourite channels in their genetic relationship with giant, elongated, mounded, and separated contourite drifts. They can be present in the upper, middle, and lower slope. Marginal valleys (scours or troughs) are elongate erosional depressions generated by the effects of a current impinging against and around topographic elevations as well as gravitational currents, they are however thought to mainly be the product of turbulent gravitational processes (Ref.). Rebesco et al. (2014), argued that, since these distinctions are mainly developed from observations in the Gulf of Cadiz, Antarctica and Argentine basins, more detailed knowledge is required on erosional features, associated oceanographic processes and, the genetic spatial and vertical relationships between erosional and depositional features.

Bedforms, related to bottom-currents have previously been divided into two types based on their spatial relationship to the flow: longitudinal, which are elongated parallel to the flow (essentially erosional), and transverse, which are considered depositional features (Rebesco et al., 2014). Stow et al. (2009, 2013a) described that both the longitudinal and transverse bedforms are related to the velocity range of the bottom current in function of the mean grain size of the available sediments.

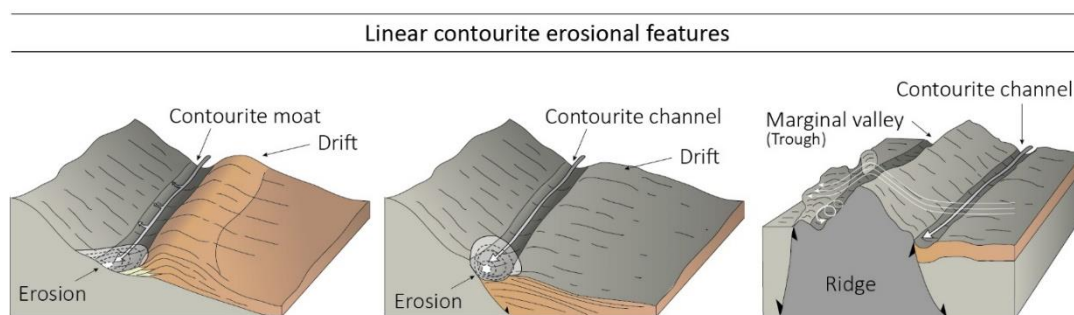


**Figure 8.3.** Main characteristics of linear, large-scale contourite erosional features. The three main types are contourite moats, contourite channels and marginal valleys. Modified from Hernández-Molina et al. (2008b).

Based on the synthesis by *Rebesco et al. (2014)*, longitudinal bedforms consist of: gravel stringers (e.g. *Hollister and McCave, 1984*), longitudinal triangular ripples (e.g. *Flood, 1981*), crag and tail (*Heezen and Hollister, 1964*), comet scours (*Masson et al., 2004*), ribbon marks (*Viana et al., 2007*), erosional furrows (*Flood, 1983; Masson et al., 2004; Stow et al., 2013a*), and, catastrophic high-energy scours (*Bulat and Long, 2001; Holmes et al., 2003; Stoker et al., 2003*). Transverse bedforms exist in various shapes and sizes, the smallest ones being ripples (e.g. *Stow et al., 2009*). Larger transverse bedforms are dunes (e.g. *Wynn and Stow, 2002*), sand waves (*Kuijpers et al., 1993*) and, sediment waves or mud waves (*Wynn and Stow, 2002; Stow et al., 2013a*).

The longitudinal bedforms have in common that they are erosional, not considering that bedforms related to the contourite channel can also be longitudinal, like the sandy transverse bedforms, deposited parallel to the flow within the contourite channel. Since *Stow et al. (2009, 2013a)* described that both the longitudinal and transverse bedforms are related to the velocity range of the bottom current in function of the mean grain-size of the available sediments, depositional bedforms should not necessarily be associated to large depositional features as they merely seem to encompass contourite drifts. Contourite drifts however are not formed by bottom-current velocities required to deposit large sandy bedforms.

Based on our findings (*Chapters IV, V, VI and VII; de Weger et al., 2020, 2021a, b, c*), contourite channels can be filled by sandy sediment, comprising a range of bedforms that are formed by the relation of flow velocity and available sediments mean grain-size as indicated by *Stow et al., (2009, 2013a)*. These bedforms are deposited parallel to the axis of the channel and should thus be grouped as longitudinal bedforms. In fact, the large sandy bedforms found in outcrop are solely found within the channel which is, confusingly, part of the erosional feature of contourites. As the contourite channel shows both a first order erosive channel, second order erosional features and channel fill sequences, the contourite channel is, intermittently, both erosive and depositional (*Chapter VII; de Weger et al., 2021c*).

## How can we improve on the terminology used for contourite depositional systems?

As became evident from working with contourite channel deposits, contourite terminology is regularly very confusing. As such I would like to propose to split contourite

depositional systems, which comprises all morphological and sedimentological features and bedforms associated to the persistent action of bottom currents, into different contourite domains (Fig. 8.4). These contourite domains are (1) the channelized domain, (2) the drift/channel transitional domain, (3) the drift domain, (4) the contouritic terrace, and, (5) the furrow domain. These domains comprise the full spectrum of contourite features, not separating them by erosional and depositional processes as both can occur within each domain. By example, contourite channels can either be erosional and depositional, contourite drifts show discontinuous sedimentation, reworking and winnowing, of which the latter two are also erosional processes. In the case of mixed-systems, contouritic domains can still be applied by adding the prefix “mixed-“ to the contourite domain in which they occur. In example, if a contourite drift is significantly affected by turbidity currents, or if turbidity currents are affected by bottom-currents in the drift, the sedimentary features are found in a mixed-drift domain. Alternatively, if a contourite channel is significantly affected by turbidity currents, or if turbidity currents are affected by a contouritic channel, the sedimentary features are found in a mixed-channelized contourite domain. If all elements of a bottom-current affected system are significantly affected by gravitational processes, we refer to this system as mixed-contourite depositional system, as for example is the case for marginal valleys.

#### (vi) How are contourite channel systems sourced with sediment?

The sediment source of contourite depositional systems can, in part, be deduced from the classification of contourite deposits as this classification of contourites is primarily based on their lithology and texture (*Stow and Lovell, 1979; Gonthier et al., 1984; Stow and Holbrook, 1984; Faugeres and Stow, 1993; Stow and Faugeres, 2008*). Muddy contourites are dominantly siliciclastic but commonly with some biogenic fraction. These components are in part locally derived, contain a pelagic contribution, and a fraction is far travelled. The local fraction results from reworking of previously deposited sediment or the erosion of a precursory lithology. The far travelled fraction is brought to the system by bottom currents, hyperpycnal flows (*e.g. Zavala, 2020*) and/or suspension fallout of a turbidity clouds (*e.g. de Castro et al., 2020a, b; Fonessu et al., 2020; Fuhrman et al., 2020*) or other gravity induced processes that can stir up muddy sediment, having an up-slope, up current sediment source. As for silty contourites, they are similar in many ways to muddy contourites and hence the processes that source the contourite depositional system with this sediment are also similar.

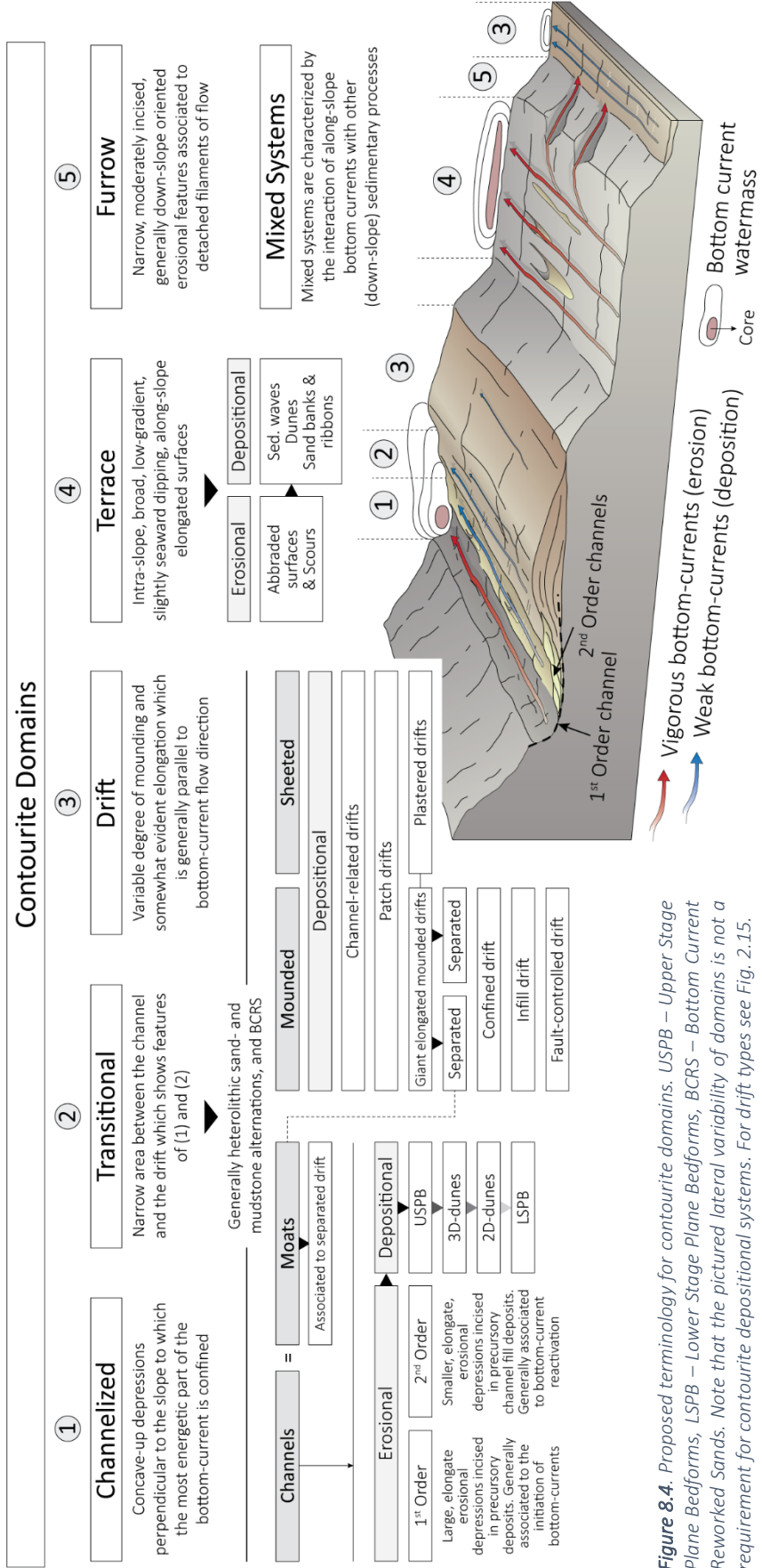


**Figure 8.4.** Proposed terminology for contourite domains. USPB – Upper Stage Plane Bedforms, LSPB – Lower Stage Plane Bedforms, BCRS – Bottom Current Reworked Sands. Note that the pictured lateral variability of domains is not a requirement for contourite depositional systems. For drift types see Fig. 2.15.



Sandy contourites are less likely to be far travelled parallel to the slope as this requires high velocity currents that need to be sustained for long distances. As such, the most likely, and generally accepted processes accountable for transporting sandy sediment to contourite depositional systems are gravitational processes. Within the contourites studied herein, large sandy slumps have been observed within the contourite channels that have been partially eroded (*Chapters IV and VII; de Weger et al., 2020, 2021c*) and sandy turbidites are common interbedded between the 1<sup>st</sup> order contourite channels or sandstone units. Less regularly, turbidite deposits are found within the channels as bottom current velocities were sufficiently high to winnow, erode and redeposit this sediment as contourite deposits. More likely than for muddy contourites, is the local sourcing of sandy sediment from reworking of previously deposited sediment or the erosion of a precursory lithology as current velocities required to deposit sandy sediments are higher. Evidence of local sourcing is found in the presence of Triassic bipyramidal quartz grains of the Keuper facies (*Herrero et al., 2020*) and middle Miocene white marl pellets (*Sani et al., 2007*), which were incorporated in the accretionary wedge against which the contourite channels are forced. The reworked dolomite rhombs are also derived from a precursory lithology, likely originating from carbonate lithologies of the Middle Atlas in the Taza-Sill region and thus, likely being far travelled down the contourite channel.

In conventional sequence stratigraphic models, deep-water clastic sediment supply is most common during periods of lowstand because of shelf erosion and direct sediment supply to the shelf edge or upper slope. *De Castro et al. (2020b)* proposed that, in terms of contourite sedimentation, these sediments can be affected by bottom currents (examples from Corsica). Based on observations in the Mozambique upper slope, the Brazilian upper slope (*Viana and Faugeres, 1998*) and, in the Capo Vaticano upper slope in the Mediterranean Sea (*Martorelli et al., 2020*), the outer-shelf environment sources sand predominantly from early sea level rise to the highstand. Once the highstand is established, the bottom currents in the contourite terrace remain active with a decreased sediment input, favoring reworking and sediment condensation in the contourite terrace (*de Castro et al., 2020b*). In the case of the contourite deposits in Morocco, the main driver of sediment supply is tectonically induced instability (*de Weger et al., 2020*) and the erosive nature of overflow water, particularly in the region of the Taza-sill and the contourite channel.

(vii) How do contourite channel systems interact with other deep-marine sedimentary processes?

The most recent contributions on mixed turbidite-contourite systems by *Fonnesu et al. (2020)* and *Fuhrmann et al. (2020)* described the interaction between, turbidite channels and bottom currents. In those publications, bottom current velocities predominantly range between 0 – 0.5 ms<sup>-1</sup>. Both these works focus on the direction of migration of turbidite channels influenced by bottom currents. This work however describes a different setting, in which contourite channels with high flow velocities (periodically over 1 ms<sup>-1</sup>) are crossed by turbidity currents. Based on our findings turbidite sedimentary facies have very poor preservation potential within the channel as these facies have hardly (“not”) been identified within the channel fill sequences. As turbidite facies (predominantly partial turbidite facies sequences) have been identified in the drift (*de Castro et al., 2020a, b; de Weger et al., 2021a*), part of the turbidity current managed to cross the contourite channel to be deposited in the channel-drift transitional and drift domain. The perpendicularly approaching turbidity current with respect to the contourite channel was likely affected while it crossed the interface between the overriding water-mass and the denser water-mass of the overflow water. This density gradient might have caused flow stripping, causing the fine-grained turbidity cloud to be deflected down-current of the overflow water. Hypothetically, this fine-grained, flow stripped cloud could also have overridden the overflow water mass to have later been deposited as hemipelagic fallout in a down-slope direction. The remainder, coarser grained fraction of the turbidity current, was likely affected by the bottom-current of the overflow water but might still have been temporarily deposited within the channel to be reworked into contourite deposits over time.

Mass transport deposits, slumps, are thought to have influenced the core of the overflow water more significantly. As indicated by *de Weger et al. (Chapter VI, submitted)*, the sudden input of slump deposits within the right flank of the contourite channel forced the overflow-water mass to migrate towards the left flank. This caused the temporary, subtle but sudden, down-slope (towards the left) migration of the 2<sup>nd</sup> order contourite channel. The natural, Coriolis force induced, migration of the contourite channel (up slope, towards the right) was re-established over time.

(viii) Which sedimentary facies typify contourite channel fill sequences?

*Stow and Smillie (2020, and references therein)*, synthesized the current understanding of deep-water sedimentary facies. They indicated that contourite sands occur as part of the bi-gradational sequence or partial sequences in mud-rich drifts but they also occur independently in sand sheets and contourite channels. *Brackenridge, et al. (2018)* recognized these different sandy contourite types as; 1) fine-grained bioturbated sandy facies with some mud, 2) fine to medium-grained, clean (mud-free) sands that are mostly structureless with rare bioturbation and lamination and, 3) medium- to coarse-grained, laminated and cross-bedded sands that are mud-free and generally without bioturbation. They furthermore argued that these facies, not representative for the C3 division of the standard contourite facies model (*Gonthier et al., 1984*), required a new facies model related to vigorous bottom currents, principally occurrent within the contourite channel systems (*Stow et al., 2013b; Hernández-Molina et al., 2014*). The sedimentary sandy contourite channel facies described in this research project would predominantly fall within the medium- to coarse-grained laminated and cross-bedded sands, they however provide significantly more sedimentary facies information for which we were able to propose a new facies model.

The sedimentary facies that are typical for contourite channel fill sequences originating from bottom-current activity, based on this research project, are predominantly related to two-dimensional (Facies F6.1 and F6.2) and three-dimensional dunes (Facies F6.3 and F6.4) (Chapters IV, V and VI); thin- (F6.1) to tick-bedded (F6.2) cross stratified, up to coarse grained mixed compositional sandstone and through- (F6.3) and tangential-cross stratified (F6.4), up to coarse grained mixed compositional sandstone. To a lesser extent, both un- (F7) and fully-bioturbated (F5), planar laminated, up to coarse grained mixed compositional sandstones are typical. Besides the depositional products of bottom-currents, convolute and contorted sandstones (F8) related to slump deposits are common within the channel fill sequences. These slump deposits can produce overpressure in the previously deposited contourite facies, resulting in soft sediment deformation and fluid escape structures. As mentioned previously, turbidite deposits (F9) have very poor preservation potential within the contourite channels as the persistent bottom-current velocities are too high. The channel-drift transitional domain is typified by sedimentary facies F3 and F4; heterolithic sand-mudstones (F4) and muddy sediment with sand laminae (F3), produced by bottom-current

velocities that are lower compared to the contourite channel but higher than in the drift. Furthermore, the heterolithic nature of these sedimentary facies indicates stronger fluctuations in the current regime. These fluctuations are likely the result of the expansion and collapse of the bottom-current core which preferentially, primarily due to the Coriolis force, is contained within the contourite channel. If the core, related to times of deposition, collapses, or decreases in size, the core is contained within the channel, decreasing the current-velocities within the channel-drift transitional and drift domain, allowing the deposition of fine-grained particles. When the core expands, or increases in size, the core or water-mass related to overflow affects the channel-drift transitional and drift domain, increasing the bottom-current velocities within these domains. During periods in which the core is expanded, coarser grained sediment is deposited within these domains and the increased current velocities might also cause winnowing and erosion. Core expansion and collapse are also evident within the contourite channel fill sequences, where, during times of core expansion, the bottom-current is more erosive, capable of forming 2<sup>nd</sup> order concave-up erosive surfaces.

The proposed new facies model (Fig. 8.5; *Chapters V and VII; de Weger et al., 2021a, 2021c*) relates the occurrent sedimentary facies to their position and distribution within; the proximal channel flank, the axis of the channel, the distal flank of the channel, the channel drift-transitional domain, and the drift. Each of these domains are characterized by different hydrodynamic conditions that are responsible for the type of deposits they contain. The results of this research project, compared to the works of *de Castro et al. (2020b)* in modern/recent contourite channels, shows a very good correlation, attesting to the validity of the model.

(ix) What are the identification criteria for sandy contourite channels?

Since the separation of muddy and sandy contourites in the 1970's (*Stow and Lovell, 1979*), the now standard bi-gradational facies model (*Gonthier et al., 1984; Stow and Faugetes, 2008*) and associated partial sequences, remain the only reliable model for contourite facies recognition. This model is regularly thought to apply to all types and

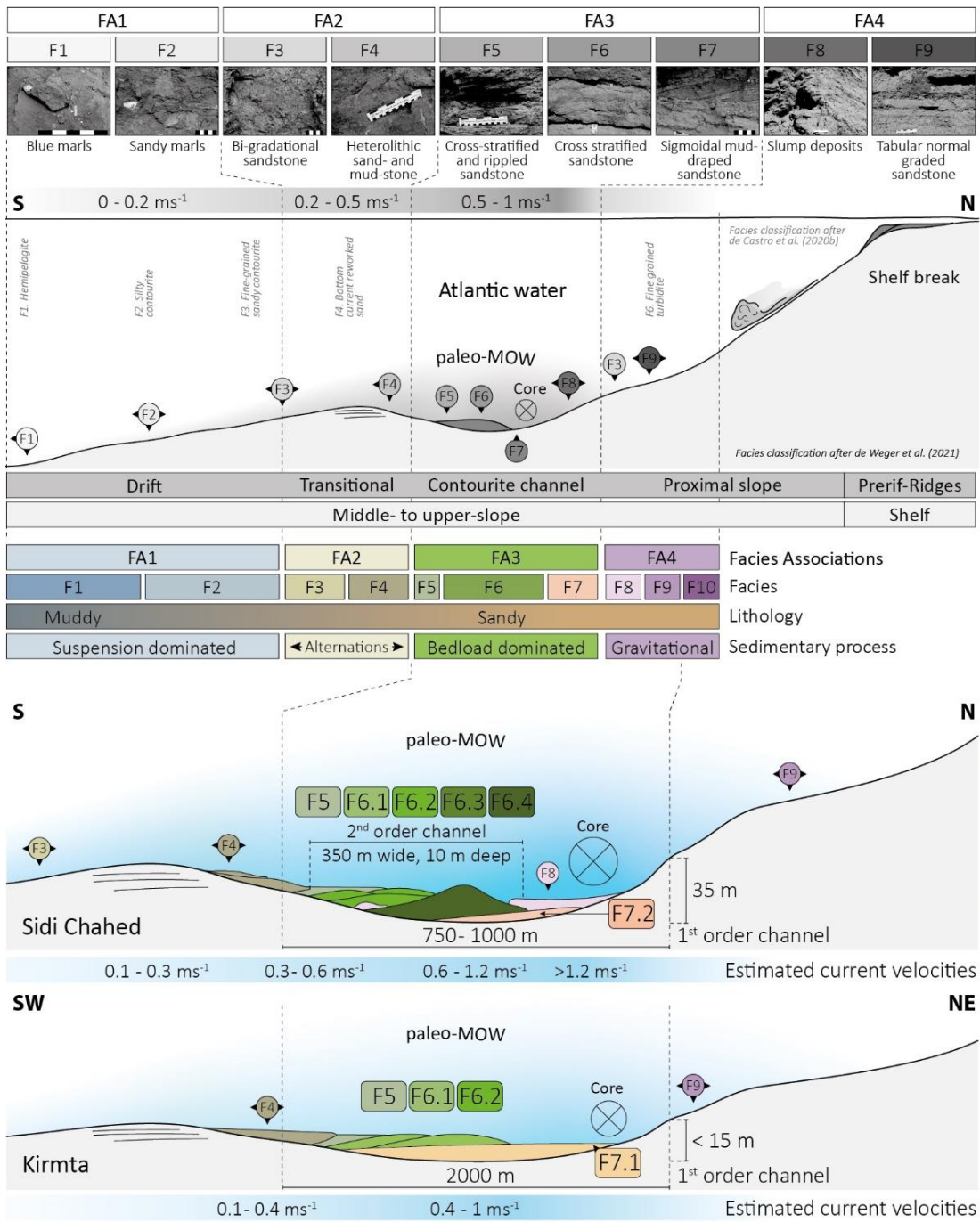


**Figure 8.5.** The top panel is derived from de Weger et al. (2021a) and shows the relation between facies F1-F9 defined therein. This facies model is used for comparison to the newly proposed facies model made herein (two bottom panels, one for the Sidi Chahed and one for the Kirmta outcrop at the bottom). This facies model shows the relation between facies and facies associations within the 1<sup>st</sup> order contourite channel, which transitions towards the drift (S/SW or left). The estimated current velocities for each depositional domain is included.

depositional settings of contourite systems. As mentioned in the previous paragraph however, *Brackenridge et al. (2018)* and *de Castro et al. (2021)* identified independent sedimentary facies for sheeted sand and contourite channels. *Shanmugam (1993b, 2008)* stated that no single criterion by itself is unique to bottom-current-reworked sands as it is difficult to establish that a given sedimentary structure in the rock record was originated by contour-following thermohaline currents without establishing the paleowater circulation pattern independently. For this reason, he introduced the term “bottom-current-reworked sands”. As this research project focuses on sandy contourite deposits related to the contourite channel, herein we try to establish diagnostic criteria for contourite channel deposits, which should have a more pronounced signature as they are related to strong bottom currents.

To do so, first we must establish the principal controls on depositions. Contourite channels are formed by the persistent action of semi-continuous, long-lived, and strong bottom-currents. These bottom-currents are capable of eroding into previously deposited sediment, forming the channel. With reducing bottom-current velocities, sediment can be deposited as sedimentary bodies which migrate down the channel. For this reason, the principal controls on sedimentation are: intermittent, long-lived bottom-currents that are confined within a contourite channel, much like a river, where the atmosphere-water boundary is replaced by different water masses, having a significantly different density gradient. The long-lived duration and persistent action of a current should be captured in the sedimentary facies of contourite deposits in the form of bedload sediment migration. Many authors previously recognized that contourite deposits should contain sedimentary structures related to bedload transport (*e.g. Shanmugam, 1997a; Martín-Chivelet et al., 2008*) however, due to most of the research being focused on contourite drifts, these criteria of persistent sediment movement are largely overprinted by bioturbation. This however is different in contourite channels, where bottom currents and sedimentation rates are sufficiently high to preserve sedimentary structures related to the persistent action of currents. Based on the results of this research project, all sedimentary structures related to persistent currents; cross-stratification, parallel lamination, ripples and tidal signatures are diagnostic for contourite deposits, given sufficient background on palaeo-environmental conditions, water-depth (at least two water-masses should have been present to allow stratification and the possibility for bottom current formation), and the possibility of strong, along-slope bottom-currents are provided. Furthermore, the paleocurrent directions should predominantly be directed perpendicular to the inferred paleo-slope, in a roughly 90 degree

offset to identified gravitational deposits. Gravitational deposits in the sedimentary succession within contourite channels should be reworked by bottom-currents or absent. The mixed siliciclastic-bioclastic composition, with higher bioclastic fractions and poorer sorting in coarse grained sand, might also attest to a contouritic origin as previously discussed in *Brackenridge et al. (2018)* and observed by several authors (*e.g. Stow, 2002; Wetzel et al., 2008; Mulder et al., 2013*).

#### (x) How is sediment distributed in contourite channels?

Despite many recent attempts to study sedimentation in contourite channels, little is currently known about the sediment distribution in these channels. Based on ROV footage from the contourite channels in the Gulf of Cadiz however, sedimentary facies change rapidly over short distances (*e.g. MOWER cruise, 2014; INPULSE cruise, 2019*). These rapid facies changes might result from the fact that the channels in the Gulf of Cadiz are currently in their erosional phase or at the beginning of their infill stage, not fully depicting contourite channels in their depositional phase. Based on the findings of this study (*Chapters V and VI*), the decrease in current velocity laterally away from the core however play the most important role in across channel facies distribution. The channels in the late Miocene Rifian Corridor show an across channel facies change from facies produced by high velocity bottom-currents (upper stage plane beds, large 3D-dunes) to facies produced by lower velocity bottom-currents (in size decreasing 2D-dunes, lower stage plane beds and heterolithic facies) towards the down slope flank of the channel. This across channel trend in flow velocity was also described in the works of *de Castro et al. (2021)*. The down-current decrease in flow velocity was already established (*Llave et al., 2001, 2003; Habgood et al., 2003; Hernández-Molina et al., 2003, 2006*) and the down-current deceleration of flow-velocities has also been inferred from the distribution patterns of sediment.

Interestingly, contourite channel deposits are primarily found in the study area at locations where the contourite channel was deflected, forming a bend (*Chapter VI*). In these bends, deposition was concentrated in the outer bend because of the Coriolis force, which forces the core of the current, related to the highest flow velocities, to the inner bend, located against the slope. The flow behaviour in channels affected by the Coriolis force has experimentally been confirmed by *Davarpanah et al. (2020)*. Similarly, much of the published evidence of sandy contourite deposits, primarily located in the Gulf of Cadiz (*e.g. Hernández-Molina et al., 2006, 2014a; Stow et al., 2013; de Castro et al., 2021*) but also in the Faero



Bank Channel area (*Akhmetzhanov, et al., 2007*), the South China Sea (*Gong et al., 2017*), onshore in the Yangtze region of China (*Zhang et al., 2020*) and in the southern Brasil Basin (*Mézeris et al., 1993*), reveals that contourite channel deposits are primarily found in areas in which the contourite channel changes its orientation, forming a bend. The preferred deposition and/or preservation of channel fill sediment in these bends are likely the result of, as of yet unidentified, changes in flow characteristics across and along the channel.

(xi) What factors control erosional and depositional features in contourite channel systems?

The primary factors controlling deposition and erosion in contourite channel systems are hydrodynamic conditions. These hydrodynamic conditions change over time, accelerating and decelerating flow velocities but they also decelerate both down current and laterally away from the core of the bottom-current (*Chapters V and VI*). Sea-floor topography and morphological features in the pathway of the current furthermore control the hydrodynamic characteristics of the bottom-current, being capable of funneling/amplifying or decelerating current velocities were the become less confined (*e.g. Hernández-Molina et al., (2006b)*).

(xii) Are the studied outcrops, related to the paleo-MOW in a confined gateway, representative for sandy contourite systems on other continental margins?

The main controls on depositional style of contourite features are flow-velocity and the characteristics of sediment availability. Taking this into account, the resulting morphology and depositional style should not be drastically different between the studied sections and other contourite systems. Current velocities generated by overflow are however high in comparison to thermohaline circulation. Having said that, the ability of flow to transport and deposit sandy sediment is a function of flow-velocity and sediment particle characteristics (*e.g. the Hjulström curve*), and thus sandy contourite deposits, independent of the style of bottom-current generation should show similar features. As such, the contourite channel system and the erosional and depositional features are unique due to the morphology of the gateway and the effects of this morphology on flow characteristics. The gateway however was sufficiently wide (> 50 km) not restricting the overflow water mass nor the core, being able to “freely” flow along the slope, controlled only by sea floor morphology, density

gradients and the Coriolis force. The morphology of the gateway however did amplify tidal forces, generating an amplified tidal control on overflow behavior. From this it can be deduced that in other contourite systems, with similar flow-velocities, not pertaining to a gateway, should likely show less pronounced tidal signatures.

#### (xiv) Why are there so few examples of contourite deposits in outcrop?

The list of examples of exposed ancient deposits affected or deposited by bottom currents is small; The Neogene Miura-Boso region, SE Japan (*Stow and Faugeres, 1990; Stow et al., 1998b, 2002*); The Oligocene-Miocene carbonate contourite drift, Cyprus (*Roberston, 1990; Stow et al., 2002; Huneke et al., 2020*); the late Cretaceous-Palaeocene carbonate contourite drifts, Danish Basin (*Lykke-Andersen and Surlyk, 2004*); The Devonian carbonate contourites, Europe and North Africa (*e.g. Huneke, 2001, 2006, 2007a, b; in Huneke and Stow, 2008*); Ordovician Jiuxi carbonate drift, China (*Duan et al., 1993*); Miocene siliciclastic contourites, Rifian Gateway succession, Morocco (*e.g. Capella et al., 2017a*); Oligocene-Pliocene muddy-sandy contourite deposits, Angola (*Cauxeiro et al., 2020*); Ordovician contourites, Ordos Basin, China (*Li, et al. 2020*). The commonality between most of these outcrops is that the signatures of contourite processes are diluted by gravitational processes. Furthermore, most of these outcrops still require further investigation. A more analytical synthesis on most of these contourite outcrops are provided in *Huneke and Stow (2008)*. Only two outcrops are currently deemed excellent contourite outcrops, Cyprus, and Morocco. These outcrops are however considerably different, Cyprus being related to a calcareous contourite drift (*Huneke et al., 2020*) and Morocco representing a mixed siliciclastic-bioclastic sandy contourite channel (*Chapters IV, V and VI*).

Contourite depositional systems, by volume, predominantly consist of fine-grained sediment belonging to the contourite drift. The contourite drift, in turn, is formed by the combination of bottom-currents, gravitational processes and pelagic/hemipelagic sedimentation. The differentiation between the processes responsible for the deposition of fine-grained sediment has proven difficult, however, the works of *de Castro et al. (2020a, 2021)* provided a method to resolve this problem. This method however is difficult to apply on fine-grained sediment in outcrop, and it furthermore needs processing rather than just field observations. Subsurface contourite drifts are recognized based on their morphological features, another aspect that can generally not be applied to fine-grained deposits in

outcrop. Finally, fine-grained deposits in outcrop are usually weathered, hindering direct field observations on both small- and large-scales sedimentary features which could reveal their depositional origin. The now standard bi-gradational facies model (*Gonthier et al., 1984; Stow and Faugeres, 2008*) is based on these fine-grained sediment, but, because of the problems addressed above, are not easily recognized in field studies. The best way to relate sandy deposits to a contouritic origin is their morphological link with fine-grained drift features, which cannot be identified in outcrop, hampering their recognition. Sandy contourite deposits furthermore only make up, by volume, a small percentage of contourite depositional systems, making them naturally scarce. The interpretation of sandy contourite deposits furthermore requires the difficult and time-consuming process of producing a solid understanding of the paleogeographic settings and the paleo-hydrodynamic conditions to attest to a contouritic origin as they can easily be mistaken with shallow-marine deposits. Furthermore, as indicated in the previous paragraph, the already small contribution of sandy contourites might further be limited to the preferred deposition/preservation of contourite channel fill deposits in bends of the contourite channel. Nevertheless, due to the poorly understood contouritic processes, many previously interpreted deposits, particularly those interpreted as turbidites and shallow marine (near shore), tidally affected sandstone deposits might be wrongly, or insufficiently interpreted.

#### (xv) What are the implications of the new findings?

The implications of the outcome of this research project are threefold. First, we will discuss the conceptual implications, followed by the climatic and the economic implications, respectively.

##### *Conceptual implications*

The main findings described and discussed in this thesis are the discovery of sandy contourites and their first ever recognition as being relics of a contourite channel system, outcropping in the ancient record. The implications regarding these findings are that they represent, to date, the only contourite channel system exposed in the ancient record, making them a valuable analogue for modern contourite depositional system and ancient subsurface exploration and research targets. As such, the data presented herein is unique and provides a solid foundation for these sedimentary systems. Many of the interpretations

made throughout this thesis, despite being based on findings from previous and, to some extent comparable studies, are original and need to be investigated further.

### *Implications in climate change*

Over the past decade there has been a significant rise in awareness of human's contribution in climate change. The google scholar search engine shows 117,000 results for "climate change" since 2020, compared to 425 for "contourites", even though contourites contain significant information on ocean circulation and past climate change (e.g. Knutz, 2008). Taking in mind, the well-known expression of: "The past is the key to the future" (*Presidential address to the Geochemical Society. October 19, 1982, New Orleans, Louisiana*), contourite research could significantly attribute to the understanding of the processes leading to climate change, a topic which despite gaining significant attention from the research community, is not well understood due to the complex interplay of all global processes affecting climate. In this thesis, we address the driving forces that affect the late Miocene contourite channel system (*Chapter IV*) and the effect the overflow has on global climate. Furthermore, we provide information regarding mechanisms that affect the overflow water, thus providing information on processes that trigger climate change. These findings should provide a framework for future considerations of the effects of ocean circulation and climate change.

### *Economic implications*

Besides the considerable economical impact of climate change induced by ocean circulation changes, contourites have significant economic impact on energy geosciences and geohazards (e.g. Viana, 2008). One of the geohazards caused by the persistent action of bottom currents is that the erosive effect of bottom currents triggers slope instability, provoking mass transport deposits (e.g. Niemi et al., 2000; Laberg et al., 2005; Viana et al., 2007; Verdicchio et al., 2007). This effect has also been deduced from the outcrops studied herein, where mass transport deposits, or slump deposits, are common in the proximal flank of the channel (*Chapters IV and VII; de Weger et al. 2020, 2021c*). In this paragraph however we will focus on the economic significance of contourites for energy geosciences.

The potential of contourite deposits for energy geosciences exploration has already been addressed by Viana et al. (2007) and Viana (2008). The most promising aspect of contourite deposits for exploration is that contourite depositional systems contain both fine-grained sediments, which might act as seals (and source rock), and coarse-grained sediment that has

the potential to form reservoir rock (Fig. 8.6). In these contourite systems, both fine-grained and coarse-grained sediment, due to the behavior of the system are well separated, being able to form extensive and relatively undisturbed reservoir and seal morphologies. Based on our findings, contourite depositional systems are furthermore likely to be self-sealing (*Chapter VII; de Weger et al., 2021c*) as the termination of processes responsible for the deposition of sand-grained sediment (high flow-velocities) is followed by the deposition of fine-grained sediment (decelerating flow-velocities). Furthermore, when flow velocities are highest, both spatial and temporal, bottom currents can form intra-slope sub-basins creating accommodation space for sand-grained sediment with reservoir potential, independent of the depositional process. These sub-basins are carved in the slope which primarily consist of fine-grained sediment. This research project furthermore elaborates on the distribution of sediment with excellent reservoir characteristics within the channel. Despite the recognition of laterally extensive, both across the channel and down-current, sand-prone contourite channel fill sequences from seismic studies (examples), herein we discussed the possibility that contourite channel fill deposits might preferentially be deposited/preserved within the bends of these channels (*Chapter VII; de Weger et al., 2021c*), possibly limiting the extent of their economical prospectivity.

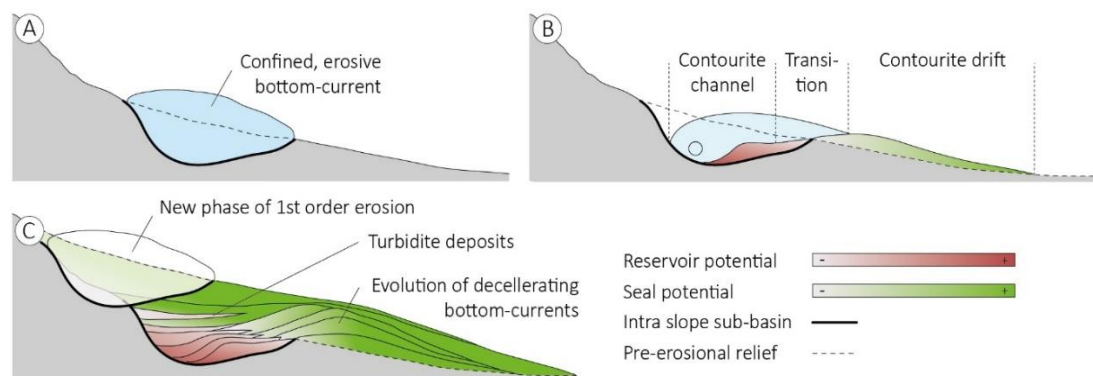


**Figure 8.6.** Evolution of contourite channels and the distribution of sediment with either reservoir (red) or seal (green) potential. A) The first stage of intra-slope sub-basin formation by the initiation and action of energetic bottom-currents. B) The across channel distribution of sediment with reservoir and seal potential. C) the final product of the natural evolution (up-slope migration) of the contourite channel and drift. A new phase of bottom-current activity is initiated by a newly generated bottom current > A.

(xvi) What are the main limitations of this research project?

As usually the case with research projects, the main limitations apply to the duration of the research project and data quantity.

- Time constraints hampered the study of more outcrops, as described in (Table 1, chapter III), by studying more outcrops related to the same system a better understanding of the behavior of the overflow water and the distribution of sediment can be generated.
- Due to the duration of the research project, we have not yet been able to properly analyze the geochemical data (work in progress).
- The lack of higher resolution age-constraints hampers the ability to differentiate between processes that control overflow behavior.
- Outcrops have been influenced by secondary processes, weathering, and dissolution, making them less suitable for determining petrophysical characteristics. Furthermore, these processes might have affected characteristics of the thin-sections, despite taking care of collecting fresh samples, not significantly affected by these processes.
- In this study, the limited number of previous studies on the research topic hampered extensive comparison. This lack of previous work however also enabled us to tackle the research questions in an “open minded” fashion.
- Due to the outbreak of the pandemic, we were not able to go on a planned fieldtrip. This missed fieldtrip was intended for additional data collection and the construction of a synthetic seismic profile in the Kirmia outcrop as a MSc research project supervised by TOTAL.

## CONCLUSIONS

Although bottom currents and their associated contourite depositional systems are increasingly more often recognized in deep-marine environments, the processes driving and controlling these systems remain poorly understood. The aim of this research project was to gain insights in the processes, controlling factors and sedimentary facies of the least well understood elements of these systems, the contourite channels, by studying contourite channel deposits in outcrop. The main conclusions resulting from this study are listed below.

Bottom currents generated by the overflow of dense water behave intermittently, controlled by tectonic processes and global and regional climate variations. Tectonic processes predominantly control the configuration of the sill, the point where overflow takes place, and the slope along which the bottom current is forced. Climate variations, induced by orbital cyclicity and seasonal variations control the characteristics of surficial and bottom water-masses, controlling the characteristics of the bottom-current. Furthermore, climate induced variations in relative sea-level control the depth of the sill and the accommodation space for overflow-water.

Tides substantially modulate the overflow behavior on a sub-annual timescale. Maximum outflow velocities are reached during the flooding phase or the maximum W-ward directed tidal current. Minimum outflow velocities occur during the ebb-phase where maximum E-ward directed tidal currents are present. These tidal signatures are observed in the rock-record as thickening-thinning foreset bundles with angular to tangential toe-set geometries. As such, tidal signatures might be characteristic for bottom-current channel associated deposits.

Sedimentological characteristics of contourite channels primarily depend on the behavior (velocity) of the bottom-current and the supply of sediment. Contourite channels are formed by vigorous bottom currents that are able to erode into the existing sediment, forming an erosional concave-up depression. This phase of channel formation is most likely associated to the initiation of the bottom current after a period without or severely reduced overflow. The contourite channel, upon deceleration of the current, is filled by sediment. The characteristics of channel-fill depend on both flow velocity and sediment supply. The sedimentary facies that make up the channel-fill sequence, primarily consisting of sandstone, show a good correlation to existing bedform stability diagrams. These facies consist of (from



high velocity to low velocity) upper stage plane bedforms, 3D and 2D dunes, lower stage plane bedforms, ripples and more heterolithic, sandstone and mudstone facies.

Within the channel, the velocity profile of the bottom current, with its highest velocities forced against the slope by the Coriolis Force and decreasing velocities towards and over the adjacent drift, determine the inter-channel facies distribution which is associated to the changes in across channel flow velocity profiles. Furthermore, down-channel decreases in flow velocity occur due to a decrease in the effect of gravity by turbulent mixing. This results in a down-channel change in sedimentary facies towards facies associated to lower bottom-current velocities.

Channel migration is primarily triggered by tectonically induced reconfiguration of both the slope and the sill, but also by pulses of gravitationally driven sediment supply to the channel. When the channel is suddenly filled by sediment in the form of e.g. slump deposits, the bottom-current is forced down-slope. The natural migration of contourite channels is up-slope, controlled by the Coriolis Force.

Although significant advances have been made in understanding contourite channels and their infill deposits as well as the establishment of newly proposed facies models in this study, further research on the topic is required. The proposed further research primarily relates to the study of both modern contourite channel systems, to better understand the hydrodynamic behavior of channelized bottom currents and the resulting depositional systems as well as to verify the proposed facies models of this study, furthermore, the results of this study need to be applied to outcrops which likely have a contouritic origin to further develop the sedimentary facies and facies distribution of contourite channels. Improving our knowledge of these systems can greatly benefit the understanding of deep-marine sedimentary processes, the impact of bottom currents on climate change, and their economic significance in deep-marine hydrocarbon exploration.

## REFERENCES

- Akhmetzhanov, A., Kenyon, N. H., Habgood, E., Van Der Mollen, A.S., Nielsen, T., Ivanov, M., & Shashkin, P. (2007). North Atlantic contourite sand channels. *Geological Society, London, Special Publications*, 276(1), 25-47.
- Armi, L., & Farmer, D.M. (1988). The flow of tar. The flow of Atlantic water through the Strait of Gibraltar. *Progress in Oceanography*, 21(1), 1-105.
- Baringer, M.O.N., and Price, J. F. (1999). A review of the physical oceanography of the Mediterranean outflow. *Marine Geology*, 155(1-2), 63-82.
- Baschek, B., Send, U., Lafuente, J.G., & Candela, J. (2001). Transport estimates in

- the Strait of Gibraltar with a tidal inverse model. *Journal of Geophysical Research: Oceans*, 106(C12), 31033-31044.
- Brackenridge, R.E., Stow, D.A., Hernández-Molina, F.J., Jones, C., Mena, A., Alejo, I., ... & Frances, G. (2018). Textural characteristics and facies of sand-rich contourite depositional systems. *Sedimentology*, 65(7), 2223-2252.
- Bruno, M., Mañanes, R., Alonso, J.J., Izquierdo, A., Tejedor, I., & Kagan, B.A. (2000). Vertical structure of the semidiurnal tidal currents at Camarinal Sill, the strait of Gibraltar. *Oceanologica Acta*, 23(1), 15-24.
- Bryden, H.L., & Kinder, T.H. (1991). Steady two-layer exchange through the Strait of Gibraltar. *Deep Sea Research Part A. Oceanographic Research Papers*, 38, S445-S463.
- Bryden, H.L., Candela, J., & Kinder, T.H. (1994). Exchange through the Strait of Gibraltar. *Progress in Oceanography*, 33(3), 201-248.
- Bulat, J., & Long, D. (2001). Images of the seabed in the Faroe-Shetland Channel from commercial 3D seismic data. *Marine Geophysical Researches*, 22(5), 345-367.
- Candela, J., Winant, C.D., & Bryden, H.L. (1989). Meteorologically forced subinertial flows through the Strait of Gibraltar. *Journal of Geophysical Research: Oceans*, 94(C9), 12667-12679.
- Candela, J., Winant, C., & Ruiz, A. (1990). Tides in the Strait of Gibraltar. *Journal of Geophysical Research: Oceans*, 95(C5), 7313-7335.
- Candela, J. (1991). The Gibraltar Strait and its role in the dynamics of the Mediterranean Sea. *Dynamics of Atmospheres and Oceans*, 15(3-5), 267-299.
- Candela, J. (2001). Mediterranean water and global circulation. In *International Geophysics* (Vol. 77, pp. 419-XLVIII). Academic Press.
- Capella, W., Hernández-Molina, F.J., Flecker, R., Hilgen, F.J., Hssain, M., Kouwenhoven, T.J., van Oorschot, M., Sierro, F.J., Stow, D.A.V., Trabucho-Alexandre, J., Tulbure, M. A., de Weger, W., Yousfi, M.Z., Krijgsman, W. (2017a). Sandy contourite drift in the late Miocene Rifian Corridor (Morocco): Reconstruction of depositional environments in a foreland-basin seaway. *Sed. Geol.*, 355, 31-57.
- Cauzeiroa, C., Lopezb, M., Hernández-Molinac, J., Miguela, A., Cauzeirod, G., & Caetano, V. (2020). Contourite vs Turbidite Outcrop and Seismic Architectures. *Angolan Mineral, Oil & Gas Journal*, 1(1), 20-26.
- Davarpanah Jazi, S., Wells, M.G., Peakall, J., Dorrell, R.M., Thomas, R.E., Keevil, G.M., ... & Valran, T. (2020). Influence of Coriolis force upon bottom boundary layers in a large-scale gravity current experiment: Implications for evolution of sinuous deep-water channel systems. *Journal of Geophysical Research: Oceans*, 125(3), e2019JC015284.
- de Castro, S., Hernández-Molina, F.J., Rodríguez-Tovar, F.J., Llave, E., Ng, Z.L., Nishida, N., & Mena, A. (2020a). Contourites and bottom current reworked sands: Bed facies model and implications. *Marine Geology*, 428, 106267.
- de Castro, S., Hernández-Molina, F.J., de Weger, W., Jiménez-Espejo, F. J., Rodríguez-Tovar, F.J., Mena, A., ... & Sierro, F.J. (2020b). Contourite characterization and its discrimination from other deep-water deposits in the Gulf of Cadiz contourite depositional system. *Sedimentology*.
- de Castro, S., Miramontes, E., Dorador, J., Jouet, G., Cattaneo, A., Rodríguez-Tovar, F.J., & Hernández-Molina, F.J. (2021). Siliciclastic and bioclastic contouritic sands: Textural and geochemical characterisation. *Marine and Petroleum Geology*, 128, 105002.
- de Weger, W., Hernández-Molina, F.J., Flecker, R., Sierro, F.J., Chiarella, D., Krijgsman, W., & Manar, M.A. (2020). Late Miocene contourite channel system reveals intermittent overflow behavior. *Geology*, 48(12), 1194-1199.
- de Weger, W., Hernández-Molina, F.J., Miguez-Salas, O., De Castro, S., Bruno, M., Chiarella, D., ... & Manar, M.A. Contourite depositional system after the exit of a strait: Case study from the late Miocene South Rifian Corridor, Morocco. *Sedimentology*.
- Duan, T., Gao, Z., Zeng, Y., & Stow, D. (1993). A fossil carbonate contourite drift on the Lower Ordovician palaeocontinental margin of the middle Yangtze Terrane, Jiuxi, northern Hunan, southern China. *Sedimentary Geology*, 82(1-4), 271-284.
- Ercilla, G., Casas, D., Vázquez, J.T., Iglesias, J., Somoza, L., Juan, C., ... & Maestro, A. (2011). Imaging the recent sediment dynamics of the Galicia Bank region (Atlantic, NW Iberian Peninsula). *Marine Geophysical Research*, 32(1), 99-126.

- Farmer, D.M., & Armi, L. (1986). Maximal two-layer exchange over a sill and through the combination of a sill and contraction with barotropic flow. *Journal of Fluid Mechanics*, 164, 53-76.
- Faugères, J.C., & Stow, D.A. (1993). Bottom-current-controlled sedimentation: a synthesis of the contourite problem. *Sedimentary Geology*, 82(1-4), 287-297.
- Faugères, J.C., Stow, D.A., Imbert, P., & Viana, A. (1999). Seismic features diagnostic of contourite drifts. *Marine Geology*, 162(1), 1-38.
- Flood, R.D. (1981). Distribution, morphology, and origin of sedimentary furrows in cohesive sediments, Southampton Water. *Sedimentology*, 28(4), 511-529.
- Flood, R.D. (1983). Classification of sedimentary furrows and a model for furrow initiation and evolution. *Geological Society of America Bulletin*, 94(5), 630-639.
- Fonnesu, M., Palermo, D., Galbiati, M., Marchesini, M., Bonamini, E., & Bendias, D. (2020). A new world-class deep-water play-type, deposited by the syndepositional interaction of turbidity flows and bottom currents: The giant Eocene Coral Field in northern Mozambique. *Marine and Petroleum Geology*, 111, 179-201.
- Fuhrmann, A., Kane, I.A., Clare, M.A., Ferguson, R.A., Schomacker, E., Bonamini, E., & Contreras, F.A. (2020). Hybrid turbidite-drift channel complexes: An integrated multiscale model. *Geology*, 48(6), 562-568.
- García, M., Hernández-Molina, F.J., Llave, E., Stow, D.A.V., León, R., Fernández-Puga, M.C., ... & Somoza, L. (2009). Contourite erosive features caused by the Mediterranean Outflow Water in the Gulf of Cadiz: Quaternary tectonic and oceanographic implications. *Marine Geology*, 257(1-4), 24-40.
- Gladstone, R., Flecker, R., Valdes, P., Lunt, D., & Markwick, P. (2007). The Mediterranean hydrologic budget from a Late Miocene global climate simulation. *Palaeogeography, Palaeoclimatology, Palaeoecology*, 251(2), 254-267.
- Gong, C., Peakall, J., Wang, Y., Wells, M.G., & Xu, J. (2017). Flow processes and sedimentation in contourite channels on the northwestern South China Sea margin: A joint 3D seismic and oceanographic perspective. *Marine Geology*, 393, 176-193.
- Gonthier, E.G., Faugères, J.C., & Stow, D.A.V. (1984). Contourite facies of the Faro drift, Gulf of Cadiz. *Geological Society, London, Special Publications*, 15(1), 275-292.
- Habgood, E.L., Kenyon, N.H., Masson, D.G., Akhmetzhanov, A., Weaver, P.P., Gardner, J., & Mulder, T. (2003). Deep-water sediment wave fields, bottom current sand channels and gravity flow channel-lobe systems: Gulf of Cadiz, NE Atlantic. *Sedimentology*, 50(3), 483-510.
- Heezen, B.C., & Hollister, C. (1964). Deep-sea current evidence from abyssal sediments. *Marine Geology*, 1(2), 141-174.
- Helfrich, K.R. (1995). Time-dependent two-layer hydraulic exchange flows. *Journal of Physical Oceanography*, 25(3), 359-373.
- Hernández-Molina, J., Llave, E., Somoza, L., Fernández-Puga, M.C., Maestro, A., León, R., ... & Gardner, J. (2003). Looking for clues to paleoceanographic imprints: a diagnosis of the Gulf of Cadiz contourite depositional systems. *Geology*, 31(1), 19-22.
- Hernández-Molina, F.J., Llave, E., Stow, D.A.V., García, M., Somoza, L., Vázquez, J.T., ... & Gardner, J. (2006). The contourite depositional system of the Gulf of Cadiz: a sedimentary model related to the bottom current activity of the Mediterranean outflow water and its interaction with the continental margin. *Deep Sea Research Part II: Topical Studies in Oceanography*, 53(11-13), 1420-1463.
- Hernández-Molina, F.J., Llave, E., & Stow, D.A.V. (2008). Continental slope contourites. *Developments in sedimentology*, 60, 379-408.
- Hernández-Molina, F.J., Maldonado, A., & Stow, D.A.V. (2008). Abyssal plain contourites. *Developments in Sedimentology*, 60, 345-378.
- Hernández-Molina, F.J., Paterlini, M., Violante, R., Marshall, P., de Isasi, M., Somoza, L., & Rebesco, M. (2009). Contourite depositional system on the Argentine Slope: An exceptional record of the influence of Antarctic water masses. *Geology*, 37(6), 507-510.
- Hernández-Molina, F.J., Llave, E., Preu, B., Ercilla, G., Fontan, A., Bruno, M., ... & Arnaiz, A. (2014). Contourite processes associated with the Mediterranean Outflow Water after its exit from the Strait of Gibraltar: Global and conceptual implications. *Geology*, 42(3), 227-230.

- Herrero, M.J., Marfil, R., Escavy, J.I., Al-Aasm, I., & Scherer, M. (2020). Diagenetic origin of bipyramidal quartz and hydrothermal aragonites within the Upper Triassic saline succession of the Iberian Basin: Implications for interpreting the burial–thermal evolution of the basin. *Minerals*, 10(2), 177.
- Hollister, C.D., & McCave, I.N. (1984). Sedimentation under deep-sea storms. *Nature*, 309(5965), 220-225.
- Hüneke, H. (2006). Erosion and deposition from bottom currents during the Givetian and Frasnian: response to intensified oceanic circulation between Gondwana and Laurussia. *Palaeogeography, Palaeoclimatology, Palaeoecology*, 234(2-4), 146-167.
- Hüneke, H. (2007). Pelagic carbonate ooze reworked by bottom currents during Devonian approach of the continents Gondwana and Laurussia. *Geological Society, London, Special Publications*, 276(1), 299-328.
- Hüneke, H., & Stow, D.A.V. (2008). Identification of ancient contourites: problems and palaeoceanographic significance. *Developments in Sedimentology*, 60, 323-344.
- Hüneke, H., & Rodríguez Tovar, F.J. (2020). Diagnostic criteria using microfacies for calcareous contourites, turbidites and pelagites in the Eocene–Miocene slope succession, southern Cyprus.
- Johnson, G.C., Lueck, R.G., & Sanford, T.B. (1994). Stress on the Mediterranean outflow plume: Part II. Turbulent dissipation and shear measurements. *Journal of Physical oceanography*, 24(10), 2084-2092.
- Knutz, P. C. (2008). Palaeoceanographic significance of contourite drifts. *Developments in Sedimentology*, 60, 511-535.
- Kuijpers, A., Werner, F., & Rumohr, J. (1993). Sandwaves and other large-scale bedforms as indicators of non-tidal surge currents in the Skagerrak off Northern Denmark. *Marine Geology*, 111(3-4), 209-221.
- Laberg, J.S., & Camerlenghi, A. (2008). The significance of contourites for submarine slope stability. *Developments in sedimentology*, 60, 537-556.
- Lafuente, J.G., Vargas, J.M., Plaza, F., Sarhan, T., Candela, J., & Bascheck, B. (2000). Tide at the eastern section of the Strait of Gibraltar. *Journal of Geophysical Research: Oceans*, 105(C6), 14197-14213.
- Li, H., van Loon, A.J., & He, Y. (2020). Cannibalism of contourites by gravity flows: explanation of the facies distribution of the Ordovician Pingliang Formation along the southern margin of the Ordos Basin, China. *Canadian Journal of Earth Sciences*, 57(3), 331-347.
- Llave, E., Hernández-Molina, F.J., Somoza, L., Díaz-del-Río, V., Stow, D.A.V., Maestro, A., & Dias, J.A. (2001). Seismic stacking pattern of the Faro-Albufeira contourite system (Gulf of Cadiz): a Quaternary record of paleoceanographic and tectonic influences. *Marine Geophysical Researches*, 22(5), 487-508.
- Llave, E., Schönfeld, J., Hernández-Molina, F.J., Mulder, T., Somoza, L., Del Río, V.D., & Sánchez-Almazo, I. (2006). High-resolution stratigraphy of the Mediterranean outflow contourite system in the Gulf of Cadiz during the late Pleistocene: the impact of Heinrich events. *Marine Geology*, 227(3-4), 241-262.
- Legg, S., Briegleb, B., Chang, Y., Chassignet, E. P., Danabasoglu, G., Ezer, T., ... & Yang, J. (2009). Improving oceanic overflow representation in climate models: the gravity current entrainment climate process team. *Bulletin of the American Meteorological Society*, 90(5), 657-670.
- Lykke-Andersen, H., & Surlyk, F. (2007). The Danish Basin: contourites in an epeiric sea. *Economic and palaeoceanographic significance of contourite deposits*, 276, 265-282.
- Martín-Chivelet, J., Fregenal-Martínez, M.A., & Chacón, B. (2008). Traction structures in contourites. *Developments in Sedimentology*, 60, 157-182.
- Martorelli, E., Bosman, A., Casalbore, D., Chiocci, F., Conte, A.M., Di Bella, L., ... & Mancini, M. (2021). Mid-to-late Holocene upper slope contourite deposits off Capo Vaticano (Mediterranean Sea): High-resolution record of contourite cyclicity, bottom current variability and sandy facies. *Marine Geology*, 431, 106372.
- Masson, D.G., Wynn, R.B., & Bett, B.J. (2004). Sedimentary environment of the Faroe-Shetland and Faroe Bank Channels, north-east Atlantic, and the use of bedforms as indicators of bottom current velocity in the deep ocean. *Sedimentology*, 51(6), 1207-1241.

- Mézerai, M.L., Faugères, J.C., Figueiredo Jr, A.G., & Massé, L. (1993). Contour current accumulation off the Vema Channel mouth, southern Brazil Basin: pattern of a "contourite fan". *Sedimentary Geology*, 82(1-4), 173-187.
- Millot, C. (1999). Circulation in the western Mediterranean Sea. *Journal of Marine Systems*, 20(1-4), 423-442.
- Mulder, T., Hassan, R., Ducassou, E., Zaragosi, S., Gonthier, E., Hanquiez, V., ... & Toucanne, S. (2013). Contourites in the Gulf of Cadiz: a cautionary note on potentially ambiguous indicators of bottom current velocity. *Geo-Marine Letters*, 33(5), 357-367.
- Niemi, T.M., Ben-Avraham, Z., Hartnady, C.J., & Reznikov, M. (2000). Post-Eocene seismic stratigraphy of the deep ocean basin adjacent to the southeast African continental margin: a record of geostrophic bottom current systems. *Marine Geology*, 162(2-4), 237-258.
- Pinardi, N., Cessi, P., Borile, F., & Wolfe, C.L. (2019). The Mediterranean sea overturning circulation. *Journal of Physical Oceanography*, 49(7), 1699-1721.
- Rebesco, M., Hernández-Molina, F.J., Van Rooij, D., & Wåhlin, A. (2014). Contourites and associated sediments controlled by deep-water circulation processes: State-of-the-art and future considerations. *Marine Geology*, 352, 111-154.
- Rodrigues, S., Roque, C., Hernández-Molina, F.J., Llave, E., & Terrinha, P. (2020). The sines contourite depositional system along the SW Portuguese margin: Onset, evolution and conceptual implications. *Marine Geology*, 430, 106357.
- Rodrigues, S., Hernández-Molina, F.J., & Kirby, A. (2021). A late Cretaceous mixed (turbidite-contourite) system along the Argentine margin: paleoceanographic and conceptual implications. *Marine and Petroleum Geology*, 123, 104768.
- Rohling, E.J., Marino, G., & Grant, K.M. (2015). Mediterranean climate and oceanography, and the periodic development of anoxic events (sapropels). *Earth-Science Reviews*, 143, 62-97.
- Sánchez-Leal, R.F., Bellanco, M.J., Fernández-Salas, L.M., García-Lafuente, J., Gasser-Rubinat, M., González-Pola, C., ... & Sánchez-Garrido, J.C. (2017). The Mediterranean Overflow in the Gulf of Cadiz: A rugged journey. *Science advances*, 3(11), ea00609.
- Sani, F., Del Ventisette, C., Montanari, D., Bendkik, A., & Chenakeb, M. (2007). Structural evolution of the Rides Prerifaines (Morocco): structural and seismic interpretation and analogue modelling experiments. *International Journal of Earth Sciences*, 96(4), 685-706.
- Sannino, G., Bargagli, A., & Artale, V. (2004). Numerical modeling of the semidiurnal tidal exchange through the Strait of Gibraltar. *Journal of Geophysical Research: Oceans*, 109(C5).
- Shanmugam, G., Spalding, T. D., & Rofheart, D. H. (1993b). Traction structures in deep-marine, bottom-current-reworked sands in the Pliocene and Pleistocene, Gulf of Mexico. *Geology*, 21(10), 929-932.
- Shanmugam, G. (2017a). The contourite problem. In *Sediment provenance* (pp. 183-254). Elsevier.
- Shanmugam, G. (2008). Deep-water bottom currents and their deposits. *Developments in sedimentology*, 60, 59-81.
- Simon, D., Marzocchi, A., Flecker, R., Lunt, D. J., Hilgen, F.J., & Meijer, P.T. (2017). Quantifying the Mediterranean freshwater budget throughout the late Miocene: New implications for sapropel formation and the Messinian Salinity Crisis. *Earth and Planetary Science Letters*, 472, 25-37.
- Stow, D.A.V., & Lovell, J.P.B. (1979). Contourites: their recognition in modern and ancient sediments. *Earth-Science Reviews*, 14(3), 251-291.
- Stow, D.A.V., & Holbrook, J.A. (1984). North , London, Special Publications, 15(1), 245-256.
- Stow, D.A.V., & Faugeres, J.C. (1990). Miocene contourites from the proto Izu-Bonin forearc region, southern Japan. *Abstract 13th Int. Sed. Cong., Nottingham*, 526.
- Stow, D.A., Faugères, J.C., Viana, A., & Gonthier, E. (1998). Fossil contourites: a critical review. *Sedimentary Geology*, 115(1-4), 3-31.
- Stow, D.A., & Mayall, M. (2000). Deep-water sedimentary systems: new models for the 21st century. *Marine and Petroleum Geology*, 17(2), 125-135.
- Stow, D. A. (Ed.). (2002). Deep-water contourite systems: modern drifts and ancient series, seismic and sedimentary characteristics. Geological Society of London.
- Stow, D.A.V., & Faugères, J.C. (2008). Contourite facies and the facies model.

- Developments in sedimentology*, 60, 223-256.
- Stow, D.A., Hernández-Molina, F.J., Llave, E., Sayago-Gil, M., Díaz del Río, V., & Branson, A. (2009). Bedform-velocity matrix: the estimation of bottom current velocity from bedform observations. *Geology*, 37(4), 327-330.
- Stow, D.A.V., Hernández-Molina, F.J., Llave, E., Bruno, M., García, M., del Río, V.D., ... & Brackenridge, R.E. (2013). The Cadiz Contourite Channel: Sandy contourites, bedforms and dynamic current interaction. *Marine Geology*, 343, 99-114.
- Stow, D., & Smillie, Z. (2020). Distinguishing between deep-water sediment facies: turbidites, contourites and hemipelagites. *Geosciences*, 10(2), 68.
- Straume, E.O., Gaina, C., Medvedev, S., & Nisancioglu, K.H. (2020). Global Cenozoic Paleobathymetry with a focus on the Northern Hemisphere Oceanic Gateways. *Gondwana Research*.
- Tsimplis, M.N., & Bryden, H.L. (2000). Estimation of the transports through the Strait of Gibraltar. *Deep Sea Research Part I: Oceanographic Research Papers*, 47(12), 2219-2242.
- Verdicchio, G., Trincardi, F., & Asioli, A. (2007). Mediterranean bottom-current deposits: an example from the Southwestern Adriatic Margin. *Geological Society, London, Special Publications*, 276(1), 199-224.
- Viana, A.R., & Faugères, J.C. (1998). Upper slope sand deposits: the example of Campos Basin, a latest Pleistocene-Holocene record of the interaction between alongslope and downslope currents. *Geological Society, London, Special Publications*, 129(1), 287-316.
- Viana, A.R. (2001). Seismic expression of shallow-to deep-water contourites along the south-eastern Brazilian margin.
- Viana, A. R., Almeida, W., Nunes, M. C. V., & Bulhões, E. M. (2007). The economic importance of contourites. *Geological Society, London, Special Publications*, 276(1), 1-23.
- Viana, A.R. (2008). Economic relevance of contourites. *Developments in Sedimentology*, 60, 491-510.
- Wang, D.P. (1993). The Strait of Gibraltar Model: Internal tide, diurnal inequality and fortnightly modulation. *Deep Sea Research Part I: Oceanographic Research Papers*, 40(6), 1187-1203.
- Wetzel, A., Werner, F., & Stow, D.A.V. (2008). Bioturbation and biogenic sedimentary structures in contourites. *Developments in Sedimentology*, 60, 183-202.
- Wüst, G. (1961). On the vertical circulation of the Mediterranean Sea. *Journal of Geophysical Research*, 66(10), 3261-3271.
- Wynn, R. B., & Stow, D. A. (2002). Classification and characterisation of deep-water sediment waves. *Marine Geology*, 192(1-3), 7-22.
- Zavala, C. (2020). Hyperpycnal (over density) flows and deposits. *Journal of Palaeogeography*, 9(1), 1-21.
- Zhang, X., Zhang, T., Lei, B., Zhang, J., & Yong, J. (2020). A giant sandy sediment drift in early Silurian (Telychian) and its multiple sedimentological process. *Marine and Petroleum Geology*, 113, 104077.

# *Chapter IX*

*Future Research*



**What would be the best step, following up on this research, in improving our understanding of contourite channel systems?**

The best steps following up on this research would be to study, in detail, the Bel Amri and Msagra sections (*Table 1, chapter III*). As addressed in *chapter III*, these outcrops have potential for contourite research, and as such, could contribute to the understanding of the evolution of the Rifian Corridor Contourite Channel System, the evolution of the paleo-channels, the distribution of contourite sediments in the Rifian Corridor, and the understanding of sandy contourite related sedimentary facies. Furthermore, to enhance the economical perspective of sandy contourite deposits, petrophysical analysis should be carried out so that besides the sedimentary facies distribution studied herein, the petrophysical characteristics can be coupled to these facies. To better understand sandy contourite deposits in general, it is of utmost importance that other outcrops with a potential contouritic origin are studied so comparisons can be made between different contourite depositional systems and their sedimentary facies.

One of our aims remains to drill a core in the Kirmta outcrop, this core could be used to unravel a significant amount of information, such as petrophysical characteristics, and would enable a better comparison with cores drilled in similar deposits in the deep-sea. Also this core would enable us to better understand the interstratified fine-grained deposits, their high resolution characterization, and by applying the methodology proposed by *de Castro et al., (2020a, 2021)* we would be able to differentiate between depositional processes occurrent when the contourite channel is inactive.

Another aspect that could significantly contribute to the understanding of the late Miocene Contourite Channel System in the Rifian Corridor is to study onshore seismic lines in the study area. Unfortunately we were not able to acquire these lines during this research project. By studying these onshore seismic lines we would potentially be able to trace the contourite channels in the subsurface and track their distribution throughout the corridor into the Atlantic. Following up on this proposed research an offshore seismic study would enable the differentiation of seismic facies from within the confined corridor into open marine conditions.

Furthermore, contourite associated flume-experiments could significantly help us to better understand the fluid-behavior within contourite channels.

# *Chapter X*

*Co-Authored work*

## Co-Authored work

The following list contains co-authored work executed in the scope of this Research Project.

### 1.1 Publications









- Macaronichnus and contourite depositional settings: Bottom currents and nutrients as coupling factors. Miguez-Salas, O., Rodríguez-Tovar, F. J., & De Weger, W. (2020). *Palaeogeography, Palaeoclimatology, Palaeoecology*, 545, 109639.
- Geochemical and Minerological Field Study of Contourite Channel Deposits in Northern Morocco. Borisov, D. G., de Weger, W., Ivanova, E. V., Korshunov, D. M., Riazanova, E. I., & Astaty, Y. (2020). *Oceanology*, 60, 142-144.
- Contourite characterization and its discrimination from other deep-water deposits in the Gulf of Cadiz contourite depositional system. de Castro, S., Hernández-Molina, F. J., de Weger, W., Jiménez-Espejo, F. J., Rodríguez-Tovar, F. J., Mena, A., ... & Sierro, F. J. (2021). *Sedimentology*, 68: 987-1027. <https://doi.org/10.1111/sed.12813>
- The Late Miocene Rifian corridor as a natural laboratory to explore a case of ichnofacies distribution in ancient gateways. Miguez-Salas, O., Rodríguez-Tovar, F. J., & de Weger, W. (2021). *Scientific Reports*, 11(1), 1-10.

# *Chapter XI*

*Appendices – (Supplementary material)*

## Supplementary material Chapter VI

**Table S4.1.** Overview of recognized sedimentary facies and facies associations. The facies consist of F1) Blue marlstone, F2) Brownish sandy marlstone, F3) Planar bi-gradational sandstones, F4) Cross-stratified sandstone, F5) Trough-cross stratified sandstones, F6) Heterolithic convolute sandstones, F7) Normal graded compound sandstone beds and, F8) Monomictic conglomerates. Besides the facies, their general thickness, sedimentary structures, composition and interpretation are provided.

Facies Association	Example	Facies	Scale	Sedimentary structures	Composition	Interpret.
Hemipelagic and Muddy contourites	 20 cm	F1. Blue marlstone	cm to 100's m scale	Structureless and gradational with sand-rich laminae	Fossil rich (mainly bivalves) marls with up to very fine-grained siliciclastic and bioclastic sand	Hemipelagites and contourite drift deposits
	 20 cm	F2. Brownish sandy marlstone	cm to m scale	Gradational to sharp with planar and undulatory laminae	Fossil rich (mainly bivalves) marls with fine-grained siliciclastic and up to coarse-grained bioclastic sand	Fine grained contourites
Sandy contourites	 5 m	F3. Planar bi-gradational sandstones	1 cm to 15 cm	Planar beds of successive normal and inverse-gradational	Fine-grained mixed siliciclastic and bioclastic sand enriched in sand-sized pellets of reworked mudstone and glauconite	Sandy contourites
	 3 m	F4. Cross-stratified sandstones	15 cm up to 1 m	Tabular low- to high-angle cross-stratified beds. Fluid-escape struct. in proximity to F6	Fine- to coarse-grained mixed silici- and bioclastic (dom. Bivalve and echinoderm fragments) sandstones.	2D contourite dunes
	 5 m	F5. Trough-cross stratified sandstones	50 cm up to 4 m	Trough cross-stratified beds with tangential foreset laminae	Mixed, medium to very coarse-grained silici- and bio-clastic sand. Bioclasts dominantly consist of bivalve and echinoderm fragments	3D contourite dunes
Gravitational deposits	 3 m	F6. Heterolithic convolute sandstones	1 m up to 5 m	Convolute and contorted beds with fluid escape structures	Fine to coarse-grained mixed siliciclastic and bioclastic sand. Beds are generally up to 10 cm thick	Slump deposits
	 70 cm	F7. Normal graded compound sandstone beds	5 cm up to 40 cm	Normal graded tabular beds with occasional basal scour erosive surfaces and ripples	Fine to coarse grained mixed siliciclastic and bioclastic sand with muddy rip-up clasts	Turbidites
	 5 m	F8. Monomictic conglomerates	Up to 2 m	Concave up basal surfaces with clast to matrix-supported conglomerates	Poorly sorted, rounded and disc shaped arenitic cobbles and boulders in a silty sand matrix	Debris-flow deposits

Note: Scale applies to width of view

Supplementary material Chapter V

**Table S5.1.** Modal analysis data based on 300-point counts in thin section. Proportions of solid rock components (i.e., all but porosity) are re-normalized to a total of 100%. Component abbreviations, from left to right: F = facies, Qm = monocrystalline quartz, Qp = polycrystalline quartz, Qt = quartz total, F = feldspar, Gg = green glauconite, Gb = brownish/yellowish glauconite, Gt = glauconite total, L = lithic fragments; c = carbonate, cp = claystone pellets, ch = chert, fa = feldspar aggregates, qm = quartz-mica aggregates, Lt = lithic total, B = bioclastic; b = bivalves, f = foraminifera, ca = calcareous algae, u = undifferentiated, Bt = bioclast total, Cc = calcite cement, Fe = iron oxides/hydroxides, P% = porosity percentage, Gs = mean grain-size (ms = medium-grained sand, vfs = very-fine grained sand), S = sorting (m = medium, w = well, vw = very well).

Sample	F	Qm	Qp	Qt	F	Gg	Gb	Gt	Lc	Ld	Lc	Lc	Lf	Lqm	Lt	Bb	Bf	Be	Bc	Bu	Bt	Cc	Fe	P%	GS	S	Fig
EA3	5	38.3	2.3	40.	0	0	0.	0.	13.	0	7.	0.	1.	0.3	22.	0.	0	0.	0	2.3	3	22.9	10.2	11.	ms	w	9C
	6			6	0	4	4	4	9	0	1	3	3	9	9	4	0	3	0	0	0	0	0	3	3		
FN1	F	19.2	2.7	21.	0	0	4.	4.	22.	2.	8.	0.	1.	1.3	36.	6.	1.	0.	0.7	13.	23.	13.7	0	2.7	ms	m-w	11
	6			9	0	5	5	5	6	7	2	3	7	8	8	5	7	7	0	5	1	0	0	0			
EA5	F	22.3	7	29.	1.	1.	1	2.	12	1.	17	0.	0	0	30.	3.	2.	6	0	0	12	17	6.7	0	vfs	w-vw	11
	8			3	7	7	7	7	3	3	3	3	0	6	7	3	3	0	0	0	0	0	0	0	0		



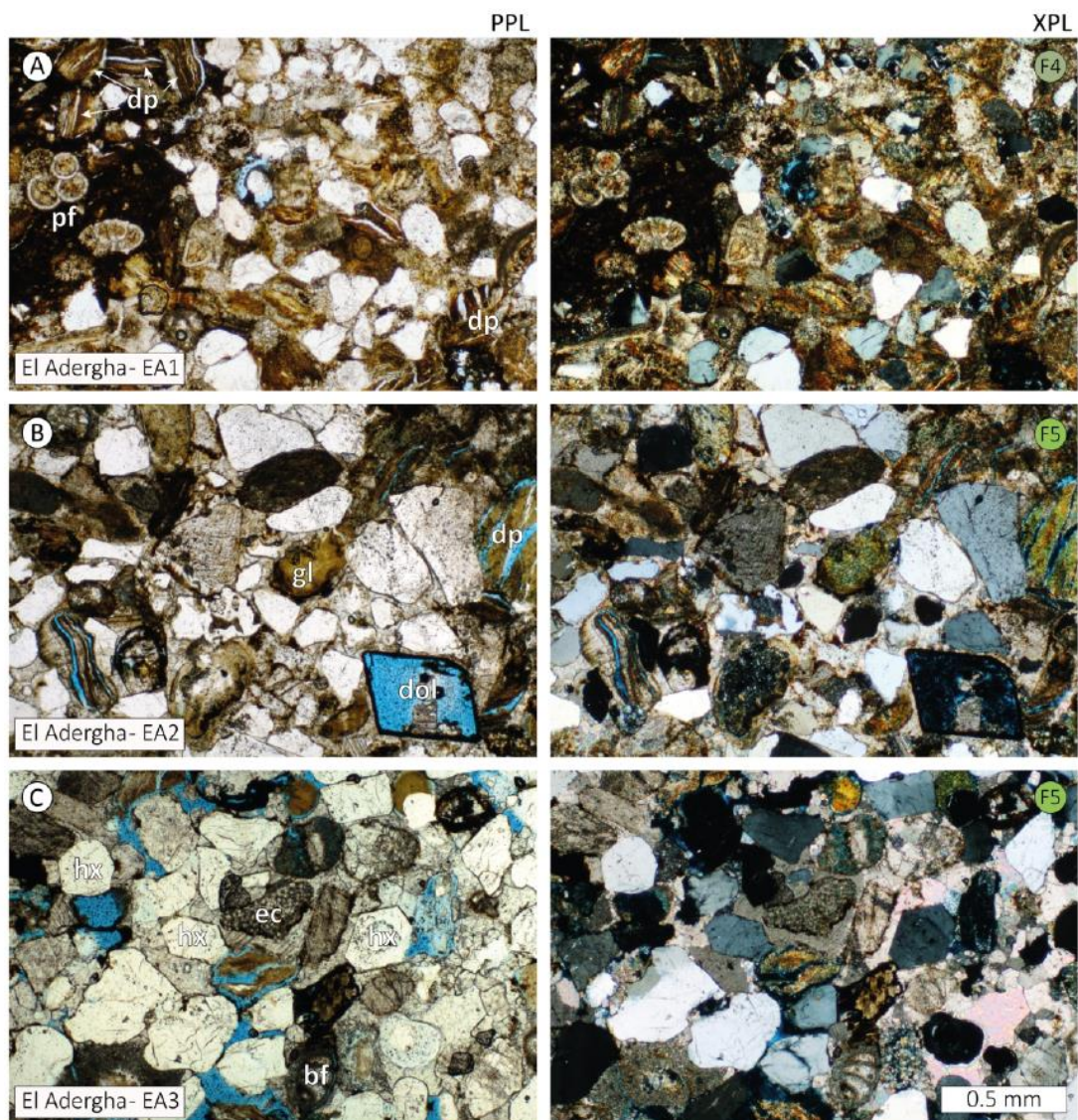


**Figure S5.1.** Microphotographs for facies F4 and F5. Abbreviations: dp = detrital pellets, pf = planktonic foraminifera, bf = benthic foraminifera, dol = dolomite, gl = glauconite, ec = echinoderm fragments, hx = hexagonal quartz. (A) Microfacies of facies F4 with detrital pellets and planktonic foraminifera. (B) and (C) Microfacies of facies F5 with brownish gl, dp and exsolved dol (B) and ec fragments and bf (C).



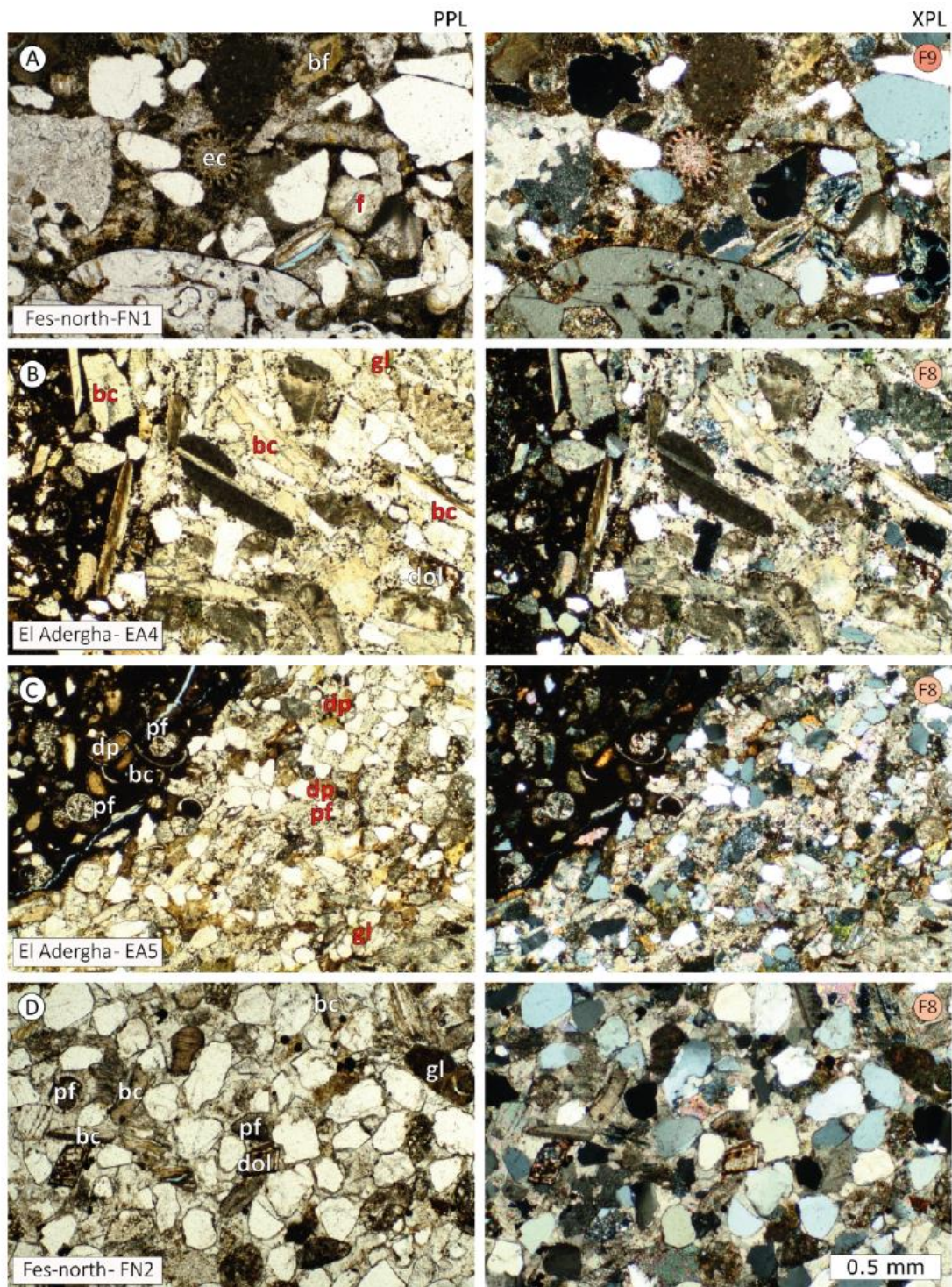


**Figure S5.2.** Microphotographs for facies F6 and F8. (A) Microfacies of F6 with *ec* spine and *bf* (see caption for Fig. S1 for abbreviations), the large crystal of calcite along the lower edge of the field-of-view contains silt-grade quartz grains and pods of argillaceous material. (B) to (D) Microfacies of F8 for El Adergha, rich in *bc*, *pf* and *gl* (B) and (C) and Fes-north, rich in *pf*, *bc*, *gl* and the occasional *dol* (D). Minute dark specs are aggregates of iron oxides dissolved from the calcite cement.



## Supplementary material Chapter VI

Note: All appendices supplementary material in this section is derived from Beelen et al., 2020. - <https://doi.org/10.2110/jsr.2020.010>

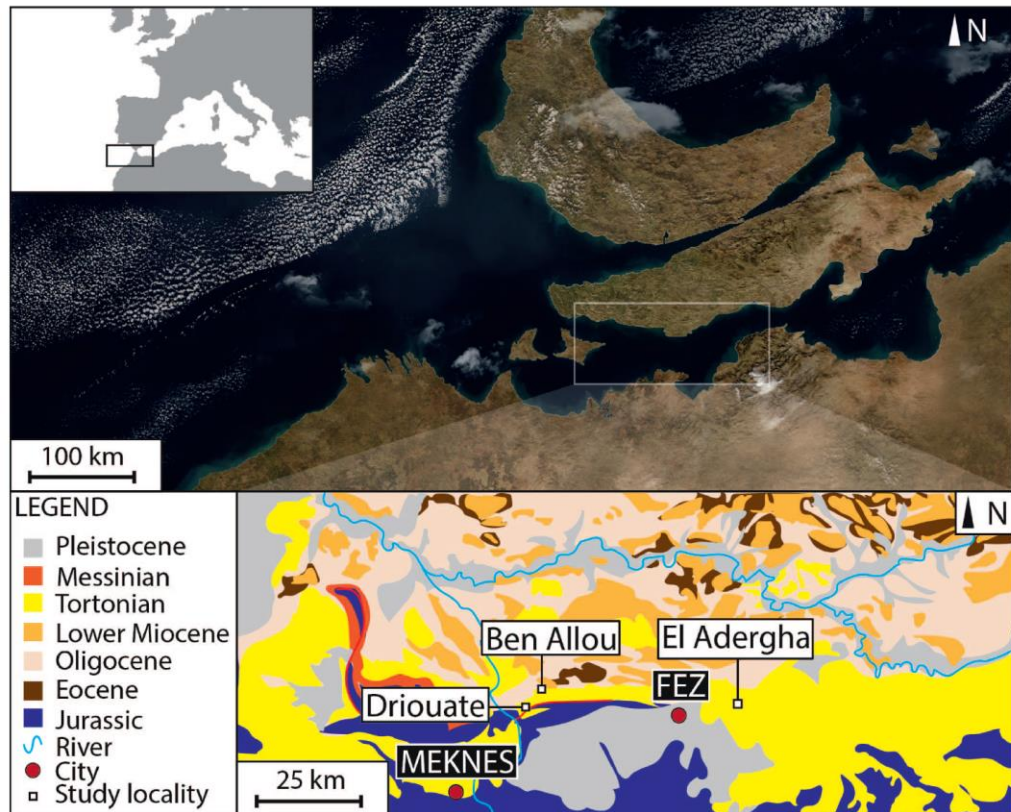


FIG. 1.—Top: Paleogeographic reconstruction of the Rifian Corridors during the late Tortonian. Note that the Gibraltar Strait had not yet formed during this time (modified from Capella et al. (2017a)). White box in top right represents area of image shown below. White inset shows present day location of the study area. Bottom: Geological map showing all three outcrop locations visited in this study: Ben Allou, El Adergha, and Driouate, relative to the cities of Meknes and Fez. Geological map is modified from Chenakeb (2004). All outcrop localities considered in this study are from the upper Tortonian interval of the Saiss sub-basin in the Rif Foreland.

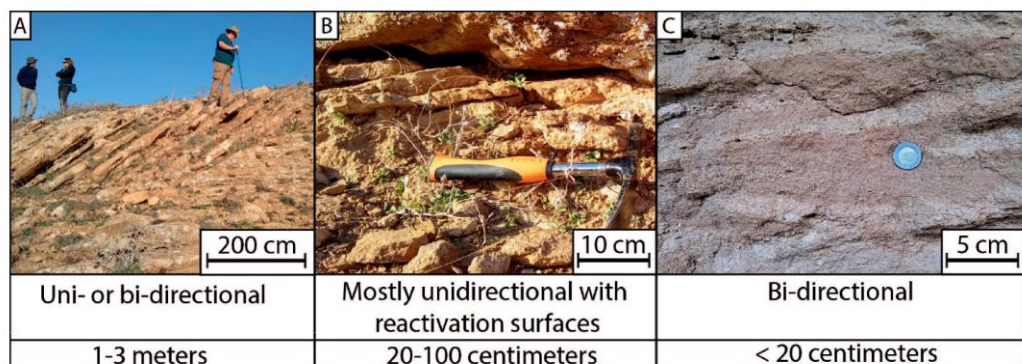


FIG. 4.—Three scale orders of cross strata in the calcarenites. A) The largest scale of 1–3-m-thick cross strata, showing both unidirectional and bidirectional cross-bedding and bounded by reactivation surfaces. B) The moderate scale has 20–100-cm-thick packages of mostly unidirectional cross strata bounded by reactivation surfaces. C) The smallest cross-strata are less than 20 cm thick and show a dominance of bidirectional cross stratification and ripples, including some herringbone strata.

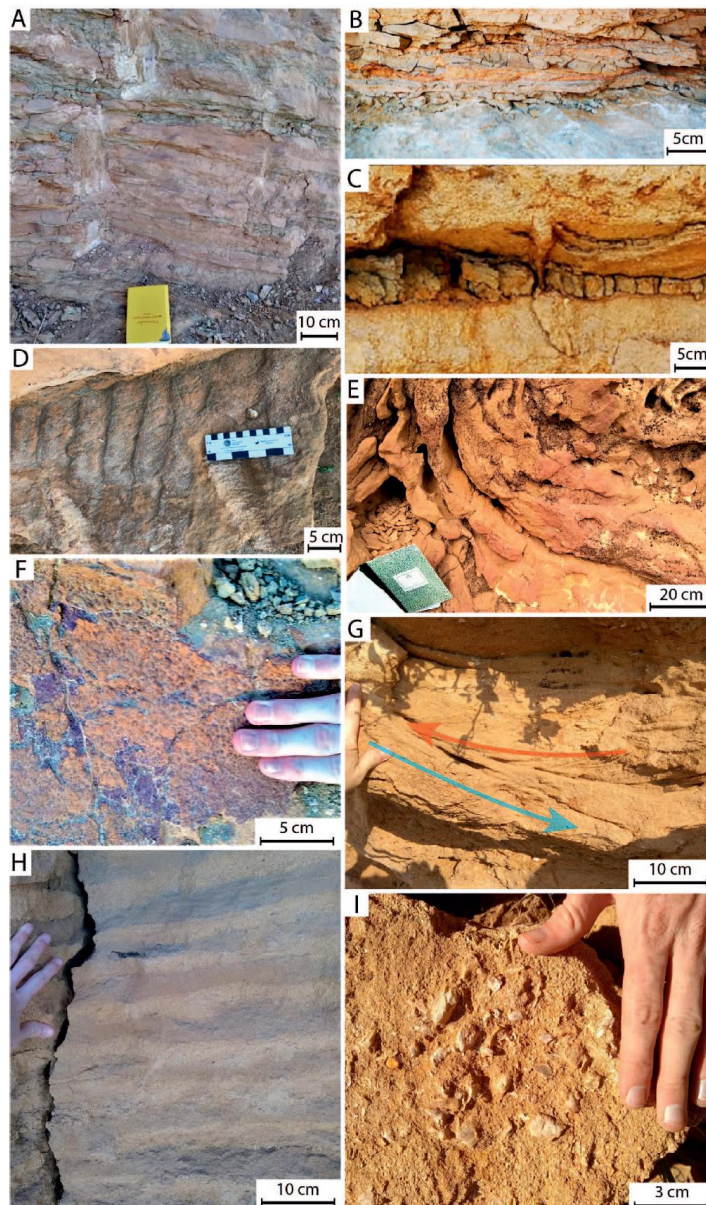


FIG. 6.—Images showing the details of subfacies 3b and 3c in the Ben Allou outcrop. A) Tabular sandstone beds bounded by mud drapes (subfacies 3c). B) 30-cm-thick intervals with bidirectional flaser bedding above a rippled surface (subfacies 3c). C) Prominent 5-cm-thick mud drape with mud crack (subfacies 3c). D) Rippled surface with *hizocorallium* (bottom left) (subfacies 3c). E) Large dewatering structure with red-colored hardgrounds at the base (subfacies 3b). F) Siderite-rich surface with pustular texture (possibly a fossil microbial mat, subfacies 3b). G) Bidirectional-current structure with dominant paleocurrent direction (blue) and subordinate paleocurrent direction (red) shown (subfacies 3b). H) Rhythmically bedded interval (subfacies 3b). I) Barnacle hash (subfacies 3b).



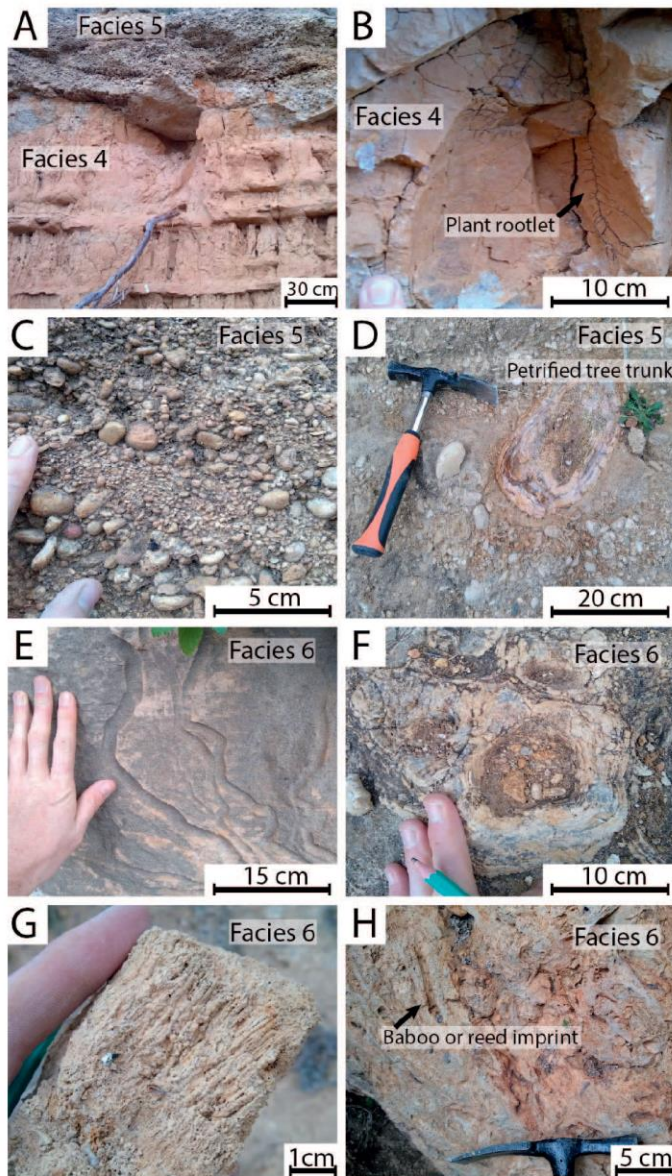


FIG. 10.—Images showing details of the Driouate outcrop. A) Pinkish, carbonaceous siltstones (facies 4) with roughly 30-cm-thick beds of micrite-rich caliche. These sediments are incised at the top by cross-stratified conglomerates (facies 5). B) Top of carbonaceous siltstones (facies 4) showing plant rootlets. C) Close-up view of cross-stratified conglomerates (facies 5) showing fining-upward beds and polymict clasts. D) Petrified tree trunk in cross-stratified conglomerates (facies 5). E) *Ptilonichnus* trace fossils in facies 6. F) Layered, tuberos stromatolite in facies 6. G) Stromatolite with numerous insect-larva burrows in facies 6. H) Close-up of facies 6 showing bamboo or reed stalk imprint.

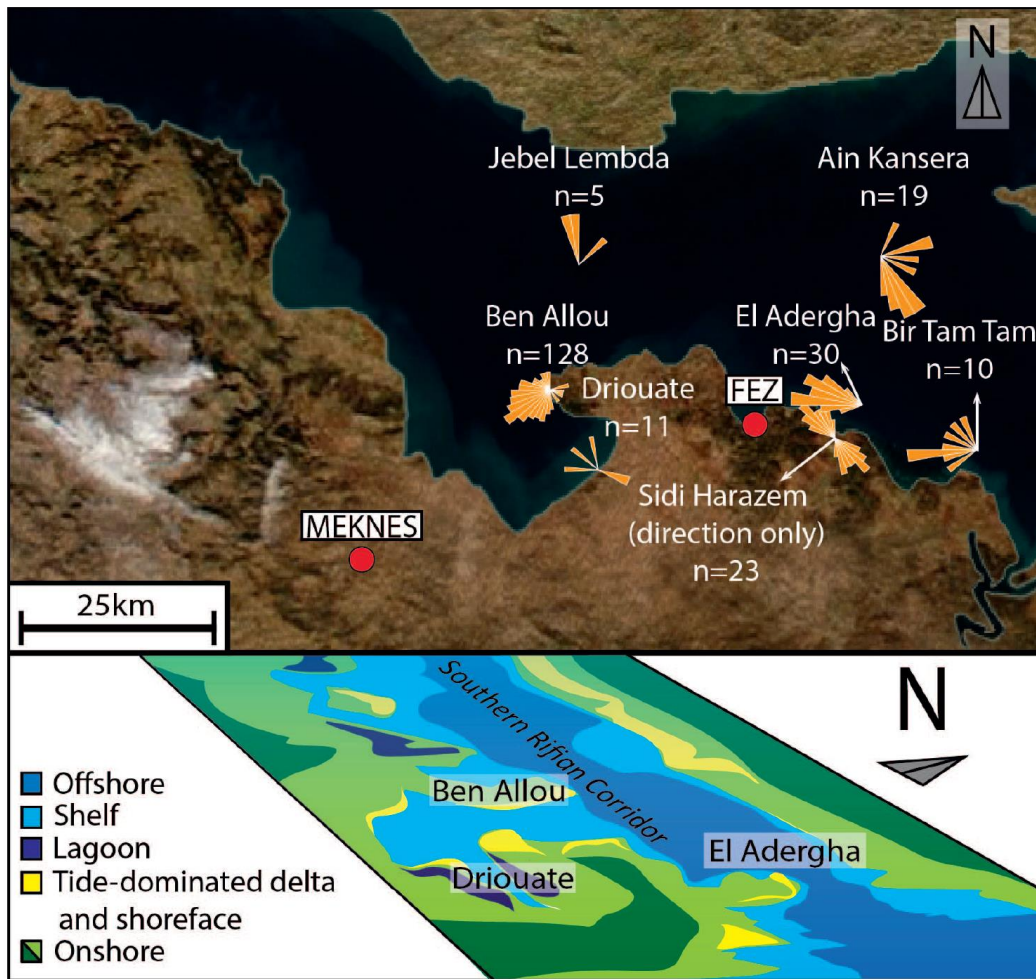


FIG. 15.—A) Exposure at Driouate. B) Interpretation: three complete cycles are identified, each having three facies. C) Possible interpretation of facies showing siltstones (facies 4) are linked to highstands while cross-stratified conglomerates (facies 5) are linked to lowstand and stromatolite bearing carbonate rocks (facies 6) are linked to transgression. Cycles are bounded at the bottom by erosional surfaces.

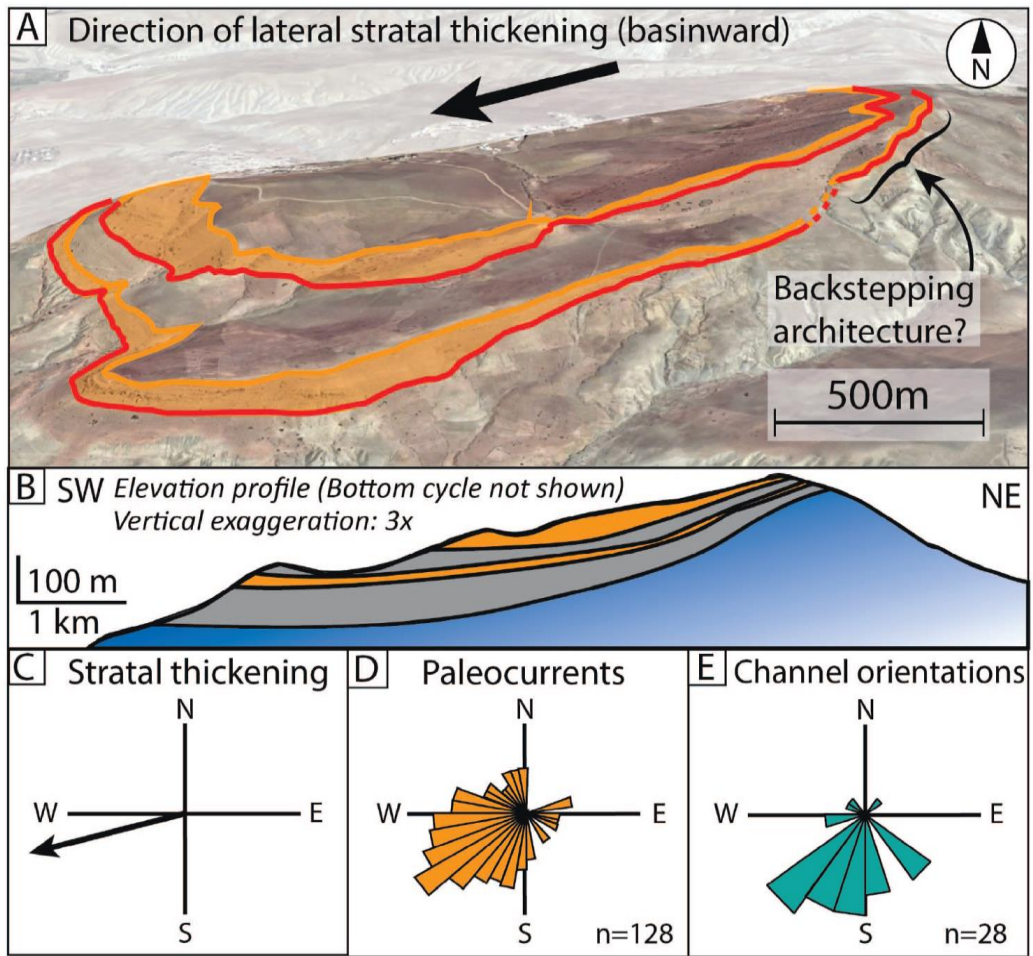


FIG. 16.—Tentative paleogeographic interpretation for the Saïss sub-basin area of the Southern Rifian Corridor. Top: five upper Tortonian outcrops and their paleocurrent directions as measured by Capella et al. (2017a), suggesting a complex, likely rugose southern coastline of the Rifian Corridor. Bottom: schematic paleogeographic interpretation for Ben Allou, El Adergha, and Driouate, showing Ben Allou situated at a bay.



Table 2 of the supplementary material by Beelen et al. 2020

Foraminiferal genera are roughly from shallow (left) to deeper (right), planktonic genera are in bold.

